

**QUANTIFICATION OF MARINE MEGAFANAL DISTRIBUTION  
PATTERNS USING A REMOTELY OPERATED VEHICLE**

by

**DAVID MATTHEW PARRY**

A thesis submitted to the University of Plymouth  
in partial fulfilment for the degree of

**DOCTOR OF PHILOSOPHY**

Institute of Marine Studies  
Faculty of Science

In collaboration with  
Plymouth Marine Laboratory

**December 2002**

UNIVERSITY OF PLYMOUTH	
Item No.	Q 08541 4538
Date	15 JAN 2003 8
Class No.	THESIS 574.52636 PAR
COPY NO.	X704522 64X
PLYMOUTH LIBRARY	

**REFERENCE ONLY**

**LIBRARY STORE**

## Abstract

# Quantification of marine megafaunal distribution patterns using a Remotely Operated Vehicle

David Matthew Parry

This thesis documents the development and application of the Automated Benthic Image Scaling System (ABISS), a novel structured lighting array for calculating image scale, accounting for perspective, to allow quantitative non-destructive megafaunal sampling using observations from a Remotely Operated Vehicle (ROV). Megafauna are important components of marine soft sediment assemblages that influence the composition of the associated assemblage and the flux of energy across the sediment–water interface, by altering the physical and chemical characteristics of the sediment during bioturbation. However, megafaunal species are not sampled adequately using traditional techniques. Megafaunal abundance estimates derived from ROV observations were validated against those derived from direct diver observations and results suggested that data were in close agreement. To quantify spatial variation of the megafaunal assemblage, spatially referenced images were collected with a maximum sample separation of 400 m within a broader area of homogeneous sediment in Plymouth Sound (United Kingdom) during May 2000 and March 2001. Results demonstrated that the spatial distribution of the megafaunal assemblage was neither uniform nor stable temporally. A hierarchy of spatial structure was detected, whereby, patches with minimum radius between 123–163 m were nested within patches up to 400 m radius. To assess the megafaunal contribution to endobenthic biomass, the population size structure and biomass of the dominant megafaunal bivalve *Lutraria lutraria* was estimated from measurements of the siphon tips. Results indicated that the population size structure was stable between years despite significant differences in abundance. In addition, *L. lutraria* contributed approximately 90% of the endobenthic biomass, indicating that traditional assessment of benthic biomass by consideration of macrofaunal samples alone will underestimate severely the biomass and respiration of the entire endobenthic assemblage. Novel techniques of quantifying the spatial distribution of megafaunal assemblages presented in this thesis offer ways forward to address how variation of megafaunal spatial structure affects macrofaunal assemblage structure, and to discuss the application of remote imaging to map and predict quantitatively the conservation value of subtidal soft sediments.

## Contents

Copyright statement .....	i
Title page .....	ii
Abstract .....	iii
Contents .....	iv
List of tables .....	viii
List of figures .....	ix
List of acronyms .....	x
List of symbols .....	xi
Acknowledgements .....	xii
Author's declaration .....	xiii
Publications .....	xiv
Conference attended and work presented .....	xv
External contacts .....	xv
 <b>Chapter 1:</b>	
<b>General introduction .....</b>	<b>1</b>
1.1 BACKGROUND TO ECOLOGICAL INVESTIGATION .....	2
1.2 THE IMPORTANCE OF DIVERSITY .....	5
1.2.1 Measurement of diversity .....	6
1.2.2 Problems of scale associated with measurement of diversity .....	7
1.2.3 Detection of diversity on large spatial scales .....	8
1.2.4 Rapid assessment of marine diversity .....	9
1.3 EFFECT OF ECOSYSTEM ENGINEERS ON DIVERSITY AND ECOSYSTEM FUNCTION .....	10
1.3.1 Mechanisms by which ecosystem engineers affect benthic ecosystem function .....	11
1.4 PATCH STRUCTURE OF BENTHIC ECOSYSTEMS .....	14
1.4.1 Role of disturbance in maintenance of patch structure .....	14
1.4.2 Landscape approach to quantifying megafaunal distribution .....	15
1.5 SAMPLING THE MEGAFUNA .....	19
1.5.1 Grabs, cores, trawls and dredges .....	19
1.5.2 Observations by SCUBA divers .....	21
1.5.3 Underwater camera observations .....	22
1.5.4 Camera deployment methods that maintain contact with the substratum .....	23
1.5.4.1 Manual deployment by SCUBA divers .....	23
1.5.4.2 Drop-down camera deployment .....	23
1.5.4.3 Sledge- and trawl-mounted cameras .....	24
1.5.4.4 Time-lapse deployment .....	25
1.5.5 Camera deployment methods where contact with the substratum is avoided .....	26
1.5.5.1 Manned scientific submersibles .....	26
1.5.5.2 Remotely Operated Vehicles .....	28
1.6 AIMS AND THESIS STRUCTURE .....	31
 <b>Chapter 2:</b>	
<b>Development of techniques to quantify scale and spatially reference remote images .....</b>	<b>33</b>
2.1 EQUIPMENT DETAILS .....	34
2.1.1 Remotely Operated Vehicle specification .....	34

2.1.2	Image-grabbing software .....	36
2.2	QUANTITATIVE UNDERWATER OBSERVATIONS .....	37
2.2.1	Platforms in contact with the seabed .....	38
2.2.1.1	<i>Objects of known dimensions in Field of View</i> .....	38
2.2.1.2	<i>Calibration images and empirical calculations</i> .....	39
2.2.2	Platforms NOT in contact with the substratum .....	40
2.2.3	Structured lighting systems .....	41
2.3	AUTOMATED BENTHIC IMAGE SCALING SYSTEM .....	43
2.3.1	Structured lighting array .....	43
2.3.2	Structured lighting trigonometry .....	44
2.3.3	Benthic Imager software .....	50
2.3.3.1	<i>Image scaling and measurement</i> .....	50
2.3.3.2	<i>Image resolution</i> .....	52
2.3.3.3	<i>Image enhancement</i> .....	52
2.3.4	Automated Benthic Image Scaling System calibration .....	54
2.3.4.1	<i>Laser alignment</i> .....	54
2.3.4.2	<i>Camera backset correction</i> .....	58
2.3.5	Laser diode wavelength .....	59
2.4	UNDERWATER ACOUSTIC POSITIONING SYSTEM .....	60
2.4.1	Basic navigation techniques .....	60
2.4.2	Underwater acoustic positioning systems .....	62
2.4.2.1	<i>Long Base Line systems</i> .....	63
2.4.2.2	<i>Short (SBL) and Ultra Short Baseline (USBL) systems</i> .....	64
2.4.3	<i>PharosLite</i> navigation system .....	65
2.5	CONCLUSIONS .....	68
<b>Chapter 3:</b>	<b>Location and description of megafaunal assemblage survey sites</b> .....	69
3.1	INTRODUCTION .....	70
3.2	JENNYCLIFF BAY, PLYMOUTH SOUND .....	70
3.2.1	Physical characteristics .....	70
3.2.2	Biological characteristics .....	71
3.2.3	Sediment resuspension .....	73
3.2.3.1	<i>Drag coefficient (<math>C_D</math>)</i> .....	73
3.2.3.2	<i>Depth mean average water current <math>\langle \bar{u} \rangle</math></i> .....	75
3.2.3.3	<i>Current shear stress (<math>\tau_0</math>)</i> .....	75
3.2.3.4	<i>Bed shear stress (<math>\tau_b</math>)</i> .....	75
3.2	LOCH CRERAN, WESTERN SCOTLAND .....	77
3.3.1	Physical characteristics .....	77
3.3.2	Biological characteristics .....	78
3.3.3	Sediment resuspension .....	78
<b>Chapter 4:</b>	<b>Validation of megafauna abundance data derived from remote (ROV) and direct (diver) observations</b> .....	80
	ABSTRACT .....	81
4.1	INTRODUCTION .....	82
4.2	MATERIALS AND METHODS .....	83
4.2.1	Site description .....	83
4.2.2	Survey design .....	84
4.2.3	Data analysis .....	85
4.3	RESULTS .....	86

4.3.1	Loch Creran .....	86
4.3.1.1	<i>Abundance estimates</i> .....	86
4.3.1.2	<i>Spatial coincidence</i> .....	87
4.3.1.3	<i>Conspicuous features</i> .....	88
4.3.1.4	<i>Features greater than 15 mm diameter</i> .....	89
4.3.2	Jennycliff Bay .....	92
4.3.2.1	<i>Abundance estimates</i> .....	92
4.3.2.2	<i>Spatial coincidence</i> .....	92
4.4	DISCUSSION.....	95
4.5	CONCLUSIONS.....	98

<b>Chapter 5:</b>	<b>Spatial and temporal pattern in community structure of a soft sediment megabenthic assemblage .....</b>	<b>99</b>
	ABSTRACT .....	100
5.1	INTRODUCTION .....	101
5.2	MATERIALS AND METHODS .....	106
5.2.1	Survey location .....	106
5.2.2	Survey design .....	106
5.2.3	Data extraction .....	107
5.2.4	Data analysis .....	109
	5.2.4.1 <i>Megafaunal assemblage composition</i> .....	111
	5.2.4.2 <i>Spatial structure of the megafaunal assemblage</i> .....	112
	5.2.4.3 <i>Spatial pattern of the megafaunal assemblage</i> .....	113
5.3	RESULTS .....	117
5.3.1	Spatial structure of the megafaunal assemblage .....	117
5.3.2	Spatial pattern of the megafaunal assemblage .....	118
	5.3.2.1 <i>May 2000 survey</i> .....	118
	5.3.2.2 <i>March 2001 survey</i> .....	121
	5.3.2.3 <i>Between-year differences in spatial pattern</i> .....	122
5.3.3	Megafaunal assemblage composition and spatial structure .....	123
5.3.4	Spatial pattern of <i>Lutraria lutraria</i> and thalassinidean openings .....	130
5.4	DISCUSSION .....	132
5.4.1	Homogeneity of habitat and fauna .....	132
5.4.2	Alternative hypotheses for heterogeneous faunal distributions .....	134
	5.4.2.1 <i>Influence of physical processes on settlement of fauna</i> .....	134
	5.4.2.2 <i>Mechanisms by which resident fauna influence settlement and survival of fauna</i> .....	135
	5.4.2.2.1 <i>Effects of megafaunal bioturbation on sediment reworking</i> .....	136
	5.4.2.2.2 <i>Effects of megafaunal bioturbation on sediment geochemistry</i> .....	136
	5.4.2.2.3 <i>Effects of resident macrofauna on megafaunal distribution</i> .....	138
	5.4.2.2.4 <i>Interaction between megafaunal and macrofaunal assemblage structure</i> .....	138
5.4.3	Legitimacy of homogeneous habitat .....	140
5.4.4	Consideration of the sampling technique .....	140
5.5	CONCLUSIONS .....	143

<b>Chapter 6:</b>	<b>Population size structure and biomass of <i>Lutraria lutraria</i> in Jennycliff Bay .....</b>	<b>144</b>
	ABSTRACT .....	145
6.1	INTRODUCTION .....	146
6.2	MATERIALS AND METHODS .....	149
6.2.1	Survey location and design .....	149
6.2.2	Data extraction .....	149
6.2.3	Data analysis .....	152
6.3	RESULTS .....	154
6.3.1	Body size distribution of the <i>Lutraria lutraria</i> population .....	154
6.3.2	Estimates of <i>Lutraria lutraria</i> biomass and respiration .....	156
6.4	DISCUSSION .....	158
6.4.1	Contribution of <i>Lutraria lutraria</i> to endobenthic biomass .....	158
6.4.2	Sources of error in biomass estimation .....	161
6.4.3	Validity of estimating biomass from size–weight relationships .....	163
6.4.3.1	<i>Lutraria lutraria</i> biomass estimates .....	163
6.4.3.2	<i>Thalassinidean mud shrimp</i> biomass estimates .....	164
6.4.4	Interpretation of size–frequency histograms .....	165
6.4.4.1	Temporal stability of size–frequency histograms .....	165
6.4.4.2	Detection of population recruitment .....	166
6.4.4.3	Between-year difference in population abundance .....	166
6.4.5	Modelling energy flux through ecosystems .....	167
6.4.6	Suggestions for sampling endobenthic biomass and respiration .....	168
6.5	CONCLUSION .....	169
 <b>Chapter 7:</b>	 <b>General discussion and conclusions .....</b>	 <b>170</b>
7.1	INTRODUCTION .....	171
7.2	ADVANCES IN REMOTE IMAGING TECHNIQUES .....	171
7.3	MEGAFUNAL ASSEMBLAGE STRUCTURE AND FUNCTION .....	173
7.3.1	Spatial pattern of the megafaunal assemblage .....	173
7.3.2	The role of megafauna in ecosystem function .....	174
7.4	IMPLICATIONS FOR QUANTIFYING SPATIAL STRUCTURE IN BENTHIC ASSEMBLAGES .....	176
7.5	CONCLUSIONS .....	177
 <b>References:</b>	 .....	 <b>179</b>
 <b>Appendix I:</b>	 <b>Description of megafaunal features .....</b>	 <b>201</b>
<b>Appendix II:</b>	<b>Raw abundance data .....</b>	<b>204</b>
<b>Appendix III:</b>	<b>Image scale information .....</b>	<b>224</b>
<b>Appendix IV:</b>	<b>Sample images .....</b>	<b>227</b>

## List of Tables

<b>Table 1.1</b>	Maximum depth of burrows constructed by megafaunal bioturbating species .....	20
<b>Table 1.2</b>	The relative merits of underwater camera deployment methods .....	31
<b>Table 4.1</b>	Mean abundance estimates of biotic features derived from direct diver and remotely operated vehicle observations of Loch Creran survey plots .....	86
<b>Table 4.2</b>	Bias between abundance estimates derived from diver and ROV observations of Loch Creran survey plots .....	87
<b>Table 4.3</b>	Abundance estimates of biotic features counted during diver and ROV observations of the Jennycliff Bay survey plot .....	92
<b>Table 4.4</b>	Mean bias ( $\pm 95\%$ CI) between diver and ROV estimates of features contained in Jennycliff Bay grid cells of $0.25\text{m}^2$ .....	93
<b>Table 5.1</b>	Spearman's rank correlation coefficients to investigate spatial structure in the megafaunal assemblage .....	118
<b>Table 5.2</b>	Two-way crossed ANOSIM to test for differences between the megafaunal assemblages ..	123
<b>Table 5.3</b>	R-values from pairwise comparison of stations using 1-way ANOSIM .....	125
<b>Table 5.4</b>	Contribution of discriminating species to between-station dissimilarity .....	126
<b>Table 5.5</b>	Two-way crossed ANOVA comparing the abundance of discriminating species between stations .....	127
<b>Table 5.6</b>	Between-station differences in the abundance of discriminating species .....	128
<b>Table 6.1</b>	Equivalent shell length and AFDW values corresponding to siphon width groups for <i>Lutraria lutraria</i> .....	155
<b>Table 6.2</b>	Two-way crossed ANOVA test comparing estimates of <i>Lutraria lutraria</i> biomass .....	156
<b>Table 6.3</b>	Gross <i>Lutraria lutraria</i> biomass and oxygen consumption estimates in Jennycliff Bay ...	156
<b>Table 6.4</b>	Relative contribution of <i>Lutraria lutraria</i> to endobenthic biomass in Jennycliff Bay .....	159
<b>Table 6.5</b>	Biomass partitioning in Northumberland, Kiel Bay, Helgoland Bight and Barents Sea ....	160
<b>Table 6.6</b>	Effect of biomass estimate artefacts on partitioning of biomass in Jennycliff Bay .....	163



## List of Figures

Figure 1.1	Schematic representation of diversity–ecosystem function models .....	6
Figure 1.2	Schematic depicting the limitations imposed by water currents on the depth and spatial extent of remotely operated vehicle (ROV) deployments .....	30
Figure 2.1	The Deep Ocean Engineering Phantom XTL remotely operated vehicle .....	34
Figure 2.2	Schematic diagram of the hardware configuration for deployment of the ROV .....	35
Figure 2.3	The structured lighting array mounted on the camera of the Phantom XTL .....	44
Figure 2.4	Schematic of the behaviour of the parallel laser spot pattern .....	45
Figure 2.5	Schematic diagram for derivation of camera inclination angle ( $\phi$ ) and camera–object distance .....	46
Figure 2.6	Schematic diagram of the geometry required to calculate the absolute scale within the vertical axis of a perspective image .....	49
Figure 2.7	<i>Benthic Imager</i> screenshot showing the 5-spot laser pattern around a burrow of the angular crab, <i>Goneplax rhomboides</i> .....	50
Figure 2.8	Laser alignment setup .....	55
Figure 2.9	Plan view of the laser array indicating the parameters required to calibrate the camera–object distance calculations in <i>Benthic Imager</i> software .....	57
Figure 2.10	The effect of changing camera backset correction on the accuracy of measurements in <i>Benthic Imager</i> software .....	59
Figure 2.11	Schematic plan view of the influence of current direction on vehicle navigation if using the compass heading only .....	61
Figure 2.12	Schematic representation of a Sonardyne International Ltd. long baseline seabed transponder beacon array .....	64
Figure 2.13	Schematic representation of a short baseline (SBL) and ultra short baseline (USBL) acoustic positioning system .....	65
Figure 2.14	Schematic representation of the Universal Transverse Mercator projection .....	66
Figure 2.15	Screenshot from the <i>PharosLite</i> navigation display .....	67
Figure 3.1	Location of sites for megafaunal assemblage investigations in the United Kingdom .....	70
Figure 3.2	Location of Jennycliff Bay, Plymouth Sound .....	72
Figure 3.3	Location of Loch Creran, western Scotland .....	77
Figure 4.1	Bland and Altman plot of difference against mean for total biotic features in Loch Creran survey plots .....	88
Figure 4.2	Bland and Altman plot of difference against mean for large conspicuous features in Loch Creran survey plots .....	90
Figure 4.3	Bland and Altman plot of difference against mean for features greater than 15 mm diameter in Loch Creran survey plots .....	91
Figure 4.4	Bland and Altman plot of difference against mean for total biotic features in the Jennycliff Bay survey plot .....	94
Figure 5.1	Location of 0.5 m <sup>2</sup> contiguous image stations .....	108
Figure 5.2	Construction of a sample distance matrix that represents distances between every pair of samples .....	113
Figure 5.3	Schematic representation for constructing ‘model’ distance matrices from the between-sample Euclidean distance matrix .....	114
Figure 5.4	Rank-correlogram that would be obtained if biotic similarity and inter-sample distances were in a perfect series for each year .....	116
Figure 5.5	Rank-correlograms for spatial pattern in Jennycliff Bay during May 2000 and March 2001 .....	120
Figure 5.6	Multi-dimensional scaling (MDS) plots of megafaunal similarity between years .....	124
Figure 5.7	Mean abundance of dominant megafaunal features at each station .....	129
Figure 5.8	Rank correlograms for <i>Lutraria lutraria</i> and thalassinidean burrow openings .....	131
Figure 6.1	Size–frequency histogram of <i>Lutraria lutraria</i> in Jennycliff Bay .....	155
Figure 6.2	Mean <i>Lutraria lutraria</i> biomass per station in Jennycliff Bay .....	157

## **List of Acronyms**

ABISS	Automated Benthic Image Scaling System
AFDW	Ash-free Dry Weight
AGDS	Acoustic Ground Discrimination System
ANOSIM	Analysis of Similarities
ANOVA	Analysis of Variance
AUV	Autonomous Underwater Vehicle
CI	Confidence Interval
DGPS	Differential Global Positioning System
ERSEM	European Regional Seas Ecosystem Model
HSD	Honestly Significantly Different
LBL	Long Base Line
MDS	Multi-dimensional Scaling
PRIMER	Plymouth Routines in Multivariate Ecological Research
QTC	Qester Tangent Corporation
ROV	Remotely Operated Vehicle
SAC	Special Area of Conservation
SBL	Short Base Line
SCOC	Sediment Community Oxygen Consumption
SCUBA	Self-contained Underwater Breathing Apparatus
SIMPER	Similarity of Percentages
TMS	Tether management system
USBL	Ultra Short Base Line
UTM	Universal Transverse Mercator
VAC	Volts alternating current
VDC	Volts Direct Current
VHS	Video High Standard

## List of Symbols

Symbol	Parameter	Unit
$\phi$	Camera inclination angle	°
$\psi$	Perspective Ratio	dimensionless
$\lambda$	Wavelength	m
$\rho$	Spearman's correlation coefficient	dimensionless
$\pi$	Pi	dimensionless
$Q_{10}$	Coefficient of temperature on metabolism	dimensionless
$\tau_0$	Current shear stress	$\text{kg.m}^{-1}.\text{s}^{-2} = \text{Pa}$
$\tau_e$	Bed shear stress	$\text{kg.m}^{-1}.\text{s}^{-2} = \text{Pa}$
$C_D$	Drag coefficient	dimensionless
$\langle \bar{u} \rangle$	Depth mean averaged water current	$\text{m.s}^{-1}$
$h$	Water depth	m
$z_0$	Bed roughness of a flat substratum	m
$z_1$	Bed roughness of a complex substratum	m
$H$	Height of biogenic mounds	m
$S$	Cross-sectional area of biogenic mounds	$\text{m}^2$
$\xi$	Horizontal area of biogenic mounds	$\text{m}^2$
$\rho_w$	Density of seawater (=1033)	$\text{kg.m}^{-3}$
$\kappa$	Von Karman's constant (=0.4)	dimensionless
$\phi_w$	Wentworth Scale	dimensionless

## ACKNOWLEDGMENTS

This thesis is the culmination of an epic voyage of discovery, both personally and professionally, which could not have been achieved without significant assistance from a variety of sources. In the remainder of this page, I would like to extend my thanks to supervisors, colleagues, friends and family alike.

The Automated Benthic Image Scaling System was the brainchild of Derek Pilgrim and without his support during further development, quantitative megafaunal investigations would not have been possible. Malcolm Jones has been a constant source of encouragement, advice and editorial skills (plus a beer or two in Aberdeen!), for which I am forever in his debt. Mike Kendall has displayed a considerable dedication to duty throughout the entire PhD process, displayed most notably by reading a draft of Chapter 6 on his way to the operating theatre; no anaesthetic needed! Mike's knowledge, enthusiasm (especially near mud!) and guidance were a continual source of inspiration, for which I am truly grateful. In addition to formal supervision, I would like to thank Steve Widdicombe, Mel Austen, Paul Somerfield, Bob Clarke, Lois Nickell and Chris Smith for many fruitful discussions and encouragement.

The many hours of fieldwork passed without (major) incident, thanks to the expertise and good humour of the crews of the RVs Tamaris, Sepia, Catfish and Soel Mara, while Peter Holt and his team at Sonardyne International Ltd. ensured that we were positioned accurately. Mike Stringer did an excellent job building the laser array, while Peter Ganderton enabled simultaneous operation of the acoustic positioning system and the ABISS with his 'box of tricks'. Graham Carter and Steve Bennetts provided technical support, and Rob Wood supervised diving operations. Thanks guys!

I have been fortunate to have a great bunch of mates ever eager to share a beer, joke and even discuss the football. It would be impossible to thank all the past and present members of 'Team IMS' by name, but you know who you are. Friday nights in the JSV will live long in the (somewhat blurred) memory!! Thanks also to Si and Dave for believing that I've been studying 'Fighting Plankton' all these years.


The support and encouragement provided by Mum, Dad, Steve, Chris and Rachel will never be forgotten. The miles may be many, but you will never know how close you really were on this journey. Last, but by no means least, I would like to thank Helen for putting up with me (especially during the torment of writing-up) and making all the hard work worthwhile by accepting the dubious honour to become my wife.

## Author's Declaration

*At no time during the registration for the degree of Doctor of Philosophy has the author been registered for any other University Award*

This study was financed with the aid of a studentship from the Natural Environment Research Council (04/98/MS/233) and conducted in collaboration with the Plymouth Marine Laboratory.

Relevant scientific seminars and conferences were attended regularly at which work was often presented; external institutions were visited for analytical and consultation purposes, and papers prepared for publication.

Signed .....  .....  
Date ..... 19/12/2002 .....

## **Publications:**

- Parry, D.M.**, Nickell, L.A., Kendall, M.A., Burrows, M.T., Pilgrim, D.A., Jones, M.B. (2002). Comparison of abundance and spatial distribution of burrowing megafauna from diver and Remotely Operated Vehicle observations. *Marine Ecology Progress Series*, **244**, 89–93.
- Parry, D.M.**, Kendall, M.A., Pilgrim, D.A., Jones, M.B. (in press) Identification of patch structure within marine benthic landscapes using a Remotely Operated Vehicle. *Journal of Experimental Marine Biology and Ecology*, **285–286**. *Special Issue on In Situ Surveillance of the Sediment–Water Interface*
- Solan, M., Germano, J.D., Rhoads, D.C., Smith, C.J., Michaud, E., **Parry, D.M.**, Wenzhöfer, F., Kennedy, R., Henriques, C., Battle, E.J.V., Carey, D.A., Iocco, L., Valente, R.M., Watson, J., Rosenberg, R. (in press). Towards a greater understanding of pattern, scale and process in marine benthic systems: a picture is worth a thousand worms. *Journal of Experimental Marine Biology and Ecology*, **285–286**. *Special Issue on In Situ Surveillance of the Sediment–Water Interface*.
- Raffaelli, D., Bell, E., Weithoff, G., Matsumoto, A.K., Cruz-Motta, J.J., Jones, M.B., Kershaw, P., Parker, E.R., **Parry, D.M.**, (in press). The ups and downs of benthic ecology: considerations of scale, heterogeneity and surveillance for benthic-pelagic coupling. *Journal of Experimental Marine Biology and Ecology*, **285–286**. *Special Issue on In Situ Surveillance of the Sediment–Water Interface*.
- Pilgrim, D.A., **Parry, D.M.**, Jones, M.B., Kendall, M.A. (2000). ROV image scaling with laser spot patterns. *Underwater Technology*, **24(3)**, 93–103.
- Parry, D.M.**, Jones, M.B., Kendall, M.A., Pilgrim, D.A. (2000). Quantitative investigation of megafaunal distribution using Remotely Operated Vehicles. *Porcupine Marine Natural History Society Newsletter*, **5**, 44–45.

## **Conferences attended and work presented:**

### **Platform presentations:**

ECSA Marine Benthic Sampling Strategies and Survey Design Workshop, 24–28 May 1999. University Marine Biological Station, Millport. '*Visual Survey of Epibenthos and Hyperbenthos using a Remotely Operated Vehicle*'.

Porcupine Marine Natural History Society Annual Meeting, 17–19 March 2000. Plymouth Marine Laboratory, United Kingdom. '*Quantifying Megafaunal Spatial Distribution using a Remotely Operated Vehicle*'.

30<sup>th</sup> Benthic Ecology Meeting, 15–18 March 2001. University of New Hampshire, New Hampshire, United States of America. '*Quantitative spatial distribution patterns of bioturbating megafauna using a Remotely Operated Vehicle*'.

Benthic Dynamics: *in situ* surveillance of the sediment water interface, 25–29 March 2002. University of Aberdeen, United Kingdom. '*Identification of patch structure within marine benthic landscapes using a Remotely Operated Vehicle*'.

### **Poster presentations:**

Porcupine Marine Natural History Society Annual Meeting, 17–19 March 2000, Plymouth Marine Laboratory, United Kingdom. '*Image scaling aids identification of sediment structures observed by Remotely Operated Vehicles*'.

36<sup>th</sup> European Marine Biology Symposium, 17–22 September 2001. University of Barcelona, Menorca, Spain. '*Quantitative spatial and temporal distribution patterns of bioturbating megafauna using a Remotely Operated Vehicle*'.

### **External contacts:**

Mr P. Holt, Sonardyne International Limited, Plymouth Trials and Training Centre, Pier House, Turnchapel Marina, Turnchapel, Plymouth, Devon, PL9 9XB, United Kingdom.

Dr L.A. Nickell, Dunstaffnage Marine Laboratory, Oban, Argyle, Scotland, PA34 4AD, United Kingdom.

Dr M.T. Burrows, Dunstaffnage Marine Laboratory, Oban, Argyle, Scotland, PA34 4AD, United Kingdom.

# **CHAPTER 1**

## **General Introduction**



## 1.1 BACKGROUND TO ECOLOGICAL INVESTIGATION

Ecosystems encompass a hierarchy of biological complexity from individuals, populations, assemblages, habitats, landscapes to biogeographical provinces. Ecologists face a daunting task to study scientifically the interactions that determine the distribution and abundance of organisms (Krebs, 1972). Although there is no single correct level in ecosystem hierarchy to describe ecological patterns (Levin, 1992), methods for understanding and predicting relationships in ecosystems may be classified as either top-down or bottom-up. Top-down investigations suggest that only by observing patterns in assemblage structure may the distribution of individual species be appreciated. Conversely, the bottom-up approach requires an appreciation of how each species in the assemblage is distributed and the way it interacts with all other species before community patterns may be determined. In practice, understanding ecosystem dynamics is a multiphase process because patterns in assemblage structure result from both top-down and bottom-up processes operating simultaneously. However, the detection and description of pattern (i.e. top-down approach) is the necessary starting point from which hypotheses may be raised, and tested experimentally, to identify the processes that establish and maintain the patterns observed (Steele, 1985; Underwood et al., 2000).

At any particular level in the ecosystem hierarchy, the arrangement of organisms is typically non-random; species distribution patterns are heterogeneous both spatially and temporally. However, matching observed patterns to particular processes has proven difficult (Hewitt et al., 1996) because the boundary conditions that support a particular distribution pattern are set by processes operating at the next highest level, while the distribution pattern is generated by processes that operate at the next lowest level (O'Neill, 1989). Additionally, higher level processes operate generally at relatively low rates and might appear constant at smaller scales of observation, while lower level processes operate at relatively high rates and may appear as noise in large-scale observations (O'Neill, 1989).

On a global scale, for example, the general pattern of high diversity at tropical latitudes compared to temperate or polar latitudes (Sanders, 1968; Crame, 2000) is made possible because atmospheric conditions support life on earth, while processes correlated with latitude, such as temperature, seasonality and area, maintain the pattern. Similarly, at the landscape scale, abiotic processes set the characteristics of a habitat while biotic interactions influence faunal distributional patterns (Schneider, 1994). Investigation of faunal abundance over a range of spatial scales usually reveals mosaics of patches nested within patches that appear homogeneous at larger spatial scales (Thrush et al., 1989; Morrissey et al., 1992; Kendall and Widdicombe, 1999), which suggests that the dominance of different structuring processes changes with spatial scales. Therefore, when investigations are planned to elucidate the relationship between faunal distribution patterns and structuring processes, the scales of observation should be linked with that of the process in question (Kotliar and Weins, 1990).

The distribution and abundance of organisms may be investigated by quantifying diversity (the number of species present and the proportion of individuals of each species within a known area). In marine benthic ecology, diversity has been assessed traditionally for samples up to 0.25 m<sup>2</sup>, but the diversity of a point sample may be a property of the sample itself rather of the assemblage from which it has been collected. To quantify diversity of an assemblage, the spatial variability in the composition of species is required (beta diversity). Beta diversity measures the spatial variability in the composition of species (Gray, 2000), so may be used to detect patterns of faunal distribution from which structuring processes may be inferred.

The intrinsic and extrinsic value of marine biodiversity in ecosystem function (Bengtsson et al., 1997; Costanza et al., 1997; Gray, 1997) has provided the impetus for resource management protocols that aim to sustain, maintain or enhance biodiversity. Furthermore,

the United Kingdom has a legislative obligation to make inventories of, and monitor changes in, biodiversity and make plans to conserve biodiversity under the Convention on Biological Diversity, which was signed in 1992 and ratified by the United Kingdom in 1994 (United Nations Environment Program, 1992). The ability to describe and predict changes in ecosystems, however, requires quantitative sampling at spatial scales greater than currently practised (Peters, 1991; Thrush et al, 1997b; Constable, 1999).

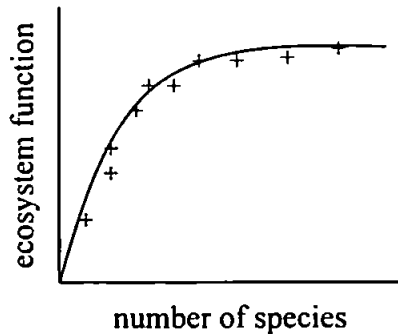
Traditionally, marine benthic ecology has considered the composition and spatial variability of meio- and macrofaunal-sized species that may be sampled adequately using grabs and cores. However, benthic assemblages also contain megafaunal-sized organisms, defined operationally as those species large enough to be visible in a photograph (Grassle et al., 1975), which are excluded currently from most studies through a lack of adequate sampling techniques. In recent years, the importance of megafaunal-sized species, particularly as ecosystem engineers, to the structure and function of benthic assemblages has been realised (Jones et al., 1994; Lawton, 1994). Ecosystem engineers are organisms that exert a greater influence on the structure and function of assemblages than their abundance alone would suggest by controlling the availability of resources to other organisms by altering the physical state of biotic and abiotic resources (Jones et al., 1997). In subtidal marine benthic habitats, megafaunal ecosystem engineers include epifaunal species such as crabs (Thrush, 1986) and fish (Summers, 1980), and infaunal species such as bivalves (Cummings et al., 1998), polychaetes (Woodin, 1978) and burrowing decapods (Posey et al., 1991). In addition to acting as ecosystem engineers, megafaunal species represent a large proportion of the benthic biomass and may, therefore, be an important route for energy flux between the benthos and the pelagial.

Traditional sampling techniques do not sample adequately the megafauna through a combination of insufficient sample unit size and their inability to sample deep-burrowing

organisms. Remotely operated vehicles (ROV) and other camera systems may offer a way forward to investigate the megafaunal fraction of marine benthic assemblages through non-destructive underwater observations of epibenthic megafaunal species and the characteristic surface openings produced by many of the burrowing megafauna. The concepts introduced thus far will be discussed in greater detail in the following Sections.

## 1.2 THE IMPORTANCE OF DIVERSITY

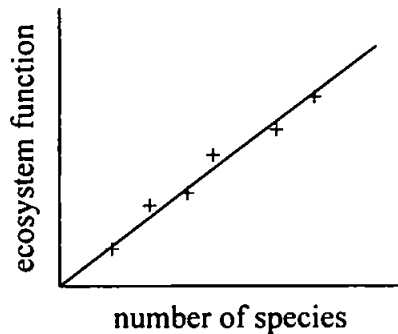
Diversity measures, the number of species and the proportion of individuals of each species present in a known area, allow quantitative investigation of the distribution and abundance of organisms within any particular level of the ecosystem hierarchy. Over the past decade, there has been a profusion of studies that investigate the role of diversity in ecosystem function (Loreau et al., 2001 and references therein) as there is growing concern that loss of diversity due to anthropogenic effects and global warming will result in the loss of ecosystem function and the goods and services that they provide to society (Costanza et al., 1997). While certain species that are exploited commercially for food and raw materials represent obvious ecosystem goods, most ecosystem functions, such as production, carbon flow and nutrient cycling, are shared amongst many of the other non-commercial species present (Duarte, 2000). Consequently, ecosystem services such as gas and climate regulation, erosion, sedimentation and waste treatment are also shared amongst the species present. Currently, the influence of biodiversity on ecosystem function is generally investigated experimentally to test whether key ecosystem functions are independent of the number of species in an assemblage, the results of which are compared with the Redundant Species, Rivet or Idiosyncratic Response Hypotheses (Lawton, 1994) (Fig. 1.1). At present, conclusive experiments that elucidate the relationship between biodiversity and ecosystem function remain elusive because of confounding factors related to the non-random selection of species in assemblages (Duarte, 2000), but there appears to be a positive relationship between species richness and ecosystem function (Tilman, 1997).



#### **Redundant Species Hypothesis:**

Few species are responsible for the majority of ecosystem functioning.

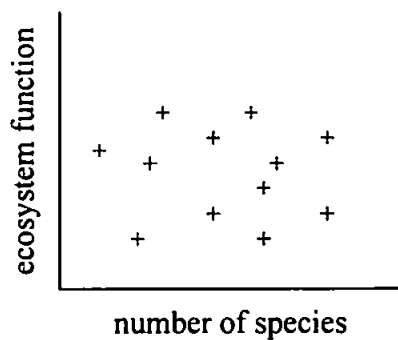
Additional species contribute little, and their removal will not affect significantly ecosystem functioning



#### **Rivet Hypothesis:**

All species make a significant contribution to ecosystem functioning.

Ecosystem function will decrease as more species are removed.



#### **Idiosyncratic Response Hypothesis:**

Ecosystem function is related to diversity, but the magnitude and direction of change is unpredictable because the roles of individual species are complex and varied.

Figure 1.1: Three hypothetical relationships between species richness and ecosystem function. The null hypothesis indicates that ecosystem function is insensitive to species addition or removal (Lawton, 1994).

### **1.2.1 Measurement of diversity**

In the simplest form, diversity is described by the number of different types of organisms co-existing in one place at the same time. It is not possible logistically to enumerate every individual of every species in an assemblage, so the number of organisms in a sample of that assemblage must be counted. Ideally, all species in a sample would be assessed, regardless of taxonomy and body size, but the size of sampler constrains both the species that may be sampled adequately and the way in which patterns of species distributions are perceived (Andrew and Mapstone, 1987). Therefore, all measures of diversity are linked inherently to scale and may be divided into three groups: alpha ( $\alpha$ ), beta ( $\beta$ ) and gamma ( $\gamma$ )

diversity. The precise definition of each group of diversity measures is the subject of much debate and controversy (e.g. Gray, 2000). Nevertheless, alpha( $\alpha$ )-diversity refers generally to diversity of a single sample and must be expressed as a function of sample size. Although there appears to be no method to define objectively the appropriate scale for measuring point diversity (Underwood, 1986), alpha( $\alpha$ )-diversity indices may be used to describe within-habitat diversity (Whittaker, 1960) by calculating the mean number of species ( $\pm$  confidence interval) in replicate samples collected over the area. Beta( $\beta$ )-diversity indices measure the degree of change in, or difference in composition among, samples from a survey (Whittaker, 1975). If the spatial extent of sampling is sufficiently large, beta( $\beta$ )-diversity measures indicate how organisms respond to gradients in environmental heterogeneity and are, therefore, measures of between-habitat diversity. Beta( $\beta$ )-diversity is dependent on the spatial arrangement and identity of species rather than a scale of diversity (as with alpha( $\alpha$ )-diversity), so may be termed more appropriately as turnover diversity (Clarke and Lidgard, 2000) and expressed in one of two ways: either as similarity between habitats or samples, or as the rate of species turnover between habitats or samples. In contrast, gamma( $\gamma$ )-diversity indices consider the number of species within a geographical region (Whittaker, 1960) and are analogous to an alpha( $\alpha$ )-diversity measure of a very large sample.

### **1.2.2 Problems of scale associated with measurement of diversity**

The detection and description of diversity and pattern within an assemblage should consider the size of sampler used and the distribution of samples within the survey location because any estimate of diversity is constrained by the characteristics of the sampler (Andrew and Mapstone, 1987; Wiens, 1989). To define sample strategy, the sample grain represents the size of an individual sample unit and the lag measures the distance between any pair of samples. Finally, the spatial extent represents the area within which all samples are contained (Wiens, 1989; Hewitt et al., 1996). In general, increasing sample grain size

will reduce variation between samples because a greater proportion of small-scale heterogeneity will be included within each sample, while variation may increase at larger spatial extent as more different habitats are sampled. Similarly, sample lag is related to the scale of distributional patterns that may be detected by a survey.

The inverse relationship between body size and population density (Peters and Wassenberg, 1983; Lawton, 1989; Blackburn et al., 1990) interacts with sample grain so that any sampler will underestimate the abundance of larger-bodied organisms or organisms that are dispersed on a scale greater than the sampler. In marine benthic ecology, the sample grain of traditional grabs and box-cores varies typically between 0.07–0.1 m<sup>2</sup>, which may be suitable for sampling meio- and macrofaunal-sized organisms (Holme and McIntyre, 1984). However, megafaunal-sized organisms are not sampled adequately by traditional grabs and cores (Thurston et al., 1994). As a result, community analyses of benthic assemblages, sampled by traditional techniques, underestimate the contribution of megafaunal-sized species to assemblage composition because few individuals are collected. To sample megafaunal organisms adequately, the sample grain may be increased, but the definition of the benthic assemblage will change because it becomes impractical to count small species as sample grain increases.

### **1.2.3 Detection of diversity on large spatial scales**

Detection of spatial pattern in benthic assemblages may provide the catalyst for inferring the structuring processes (Steele, 1985; O'Neill et al., 1991). Previously, such linkage has proven difficult because ecological patterns are a function of top-down and bottom-up processes operating simultaneously. Patterns in macrofaunal assemblage structure are used traditionally to assess the general processes that influence benthic diversity, but the scales at which organisms interact with the environment are usually a function of body size, feeding area and mode, and mobility (Addicot et al., 1987; Milne, 1992; Hewitt et al.,

1996). As a result, macrofaunal assemblage patterns may be maintained by small-scale processes, the influence of which cannot necessarily be scaled up to assess directly patterns in assemblage structure on larger spatial scales (Thrush et al., 1997b). To identify the processes that structure benthic assemblages at large spatial scales, information required by resource managers, techniques that detect pattern in fauna at larger scales are required.

#### **1.2.4 Rapid assessment of marine diversity**

To address issues of landscape, regional or global change, the influence of large-scale processes on ecological processes at local scales, and how the effects will vary from place to place, are required. To achieve high confidence in results, replication may be increased with an associated increase in effort. In contrast, to increase generality of results, the separation between samples may be increased. The balance between generality and confidence must be considered carefully, therefore, because excessive attention to confidence risks learning more and more about less and less, while increasing generality leads to learning less and less about more and more (Thrush et al., 1997b). Nevertheless, ecological management and conservation requires indicators of generality that may be applied with high confidence. In terrestrial ecology, rapid assessment techniques have been developed to provide general assessment of faunal distribution patterns with confidence, whereby the diversity of a subset of taxa may be used as a surrogate to estimate indirectly the diversity of whole assemblages (Oliver and Beattie, 1993; Gaston and Blackburn, 1995; Jones and Eggleton, 2000). Efforts to develop equivalent techniques in marine ecology lag behind their terrestrial counterparts, but identification of surrogates for marine and coastal biodiversity have become an important research area (Feral, 1999). On a regional scale, the composition of death assemblages offers a promising approach to rapid assessment of molluscan diversity (gamma [ $\gamma$ ]-diversity) (Kidwell, 2001; Warwick and Light, 2002), but questions remain as to how molluscan diversity relates to the total diversity of all groups in the region. At local scales, the composition of macrofaunal



assemblages may be assessed rapidly by reducing the taxonomic resolution of data analyses (Olsgard et al., 1998). To assess rapidly the variation in benthic diversity at larger scales (i.e. beta( $\beta$ )-diversity), however, those aspects of the seafloor habitat that are most related to diversity must be defined and/or investigated. Additionally, for benthic diversity surrogates to be effective rapid assessment techniques, it must be possible to quantify their spatial distribution over potentially large areas cost-effectively. Marine megafauna, and the biogenic sediment structures they produce, are an important component of benthic diversity and megafaunal distributional patterns may represent a convenient method to assess rapidly the diversity of benthic assemblages. The mechanisms by which they might influence macrofaunal assemblages will be addressed in the following Section.

### 1.3 EFFECT OF ECOSYSTEM ENGINEERS ON DIVERSITY AND ECOSYSTEM FUNCTION

Various species appear to exert a greater influence on the structure and function of assemblages than their abundance alone would suggest, so quantification of their distribution may act as a convenient technique to assess rapidly the composition of the entire assemblage. Of particular interest, is the role of physical ecosystem engineers, which are organisms that control the availability of resources to other organisms by altering the physical state of biotic and abiotic resources (Jones et al., 1997). Autogenic engineers, such as coral reefs, modify the environment via their own physical structures and remain part of the engineered environment, while allogenic engineers transform biotic/abiotic materials that are available to others and do not necessarily remain part of the engineered environment (Lawton, 1994). To predict the influence of physical ecosystem engineers on ecosystem processes and infaunal assemblage structure, it is important to identify the engineers that are present and which resources are being engineered (Jones et al., 1997), because species may respond to changes in resource availability in different ways. At local scales, autogenic engineers may be associated with increased species

richness as they provide habitats that would otherwise be unavailable. However, the response to allogenic ecosystem engineers will depend on the magnitude and types of changes that occur, the resources that are controlled, the number of species that depend on these resources and whether these resources are able to support persistence in the new habitat (Jones et al., 1997).

### **1.3.1 Mechanisms by which ecosystem engineers affect benthic ecosystem function**

In marine soft sediment environments, the physical characteristics of the sediment constitute an important resource that may influence the structure of associated assemblages and the flux of nutrients across the sediment–water interface (Gray, 1974; Rhoads, 1974; Snelgrove and Butman, 1994). At large (10s to 100s of kilometres) spatial scales, abiotic processes such as storm events (Rees et al., 1977; Posey et al., 1996) and demersal trawling (Schwinghamer et al., 1996; Kaiser et al., 1998; Thrush et al., 1998) may affect the composition of benthic assemblages through active removal of fauna and disturbance of sediment characteristics. In areas of low abiotic disturbance, however, the role of allogenic ecosystem engineers may be important in the creation and maintenance of diversity in otherwise homogeneous sediment habitats (Levin, 2000). Experimental evidence has shown that burrowing (bioturbation) and feeding by infaunal and epifaunal organisms may influence assemblage structure and nutrient flux across the sediment–water interface by altering sediment permeability, granulometry and stability (Suchanek, 1983; Hall, 1994; Widdicombe and Austen, 1998; Snelgrove et al., 2000); burrowing species act as allogenic ecosystem engineers (Jones et al., 1994). In the context of ecosystem function models (Fig. 1.1), assemblages that contain effective ecosystem engineering species may, therefore, conform to the Redundant Species Hypothesis (Lawton, 1994) as the engineer species are responsible for the majority of ecosystem function.

The scales of bioturbation may vary spatially and temporally as a function of both the mode of activity and mobility of the bioturbating species themselves. Feeding activity of epifaunal organisms, such as eagle rays (*Myliobatis tenuicaudatus* [Thrush et al., 1991], blue crabs (*Callinectes sapidus* [Blundon and Kennedy, 1982]) and flounder (*Platichthys flesus* [Summers, 1980]), may produce feeding pits several centimetres in diameter. Similarly, gray whales (*Eschrichtus robustus*) may produce pits or trenches several metres in diameter when feeding on benthic amphipods (Oliver and Slattery, 1985; Grebmeier and Harrison, 1992). Sediment disturbance by epifaunal feeding depends on the frequency of return to a particular piece of sediment and may be limited to the surface layers. In contrast, infaunal bioturbation and feeding may influence local sediment characteristics to greater depths and on a continuous basis, while the changes to sediment characteristics may be related to the type of burrowing activity.

Mobile infaunal organisms disturb sediment either by 'biological bulldozing' or by 'backfilling' as they move through the sediment fabric. Biological bulldozers displace sediment laterally as they move (e.g. *Cerastoderma edule* [Coffen-Smout and Rees, 1999]), while backfillers excavate sediment from the anterior end of the body, which is passed along the outside of the body and deposited behind the individual (Kanazawa, 1995) (heart urchin, *Brissopsis lyrifera* [DeRidder and Lawrence, 1982]). Nevertheless, mobile burrowers have been shown to reduce the abundance of surface deposit feeders, enabling the proportion of suspension feeders and subsurface deposit feeders to increase (Brenchley, 1981). In contrast, infaunal organisms that live in permanent burrows and tubes may, at least temporarily, increase sediment stability and alter granulometry during burrow construction and maintenance, which creates local patches of unstable ejected sediment that may smother animals with low mobility and inhibit larval settlement and/or recruitment (Meadows and Tait, 1989; Posey et al., 1991). Burrow-dwelling species may influence sediment granulometry further through the production of faecal pellets, which

may also enhance bioresuspension of sediment and organics into the water column (Graf and Rosenberg, 1997). In addition to the direct effects of bioturbation on sediment characteristics, surface openings and ejecta mounds alter the topography of the sediment surface, affecting water flow at the sediment–water interface (Eckman et al., 1981). The interaction between hydrography and biogenic sediment features, such as burrow openings and tubes, may enhance further biodeposition and bioresuspension of sediment, with the associated effects on nutrient fluxes and assemblage structure (Graf and Rosenberg, 1997).

Benthic assemblage structure has been investigated for different size fractions of the sediment infauna; meiofauna are retained on a 63  $\mu\text{m}$  mesh and macrofauna are retained on a 0.5 mm mesh (Holme and McIntyre, 1984). The limited body size of meio- and macrofaunal organisms suggests that the volume of sediment disturbed by each individual may be small, so macro- and meiofauna may engineer the ecosystem allogenicly for protozoans. In contrast, megafaunal bioturbating species, which are larger than meio- and macrofaunal species, may disturb larger volumes of sediment and, hence, have the potential to act as important allogenic ecosystem engineers for macrofauna, meiofauna and protozoans, particularly in habitats that experience weak abiotic sediment disturbance processes. For example, the megafaunal thalassinidean ghost shrimp *Callianassa subterranea* may expel 1–2  $\text{cm}^3$  of sediment from the burrow every hour (Stamhuis et al., 1987, Rowden and Jones, 1993), equivalent to transporting a 75 cm thick layer of sediment to the surface each year (Rhoads, 1974). The most effective form of bioturbation appears to be ‘biological bulldozing’ (Thayer, 1983; Hall, 1994), but different elements of infaunal assemblages respond independently to different bioturbating mechanisms, suggesting that both the intensity and identity of bioturbating species will affect assemblage structure and nutrient flux rates (Widdicombe and Austen, 1999). The distribution of megafaunal ecosystem engineers, and the habitat characteristics they produce might, therefore,

represent a viable surrogate for rapid assessment of macrofaunal diversity (Thrush et al., 2001).

## 1.4 PATCH STRUCTURE OF BENTHIC ECOSYSTEMS

### 1.4.1 Role of disturbance in maintenance of patch structure

Several 'non-equilibrium' hypotheses have been raised to predict the role of disturbance in the creation and maintenance of diversity in marine soft sediment habitats. The Intermediate Disturbance Hypothesis proposes that the intensity and frequency of disturbance are key elements in setting and maintaining diversity (Connell, 1978); maximum species diversity occurs at an intermediate level of disturbance where competitive exclusion to a limiting resource is reduced, allowing co-existence of potentially competing species. The Intermediate Disturbance Hypothesis and variations thereon (e.g. Dynamic Equilibrium Model that includes the effects of organic enrichment [Huston, 1979]) predict that diversity depends on a disturbance regime that acts homogeneously over the habitat or assemblage under observation. Considering ecosystems as a hierarchy of structural complexity, however, disturbance from bioturbation may occur randomly both spatially and temporally at scales within habitats or assemblages.

To understand how the predictions of non-equilibrium hypotheses may be manifested within habitat-sized areas, disturbance processes should be considered within a spatial/temporal framework. The concept of patch dynamics provides such a framework, within which the size, frequency and intensity of disturbance is considered together with recolonisation of patches (succession), temporal change within patches and the relation of patches to each other (Pickett and Thompson, 1978; White and Pickett, 1985; Reise, 1991). The way in which disturbance processes act upon the seabed may be visualised within the Spatio-temporal Mosaic Model (Grassle and Morse-Porteous, 1987), which considers the seabed as a mosaic of assemblages at different stages of recovery from physical

disturbance processes that operate at a range of scales and frequencies. At any location in the mosaic, the composition of the associated assemblage would depend on the area disturbed, intensity of the initial disturbance and the time since the disturbance ceased. Hence, the species richness of a large area depends on the average state of succession of all the patches within the mosaic (Grassle and Morse-Porteous, 1987).

In the Spatio-temporal Mosaic Model (Grassle and Morse-Porteous, 1987), disturbance was a discrete event that removed all organisms from the affected area, but bioturbating megafauna do not influence macrofauna in this way. Megafaunal bioturbation is a more continuous sub-lethal process in the vicinity of megafaunal individuals themselves that affects species differentially and is reflected in the composition of associated assemblages (Section 1.3.1). Within an assemblage, the spatial distribution of megafaunal, macrofaunal and meiofaunal species may be aggregated at a variety of spatial scales, each of which may be considered as patches of bioturbatory activity. At the largest scale, patches may be defined on the presence or absence of a particular megafaunal species. Within bioturbated habitats, however, the distribution of megafaunal individuals will seldom be uniform throughout the habitat, so areas of different bioturbating intensity will exist (Thrush et al., 1997a). At the smallest scale, megafaunal individuals will create patches of bioturbated sediment around them with patches of less bioturbated sediment separating them from conspecifics, which will be particularly evident for territorial species. The different scales of aggregation for individual megafaunal species may be evident for all megafaunal species in an assemblage, which will interact to produce a hierarchy of nested patches that contribute to landscape heterogeneity (Reise, 1991; Hall et al., 1992).

#### **1.4.2 Landscape approach to quantifying megafaunal distribution**

The mechanisms by which some megafaunal ecosystem engineers affect ecosystem processes, assemblage structure and energy-flux across the sediment–water interface have

been determined through experimental and *in situ* manipulation of benthic assemblages (e.g. Branch and Pringle, 1987; Gilbert et al., 1998; Widdicombe and Austen, 1998). In general, the maximum spatial extent of experimental plots may be 10s of metres, yet there is a growing need to quantify megafaunal distribution patterns at larger spatial scales to improve the ability to describe and predict changes in ecosystems (Peters, 1991; Thrush et al., 1997b; Constable, 1999).

Landscape ecology originated in terrestrial ecology as a top-down approach to understanding ecosystem dynamics, where all landscapes are considered as a mosaic of landscape units that may be repeated at intervals over space within a background matrix (Turner et al., 1989; Forman, 1995; Kent et al., 1997). In common with the ecosystem hierarchy, landscape units may occur at any level of organisation (Forman, 1995). Hence, the stability of a particular landscape unit, such as a habitat patch, may be affected by processes operating in encompassing landscape units at the next highest level, between nearby units at the same level, and in component units at the next lowest level. The focus of landscape ecology on patterns and processes suggests that a similar approach may be applied to understand marine ecosystem dynamics and predict the consequences of change.

In terrestrial landscape ecology, habitat patches are defined usually on the basis of vegetation type and/or anthropogenic structures, whereby, the background matrix may be woodland, while woods, fields and housing estates represent conspicuous patches that may be linked by corridors such as hedgerows, rivers and roads (Forman, 1995). In marine benthic landscapes, the background matrix may be either rock or sediment substrata, in which habitat patches may be defined using different types of macroalgae (Dayton, 1992) or seagrass (Irlandi, 1994; Robbins and Bell, 1994). To apply a landscape ecology approach to unvegetated sediment substrata, however, requires habitat patches being

defined on the basis of the physical characteristics of the sediment rather than biological structures (Zajac, 1999).

It has long been recognised that benthic macrofaunal communities are related to the physical characteristics of substrata (Petersen, 1913; Jones, 1950; Gray, 1974), which reflect patterns of tidal stress, grain size and availability of sediment (Warwick and Uncles, 1980). The physical characteristics of the seabed may be mapped on a landscape scale using acoustic imaging techniques such as side-scan sonar, a system which ensonifies a swathe of seabed either side of the research vessel and produces maps of acoustic reflectance of the seabed (Warwick and Davies, 1977). In the past decade, acoustic ground discrimination systems (AGDS) have been developed to classify the type of substratum from the characteristics of acoustic signals reflected from the seabed. The first commercially-available AGDS was RoxAnn™ (Stenmar Micro Systems Ltd., Aberdeen, Scotland) which measures the strength of the first and second reflections of the signal from a standard echo-sounder to estimate the roughness (E1) and hardness (E2) of the seabed respectively (Chivers et al., 1990). Acoustically-distinct areas of seabed may be defined on the grouping of E1 and E2, and converted to maps of different sediment types after the E1 and E2 groupings have been calibrated for known sediment types in the region under investigation.

A variety of AGDSs has been developed subsequently, including QTC View™ (Quester Tangent Corporation, Vancouver Island, Canada). In contrast to RoxAnn™, QTC View™ uses a thorough analysis of the E1 signal only, from which a series of algorithms produces 166 acoustic feature descriptors. The most useful acoustic feature descriptors are identified by principal components analysis (PCA), which are expressed as three 'Q' values, the combination of which are compared to acoustic signatures to infer sediment type (Collins et al., 1996; Preston and Collins, 1999). Both RoxAnn™ and QTC View™



give a continuous classification of seabed directly below the acoustic beam (Greenstreet et al., 1997; Morrison et al., 2001), so sediment maps are produced by interpolation between data points. Acoustic ground discrimination by RoxAnn™ and QTC View™ provides valuable information on the distribution of different sediment types at landscape scales, despite different approaches to seabed classification (Hamilton et al., 1999), and may be used to infer the general composition of the associated faunal assemblages. However, patterns of sediment grain size distribution are formed ultimately by hydrodynamic and geotechnical processes (Buller and McManus, 1979), so acoustic imaging techniques identify the boundary conditions within which faunal assemblages occur rather than provide information on the variability within the assemblages themselves.

The activity of bioturbating organisms may influence sediment granulometry and porosity, each of which affects the acoustic reflectance of soft sediments. Acoustic imaging techniques may, therefore, offer a way forward to quantify the spatial distribution of bioturbating activity within habitat patches (Magorrian et al., 1995; Briggs and Richardson, 1997). A RoxAnn™ survey in the Greater Minch appeared to support such an approach by suggesting that *Nephrops norvegicus* burrow density explained 95% of the variability of the E1 signal from a RoxAnn™ survey (Pinn and Robertson, 1998). The strong relationship between E1 and burrow density was lost, however, following subsequent deployments at different locations (Pinn and Robertson, 2001), indicating that acoustic imaging is limited to detecting landscape scale patterns of sediment granulometry rather than variation in burrow density. Consequently, alternative methods for quantifying the abundance and distribution of megafaunal organisms, both epifaunal and infaunal, at intermediate spatial scales are required.

## 1.5 SAMPLING THE MEGAFUNA

The previous Sections indicate that the activity of large bioturbating fauna is important in structuring soft-sediment communities and that these organisms are a poorly understood component of energy-flux models. In addition, there is a growing requirement to assess the defining characteristics of habitats, and the dynamics of those habitats to bridge the gap between local deterministic studies and observations of broad-scale patterns. In the following Sections, methods for sampling the megafauna will be discussed in terms of sample grain (the size of an individual sample unit), survey extent (the area within which all samples are contained) and sample lag (the inter-sample distance) (Wiens, 1989; Hewitt et al., 1996).

### 1.5.1 Grabs, Cores, Trawls and Dredges

Traditional methods for describing and monitoring subtidal soft-sediment communities usually involve collection of samples using grabs, box-corers, benthic trawls or dredges. The dimensions of the grab or core determine the sample grain, while that of trawls and dredges may be calculated by multiplying the width of the trawl/dredge opening by the distance for which they were towed. However, 'blind' deployment of these samplers precludes the accurate calculation of sample lag. Any sampler will underestimate the abundance of organisms that are dispersed on a scale greater than the dimensions of the sampler. Similarly, the inverse relationship between body size and population density (Peters and Wassenberg, 1983; Lawton, 1989; Blackburn et al., 1990) interacts with sample grain so that any sampler will underestimate the abundance of larger-bodied organisms. Given the relationship between body size and scale of dispersion, grabs and box-corers with a typical sample grain of 0.07–0.1m<sup>2</sup> may be suitable for sampling meio- and macrofaunal-sized organisms (Holme and McIntyre, 1984), but will not sample adequately megafaunal-sized organisms (Thurston et al., 1994). Trawls and dredges may be more appropriate for sampling epifaunal and shallow-burying megafaunal organisms

because the sample grain is greater than for grabs and box-corers (hundreds to thousands of square metres); thus the relationship between body size and sample grain should not be as strong. However, each trawl or dredge must be considered as a single sample, so important information on spatial heterogeneity will be lost by integration of the sample.

Table 1.1: Maximum depth of burrows constructed by megafaunal bioturbating species.

Megafaunal Species	Maximum depth (cm)	Reference
Thalassinidean crustacean		
<i>Axius serratus</i>	300	Pemberton et al. (1976)
<i>Callichurus laureae</i>	200	de Vaugelas and Buscail (1990)
<i>Upogebia deltaura</i>	68	Hall-Spencer and Atkinson (1999)
<i>Upogebia omissa</i>	86	Coelho et al. (2000)
<i>Callianassa subterranea</i>	65 ± 17	Nickell and Atkinson (1995)
<i>Calocaris macandarea</i>	22	Nash et al. (1984)
<i>Jaxea nocturna</i>	92	Nickell and Atkinson (1995)
Bivalve mollusc		
<i>Lutraria angustior</i>	40	Hall-Spencer and Atkinson (1999)
<i>Mya arenaria</i>	16–18	Zwarts and Wanink (1989)
	25	Blundon and Kennedy (1982)
<i>Mya truncata</i>	52	Hall-Spencer and Atkinson (1999)
<i>Ensis arcuatus</i>	32	Hall-Spencer and Atkinson (1999)
<i>Cerastoderma edule</i>	1–2	Zwarts and Wanink (1989)
<i>Macoma balthica</i>	5	Zwarts and Wanink (1989)
<i>Scrobicularia plana</i>	12	Zwarts and Wanink (1989)
Spatangoid echinoderm		
<i>Brissopsis lyrifera</i>	3	de Ridder and Lawrence (1982)
Echiuran worm		
<i>Maxmuelleria lankesteri</i>	80	Hughes et al. (1996)

In addition to the influence of the body size/sample grain relationship on estimates of megafaunal abundance, many burrowing megafaunal species bury beyond the reach of most traditional sampling equipment (Table 1.1). The depth of penetration into the seabed

by grabs and cores is a function of equipment weight, equipment velocity at impact with the seabed, deployment depth and the physical characteristics of the sediment being sampled, but maximum penetration rarely exceeds 50 cm. Consequently, the combination of large body size and deep burrowing lifestyle of many megafaunal species renders traditional equipment inappropriate for their sampling. Abundance and distributional patterns may, however, be investigated using quantitative observations of epibenthic megafauna (Thrush and Townsend, 1986), and of the characteristic surface openings and mounds associated with many of the burrowing megafaunal species. For example, thalassinidean shrimps produce characteristic burrow openings and mounds (Atkinson and Nash, 1985; Griffis and Suchanek, 1991) that may be used to infer abundance and identity (Rowden et al., 1998). Similarly, echinuran worms are identified and counted generally using observations of ejecta mounds and stellate surface traces produced by the proboscis (Hughes et al., 1993; Bett et al., 1995) as they are difficult to collect intact and retract rapidly into the sediment when approached (Hughes et al., 1996).

### **1.5.2 Observations by SCUBA Divers**

Observations by SCUBA (Self Contained Underwater Breathing Apparatus) divers have long been used to quantify the distribution of conspicuous epifaunal species (Suchanek, 1983; Thrush and Townsend, 1986) and, in combination with resin casting, have been used to characterise burrow morphology and surface openings associated with burrowing fauna (Suchanek and Colin, 1986; Atkinson and Nash, 1990; Nickell et al., 1995). However, quantification of megafaunal abundance and distribution using observations by SCUBA divers has been limited by the logistic and physiological constraints of dive depth and duration to shallow (<30 m) coastal habitats.

### 1.5.3 Underwater camera observations

Megafaunal abundance and distribution data that are comparable to that derived from diver observations may be collected from images from underwater cameras, which are not subject to the same constraints of deployment depth and duration as divers. Consequently, camera observations may be used to quantify the abundance and distribution of conspicuous megafauna, and the characteristic sediment structures associated with many burrowing megafaunal species, in habitats not accessible to SCUBA divers. In addition to extending the conditions under which data may be collected, cameras provide a permanent record of observations, which may be analysed further by other scientists.

The sample grain of all photographic investigations is determined by the orientation of the camera and camera-object distance associated with the way in which the camera is mounted on its frame. For photographic surveys, sample lag depends on the number of images that may be captured on the film and is a function of the velocity of the camera relative to the substratum. In contrast, video cameras provide continuous observations, so selecting a contiguous series of overlapping images may control sample grain, while sample lag may be varied to increase or decrease the spatial resolution of investigations.

Underwater cameras may be deployed and controlled in a number of ways depending on the accessibility and spatial extent of the survey location, and the budget available. To obtain quantitative data from any underwater image, however, the area of seabed contained within each image must be calculated, so that a constant sample grain may be defined. The absolute area contained within any image is a function of the distance between the camera and the object, the orientation of the camera with respect to the object (i.e. camera inclination angle) and the acceptance angle of the lens (Wakefield and Genin, 1987). Additionally, the orientation of the camera affects the resolution of observations; image resolution (Section 2.3.3.2) decreases as camera-object distance increases. In the majority

of underwater camera deployments, camera–object distance and inclination angle are maintained by mounting the camera within a frame supported by the substratum when images are collected. Underwater cameras may be deployed also in such a way that no part of the camera or mounting frame makes contact with the seabed; hence, camera–object distance and inclination angle may be variable and unknown, which requires alternative techniques to quantify image scale. The different methods of camera deployment, and the circumstances in which they may be deployed, will be introduced in the following Sections, while the methods of calculating image scale will be addressed fully elsewhere (Chapter 2).

#### **1.5.4 Camera deployment methods that maintain contact with the substratum**

##### **1.5.4.1 Manual deployment by SCUBA divers**

Underwater cameras, both photographic and videographic, may be deployed and operated by SCUBA divers, enhancing direct observational data by providing a permanent record of the underwater scene. Camera–object distance may be maintained by attaching a pair of rods of known length to the camera housing but, to maintain camera inclination angle, a camera frame is required (Lundälv, 1971, 1976). Diver-operated cameras are used most commonly for monitoring temporal change at fixed locations, where a single image or a series of overlapping images may be collected (Hiscock, 1987). Physiological processes associated with the depth and duration of dives restricts the survey extent, while diver-deployed cameras are restricted to shallow (<30 m) coastal habitats.

##### **1.5.4.2 Drop-down camera deployment**

To investigate spatial variation in abundance of conspicuous flora and fauna beyond depths reached by divers, underwater cameras may be deployed on a frame that is lowered to the seabed using a warp from a surface vessel (i.e. drop-down camera deployment). The location of images may be controlled from the surface by raising and lowering the camera

on the tether to make contact with the substratum. To ensure that images are collected at a standard camera-object distance, photographic cameras may be controlled by a switch mounted on the frame that is activated on contact with the substratum (Vevers, 1951). Alternatively, a forerunner weight that hangs a set distance below the camera may be attached to the shutter release; the camera is activated by the release of tension as the weight makes contact with the seabed (Piepenburg and Schmid, 1997; Lamont and Gage, 1998). The spatial extent of drop-down camera surveys may be considerable because a series of images may be collected by 'bouncing' the frame (or trigger weight) along the substratum as the vessel drifts or is underway at slow speeds. In many ways, drop-down photography is analogous to grab and core sampling of the sediment-water interface, and cameras may be attached to grab and box-core equipment to target sampling towards particular substrata (Mortensen et al., 2000) and place infaunal samples in context with the local sediment habitat (Collie et al., 2000). Disadvantages of drop-down cameras are introduced by the impact of the camera frame (or grab/core) on soft sediment, causing sediment resuspension that obscures the seabed. As with grabs and cores, 'blind' deployment precludes calculation of sample lag as the exact location of the camera on the seabed, either in real or relative co-ordinates, is usually unknown (Patterson, 1984; Barthel et al., 1991).

#### 1.5.4.3 Sledge- and Trawl-mounted Cameras

In addition to their deployment on grabs and cores, cameras may be attached to trawl equipment (Rice et al., 1982). In this configuration, cameras enhance trawl sampling by providing an indication of the spatial heterogeneity of the benthos within each sample. However, underwater cameras are often mounted on sledges that do not physically collect the epifaunal species encountered (Machan and Fedra, 1975; Holme and Barrett, 1977). In recent years, towed underwater camera systems have been deployed on positively buoyant frames weighed down by chains that drag across the seabed, hence camera-object distance

is maintained when neutral buoyancy is reached (Barker et al., 1999; Bax et al., 1999). In common with drop-down deployment, the spatial extent of sledge-mounted surveys may be considerable because the equipment is towed while the vessel is underway, the distance travelled being measured by an odometer wheel in contact with the seabed. Towed camera surveys may use either photographic cameras, activated at pre-determined frequency, or video cameras that record a continuous stream of images. Consequently, photographic surveys provide images with constant sample grain where sample lag is related to the velocity of the sledge over the seabed. In contrast, the sample grain of video surveys may be manipulated after deployment by considering series of contiguous images. Nevertheless, sample lag is related to the velocity of the sledge over the seabed.

Sledge-mounted video surveys have been particularly successful in surveying large conspicuous fauna such as scallops (Franklin et al., 1980) and *Nephrops norvegicus* fishing grounds where the characteristic burrows are counted (Chapman, 1979; Hensley, 1996; Tuck et al., 1997). However, the main disadvantage with sledge-mounted cameras is sediment resuspension as the sledge tracks drag across soft substrata. The minimum speed at which sledges are towed across the substratum is difficult to control accurately from the surface vessel, but a speed of approximately 1 knot is common. However, faster towing speeds are often required to 'out-run' the clouds of resuspended sediment (Hughes and Atkinson, 1997). Although the survey extent per unit time will be broadened by increased sledge velocity in relation to the seabed, the resultant images become blurred, reducing the ability to identify and count organisms or burrows encountered.

#### 1.5.4.4 Time-lapse deployment

In time-lapse deployment, the camera is mounted on a fixed frame that is not connected physically to the surface; a benthic lander. Time-lapse photographs are generally collected from single landers deployed on temporal scales approaching one year (Gardner et al.,



1984) to investigate temporal variation in local processes such as rates of organic input (Lampitt et al., 1995) and activity of mobile megafauna (Smith et al., 1993). When deployed in isolation, the sample grain of time-lapse photographs, which may be a few square metres, is analogous to the spatial extent of the survey. Orienting the camera to look straight down at the seabed (i.e. perpendicular camera inclination) provides the minimum sample grain of time-lapse images, whilst oblique inclination angles increase sample grain and allow observation of regions of seabed undisturbed by the lander (Thorndike, 1959; Lampitt and Burnham, 1983). The sample grain (and spatial extent) of time-lapse photography may be increased indirectly by using bait to attract mobile fauna (Priede et al., 1994), but the absolute sample grain depends on dispersal of the bait odor and sensitivity of the fauna attracted to the bait. Consequently, baited time-lapse cameras are limited generally to quantifying temporal variation in local process in the same way as non-baited time-lapse cameras. However, plans for deployment of arrays of benthic landers equipped with time-lapse cameras are being developed to address the spatial component of temporal processes observed currently in the deep sea (Priede [Oceanlab, University of Aberdeen] pers. comm.).

### **1.5.5 Camera deployment methods where contact with the substratum is avoided**

#### **1.5.5.1 Manned scientific submersibles**

Manned submersibles, autonomous underwater vehicles that support a pilot and crew of one or two scientists, allow direct observation of biota in water depths well beyond the reach of SCUBA divers (Bowen and Walden, 1992). Although manned submersibles allow direct observations in the deep sea, organismal abundance is often over-estimated (Grassle et al., 1975), while observations through convex viewports, the optimum design for withstanding the immense pressures at depth, reduces the apparent size of objects (Caddy, 1973). Consequently, a variety of underwater cameras, both photographic and video, is attached to the outside of manned submersibles to collect consistent underwater

images. Although the pioneer manned submersible deployments maintained contact with the seabed to control the area of seabed contained within underwater images (Caddy, 1973; Grassle et al., 1975), the benefits of submersible manoeuvrability are restricted as similar data could be obtained using towed camera sledges for a fraction of the cost.

The maximum depth achieved currently by a manned scientific submersible is 6000 m (Deep Submersion Vehicle [DSV] Nautile, IFREMER), but the actual dive depth and duration is related directly to the length of time the batteries can supply sufficient power to operate the submersible. For example, the duration of a typical dive in DSV ALVIN is 7 hours, which corresponds to a maximum depth of 2050 m (Woods Hole Oceanographic Institution). However, approximately 4 hours of the total dive time may be assigned to descent and ascent to the operating depth; hence bottom time may be only three hours per dive. To maximise the time available for benthic observations, and utilise submersible manoeuvrability, manned submersibles are generally deployed to collect detailed data from specific locations, such as hydrothermal vents (Lutz et al., 1998) or whale carcasses (Smith et al., 1998), within a limited spatial extent. In essence, manned submersibles provide similar data to diver observations, but at greater depth and at significantly greater cost.

In all the camera deployment arrangements described thus far, cameras were mounted on a frame that maintained camera-object distance and inclination angle by physical contact with the substratum. In most manned submersible deployments, however, contact of the submersible with either the substratum or feature of interest may be undesirable due to the risk of damage to both the submersible and the object being studied. Consequently, the underwater cameras are mounted on pan and tilt mechanisms that permit control of camera orientation horizontally or vertically, a combination of which allow the camera to be pointed at the subject while the submersible hovers in the vicinity. The sample grain of

underwater images collected from manned submersibles may, therefore, be variable and unknown due to the lack of contact between submersible and substratum. To apply scale to underwater images, various techniques have been developed and tested. However, a novel approach to calculating image scale, the Automated Benthic Image Scaling System (ABISS), has been developed during the course of the current project. The specific details of the ABISS will be addressed in Chapter 2.

The deployment of manned submersibles is limited to a few large research institutions in the United States (Woods Hole Oceanographic Institution [DSV ALVIN] and Harbor Branch Oceanographic Institute [Johnson Sea-Link Submersibles I and II]), France (IFREMER [DSV NAUTILE]) and Russia (Shirshov Institute of Oceanology [DSV Mir I and II]) which have sufficient financial and logistical support. In addition, the survey extent of manned submersible observations is limited by the constraints of dive depth and duration. The development of unmanned submersibles would, therefore, allow comparable data to be collected over longer time scales and at greater depth, and increase the spatial extent of benthic observations.

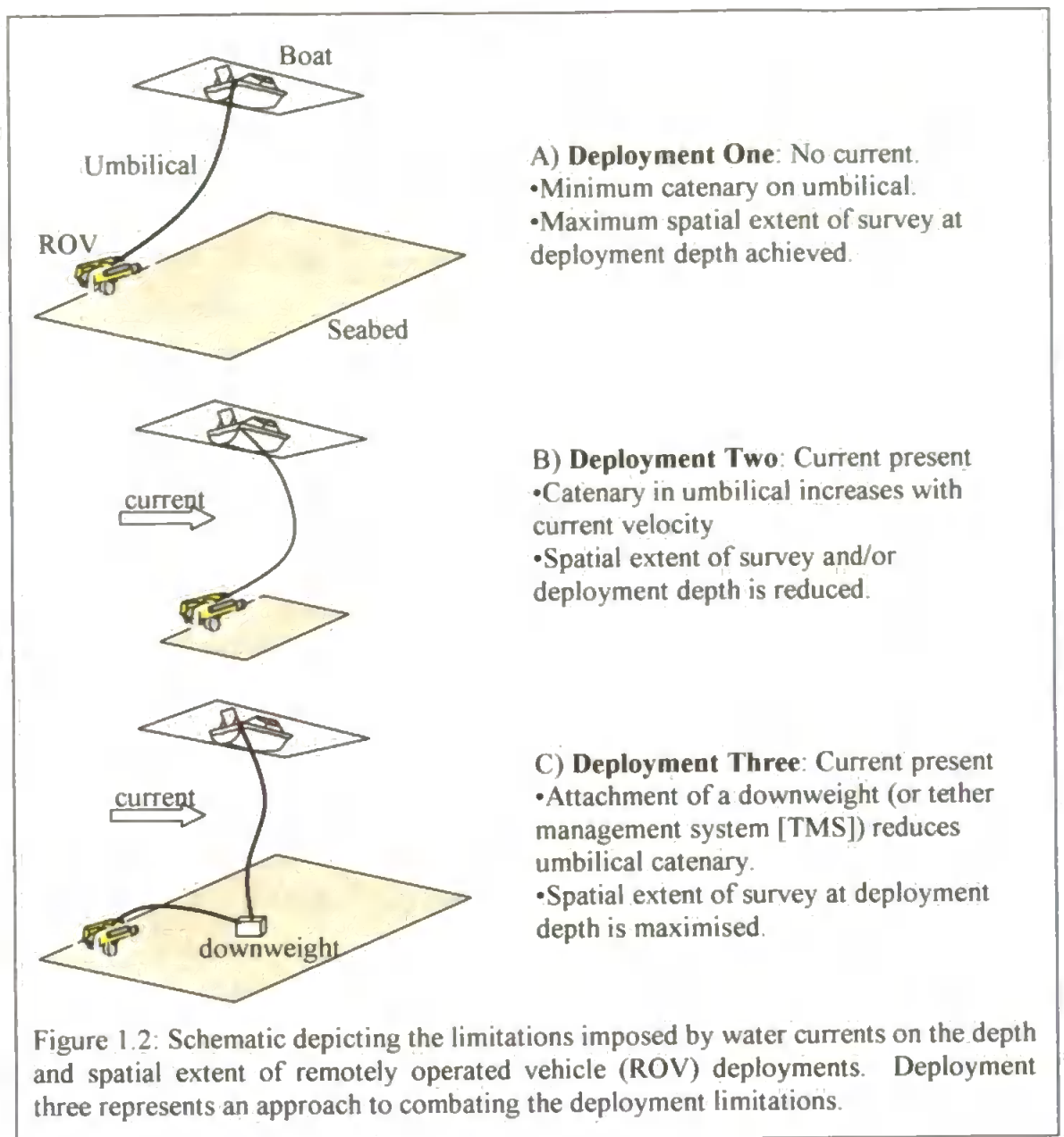
#### 1.5.5.2 Remotely Operated Vehicle

A remotely operated vehicle (ROV) is a tethered unmanned submersible linked to the surface by an umbilical cable through which power, control commands and observation data travel. The basic inspection ROV carries a video camera, auxiliary lighting and a compass, all of which provide information to a pilot who controls the vehicle in real-time by activating four or more independent thruster motors. Work-class ROVs are larger than the basic inspection ROV, with more powerful thruster motors that increase the amount of additional equipment that may be deployed. To operate the additional equipment in real-time, sufficient cables must be available within the umbilical, also increasing the weight and cost. Nevertheless, work-class ROVs have been deployed with manipulator arms

(Etchemendy and Davis, 1991), midwater sample boxes (Robison, 1992), sonar (Greene et al., 1991) and cores for limited sediment collection (Dawber and Powell, 1997). It is, however, the capability of ROVs to collect video images that have attracted their attention for most scientific investigations.

Remotely operated vehicles are suited particularly to working in topographically complex habitats, such as iceberg scour zones (Dawber and Powell, 1995; Hamada et al., 1986; Gutt et al., 1996) and marine canyon regions (Harrold et al., 1998), where the camera must be moved into position and intervention by an operator may be hazardous. Supply of power from the surface and lack of crew, however, lifts the constraints of dive depth and duration associated with manned submersibles, thus widening the circumstances under which ROVs may be deployed. Indeed, a Japanese ROV ('Kaiko') reached the bottom of Challenger Deep in the Marianas Trench which, at 10911.4 m, is the deepest place on the planet (Takagawa, 1995).

The length of umbilical limits the maximum depth, or survey extent, of an ROV deployment, which may be achieved in locations where no water currents flow. Drag on the umbilical increases with current velocity, however, imposing a catenary that reduces the effective depth, or spatial extent, that the vehicle may achieve (Fig. 1.2). Additionally, the ability to control and manoeuvre the ROV decreases as current velocity increases (Dowdeswell and Powell, 1996). Ideally, ROVs should be deployed in low current conditions, but a downweight may be attached to the umbilical to reduce the catenary in regions where current velocity is significant (Sprunk et al., 1992; Brodeur, 1998) (Fig. 1.2); thus, maximum depth or spatial extent may be approached.



Most inspection ROVs are designed to operate to a maximum depth of approximately 150 m, so the umbilical may be managed manually. To manage the additional length (and weight) of work-class ROV umbilicals, however, mechanical tether management systems (TMS) are necessary (Shepherd and Juniper, 1997). Although the depth and survey extent of ROV deployment may exceed that of manned submersibles, the ability to make fine resolution within-habitat observations is retained by control of the ROV from the surface (Hovland et al., 1998). Hence, ROV deployments offer the potential to make controlled non-destructive observations from small (Hardin et al., 1992), to intermediate spatial scales (Watters et al., 1995).

Table 1.2: The relative merits of underwater camera deployment methods. Each attribute is ranked in ascending order. 1 = lowest, 2 = intermediate, 3 = high, 4 = highest.

	Contact with substratum				No contact with substratum	
	Time-lapse	Diver-deployed	Drop-down	Sledge	Manned submersible	ROV
Control and navigation	1	3	2	2	3	3
Spatial extent	1	2	4	4	2	3
Depth	3	1	3	3	2	3
Cost (£)	1	1	1	1	3	2

The relative merits of the camera deployment techniques discussed in this chapter are summarised in Table 1.2. It is clear that remotely operated vehicles are most appropriate for controlled, non-destructive observation of benthic habitats at intermediate spatial extent, independent of water depth. For these reasons, the ROV is a valuable method of deploying underwater cameras and is becoming an increasingly valuable piece of equipment for the marine scientist.

## 1.6 AIMS AND THESIS STRUCTURE

The aims of this thesis were:

1. To develop sampling techniques to extract quantitative data from images collected by remotely operated vehicles.
2. To quantify the spatial and temporal distributional patterns within a marine megafaunal assemblage using observations from a remotely operated vehicle.
3. To estimate biomass of the dominant species within a marine megafaunal assemblage using observations from a remotely operated vehicle.

To achieve these aims, novel techniques to allow extraction of quantitative data from underwater images and to provide accurate spatial referencing to all images collected were developed. The design, calibration and operation of the Automated Benthic Image Scaling

System (ABISS), which calculates scale within underwater images and, hence sample grain, accounting for perspective, is discussed in Chapter 2. The basic principles and operation of an underwater acoustic positioning system (*PharosLite*), developed in collaboration with Sonardyne International Ltd., are also discussed in Chapter 2. Megafaunal distributional patterns were quantified at two locations in the United Kingdom: Jennycliff Bay in Plymouth Sound and Loch Creran on the west coast of Scotland, and details of the study sites are provided in Chapter 3. To assess the validity of megafaunal abundance data derived from remotely operated vehicle observations, agreement with abundance estimates derived from direct observation by SCUBA divers was investigated on a limited spatial extent (Chapter 4). To quantify spatial variation in megafaunal assemblages within habitats that might be considered homogeneous at a regional scale, the ROV was deployed within a patch of sediment, which was defined as homogeneous muddy sand using acoustic imaging techniques, on a spatial extent of 400 m (Chapter 5). To investigate the contribution of marine megafauna to the biomass of soft sediment assemblages, measurements of characteristic surface openings were used to derive the body size distribution of the infaunal bivalve, *Lutraria lutraria*, and produce gross estimates of biomass as an indicator of total megafaunal biomass (Chapter 6). The conclusions from Chapters 2–6 are synthesised and discussed in Chapter 7, allowing the quantification of marine megafaunal assemblage distributions using remotely operated vehicles to be assessed critically.

## **CHAPTER 2**

### **Development of techniques to quantify scale and spatially reference remote images**

Sections of this chapter are contained in:

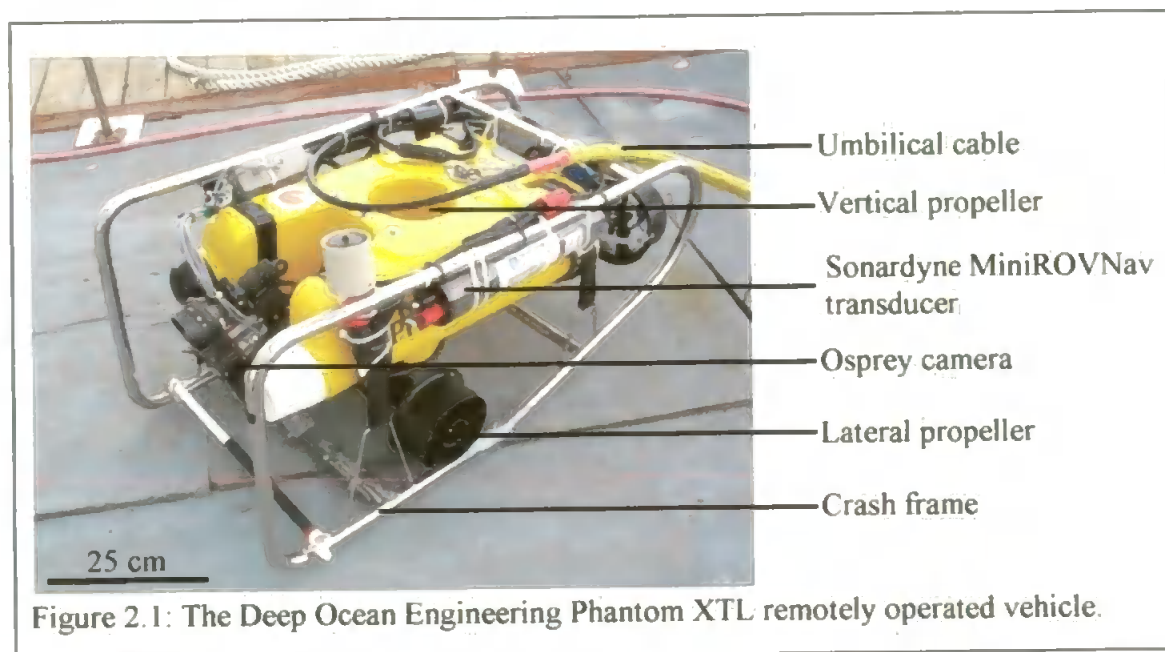
Pilgrim, D. A., Parry, D.M., Jones, M.B., Kendall, M.A. (2000). ROV image scaling with laser spot patterns. *Underwater Technology* **24**, 93–103.



## 2.1 EQUIPMENT DETAILS

### 2.1.1 Remotely Operated Vehicle specification

The remotely operated vehicle (ROV) used during the investigations presented in this thesis was a Phantom XTL (Deep Ocean Engineering, San Leandro, California) (Fig. 2.1).



This is a portable, low-cost (replacement value approximately £65,000) ROV designed for underwater inspection to depths of 150 m. The vehicle is operated from a surface console from which all control signals, telemetry and power supplies are passed to the vehicle via a 120 m umbilical cable that is neutrally buoyant. A schematic of the ROV hardware configuration is shown in Figure 2.2.

The ROV is fitted with an Osprey colour zoom camera (Kongsberg Simrad OE1366) with horizontal resolution of 450 TV lines, auto- and manual-focus, and auto-iris. The lens is water compensated with a focal length of 5.4–65 mm (capable of 12:1 magnification), such that the diagonal angle of view ranges from 55° (minimum zoom) to 5.3° (maximum zoom). The camera is mounted on a motorised tilt actuator controlled from the console, permitting observation  $\pm 90^\circ$  from horizontal. Illumination is provided by two 150 watt

tungsten-halogen lamps, one of which is mounted on the ROV hull to point forward and the other on the motorised tilt actuator to illuminate the field of view.

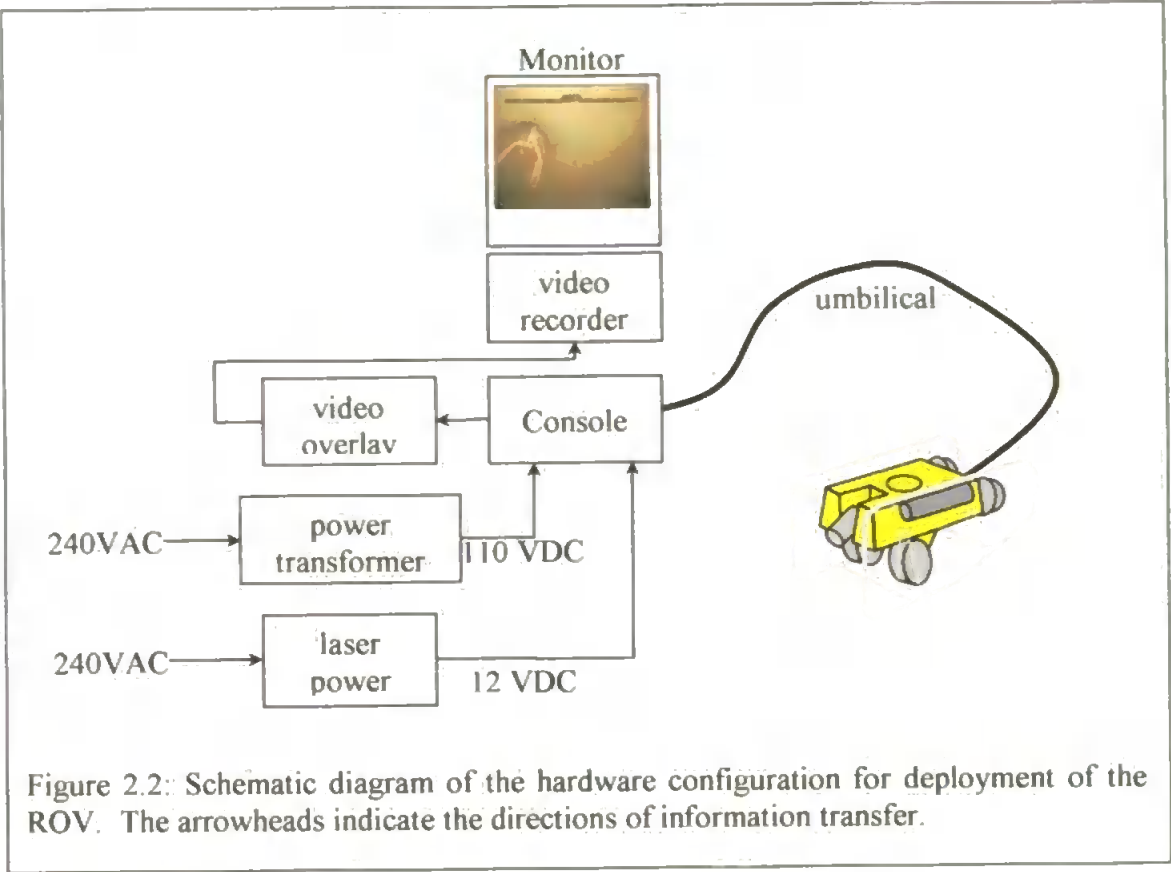


Figure 2.2: Schematic diagram of the hardware configuration for deployment of the ROV. The arrowheads indicate the directions of information transfer.

The video signal is returned to the surface via a co-axial cable within the umbilical and is passed through a video overlay system before being displayed on a monitor. The Pisces Video Plus II video overlay (Pisces Design, San Diego, California) is a programmable unit that allows up to 25 rows of information to be displayed over the video image. The first two rows at the top of the screen display the ROV compass orientation to assist the pilot with navigation. The ROV position information, which is derived from the Sonardyne International underwater acoustic positioning system (Section 2.5), is displayed with the date and time on a single row below the ROV orientation information. The overlaid information is recorded with the video signal onto VHS videotape to provide a unique reference for images during subsequent analysis.

The pilot uses the compass orientation displayed on the video images to manoeuvre the ROV using a combination of longitudinal, lateral and vertical propellers that are controlled by two joysticks on the console. The longitudinal propellers generate a maximum forward velocity of 2.5 knots. The payload of the ROV is limited to 6 kg.

The ROV was deployed from RV Catfish (University of Plymouth) and RV Tamaris (Plymouth Marine Laboratory) in Plymouth Sound and from RV Soel Mara (Dunstaffnage Marine Laboratory) in Loch Creran. Each of these research vessels is equipped with generators that supply 240 VAC required by the Phantom and associated hardware. The vessels were at anchor whilst the vehicle was deployed, so that vessel movement did not affect navigation of the vehicle. The maximum depth encountered at either of the study locations was 40 m and tidal currents did not exceed 1 knot. Consequently, the umbilical length of 120 m allowed the maximum extent of ROV deployment to reach approximately 80 m radius from the anchored vessel.

### **2.1.2 Image-grabbing software**

Laboratory analysis and application of scale to the video images collected from ROV deployments (Section 2.3) requires still images to be collected from the videotape. The video player may be linked to a personal computer, via PCimage-SC hardware, which is equipped with *MVPilot* frame grabbing software (MATRIX Vision GmbH, Oppenweiler, Germany) to display the video image on the computer monitor. The software converts the video signal into a still image, which may be saved as a standard bitmap file, on the command of the operator.

## 2.2 QUANTITATIVE UNDERWATER OBSERVATIONS

The main problem with underwater photography is that the size of features and areas of seabed contained within a single image are unknown. For example, an object that fills half an image may be either a small object observed from close-up or a large object observed from a large distance. Quantification of scale within images collected for scientific investigation provides:

- a) assistance with identification of features contained within an image,
- b) quantification of the area of seabed contained within an image (i.e. absolute field of view) which allows sample unit size to be defined, and
- c) measurement of the minimum size of objects contained within an image.

Consequently, quantification of image scale is required if data from different images and/or different camera systems are to be compared.

Although a number of camera deployment methods exist (Chapter 1), the absolute field of view is a function of camera-object distance, the orientation of the camera with respect to the subject (i.e. camera inclination angle) and the acceptance angle of the lens (i.e. camera zoom) (Wakefield and Genin, 1987). The values of these parameters may be maintained when the camera frame is deployed in contact with the seabed, but are unknown and variable when the camera frame is not in contact with the seabed. The methods of quantifying image scale will be discussed for the situation in which the camera is deployed on a frame in contact with the seabed (Section 2.2.1) and when the camera frame is not in contact with the seabed (Section 2.2.2). A description of the novel approach, developed during the course of this project, to apply scale to images collected from ROVs, where the parameters that describe camera orientation are variable and unknown will be presented in section 2.4.

### 2.2.1 Platforms in contact with the seabed

The majority of underwater camera systems consist of a camera attached to a frame that is deployed in contact with the seabed. In this configuration, the operator must assume that camera-object distance and camera inclination are maintained in the same arrangement as set on the surface. Since the cameras are focussed to the relevant camera-object distance, the acceptance angle of the lens is constant within each deployment. An indication of scale may be obtained by referring to an object of known size that has been positioned in the field of view. Alternatively, scale may be calculated using known values of the camera-object distance, the camera inclination angle and the acceptance angle of the lens (Wakefield and Genin, 1987).

#### *2.2.1.1 Objects of known dimensions in the Field of View*

The scale within diver-deployed and drop-camera systems is often estimated by placing an object of known size, such as a quadrat (Lundälv, 1971), drop-camera trigger switch/weight (Armstrong et al., 1992) or a compass (Piepenberg and Schmid, 1997) in the field of view. Although objects have been positioned in relation to cameras mounted perpendicular (Gutt and Ekau, 1996) and oblique to the seabed (Lampitt and Burnham, 1983), the scale can be estimated for the whole image only when the camera is perpendicular to the seabed. Since scale within images collected by obliquely mounted camera changes from the bottom to the top due to perspective, scale within perspective images may be estimated only near the reference object. A second disadvantage of placing reference objects in the field of view arises from variation in scale from the centre to the outside of an image, which can be resolved only if the acceptance angle of the lens is known. However, the change in scale associated with the acceptance angle is standardised in fixed-frame camera systems; constant camera-object distance requires a fixed focal length lens, and hence, fixed acceptance angle.

The problem of variable scale associated with perspective images and the acceptance angle of the lens may be addressed using empirical calculations that were applied during large scale mapping of Canada's Laurentian Plateau using oblique aerial photography (Crone, 1963) and will be addressed in the following section.

#### *2.2.1.2 Calibration images and empirical calculations*

Mounting the camera at an oblique inclination angle increases the area of seabed contained within an image but introduces a change in scale from the bottom to the top of the image i.e. perspective. However, perspective images are particularly useful in association with frame-mounted cameras because the camera observes areas of seabed that have not been directly impacted by the frame itself (Hughes and Atkinson, 1997).

The change in scale across perspective images may be calculated empirically using known values of camera-object distance, camera inclination angle (measured between the seabed and the optical axis) and acceptance angle of the lens (Wakefield and Genin, 1987). In practice, perspective grids are obtained usually by placing a square grid of known dimensions in the field of view on the surface. An image may be collected in which the square grid appears as a trapezium and the position of the grid nodes may be recorded and overlaid on all other images collected (Grassle et al., 1975; Uzmann et al., 1977; Rice et al., 1979; Smith and Hamilton, 1983; Harrold et al., 1998).

The use of calibration images and empirical calculations to quantify scale within perspective images assumes that:

- a) the seabed is flat and lies in the same horizontal plane as the base of the frame, and
- b) the camera orientation is maintained in the same arrangement as set on the surface.

However, subtle differences in image scale will occur because the seabed is seldom flat and camera frames are liable to sink into soft sediments (e.g. Bergstedt and Anderson,

1990). Camera sledges often lose contact with the seabed as they are towed (Lauerman et al., 1996), which results in variable camera orientation. Consequently, empirical calculations and calibration images cannot be applied to images collected when the sledge loses contact with the sediment. Switch mechanisms that are activated on contact with the seabed may be attached to sledges (Rice et al., 1979) whereby photographs can only be collected when the sledge rests on the sediment. However, the use of video cameras and camera platforms that do not maintain contact with the seabed required the development of alternative methods to apply scale to images.

### **2.2.2 Platforms NOT in contact with the substratum**

Manned submersibles, remotely operated vehicles (ROV) and autonomous underwater vehicles (AUV) are all designed to make underwater observations where contact with the seabed is to be avoided. The cameras are mounted obliquely to observe the seabed in front of the vehicle, as their primary role on manned submersibles and ROVs is to assist the pilot with navigation of the vehicle. In addition, variable zoom cameras are employed generally to observe features in detail because camera-object distance fluctuates as the vehicle progresses. Consequently, quantification of scale within images collected from cameras mounted on submersibles, ROVs and AUVs is complicated by variation in camera-object distance, perspective and zoom.

Although submersibles may be flown in contact with the substratum to maintain camera orientation in a similar manner to frame-mounted cameras (Grassle et al., 1975), this defeats their purpose. Early attempts to apply scale to oblique images involved estimating feature dimensions as they passed underneath a scale bar (Caddy, 1973), or through attached quadrats (Ellis and Heim, 1985) that were positioned in the field of view. Positioning scale bars in images from submersibles and ROVs was limited to perpendicular camera inclination angles as discussed earlier, and also gave parallax problems because the

distance between the scale bar and the seabed fluctuated with the position of the submersible. However, the effects of parallax between the scale bar and the seabed could be accommodated by the introduction of structured lighting systems.

### **2.2.3 Structured lighting systems**

A structured lighting system uses two or more laser diode modules that project focussed beams, which form spots when they fall on a solid surface. The simplest structured lighting system comprises a single pair of parallel lasers that project two spots of known distance apart, which is maintained independently of the camera-object distance. Camera-object distance of a fixed acceptance angle camera may be calculated from the laser spot separation in an image, but the change in scale caused by variable zoom must be resolved with the addition of a third laser to indicate camera-object distance. A single pair of parallel lasers is analogous to placing an object of known dimensions in the field of view (e.g. MacDonald, et al., 1989; Tusting, et al., 1989; Davis and Pilskalns, 1992) and the effects of oblique camera inclination angles remain.

Structured lighting systems using four parallel lasers, which project a square of known dimensions onto the seabed, were developed to indicate camera inclination angle. The projected square appeared as a trapezium in the image when camera inclination angle deviated from perpendicular. The remote images were analysed only if the projected square was not badly skewed; the distance between the top and bottom pair of laser spots being less than 10% of the distance between the bottom pair of laser spots (Grassle et al., 1975; Thrush et al., 1998). Although the pattern projected by four parallel lasers ensured that variation in image scale due to perspective were minimised, image scale may be calculated by analysis of the projected pattern itself.



A structured lighting array was developed during the course of the present project to enable all images collected from the Phantom ROV camera to be scaled, and objects within the images to be measured. The pattern of laser spots projected by the structured lighting array is analysed in the *Benthic Imager* software, which calculates camera inclination angle and camera-object distance; thus scale across entire perspective images may be calculated. The software accommodates the unknown fields of view and inclination angles associated with camera zoom and tilt facilities and the variable camera-object distances experienced as remotely operated vehicles manoeuvre above a non-horizontal seabed. The remotely operated vehicle, structured lighting array and *Benthic Imager* software package have been combined to form the Automated Benthic Image Scaling System (ABISS).

## 2.3 AUTOMATED BENTHIC IMAGE SCALING SYSTEM (ABISS)

The Automated Benthic Image Scaling System (ABISS) was conceived by Dr D.A. Pilgrim at the University of Plymouth and has been developed into an operational tool during the present project. The ABISS comprises a remotely operated vehicle and camera, a structured lighting array of five diode lasers mounted around the camera housing, and a software package, *Benthic Imager*, which analyses the laser spot pattern to calculate real scale in images. The structured lighting hardware has been developed so that it is sufficiently robust for field deployment, and the laser alignment protocol has been designed and tested thoroughly during the present project. Improvements to the *Benthic Imager* software package were implemented as the hardware advanced by Dr D.A. Pilgrim.

### 2.3.1 Structured lighting array

The structured lighting array comprises four laser diodes that must be aligned parallel to the camera optical axis, and hence each other, to project the corners of a square when the camera is perpendicular to the substratum in both horizontal and vertical planes. A fifth laser is aligned at an angle to, but in the same plane as, the bottom pair of lasers. The fifth laser projects a spot whose position relative to the bottom laser spots is used to calculate camera-object distance (Fig. 2.3).

The laser array mounting is constructed from a block of ABS plastic that has been designed to allow the alignment of individual laser modules. Each laser module fits into an ABS collar that behaves as a universal ball joint when positioned within the barrel of the mounting bracket. Alignment and locking of the position of each module is achieved by adjustment of horizontal and vertical screws located either side of the universal joint.

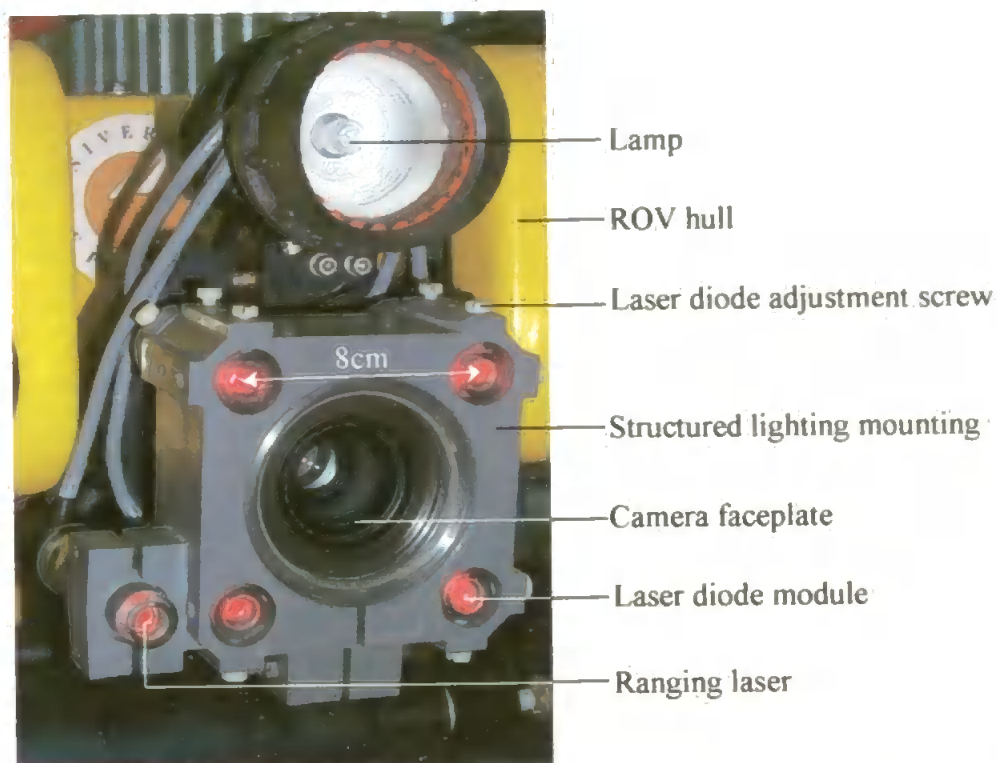


Figure 2.3: The structured lighting array mounted on the camera of the Phantom XTL.

The laser diodes, powered by a 5 VDC supply, emit red light (633 nm wavelength) that is focussed to a circular beam by a plastic lens (Imatronic LDMP 115/633/1). The laser diodes are modified for underwater use by sealing them in acrylic tubes that are joined to the umbilical through an underwater connector.

### 2.3.2 Structured lighting trigonometry

The four parallel laser modules project spots in a square of known, fixed dimensions only when the camera is perpendicular to the plane of the substratum in both horizontal and vertical planes. As the inclination angle ( $\phi$ ), measured between the substratum and the camera optical axis, deviates from perpendicular (i.e.  $\phi = 90^\circ$ ), the pattern of spots changes in a predictable manner. Although the parallel spots are actually projected as a rectangle onto the substratum when viewed from above, they appear as a trapezium in the resulting image (Fig. 2.4).

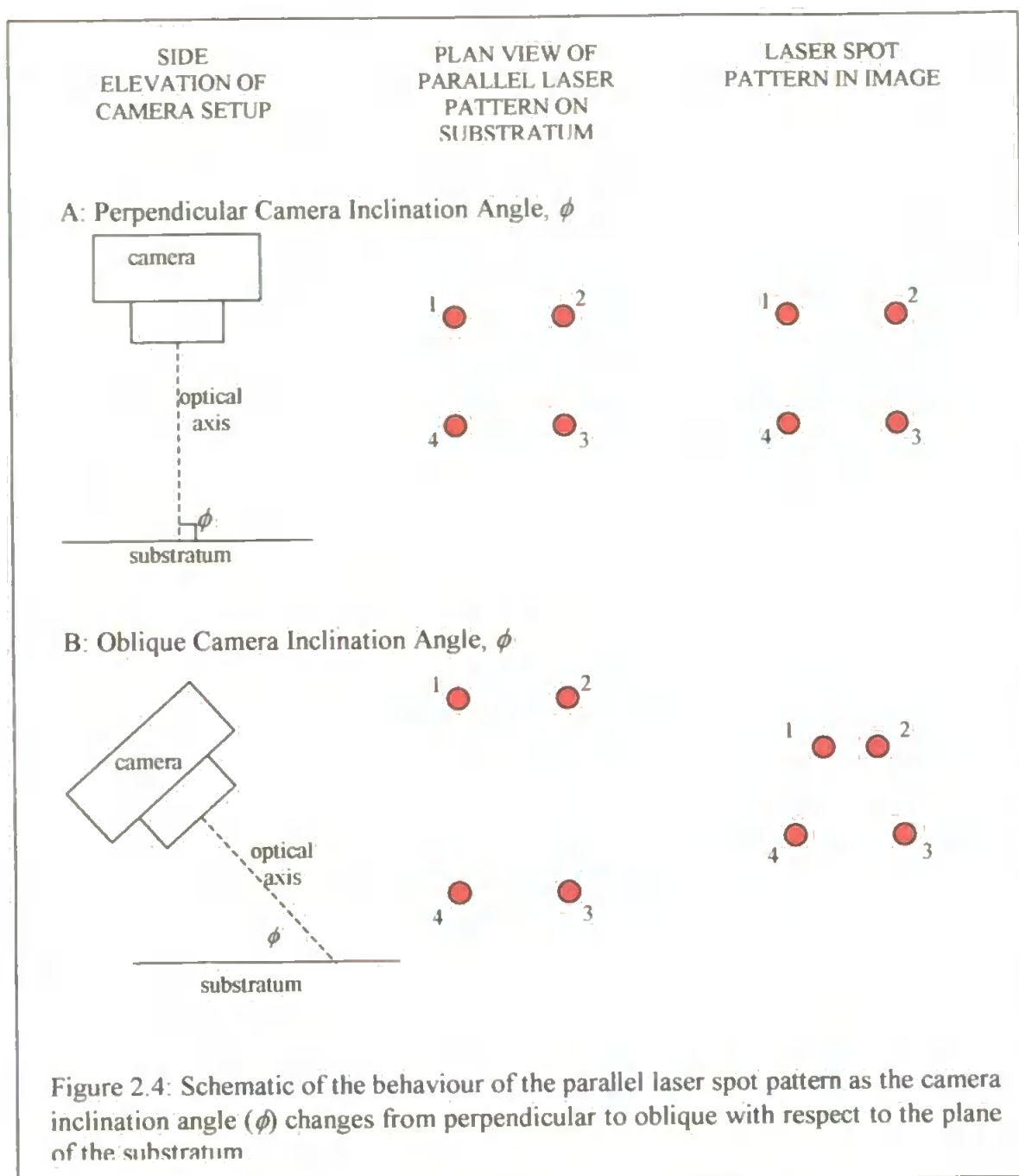


Figure 2.5 shows the geometry and the pattern of projected laser spots of a particular camera orientation, from which camera inclination angle and camera-object distance may be calculated using standard trigonometrical equations. The four laser diodes (originating from  $L_{(1,2)}$  and  $L_{(3,4)}$ ) are aligned parallel to, and at a known separation from, each other and the optical axis of the camera ( $CP$ ), while the fifth laser ( $L_{(5)}$ ) is aligned at a known angle in the plane of  $L_{(3,4)}$ .

Laser spot pattern that appears in the 'virtual' image plane

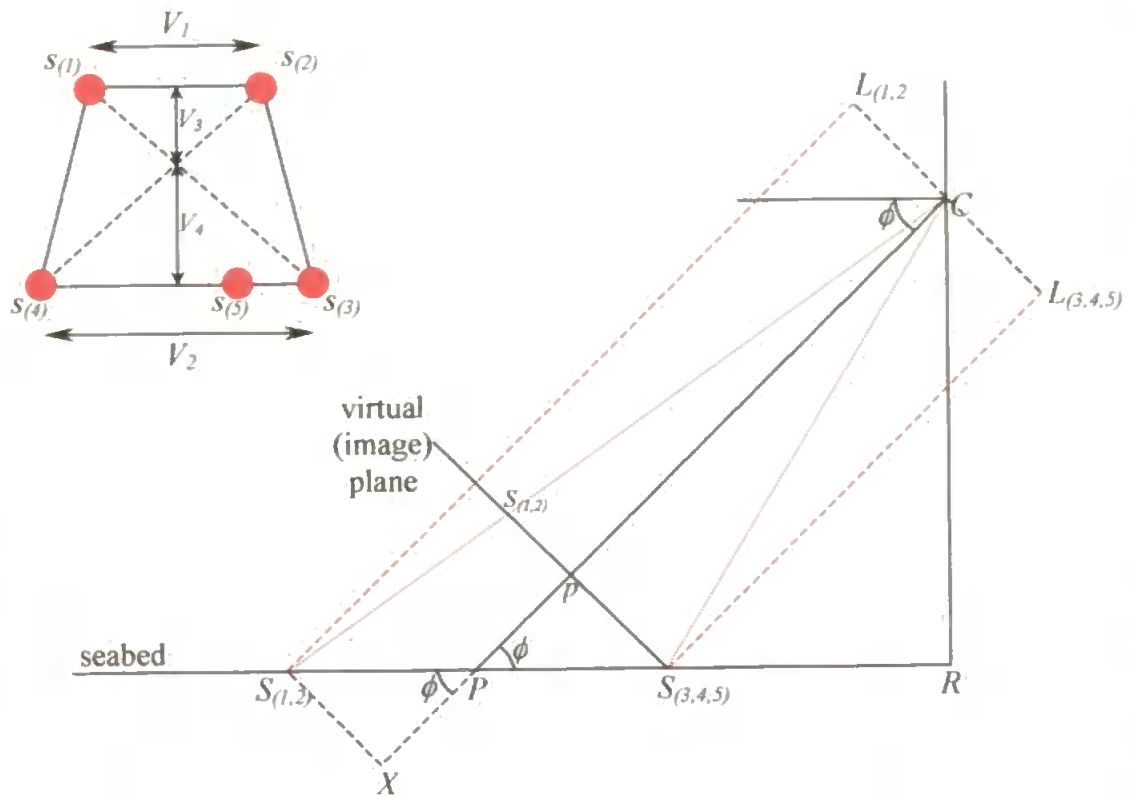


Figure 2.5: Schematic diagram for derivation of Camera inclination angle ( $\phi$ ) and camera-object distance measured along the optical axis ( $CP$ ). See text for explanation of remaining symbols.

The perspective ratio ( $\psi$ ) of any image is defined as:

$$\text{Perspective Ratio, } \psi = \frac{V_1}{V_2} = \frac{V_3}{V_4} \dots \dots \dots \text{Equation 1}$$

where  $V_1$  and  $V_2$  are the horizontal distances, measured in pixels from the image, between spots  $s_{(1)}$  and  $s_{(2)}$  and spots  $s_{(3)}$  and  $s_{(4)}$ , respectively;  $V_3$  and  $V_4$  are the vertical distances between the intersection of the lines joining the diagonally opposite laser spots  $s_{(1)}$  to  $s_{(4)}$  and the horizontal lines joining spots  $s_{(1)}$  and  $s_{(2)}$  and  $s_{(3)}$  and  $s_{(4)}$ , respectively (Fig. 2.5).

Since triangles  $Cps_{(1,2)}$  and  $CXS_{(1,2)}$  are similar:

$$\frac{ps_{(1,2)}}{XS_{(1,2)}} = \frac{\psi \cdot pS_{(3,4,5)}}{XS_{(1,2)}} = \frac{\psi \cdot XS_{(1,2)}}{XS_{(1,2)}} = \frac{Cp}{Cp + Xp}$$

Consequently, the virtual distance between the camera faceplate and the principal point of the image ( $Cp$ ) may be expressed as:

$$Cp = \psi(Cp + Xp) = L_{(3,4,5)}S_{(3,4,5)} \dots\dots\dots \text{Equation 2}$$

The angle at which the fifth laser is aligned is calibrated prior to each deployment (Section 2.3.4), so that the position of the fifth laser in relation to spots three and four may be used to calculate the distance between the bottom edge of the parallel laser box and the camera,  $L_{(3,4,5)}S_{(3,4,5)}$ .

Rearranging equation 2:

$$\psi.Xp = Cp - \psi.Cp$$

and

$$\psi.Xp = Cp(1 - \psi)$$

Therefore,

$$Xp = \frac{Cp(1 - \psi)}{\psi} \dots\dots\dots \text{Equation 3}$$

where the perspective ratio ( $\psi$ ) and  $Cp$  are derived from equations 1 and 2.

Since

$$Pp = \frac{Xp}{2}$$

$$Pp = \frac{Cp(1 - \psi)}{2.\psi} \dots\dots\dots \text{Equation 4}$$

Therefore, calculation of the camera inclination angle ( $\phi$ ) from triangle  $PpS_{(3,4,5)}$  may be expressed as follows:

$$\text{Camera inclination angle, } \phi = \tan^{-1}\left(\frac{pS_{(3,4,5)}}{Pp}\right) \dots\dots \text{Equation 5}$$

Camera-object distance measured along the optical axis ( $CP$ ) is calculated using Equations 2 and 4, whereby:

$$CP = Cp + Pp \dots\dots\dots \text{Equation 6}$$

The camera inclination angle ( $\phi$ ) and camera-object distance along the optical axis ( $Cp$ ) have been derived using Equations 5 and 6. Therefore, the geometry of the camera orientation may be derived from triangle  $CRP$  (Fig. 2.5) as follows:

$$\text{Perpendicular camera height, } alt \quad CR = CP \cdot \sin \phi$$

$$\text{Horizontal distance to principal point, } PR = CP \cdot \cos \phi$$

Having calculated camera-object distance and inclination angle, quantification of absolute scale within images is a repetitive process of converting 'image distances' that are measured in pixels into absolute distances. Figure 2.6 represents a side elevation of the camera orientation of a perspective image;  $RA$  represents the plane of the substratum and the camera faceplate is at a point  $C$ , thus the field of view in the vertical plane corresponds to  $ACB$ . The image plane is represented by  $A'B'$  (within the camera), but may also be represented by  $Bd$  (as triangles  $BCd$  and  $A'CB'$  are similar) to assist with trigonometrical calculations. The actual position of the lasers that mark the top and bottom of the parallel laser box are represented by  $L_{(1,2)}$  and  $L_{(3,4)}$ , projecting spots onto the substratum at  $S_{(1,2)}$  and  $S_{(3,4)}$ , which appear in the image plane at points  $s_{(1,2)}$  and  $s_{(3,4)}$  respectively. Similarly, the optical axis of the camera is denoted by  $PP'$  such that the centre of the image lies at point  $p$ , the principal point.

The common parameter between an absolute distance,  $PY$ , on the seabed and an 'image distance' ( $py$ ) is the common angle  $\alpha$  in triangles  $PCY$  and  $pCy$  (Fig. 2.6). It is apparent that:

$$\alpha = \tan^{-1} \left[ \frac{py}{Cp} \right]$$

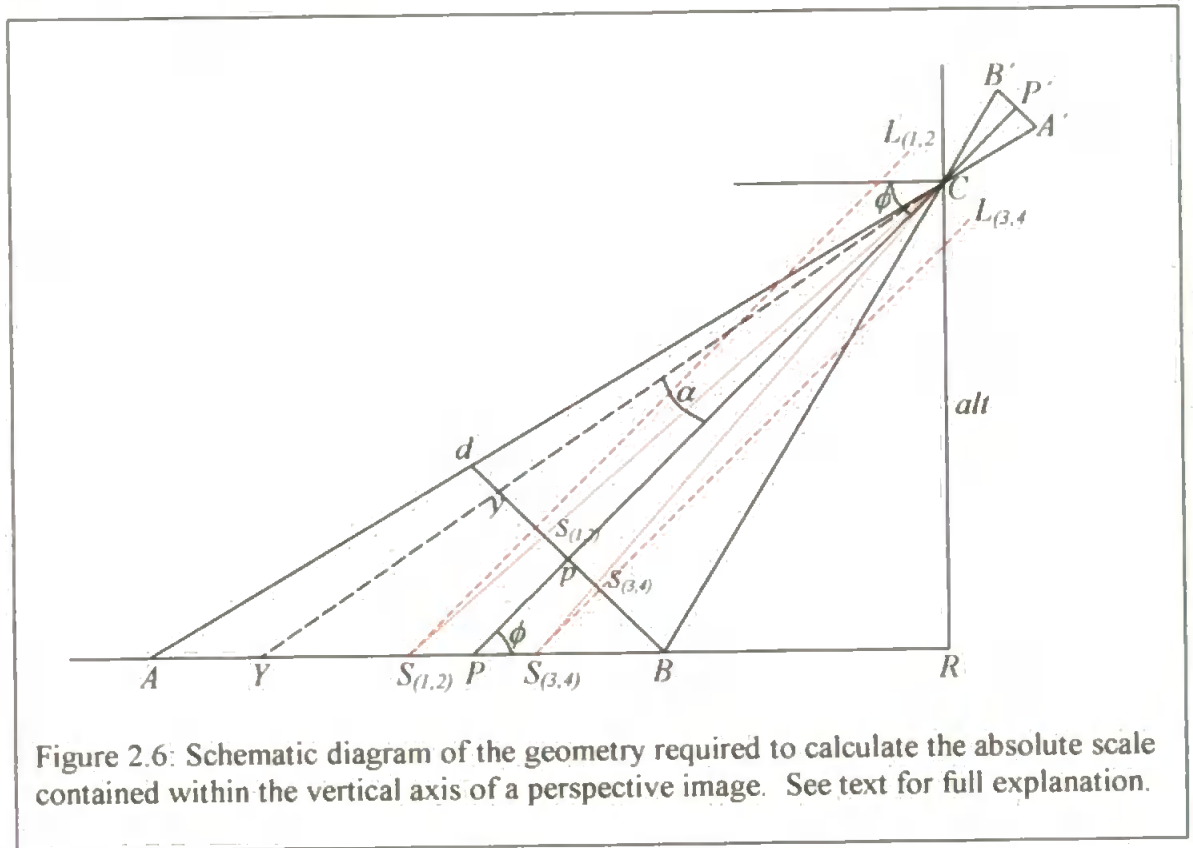
where  $py$  is the image distance measured in pixels and  $Cp$  is a virtual distance (also measured in pixels), which is calculated from Equation 1. Therefore, in triangle  $RCY$ :

$$\tan \left( \alpha + \frac{\pi}{2} - \phi \right) = \left( \frac{RP + PY}{alt} \right)$$

and thus:

$$PY = (\tan[\alpha + \pi/2 - \phi] \times alt) - RP$$

where  $\phi$  is the camera inclination angle,  $alt$  is the altitude of the camera above the substratum and  $RP$  is the horizontal distance between the principal point and the point from which camera altitude is measured.



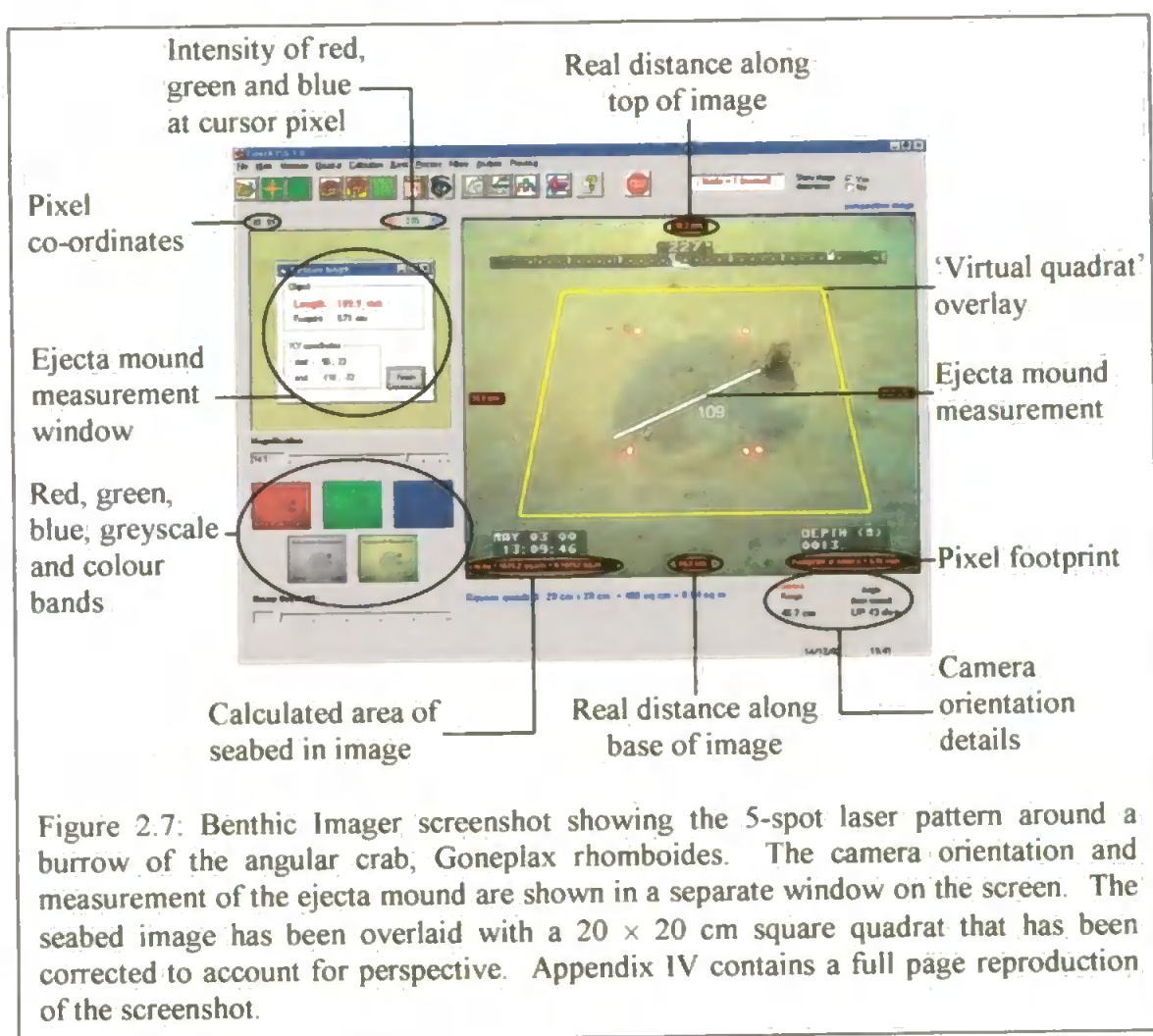
A similar procedure may be applied to scale the horizontal axis of a perspective image. Hence, quantification of scale across the whole of an image is achieved by multiple repetitions of these processes, which has been automated by the development of *Benthic Imager* software.



### 2.3.3 Benthic Imager software

#### 2.3.3.1 Image scaling and measurement

The *Benthic Imager* software was written by Dr D.A. Pilgrim using Microsoft® Visual Basic 6.0, so that it is compatible with the Microsoft® Windows format. The software displays still images that have been collected from the videotape using *MVPilot* frame-grabbing software (Section 2.1.2), and the five laser spots are located manually using the cursor to provide the co-ordinates  $s_{(1)}$  to  $s_{(5)}$  (Fig. 2.5). The program uses the trigonometrical equations described in section 2.2 to calculate the camera inclination angle, camera-object distance, total area of seabed in the image and the real dimensions represented by the image margins, which are displayed around the image (Fig. 2.7).



It is not possible to extract data from the entire image because the video overlay has been programmed to display the navigation and time telemetry at the top of the image, which obscures this portion of each image. The top of the screen was chosen because camera-object distance increases towards the top of a perspective image, which causes greater changes in scale and blurring of underwater images. Consequently, the navigation telemetry could be included to uniquely identify images without reducing the amount of useful data that could be extracted from each image.

Quantitative benthic investigations require that the data be extracted from samples of the same size. When the total area of seabed contained within an image exceeds the area of each sample, quadrats of known size that have been corrected for perspective may be overlaid within the images. Square or circular quadrats are projected as trapezoid or ovoid 'virtual quadrats' respectively (Fig. 2.7). If the total area contained within each image is less than the required sample area, a series of contiguous images may be collected to achieve a standard sample area. Since the video overlay information obscures a section of the video image, *Benthic Imager* software will calculate the real area of unobscured seabed (or the area of features, such as scallop shells or burrow openings) that has been defined by manually locating area boundaries. The area calculation routine allows the area of seabed that is obscured by the video overlay information to be subtracted from the total image area when aggregating a series of contiguous images to form a sample of standard size.

In addition to calculating absolute area within images, the dimensions or distances between features, such as burrow openings and mounds, may be measured from the images by identifying the start and end of each feature with the cursor. This procedure was used to obtain size distribution data for large bivalve siphon openings that will be presented in Chapter 6.

#### 2.3.3.2 Image resolution

Image resolution refers to the ability to distinguish between two objects in photographic and video images that are in close proximity in the object scene. Absolute resolution is particularly important in the application of remote observation in benthic ecological investigations as it provides an estimate of the minimum size of an object or organism that may be identified in the survey. Therefore, quantification of image resolution is required if data from different surveys are to be compared. Image resolution is analogous to the sieve mesh sizes that define macro- and meiofaunal studies.

*Benthic Imager* measures image resolution in terms of the 'pixel footprint', which represents the size of a single pixel in the real world. The pixel footprint of a satellite image may be measured in hundreds or thousands of metres, but the underwater image footprint scale is measured in millimetres. Since the dimensions of the image footprint will increase from the bottom to the top of a perspective image, *Benthic Imager* displays the pixel footprint as measured at the principal point, top corner (maximum size) and bottom centre (minimum size) of each image.

#### 2.3.3.3 Image enhancement

Colour video cameras compose an image as a combination of red, green and blue light intensity (Chapter 1). Since the intensity of each band ranges from 0 to 255, still images may be enhanced by manipulating the intensity values of each pixel. A variety of image enhancement filters that have been incorporated from *Inventions Software* image enhancement libraries are available within *Benthic Imager* software.

Although the intensity of the red, green and blue channels is displayed for the cursor pixel at the top right of the still image (Fig. 2.7), the intensity of pixels in the entire image are represented by the image histogram. The light intensity axis of the image histogram ranges

between 0 and 255, yet the frequency histogram of underwater images often occupies only a small proportion of the full range. A histogram stretch routine improves the contrast in an image by reallocating the pixel intensity so that the frequency histogram covers the maximum range. Spatial filtering routines may also be applied to enhance or suppress features within an image. 'Low pass filters' emphasise larger homogeneous areas of similar intensity in an image which reduces the detail, and hence noise, while 'high pass filters' increase detail by emphasising small areas where the difference in pixel intensity is high.

Although image enhancement techniques improved the quality of video images, they did not affect extraction of abundance data presented in this thesis, as the contrast between burrow openings and surface sediment was sufficient for discrimination of individual features from the unprocessed images.

### 2.3.4 Automated Benthic Image Scaling System (ABISS) calibration

The ABISS must be calibrated in the laboratory prior to deployment in the field. The following adjustments are required:

- a) *Laser alignment*: the ABISS system depends on the parallel alignment of the four main lasers, with the fifth laser aligned at an angle to these for calculation of camera–object distance. The *Benthic Imager* software must be calibrated using the dimensions of the square that is projected by the four parallel lasers i.e. ‘box size’ and the angle of the fifth laser. Consequently, the laser alignment procedure must be performed prior to each deployment of the ROV.
- b) *Camera backset correction*: the geometry associated with calculation of camera orientation using a structured lighting array assumes that light converges at the camera faceplate (point *C* in Figs 2.5 and 2.6). The convergent point actually occurs within the camera, so a small ‘camera backset correction’ is required to account for the distance between the camera faceplate and the point that the light converges. Calibration of the camera backset correction is only required for each camera that may be used in conjunction with the ABISS.

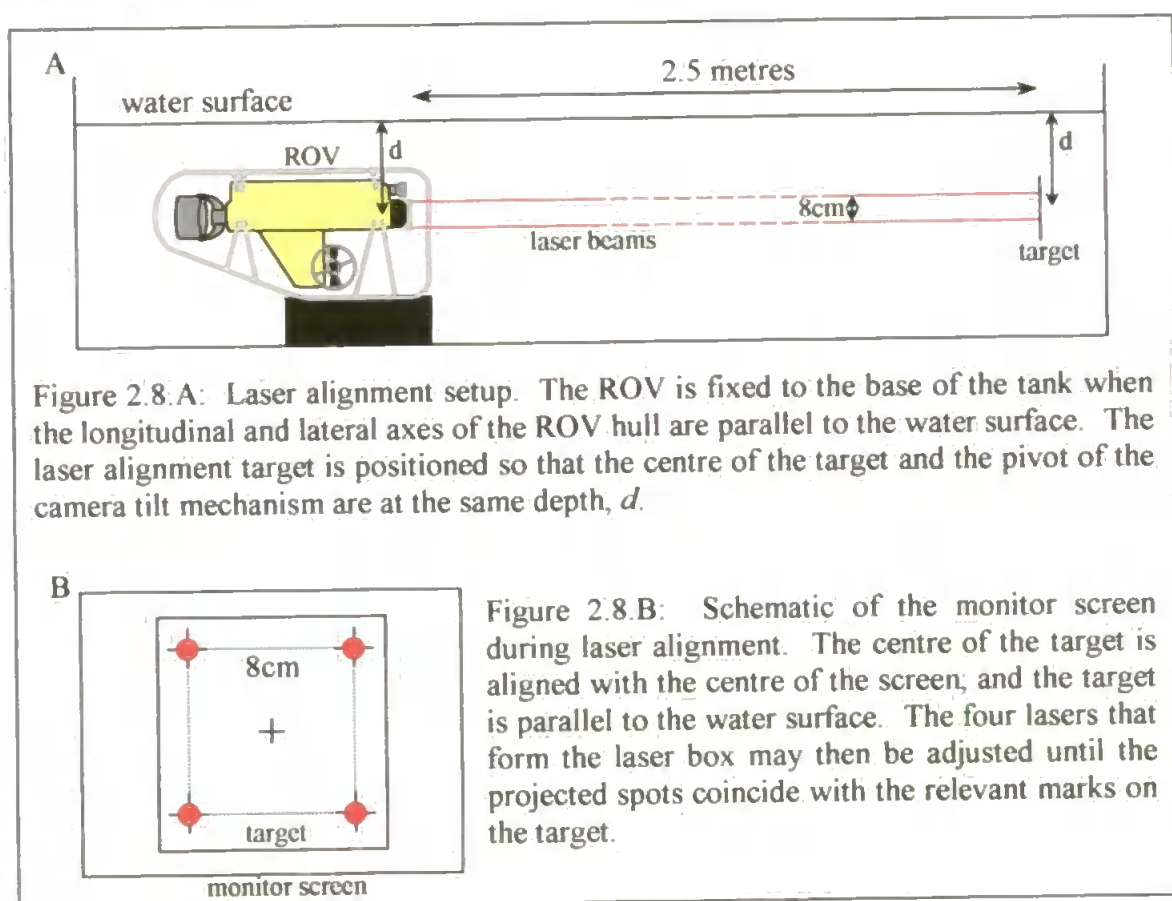
#### 2.3.4.1 Laser alignment

The ABISS system depends on the parallel alignment of the four main lasers in relation to each other and to the optical axis of the camera (Figs 2.5 and 2.6). This ensures that the corners of a square of known dimensions are projected onto a flat surface that is perpendicular to the camera optical axis. The dimensions of the projected square are called the ‘box size’, which is recorded for calibration of *Benthic Imager* software. The fifth laser is aligned at an angle to, but in the same horizontal plane as lasers three and four for calculation of camera–object distance (Fig. 2.5). Laser alignment must be performed under water, as there may be significant refraction at the air–acrylic–water interfaces of the laser modules.

To calibrate the lasers, the ROV is secured to the bottom end of a large laboratory tank, such that the ROV hull is parallel to the water surface in both longitudinal and lateral axes (Fig. 2.8.A). A target marked with the corners of a square corresponding to the box size is positioned at the other end of the tank so that:

- the top of the target is parallel to the water surface, and
- the centre of the target and the pivot point of the camera tilt mechanism are at the same depth ( $d$ ) below the water surface.

The camera tilt is adjusted until the centre of the target coincides with the centre of the video image (Fig. 2.8.B), which ensures that the target is perpendicular to the optical axis ( $CP$  in Figs 2.5 and 2.6).



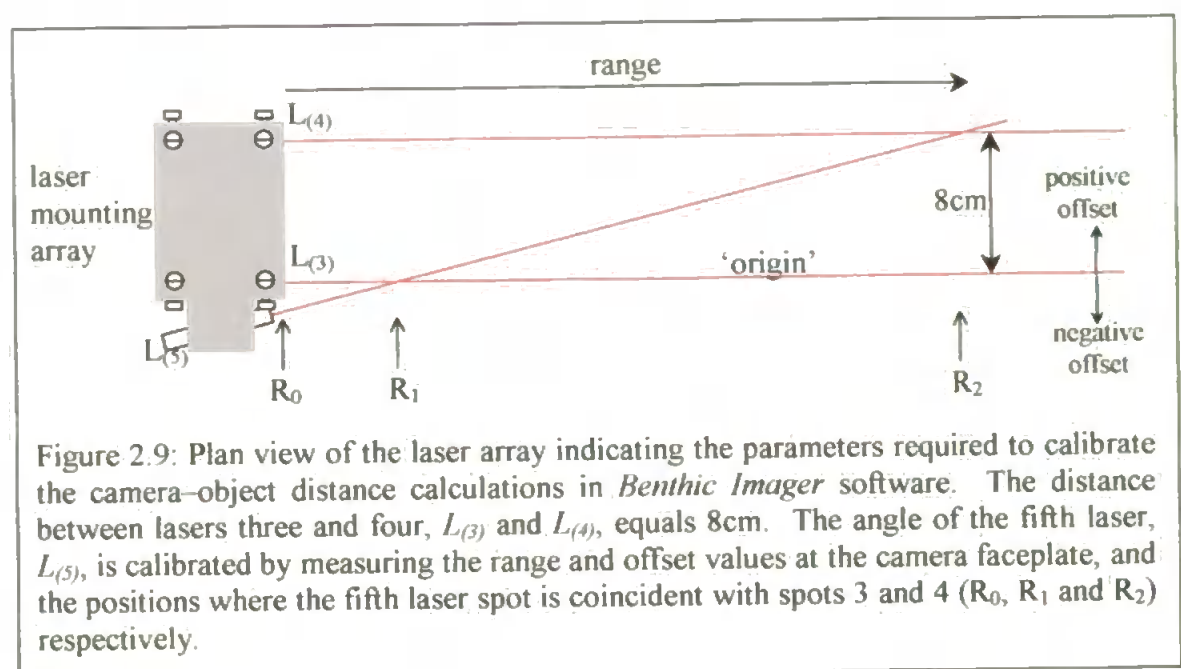
The four laser modules are adjusted and locked into position so that the spots that they project correspond with the relevant marks on the target. The four main lasers may now be considered to be parallel over the alignment range because the laser beams project the corners of a square of the same dimensions as the camera-mounted diode array. The

minimum dimensions of the laser box must be sufficient for all the laser spots to be visible in images collected at small camera–object distances, while maximising the box size will increase the accuracy of the calculations for images collected at larger camera–object distances. In practice, the box size on the Phantom ROV was limited to an 8 cm square due to the proximity of the camera mechanism and the ROV hull (Fig. 2.3). However, an 8 cm box size was appropriate for the turbid waters of Plymouth Sound and Loch Creran because the seabed became blurred in video images as camera–object distance increased before box size effects were detected. Larger box sizes may be required to maintain the accuracy of calculations for images collected in less turbid water where greater camera–object distances, and hence area of seabed contained within each image, may be achieved. The calibration procedure for *Benthic Imager* software accommodates different box size dimensions.

Once the parallel lasers have been aligned, the fifth laser must be aligned at an angle to, but in the same plane as the bottom pair of lasers. As a result, the fifth spot moves towards the left side of the video image as camera–object distance increases, and *vice versa*. Alignment of the fifth laser may be modified for each deployment so that the fifth spot will appear as close to the left side of the video image as possible at maximum camera–object distance. The angle of the fifth laser beam must be calibrated so that the position of the fifth laser in relation to the bottom pair of laser spots may be used to calculate camera–object distance.

The fifth laser is calibrated by deriving an equation for the beam angle. This is achieved by measuring the range and ‘laser offset value’, which is the real distance between spots three and five, at three locations in front of the camera. The third laser beam is defined as the origin for calibration of the fifth laser beam, so that a positive laser offset value indicates that the fifth laser lies to the left of the third laser spot, and *vice versa* (Fig. 2.9).

Although any three combinations of range and laser offset values would be sufficient, the angle of the fifth laser is described by measuring these parameters at the camera faceplate and when the projected spot is coincident with the spots projected by lasers three and four (Fig. 2.9).



The fifth laser calibration values and box size must be entered into the *Benthic Imager* calibration sequence prior to analysis of the images. *Benthic Imager* software calculates the distance (measured in pixels) between spots three and four in the image, which corresponds to the box size (measured in centimetres). The pixel co-ordinates of the fifth laser spot may be used to calculate the laser offset value (also measured in centimetres). Consequently, the range (equivalent to  $L_{(3,4,5)}S_{(3,4,5)}$  and  $C_p$  in Fig. 2.5) may be derived using the equation that describes the angle of the fifth laser beam.



#### 2.3.4.2 Camera backset correction

The geometry associated with scaling perspective images implies that all observations converge at the camera faceplate (point *C* in Figs 2.5 and 2.6). In reality, this imaginary convergent point is located at some distance behind the camera faceplate within the camera itself. Therefore, a small correction is required to account for the distance between the camera faceplate and the convergent point i.e. the 'camera backset correction'. The appropriate camera backset correction was found by collecting images of a calibration board, marked with 10 × 10 cm black and white squares, using a variety of camera-object distances and inclination angles. Scale within each image was calculated by entering the pixel co-ordinates of each laser spot directly into *Benthic Imager*, rather than locating the spots manually. Each image was re-scaled using camera backset corrections that ranged from +12 to -12 cm. Direct input of pixel co-ordinates ensured that variation in scale calculations was due to changes in camera backset correction rather than the ability to identify the spots manually.

The change in scale caused by the camera backset correction was investigated by measuring the calibration squares in the vertical and horizontal image planes, using different camera backset correction values. The percentage errors of the *Benthic Imager* measurements were calculated and plotted against the camera backset correction (Fig. 2.10). Horizontal measurement errors were found to be independent of backset correction providing an accuracy of  $\pm 2\%$ , while a backset correction value of 2 cm produced the optimum accuracy of  $\pm 5\%$  in the vertical image plane.

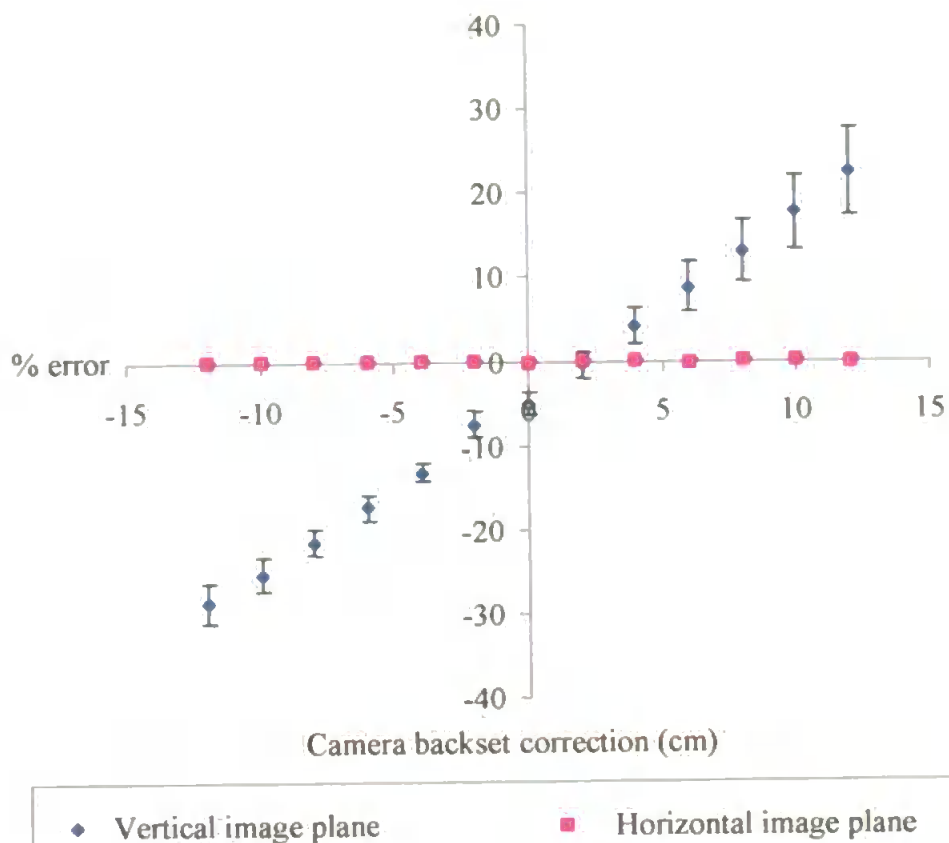


Figure 2.10: The effect of changing camera backset correction on the accuracy of measurements in *Benthic Imager* software. Mean values  $\pm 95\%$  confidence intervals: N=15.

### 2.3.5 Laser diode wavelength

The laser diode modules used in the ABISS project red light spots (wavelength,  $\lambda = 633$  nm) onto the seabed. At first, red light may not appear to be the most appropriate wavelength for underwater applications because red light is attenuated selectively underwater in comparison to blue light (Pilgrim, 1998). Consequently, a blue-green laser could project a spot onto the seabed at greater distances than a red laser of the same power. Red lasers were chosen in preference to blue-green lasers, however, because red spots were easier to see in the images, due to greater colour contrast between the red spots and the seabed.

## 2.4 UNDERWATER ACOUSTIC POSITIONING SYSTEM

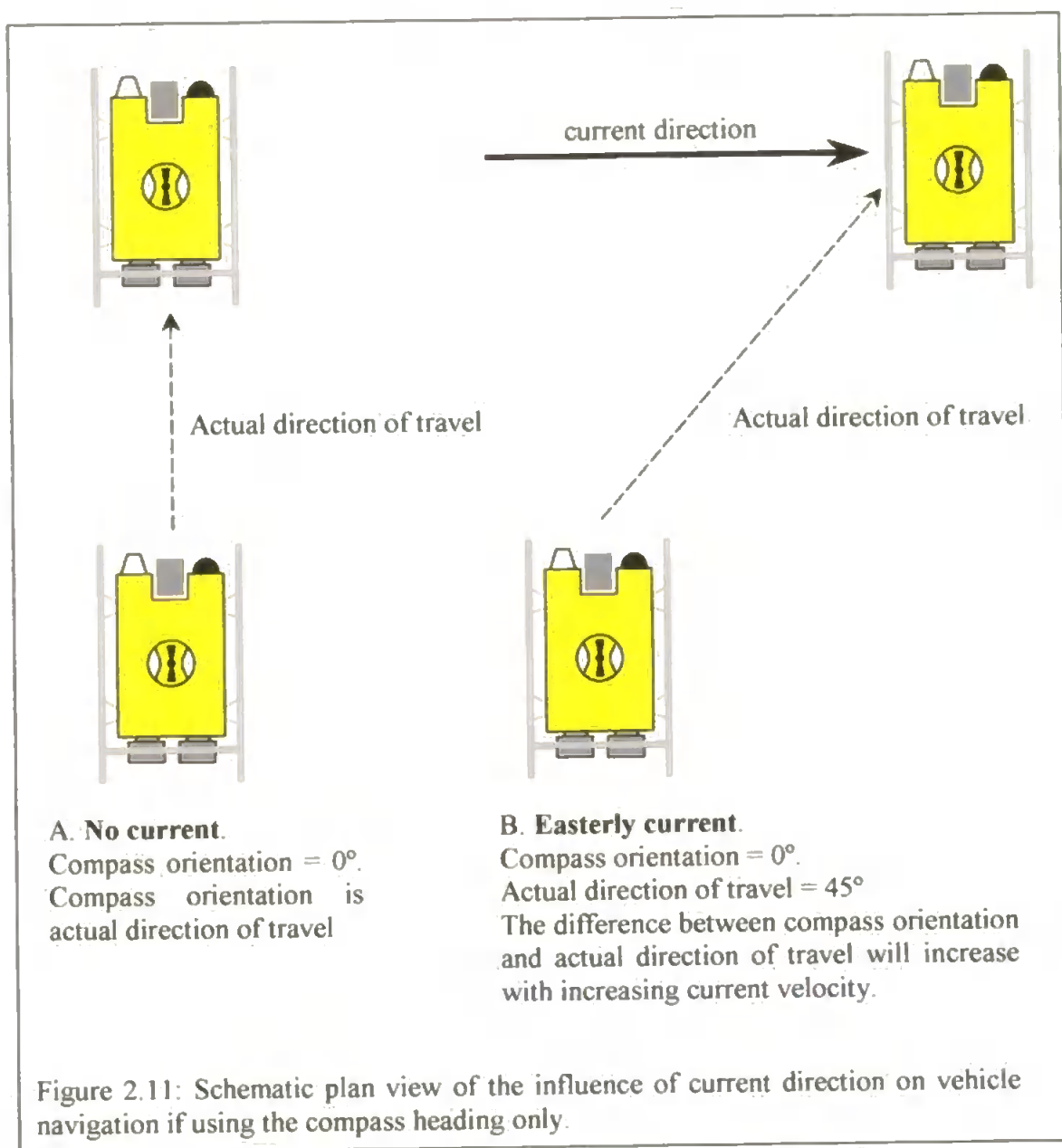
There is a basic requirement for navigation of equipment deployed in the field to avoid obstacles, yet the ability to accurately navigate vehicles back to specific locations allows investigation of temporal change in, for example, epifaunal assemblages and sediment structures at the snouts of glaciers (Hamada et al., 1986; Dawber and Powell, 1995). However, the detection and description of patterns within a megafaunal assemblage involves the comparison of variation between quantitative estimates of abundance and biomass. Since the precision of estimates of mean abundance or biomass is affected by the total number of samples collected and variability between replicate samples (Vézina, 1988), the ability to detect pattern is a function of the sample grain, lag and extent (Wiens, 1989) (Chapter 1).

In a video deployment, a series of many individual images may be recovered from the videotape and, in theory at least, each is an independent sample of the benthos. Video surveys often substitute distance travelled and image area with time as a denominator for calculation of sample grain and lag (e.g Michalopoulos et al., 1992; Magorrian and Service, 1998). Species-time methods produce estimates of relative abundance that are highly dependent on the speed of the vehicle in relation to the substratum. Consequently, navigation of vehicles carrying video cameras greatly increases the value of these images because individual images may be spatially registered.

### 2.4.1 Basic navigation techniques

The Phantom ROV is equipped with a flux-gate compass that indicates the orientation of the hull on the video overlay. The compass orientation may be used for basic navigation of the vehicle under quiescent hydrographic conditions, such as those experienced in Loch Creran. However, tidal currents can influence significantly the actual position of a vehicle

that is navigated on a constant compass heading. Figure 2.11 represents the effect of an easterly current on the location of a vehicle that is following a compass heading due north.



In the simplest form of ROV position fixing, a surface marker buoy may be attached to the vehicle and position may be calculated using either the range and bearing to the surface vessel or by attaching a GPS unit to the buoy itself (e.g. Veisze and Karpov, 2002). However, the accuracy and precision of position fixing in this way will decline as depth and currents increase because the surface buoy will not necessarily be directly above the vehicle. Vehicle position relative to a surface vessel may also be monitored by continuous echo-sounding (Dawber and Powell, 1997) to guide the vehicle to specific locations, such

as the snouts of marine glaciers, to investigate temporal variation in processes (e.g. Hamada et al., 1986; Dawber and Powell, 1995; Gutt et al., 1996). The investigation of spatial variation in megafaunal assemblages requires the spatial reference data to be incorporated with the photographic or video images.

#### **2.4.2 Underwater acoustic positioning systems**

Underwater acoustic positioning systems consist of an array of acoustic beacons, at known fixed positions underwater, and a single acoustic beacon attached to the vehicle to be navigated. The time between transmission and reception of acoustic signals produced by the beacons is recorded, from which the distance between each beacon may be calculated as a function of the speed of sound through water. Ultimately, the actual vehicle position is calculated by triangulation of distance from the beacons in the known array.

Underwater acoustic positioning systems were developed initially for the offshore oil and gas industry to position drilling rigs and bury pipelines on the correct route to land. Eventually, the technology became available on the commercial market, and early scientific applications included acoustically monitoring positioning of deep-sea sledges and submersibles with spatial resolutions of 5–10 m (Phillips et al., 1979). Acoustic positioning systems have been limited to deployment on large deep-sea vehicles, such as the ANGUS sledge (Phillips et al., 1979), which have sufficient payload capability to carry the large beacons required to detect the acoustic signals. Accurate acoustic positioning of vehicles in shallow water is more complicated than in deep water because of interference of the acoustic signal by reflection from the water surface as well as the seabed, while changes in salinity around estuaries affect the speed of sound through water.

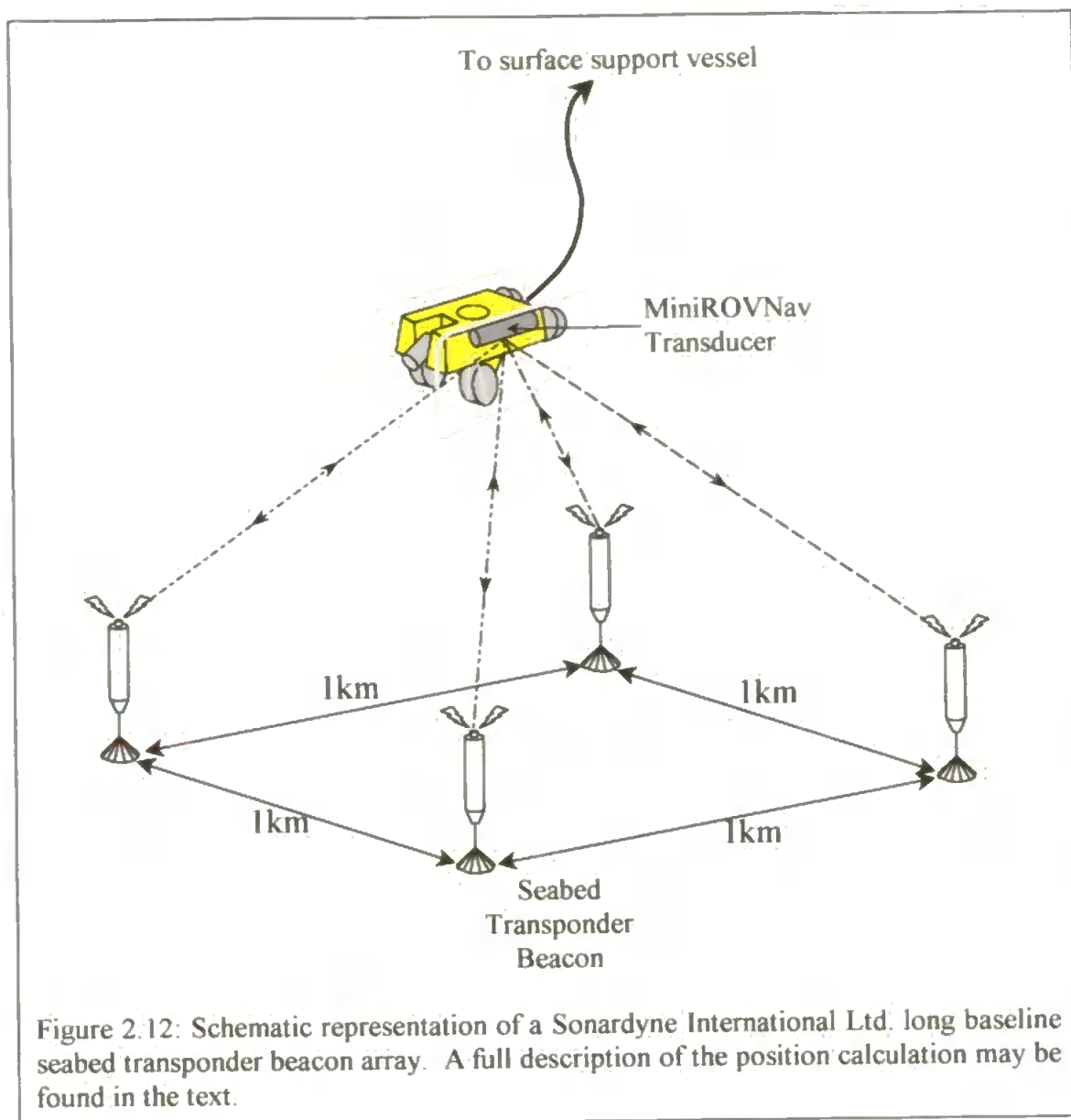
An underwater acoustic positioning system was developed for this project in collaboration with Sonardyne International Ltd., who have miniaturised the hardware for deployment on

smaller underwater vehicles. The use of an acoustic positioning system in shallow water is complicated by multiple reflections of the acoustic signal between the seabed and water surface and by salinity fluctuations which affect the velocity of the acoustic signal. However, advanced software has been designed to overcome the problems associated with shallow-water operations. Beacon arrays may be deployed in a variety of configurations, and these will be described and discussed in the following section.

#### *2.4.2.1 Long Base Line systems*

A long base line (LBL) acoustic positioning system may be sub-divided into two different elements. The first element consists of an array of acoustic transponder beacons moored in fixed locations on the seabed; the second element consists of an acoustic transducer and transceiver attached to the vehicle to be tracked (Fig. 2.12). The vehicle-mounted transducer emits a brief acoustic signal that is detected by the transponder beacons, prompting a unique acoustic signal in response. The vehicle-mounted transceiver records the time between transmission of the initial signal and receiving the response signal, and estimates the distance to each beacon based on the speed of sound through water.

In theory, vehicle navigation may be achieved using two seabed transponders, although vehicle depth must be assumed and there may be ambiguity as to which side of the base line (a line drawn between the beacons) the vessel is positioned. Three transponder beacons allow unambiguous navigation in three dimensions, while four beacons introduce a degree of redundancy that may be used to check the navigation quality.

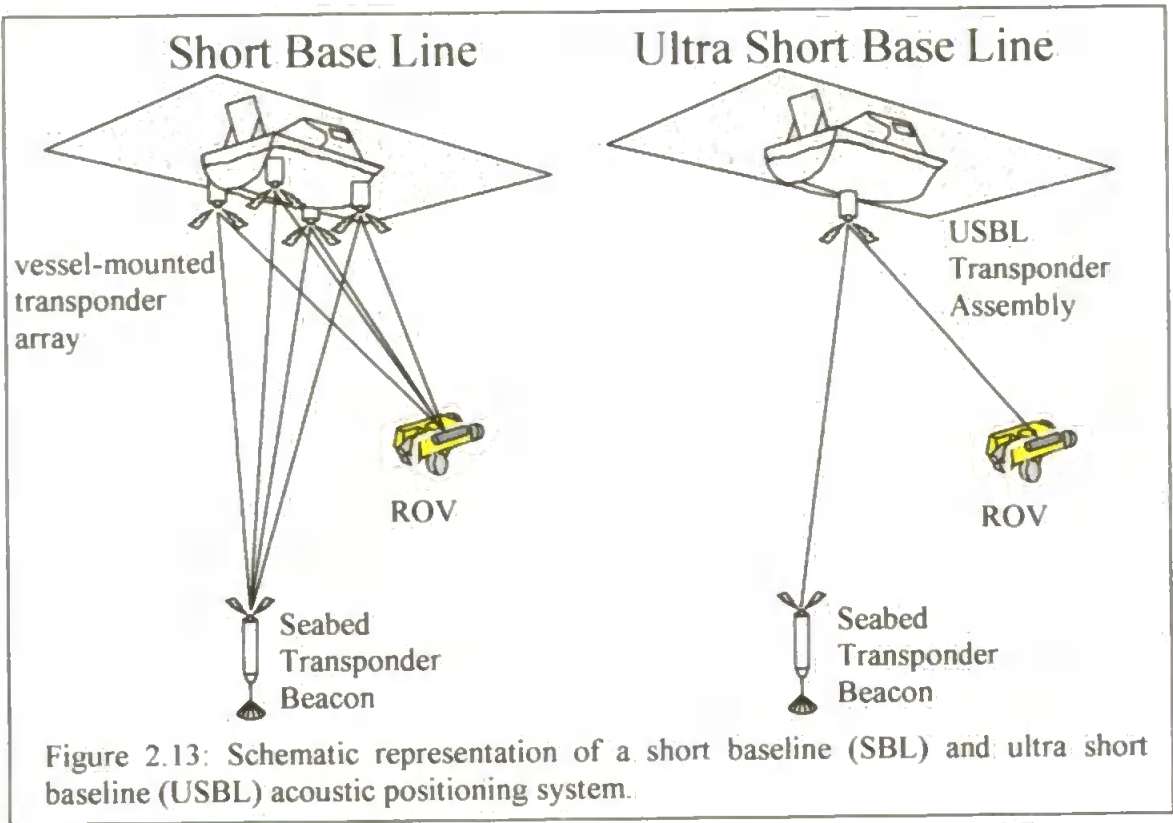


#### 2.4.2.2 Short (SBL) and Ultra Short Baseline (USBL) systems

The typical separation between each seabed transponder beacon in a long base line array may be one kilometre. The same principles of position fixing may be applied to short and ultra short base line arrays. Usually, short base line arrays are mounted on a vessel, such that transponder separation is as large as possible within the confines of the vessel itself (e.g. bow and stern). A single seabed acoustic beacon provides the origin from which vessel position may be calculated, while the short base line is used to calculate the position of deployed equipment. The ultra short base line system is similar to the short base line,

except that the separate transponder beacons are built into a single transponder assembly.

(Fig. 2.13)



Long base line arrays offer two significant advantages over either short or ultra-short arrays, despite requiring more hardware deployment. The large size of a long base line array allows position calculations to be much more accurate than are possible using short- and ultra-short baseline arrays. In addition, with long base line arrays, the tracked vessel is positioned directly within a fixed co-ordinate frame, while vessel movement affects the SBL and USBL co-ordinate frames.

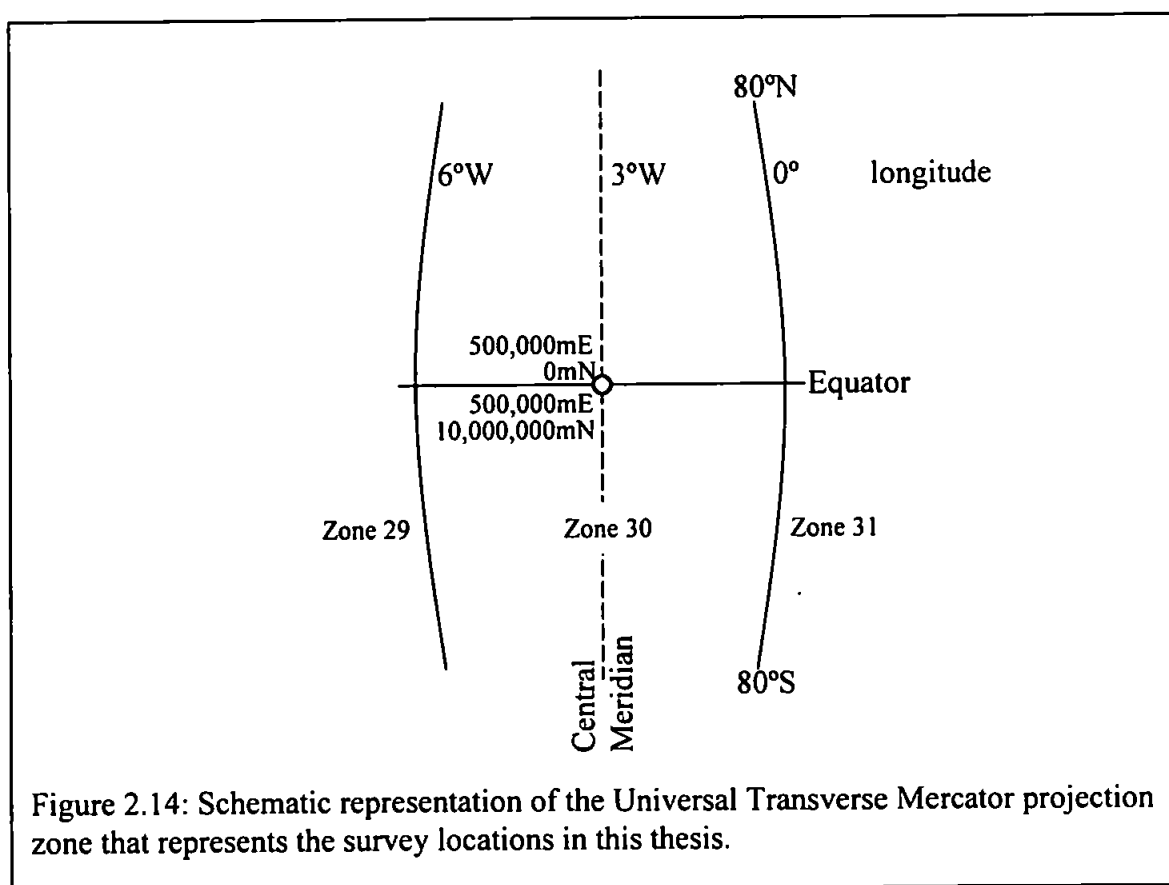
### 2.4.3 *PharosLite* navigation system

The *PharosLite* underwater navigation system was designed and constructed by Sonardyne International Ltd. for use in the offshore market. During the course of the present project, the system was tested thoroughly under controlled conditions at the Sonardyne Sea Trials Centre in Plymouth. The first field deployments of the *PharosLite* system resulted in navigation of the Phantom ROV along predefined survey lines in Plymouth Sound. These



surveys provided the data that constitute the investigation of spatial and temporal variation of a megafaunal assemblage in Plymouth Sound (Chapter 4).

The *PharosLite* system uses a long base line acoustic transponder array, the position of which is calibrated with a Differential Global Positioning System (DGPS) receiver. Vessel navigation is managed through *PharosLite* software, which calculates the position of one or more tracked vehicles in Universal Transverse Mercator (UTM) units. The Universal Transverse Mercator is a projection in which the Earth's surface is separated into sixty zones each corresponding to 6° longitude; these are subdivided into north or south hemisphere, and extend from the equator to 80° latitude. All positions are expressed in a metric co-ordinate system that originates from the intersection between the equator and the central meridian of each zone. The origin of each zone is given an Easting value of 500,000 m to ensure that all co-ordinates are positive, while the Northing value is 0 m for working north of the equator and 10,000,000 m for zones south of the equator (Smith, 1997). Accordingly, the majority of the United Kingdom lies in zone 30 North (Fig. 2.14).



The *MiniROVNav* transceiver interrogates all the seabed transponder beacons, measuring the ranges to each beacon, to calculate vehicle position every three seconds. The *PharosLite* software uses an advanced Kalman filter, which is a series of complex equations that combine all available measurement data, plus prior knowledge about the array and measuring devices, to produce an estimate of position in such a manner that the error is minimised statistically (Maybeck, 1979). *PharosLite* converts the position calculations into a graphical representation of all vehicles and beacons in the array, along with range lines and the status of the range measurements being used, while the estimated position error is represented by an error ellipse surrounding the vehicle icon (Fig. 2.15). Additional ROV compass information may also be included such that the vehicle orientation is incorporated in the display to assist with guidance of the vehicle.

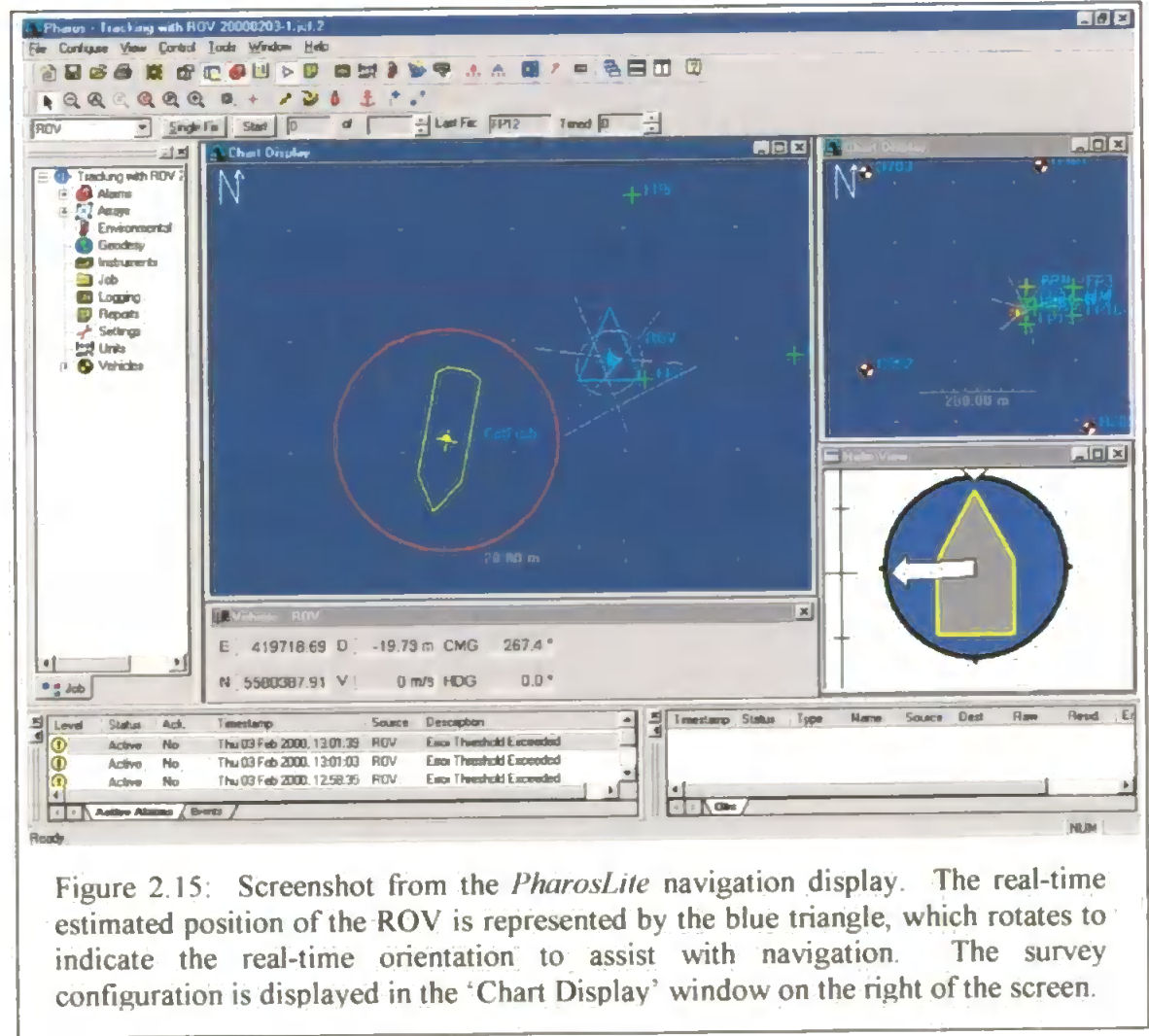


Figure 2.15: Screenshot from the *PharosLite* navigation display. The real-time estimated position of the ROV is represented by the blue triangle, which rotates to indicate the real-time orientation to assist with navigation. The survey configuration is displayed in the 'Chart Display' window on the right of the screen.

Survey configurations may be constructed to allow real-time guidance along transects to arrive at certain waypoints or avoid known obstacles. Although all position data are stored as a Microsoft® Access™ database, the software also generates a data string containing time and position co-ordinates in real-time, which may be overlaid onto the video monitor and recorded onto the videotape.

## 2.5 CONCLUSIONS

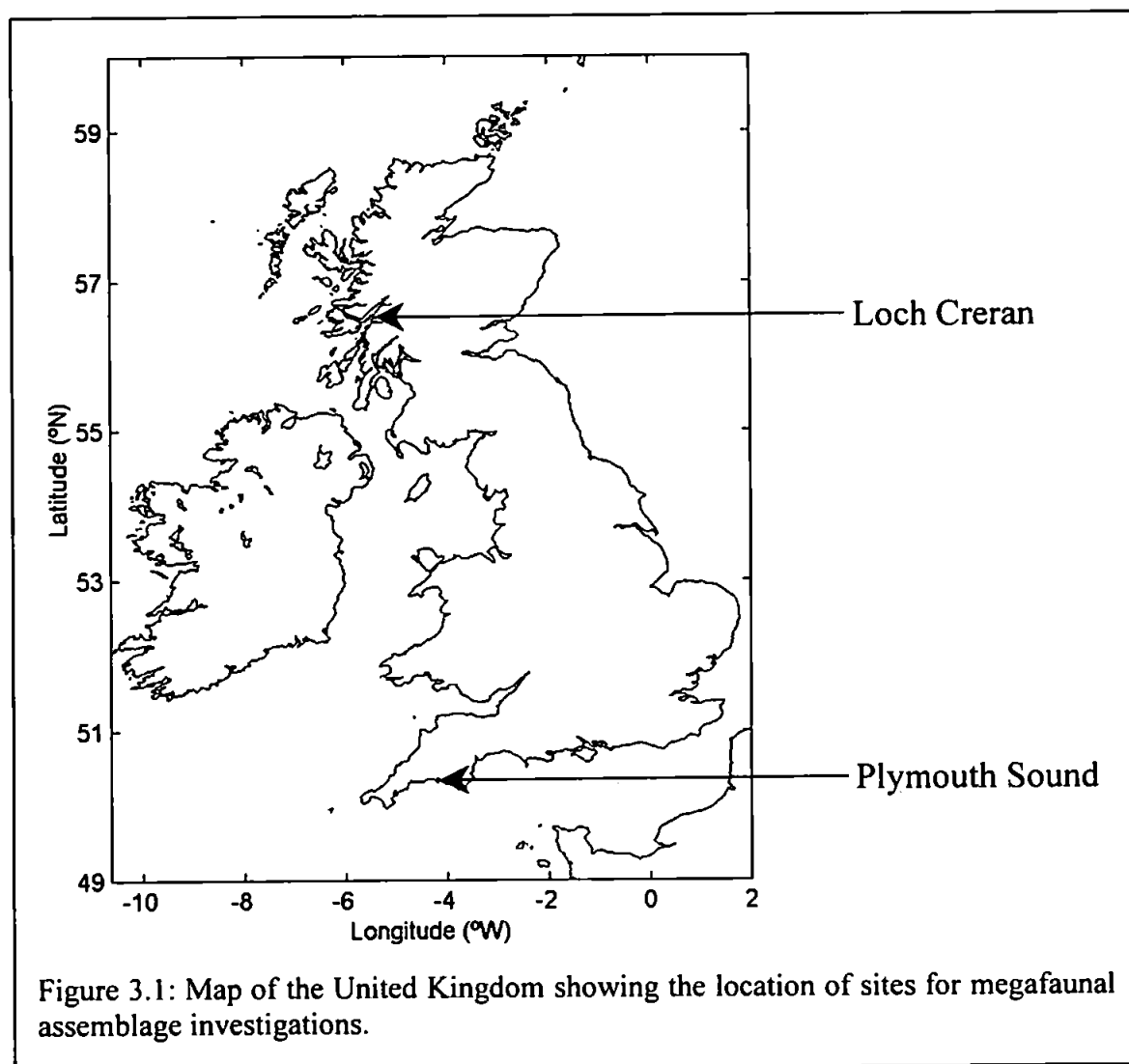
The Automated Benthic Image Scaling System (ABISS) allows quantification of scale within remotely collected images, while the location from which remote images were collected may be derived from the Sonardyne International underwater acoustic positioning system. These technological developments allow collection of quantitative images by remotely operated vehicles with greater spatial resolution than previously possible. The benchmark for quantification of megafaunal biotic features is direct observation by divers. Consequently, remotely collected data must be validated against data from direct diver observations before being used with confidence to extend biological surveys to greater depths and to wider applications than divers may achieve. In the following Chapter, the validity of remotely collected data was assessed by comparing estimates of megafaunal abundance and spatial distribution from fixed locations in Loch Creran and Jennycliff Bay derived from ROV and direct diver observations.

## **CHAPTER 3**

### **Description of megafaunal assemblage survey sites**

### 3.1. INTRODUCTION

The Remotely operated vehicle (ROV) and diver observations of megafaunal assemblages reported in this thesis were carried out at two locations that support different megafaunal densities; Jennycliff Bay in Plymouth Sound on the south-west coast of England and Loch Creran on the west coast of Scotland (Fig. 3.1).



### 3.2 JENNYCLIFF BAY, PLYMOUTH SOUND

#### 3.2.1 Physical characteristics

Plymouth Sound is an enclosed and sheltered ria formed by the submergence of the River Tamar, which currently discharges into it from the west (Marine Biological Association, 1957). A second tidal river, the River Plym, discharges into the Sound from the east (Fig. 3.2). The Sound and its estuaries have been designated a Special Area of Conservation

(SAC) under the Habitats Directive (Council of the European Communities, 1992) due to the high diversity of habitats and communities in the area. Jennycliff Bay (50°21.0' N, 04°07.8' W) is located on the eastern side of Plymouth Sound, where water depth varies between 10–15 m below chart datum. The substratum in Jennycliff Bay has been described as a “*fairly extensive stretch of sandy mud*” (Marine Biological Association, 1957) and classified as apparently homogeneous muddy sand, using side-scan sonar (Moore et al., 1999). Mean spring and neap tide ranges are 4.7 and 2.2 m respectively (The Hydrographic Office, 1991). Tidal flow on the flood tide is north-north-westerly and south-south-westerly on the ebb tide, with maximum spring tidal currents reaching 0.6 knots (The Hydrographic Office, 2001). The water temperature, monitored at station L2 (50°19.8' N, 04°10.2' W, Fig. 3.2), has a seasonal range from approximately 10–15 °C (Siddorn et al., submitted).

### 3.2.2 Biological characteristics

The most abundant species collected by trawls and dredges in Jennycliff Bay are *Philine* sp., the netted dog whelk (*Nassarius [=Hinia] reticulatus*), the little cuttlefish (*Sepiola atlantica*) and the amphipod *Gammarus locusta* (Marine Biological Association, 1957). The macrofaunal assemblage, sampled by grabs and cores, is dominated by sedentary polychaete taxa such as cirratulids, maldanids and the highly abundant ampharetid *Mellina palmata* (Gibbs, 1969; Parry et al., 1999). The sediment within Jennycliff Bay is highly bioturbated and covered with mounds of sediment ejected from the burrows of thalassinidean shrimps (Kendall and Widdicombe, 1999), but trawling and dredging techniques used in the Plymouth Marine Fauna (Marine Biological Association, 1957) may not describe adequately the megafaunal assemblage.

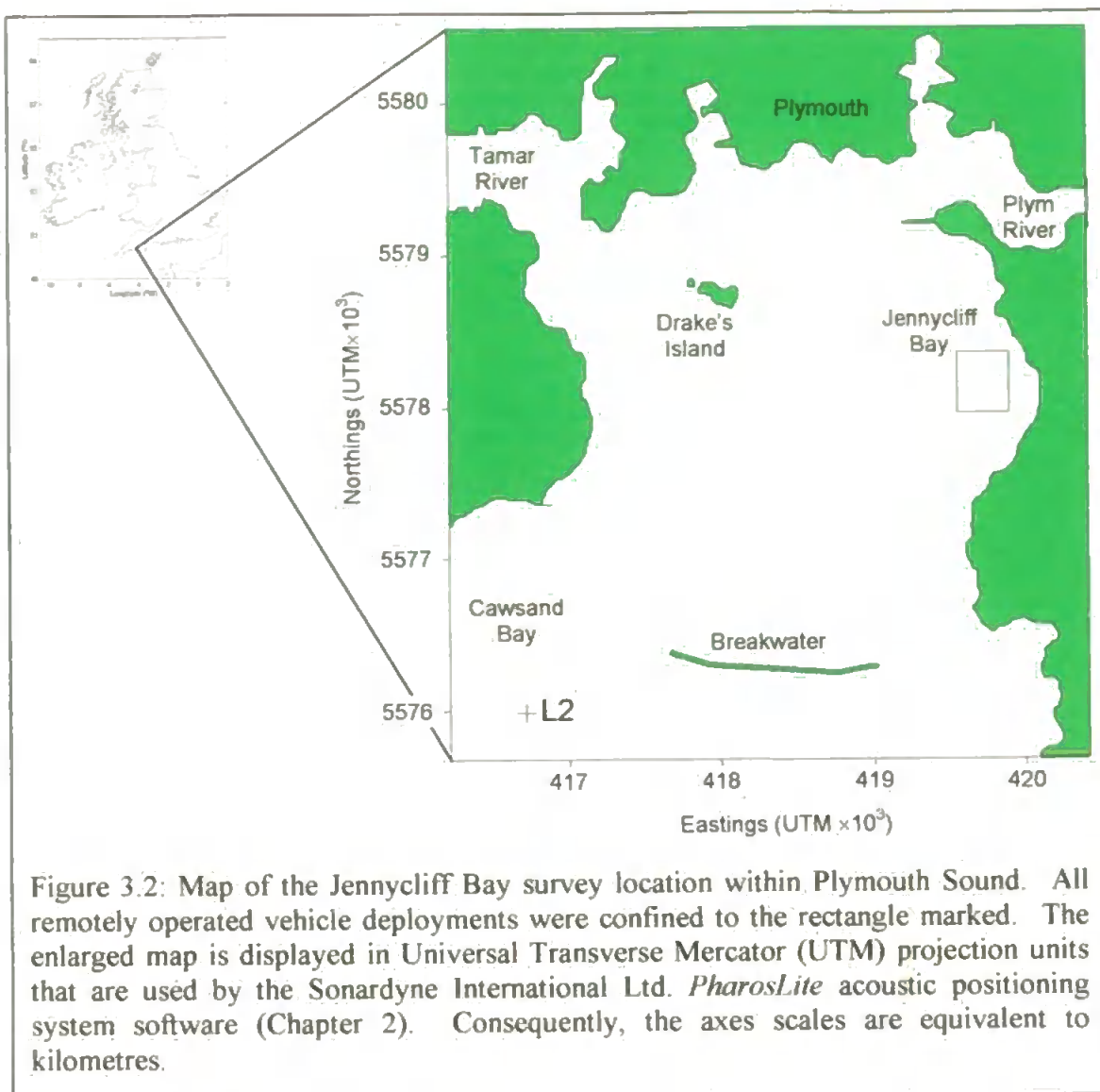


Figure 3.2: Map of the Jennycliff Bay survey location within Plymouth Sound. All remotely operated vehicle deployments were confined to the rectangle marked. The enlarged map is displayed in Universal Transverse Mercator (UTM) projection units that are used by the Sonardyne International Ltd. *PharosLite* acoustic positioning system software (Chapter 2). Consequently, the axes scales are equivalent to kilometres.

Megafaunal-sized individuals have been collected using boxcores of  $0.1 \text{ m}^2$ . The most abundant megafaunal species collected include thalassinidean mud shrimps (*Upogebia deltaura* and *Callianassa subterranea*); the angular crab *Goneplax rhomboides* and several large infaunal bivalve species. The razor shell (*Phaxas pellucidus*) is common in Jennycliff Bay, while the prickly cockle (*Acanthocardia echinatum*), common otter shell (*Lutraria lutraria*) and the blunt gaper (*Mya arenaria*) may be found commonly on similar sediment types inside and outside of the Sound (Marine Biological Association, 1957).

### 3.2.3 Sediment resuspension

Tidal currents may affect underwater observations by resuspending sediment that may obscure the seabed. In addition to resuspension of sediment, tidal currents may resuspend newly-settled megafaunal individuals, such as infaunal bivalves (Norkko et al., 2001), which may influence the spatial distribution of adults. The dynamics of cohesive sediments may be described by the bed shear stress ( $\tau_c$ ) which measures the force required to erode particles from the seabed, and by current shear stress ( $\tau_0$ ) which measures the force exerted by water currents on the seabed. Hence, sediment resuspension occurs only when current shear stress exceeds bed shear stress.

Current shear stress ( $\tau_0$ ) is a function of water density, current speed and may be expressed as follows:

$$\tau_0 = \rho_w \times C_D \times \langle \bar{u} \rangle^2 \quad \text{Equation 1}$$

where  $\rho$  is water density ( $\text{kg.m}^{-3}$ ),  $C_D$  is drag coefficient and  $\langle \bar{u} \rangle^2$  is the depth mean averaged water current ( $\text{m.s}^{-1}$ ) (Soulsby, 1997).

#### 3.2.3.1 Drag coefficient, $C_D$

The drag coefficient ( $C_D$ ) measures the friction generated as the water current passes over the seabed and is defined as follows:

$$C_D = 2 \frac{\kappa^2}{\left( \ln \left( \frac{30h}{z_0} - 1 \right) \right)^2} \quad \text{Equation 2}$$

where  $\kappa$  is the Von Karman constant ( $\sim 0.4$ ),  $h$  is the water depth (m) and  $z_0$  is the bed roughness (m) (Dyer, 1986).

The bed roughness parameter ( $z_0$ ) is a function of the sediment granulometry at a site and may be defined, for a flat substratum, as follows:



$$\text{Bed roughness, } z_0 = \frac{\text{median sediment grain diameter}}{15} \quad \text{Equation 3}$$

(Dyer, 1986)

The median diameter of sediment grains in Jennycliff Bay was  $3.87 \pm 0.11\phi_w$  (Parry et al., 1999), which corresponds to a median diameter of approximately 0.062–0.088 mm (Buchanan, 1984). Therefore, the maximum and minimum values of drag coefficient associated with Jennycliff Bay sediment may be calculated as follows:

$$\text{Maximum bed roughness} = \frac{0.088 \times 10^{-3}}{15} = 5.9 \times 10^{-6} \text{ m} \quad \text{Equation 4}$$

$$\text{Minimum bed roughness} = \frac{0.062 \times 10^{-3}}{15} = 4.1 \times 10^{-6} \text{ m} \quad \text{Equation 5}$$

The water depth in Jennycliff Bay varies between 10–15 m below chart datum, so maximum and minimum values of drag coefficient may be derived by substituting the result of Equations 4 and 5 into Equation 2 as follows:

$$\text{Maximum } C_D = 2 \frac{0.4^2}{\left( \ln \left( \left[ \frac{30 \times 10}{5.9 \times 10^{-6}} \right] - 1 \right) \right)^2}$$

$$\text{Maximum } C_D = 2 \frac{0.4^2}{17.7^2} = 1.01 \times 10^{-3} \quad \text{Equation 6}$$

Similarly, 
$$\text{Minimum } C_D = 2 \frac{0.4^2}{\left( \ln \left( \left[ \frac{30 \times 15}{4.1 \times 10^{-6}} \right] - 1 \right) \right)^2}$$

$$\text{Minimum } C_D = 2 \frac{0.4^2}{18.5^2} = 0.93 \times 10^{-3} \quad \text{Equation 7}$$

### 3.2.3.2 Depth mean average water current ( $\langle \bar{u} \rangle$ )

The depth mean averaged water current,  $\langle \bar{u} \rangle$ , may be estimated using:

$$\langle \bar{u} \rangle = \text{surface water velocity} \times 0.934 \quad \text{Equation 8}$$

(Soulsby, 1997)

In Jennycliff Bay, maximum tidal current reaches 0.6 knots between 4–5 hours after high spring tides (The Hydrographic Office, 1991). Using the conversion of 1 knot = 0.514 m.s<sup>-1</sup>:

$$\text{Maximum surface current} = 0.514 \times 0.6 = 0.31 \text{ m.s}^{-1}$$

Therefore, the maximum depth mean averaged tidal current,  $\langle \bar{u} \rangle$  is found as follows:

$$\text{Maximum } \langle \bar{u} \rangle = 0.31 \times 0.934 = 0.29 \text{ m.s}^{-1} \quad \text{Equation 9}$$

### 3.2.3.3 Current shear stress ( $\tau_0$ )

In Jennycliff Bay, the maximum shear stress exerted by the current will occur when maximum depth average current flows in areas where maximum drag coefficient occurs (i.e. shallowest water). The value of maximum current shear stress ( $\tau_0$ ) may be calculated by substituting the results from Equations 6 and 9 into Equation 1 using a standard seawater density,  $\rho_w = 1033 \text{ kg.m}^{-3}$ . Hence:

$$\text{Maximum current shear stress, } \tau_0 = 1033 \times (1.01 \times 10^{-3}) \times 0.29^2$$

$$\text{Maximum current shear stress, } \tau_0 = 0.088 \text{ kg.m}^{-1}.\text{s}^{-2} \quad \text{Equation 10}$$

### 3.2.3.4 Bed shear stress ( $\tau_e$ )

The bed shear stress ( $\tau_e$ ) measures the forces required to erode particles from the sediment surface and varies for different types of substratum. The reference bed shear stress ( $\tau_e$ ) for tidally-deposited coastal and estuarine mud is 0.1–1 kg.m<sup>-1</sup>.s<sup>-2</sup> (Paterson and Black, 1999),

which exceeds the maximum current shear stress in Jennycliff Bay (Equation 10). Therefore, in Jennycliff Bay, sediment resuspension due to water currents is negligible. The reference bed shear stress was calculated for a flat mud substratum, but the presence of burrow openings and mounds increases the complexity of sediment topography, which influences the bed roughness ( $z_0$ ). For topographically complex substrata, bed roughness may be defined as:

$$z_1 = \frac{0.5HS}{\xi} \quad \text{Equation 11}$$

(Lettau, 1969)

where  $H$  is the height (m),  $S$  is the cross-sectional area ( $\text{m}^2$ ) and  $\xi$  is the horizontal area ( $\text{m}^2$ ) of mounds. In the North Sea, the presence of *Callianassa subterranea* mounds provides bed roughness values of 0.0079 m (Rowden et al., 1998), which would increase greatly the maximum drag coefficient ( $C_D$ ) (Equation 6) compared to a flat substratum. Therefore, the current shear stress is greater in the presence of mounds than that of a current of the same velocity flowing over a flat substratum. Hence, current shear stress in the presence of biogenic mounds may exceed the bed shear stress, thereby inducing sediment resuspension. In Jennycliff Bay, the megafaunal assemblage creates a variety of surface mounds, burrow openings and tubes, all of which affect bed roughness, which will influence the physical characteristics of the sediment indirectly.

### 3.3 LOCH CRERAN, WESTERN SCOTLAND

#### 3.3.1 Physical characteristics

Loch Creran ( $56^{\circ}32.9' \text{ N}$ ,  $05^{\circ}16.1' \text{ W}$ ) lies on the west coast of Scotland. It is a double basin sea loch, interconnected at the Creagan Narrows and separated from the Firth of Lorne, by shallow rock sills, which are 3 and 5 m deep respectively (Fig. 3.3). Freshwater run-off to the Upper Basin may affect surface salinity seaward of the Creagan Narrows, but salinity at the seabed is comparable to the open sea in the Firth of Lorne (Gage, 1972). The maximum depth in the Upper Basin is approximately 40 m, while the Lower Basin is divided into four sub-basins, the deepest of which is approximately 46 m. Mean spring and neap tide ranges are 3.3 and 1.1 m respectively (The Hydrographic Office, 1991), producing a maximum spring current velocity of 5 knots at the sills (Gage, 1972). The loch basins have a quiescent hydrodynamic regime, although tidal currents are sufficient to support suspension feeding and to ventilate the bottom waters (Gage, 1972). The water temperature varies from approximately  $6^{\circ}\text{C}$  in February/March to a maximum of  $13\text{--}15^{\circ}\text{C}$  in August/September (Gage, 1972).

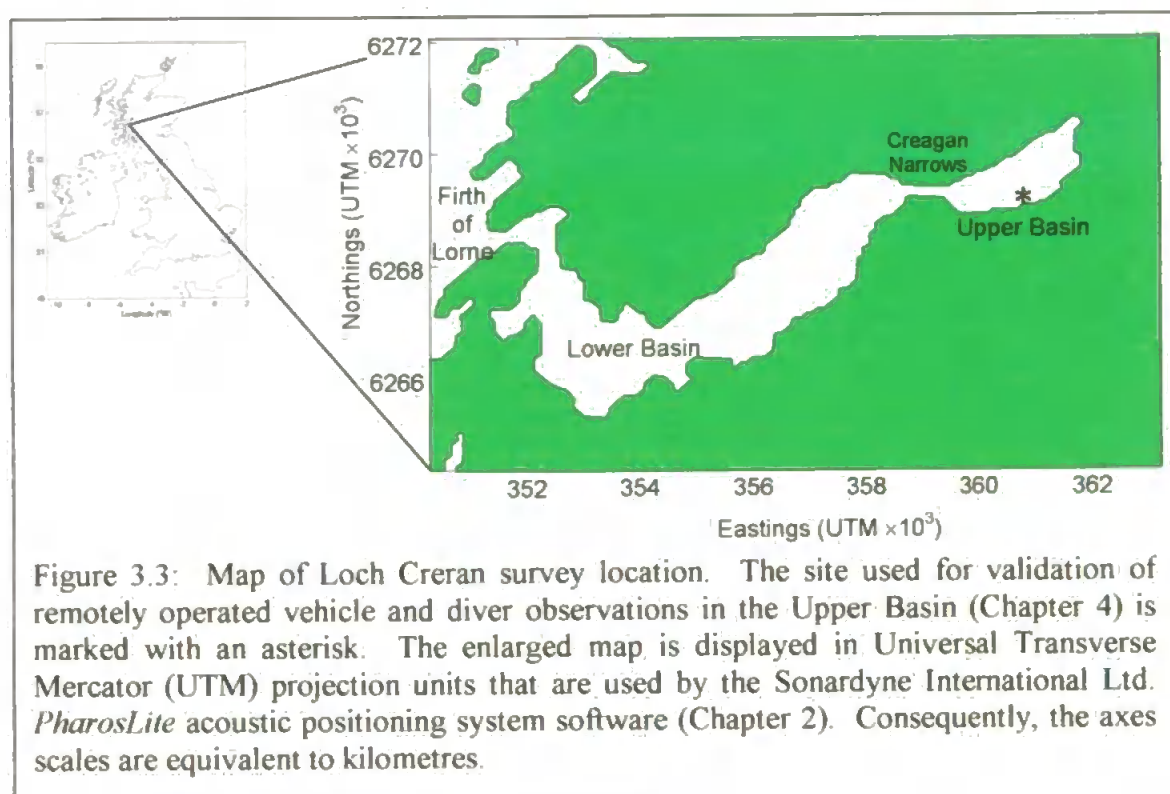


Figure 3.3: Map of Loch Creran survey location. The site used for validation of remotely operated vehicle and diver observations in the Upper Basin (Chapter 4) is marked with an asterisk. The enlarged map is displayed in Universal Transverse Mercator (UTM) projection units that are used by the Sonardyne International Ltd. *PharosLite* acoustic positioning system software (Chapter 2). Consequently, the axes scales are equivalent to kilometres.

Diver and ROV observations were limited to the Upper Basin. The survey site was approximately 50 m from the southern shore, and the substratum was muddy sand (Gage, 1974) lying at a depth of 15–20 m below chart datum (Fig. 3.3).

### 3.3.2 Biological characteristics

The benthic fauna of the Upper Basin has, thus far, received little attention (Nickell [Dunstaffnage Marine Laboratory], pers. comm.). However, the Upper Basin is known to support low densities of large megafaunal species such as the Norway lobster (*Nephrops norvegicus*), the echiuran worm *Maxmuelleria lankesteri* and the sea pen *Virgularia mirabilis* (Nickell [Dunstaffnage Marine Laboratory], pers. comm.). Macrofaunal abundance may be low (Kendall [Plymouth Marine Laboratory], pers. com.).

### 3.3.3 Sediment resuspension

In the Upper Basin of Loch Creran, the substratum was similar to that at Jennycliff Bay, so the bed shear stress ( $\tau_e$ ) will be approximately  $0.1\text{--}1 \text{ kg.m}^{-1}.\text{s}^{-2}$  (Patterson and Black, 1999). At the Loch Creran survey site, the current velocity was lower than at Jennycliff Bay; hence, depth mean averaged current ( $\langle \bar{u} \rangle$ ) will be lower than at Jennycliff Bay. In addition, the Loch Creran survey site was deeper than Jennycliff Bay, which will reduce the drag coefficient,  $C_D$ . The reduced magnitude of  $\langle \bar{u} \rangle$  and  $C_D$  will interact, so that current shear stress ( $\tau_0$ ) in the Upper Basin of Loch Creran will be less than in Jennycliff Bay. Therefore, there will be no erosion of sediment in the Upper Basin of Loch Creran due to water currents because current shear stress will not exceed bed shear stress.

The validity of megafaunal abundance estimates derived from ROV observations was tested by assessing the agreement between abundance estimates derived from direct diver observations at marked sites within both locations (Chapter 4). The spatial and temporal distribution patterns within the megafaunal assemblage were quantified for Jennycliff Bay only (Chapter 5). Similarly, assessment of megafaunal biomass through estimation of the common otter shell (*Lutraria lutraria*) biomass was performed in Jennycliff Bay only (Chapter 6).

## **CHAPTER 4**

### **Validation of megafauna abundance data derived from remote (ROV) and direct (diver) observations**

Sections of this chapter are contained in:

Parry, D.M., Nickell, L.A., Kendall, M.A., Burrows, M.T., Pilgrim, D.A., Jones, M.B. (2002) Comparison of abundance and spatial distribution of burrowing megafauna from diver and Remotely Operated Vehicle observations. *Marine Ecology Progress Series*, **244**, 89–93.

## ABSTRACT

The standard method for collecting information on the abundance and distribution of surface-dwelling megafauna and biotic sediment features associated with burrowing megafauna has been direct observation and counting by divers. However, remote observations allow information comparable to diver observations to be applied to investigations at greater depths and over wider spatial extents than divers may achieve. The present chapter compares abundance estimates of megafaunal biotic sediment features obtained from diver and remotely operated vehicle-mapping techniques. Results show strong agreement between abundance estimates, providing assurance that remote observation techniques are not subject to systematic errors in estimation of feature abundance.



## 4.1 INTRODUCTION

A number of hypotheses that explain the role of disturbance on the structure and maintenance of biodiversity in natural assemblages (Connell, 1978; Huston, 1979; Brenchley, 1981; Grassle and Morse-Porteous, 1987) were discussed in Chapter 1. The mechanisms and effects of disturbance caused by bioturbation (i.e. burrowing activity of large individuals), have received much attention (e.g. Suchanek, 1983; Suchanek and Colin, 1986; Posey et al., 1991; Valentine et al., 1994). The disproportionately large effect of burrowing animals, relative to their abundance, on assemblage structure has led to these organisms being considered as 'ecosystem engineers' (Jones et al., 1994). Although the disturbance hypotheses are based on the amplitude and frequency of disturbance, the mode of bioturbation by different engineering species may elicit different community responses (Widdicombe et al., 2000). Consequently, it has been suggested that quantification of the identity, abundance and spatial distribution of bioturbating species will enable greater understanding of the dynamics of soft-sediment assemblages (Widdicombe, 2001) and may be used as a surrogate for quantitative predictions of macro- and meiofaunal diversity patterns (Thrush et al., 2001). Unfortunately, the grain of traditional grab and core sampling significantly underestimates the abundance of megafaunal bioturbating organisms (Kendall and Widdicombe, 1999), while many bioturbating species bury deeper into the sediment than grabs and cores can penetrate. Consequently, alternative methods are required to accurately sample this important fraction of the benthic fauna.

As many bioturbating species construct burrows and tubes that produce characteristic openings or features on the sediment surface (e.g Nash et al., 1984; Atkinson and Nash, 1990; Atkinson et al., 1998), direct observations by SCUBA divers of surface openings and features may be used to infer abundance and local distributional patterns of the bioturbating species responsible for their construction. The scale of such observations, however, is not appropriate for monitoring and prediction of larger-scale (hundreds to

thousands of metres) diversity patterns (Constable, 1999). The use of underwater cameras permit observation of surface features and burrow openings without the constraints of depth and deployment time associated with SCUBA diving. Although underwater cameras may be deployed on a variety of platforms (Chapter 1), deployment on remotely operated vehicles (ROV) provides non-destructive sampling with greater control of observations than possible with cameras mounted on towed vehicles. Before remote observations may be used with confidence to investigate larger-scale (100s of metres) megafaunal spatial distribution patterns, a comparison between remote observations and the current standard method of diver observations is required.

In the present chapter, ROV techniques were compared with direct diver observation by recording all megafaunal features within the same clearly defined plots from two shallow subtidal soft sediment environments. The validity of data extracted from each observation method was assessed by comparing diver and ROV-derived estimates of:

- a) total feature abundance,
- b) feature identification, and
- c) spatial coincidence between estimates.

## 4.2 MATERIALS AND METHODS

### 4.2.1 Site description

The identity and location of biotic features within survey plots were mapped in Jennycliff Bay, Plymouth Sound (50°21.0'N 04°07.8'W) and Loch Creran, Scotland (56°32.9'N 05°16.1'W) on 31<sup>st</sup> May and 26<sup>th</sup> July 2000 respectively. A full description of the survey sites may be found in Chapter 3.

#### 4.2.2 Survey design

Four plots were established at 10–15 m depth at both locations. These locations were chosen because they supported different megafaunal species and different densities of surface features. Each plot consisted of a 3×3 m steel frame subdivided into a grid of thirty-six 50×50 cm quadrats to assist with feature mapping. The plots were fixed by embedding the steel legs, at each corner of the frame, firmly into the sediment. All surface dwelling megafauna and megafaunal biotic sediment features, including burrow openings, mounds and tubes were counted and their position within each plot recorded by divers and ROV observations. The identity of the species responsible for burrow construction was determined wherever possible using the morphological characteristics of burrows described by Marrs et al. (1996). Divers mapped onto slates the identity and location of biotic features within survey plots, while similar maps were generated from the videotape that was recorded as the ROV was flown over the same area. The interval between diver and ROV surveys in Loch Creran was 5 days, while at Jennycliff Bay, plots were surveyed by both techniques within 1 hour.

Since the ROV camera was fitted with the ABISS structured lighting array that permits image scaling (Pilgrim et al., 2000; Chapter 2), still images were selected and captured from the videotape, such that the entire survey plot was represented and allowed measurement of all the biotic features observed.

The diver and ROV feature maps were digitised using *Scion Image* software (Scion Corporation, USA) and *Surfer 6.03* software (Golden Software Inc., USA), from which grid co-ordinates of biotic features were extracted. The dimensions of features contained in the diver maps were extracted using *Scion Image* software, while dimensions of features appearing in the ROV-derived maps were measured from the corresponding still images using *Benthic Imager* software.

### 4.2.3 Data analysis

Total biotic feature abundance estimates for each survey plot were derived from diver and ROV observation techniques by aggregating the abundance estimate of each biotic feature type from each grid cell of the relevant survey plot. In order to assess the ability to detect different size fractions of the megafauna using each observation technique, total megafaunal abundance data for each plot were subdivided to calculate abundance estimates of 'conspicuous feature' and 'all features greater than 15 mm diameter' groups for each survey plot. The 'conspicuous feature' group consisted of the Norway lobster (*Nephrops norvegicus*), echiuran worm (*Maxmuelleria lankesteri*), sea pen (*Virgularia mirabilis*), polychaete worm (*Myxicola infundibulum*), funnel-shaped openings and large circular holes without a funnel. Megafaunal features were assigned to the 'features greater than 15 mm diameter' group for both diver and ROV observations using feature measurements extracted from *Scion Image* or *Benthic Imager* software respectively (Section 4.2.2). The abundance estimates of features detected by each method in each survey plot were compared using a non-parametric Wilcoxon signed rank test.

Analyses were performed at a range of sample grain sizes, which were obtained by aggregating adjacent grid cells (to give sample grains of 0.5 and 1.0 m<sup>2</sup>), to investigate whether larger samples minimise errors due to parallax. The extent of agreement between diver and ROV-derived estimates of biotic feature abundance was examined using the Bland and Altman method, a descriptive technique in which the difference between abundance estimates was plotted against the mean of the two estimates for each sample (Bland and Altman 1986). The difference between estimates was calculated by subtracting the diver abundance estimate from the ROV abundance estimate; hence positive values indicate that more features were observed in ROV images. The Bland and Altman method was preferred to product-moment correlation as it indicates the extent of bias (the average difference between estimates) rather than demonstrating covariance; it is also independent

of the range of the data (Bland and Altman 1986). Limits of agreement between diver and ROV estimates were calculated using two standard deviations of the mean difference between estimates (Bland and Altman, 1986).

### 4.3 RESULTS

The combination of high feature density in Jennycliff Bay and restricted time for SCUBA diving limited the investigation by both diver and ROV to a single survey plot at this location. However, the lower density of features in Loch Creran allowed all four plots to be surveyed by both diver and ROV in the available time. Therefore, the results from each location are presented separately.

#### 4.3.1 Loch Creran

##### 4.3.1.1 Abundance estimates

In Loch Creran, abundance estimates of total biotic features, conspicuous megafaunal features and features greater than 15 mm diameter, made from direct diver observations and from ROV images, were not significantly different at the scale of the entire survey plot (Table 4.1).

Table 4.1: Mean abundance estimates of biotic features derived from direct diver and remotely operated vehicle observations of Loch Creran survey plots (sample grain = 9 m<sup>2</sup>). Significant differences tested with non-parametric Wilcoxon signed rank test; *p*-values in parentheses. N=4.

	Total biotic features	Conspicuous megafaunal features	Features greater than 15 mm diameter
Diver ±95% CI	70.8 ±7.8	29.5 ±7.2	64.0 ±8.0
ROV ±95% CI	65.8 ±6.7	25.8 ±7.9	32.0 ±8.3
Wilcoxon signed rank test statistic	0.55 (0.58)	1.28 (0.20)	1.64 (0.10)

#### 4.3.1.2 Spatial coincidence

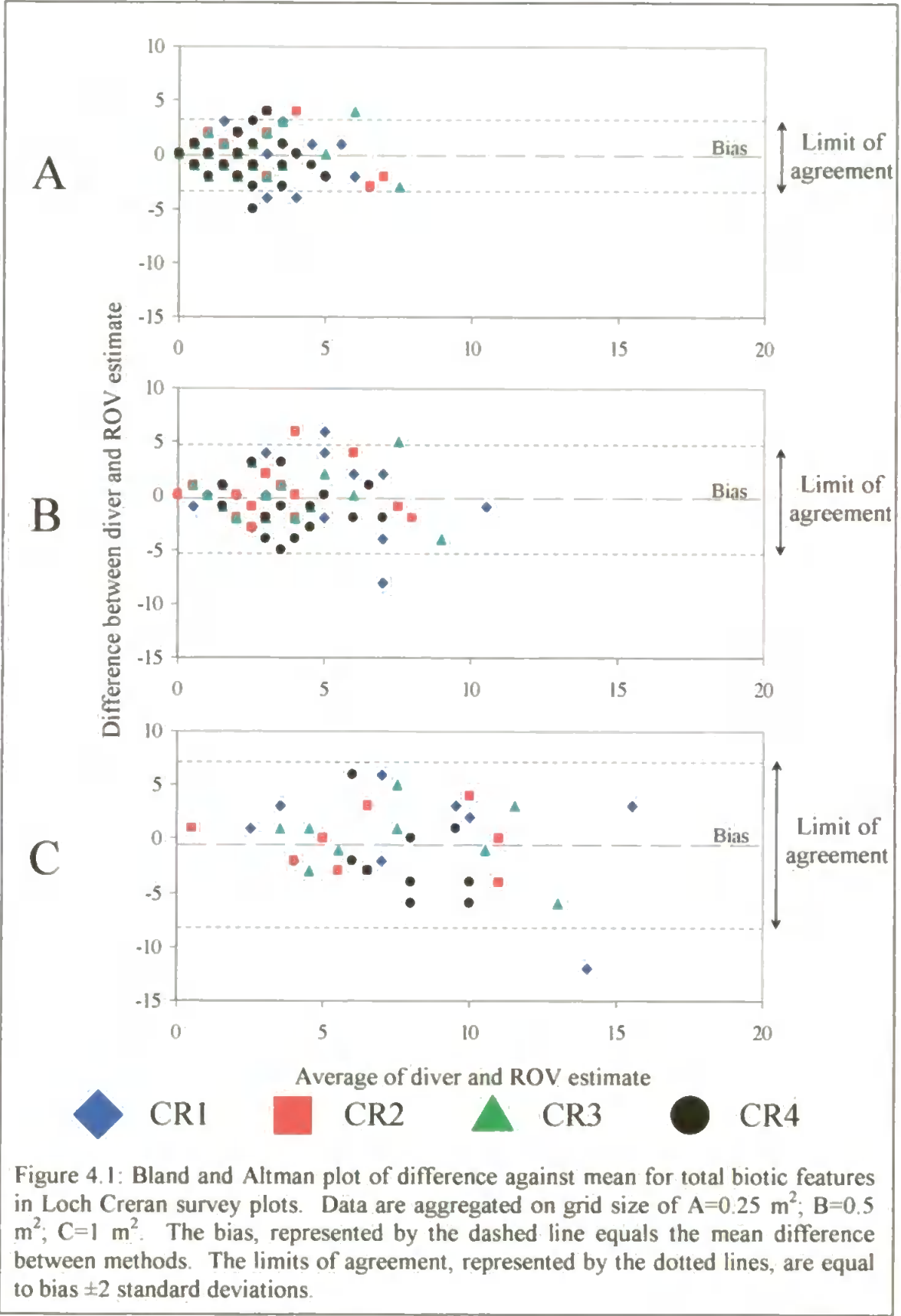
There was no significant bias between diver and ROV estimates of total biotic features or conspicuous megafaunal features, yet ROV estimates of features greater than 15 mm diameter were significantly lower than diver estimates for sample grains of 0.25, 0.5 and 1.0 m<sup>2</sup> (Table 4.2). Increasing grid cell size caused the limits of agreement between diver and ROV estimates of total biotic feature abundance to increase, while the number of data points that fell outside the limits of agreement decreased (Fig. 4.1). The majority of data points that fell outside the limits of agreement at the smallest grid cell size converged on the mean difference between estimates as grid cell size increased, indicating that parallax at the edges of grid cells was the major cause of variation between estimates.

Table 4.2: Mean bias ( $\pm$  95% CI) between abundance estimates derived from diver and ROV observations of Loch Creran survey plots. Negative values indicate that ROV estimates were less than diver estimates. Differences tested using Wilcoxon signed rank; ns:  $p > 0.05$ ; \*\*  $p < 0.01$ .

Quadrat size (m <sup>2</sup> )	N	Total biotic features	Conspicuous megafauna features	Features greater than 15 mm diameter
0.25	144	$-0.14 \pm 0.3^{ns}$	$-0.10 \pm 0.1^{ns}$	$-0.89 \pm 0.2^{**}$
0.5	72	$-0.28 \pm 0.6^{ns}$	$-0.21 \pm 0.2^{ns}$	$-1.78 \pm 0.4^{**}$
1	36	$-0.56 \pm 1.3^{ns}$	$-0.42 \pm 0.4^{ns}$	$-3.56 \pm 1.0^{**}$
9	4	$-5.00 \pm 14.4^{ns}$	$-3.75 \pm 5.6^{ns}$	$-32.0 \pm 10.5^{ns}$

Since data points that remained outside the limits of agreement represented either the effects of parallax at the edges of the 1 m<sup>2</sup> quadrat, or a real discrepancy between identification of megafaunal features, closer examination of the raw data was required. Tracking data points through the Bland and Altman plots as grid cells were aggregated revealed that the outlying point in Figure 4.1 resulted from the diver observing extra “unidentified holes” in two adjacent 0.25 m<sup>2</sup> cells from plot CR1. The still images

collected from the ROV videotape for the corresponding grid cells were re-analysed, yet the 'missing' features could not be accounted for.



#### 4.3.1.3 Conspicuous features

There was good agreement between diver and ROV estimates of large conspicuous features, with no significant bias between estimates ( $p>0.05$ ) (Fig. 4.2 and Table 4.2). The difference between diver and ROV abundance estimates decreased as grid cells were aggregated, suggesting that most of the variation between estimates may be due to the effects of parallax. Although the limits of agreement increased slightly as grid cells were aggregated, much of this variation was caused by the outlying value from grid CR1. The features that appeared to have been missed by the ROV observations were present in the ROV still images, and all measured less than 15 mm diameter. Consequently, the outlying value was an artefact of the criteria for grouping of features rather than a methodological difference.

#### 4.3.1.4 Features greater than 15 mm diameter

There was a significant negative bias ( $p<0.01$ ) between abundance estimates of features greater than 15 mm diameter derived from ROV observations in comparison to estimates derived from diver observations at sub-grid scales (Table 4.2), suggesting that the ROV consistently failed to detect the smallest megafaunal features. However, diver and ROV estimates of total features and conspicuous feature abundance were not significantly different, suggesting that the apparent differences were caused by differences between feature measurement techniques rather than the ability to detect the features *per se*. The effects of parallax on assigning feature location were evident because the limits of agreement were of the same magnitude as for total biotic feature abundance estimates (Fig. 4.3).



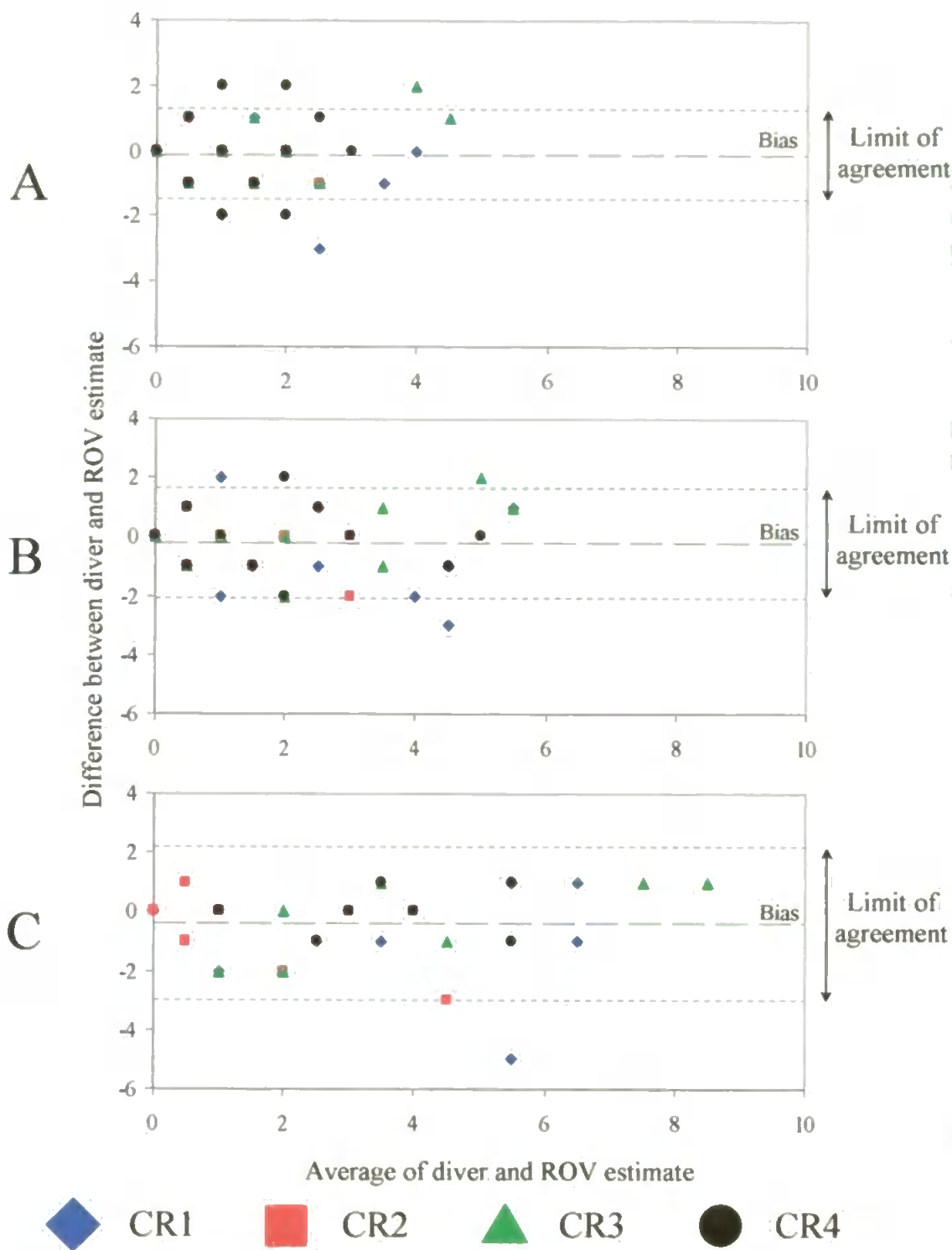


Figure 4.2: Bland and Altman plot of difference against mean for large conspicuous features in Loch Creran survey plots. Data are aggregated on grid size of  $A=0.25 \text{ m}^2$ ;  $B=0.5 \text{ m}^2$ ;  $C=1 \text{ m}^2$ . The bias, represented by the dashed line equals the mean difference between methods. The limits of agreement, represented by the dotted lines are equal to bias  $\pm$  2 standard deviations.

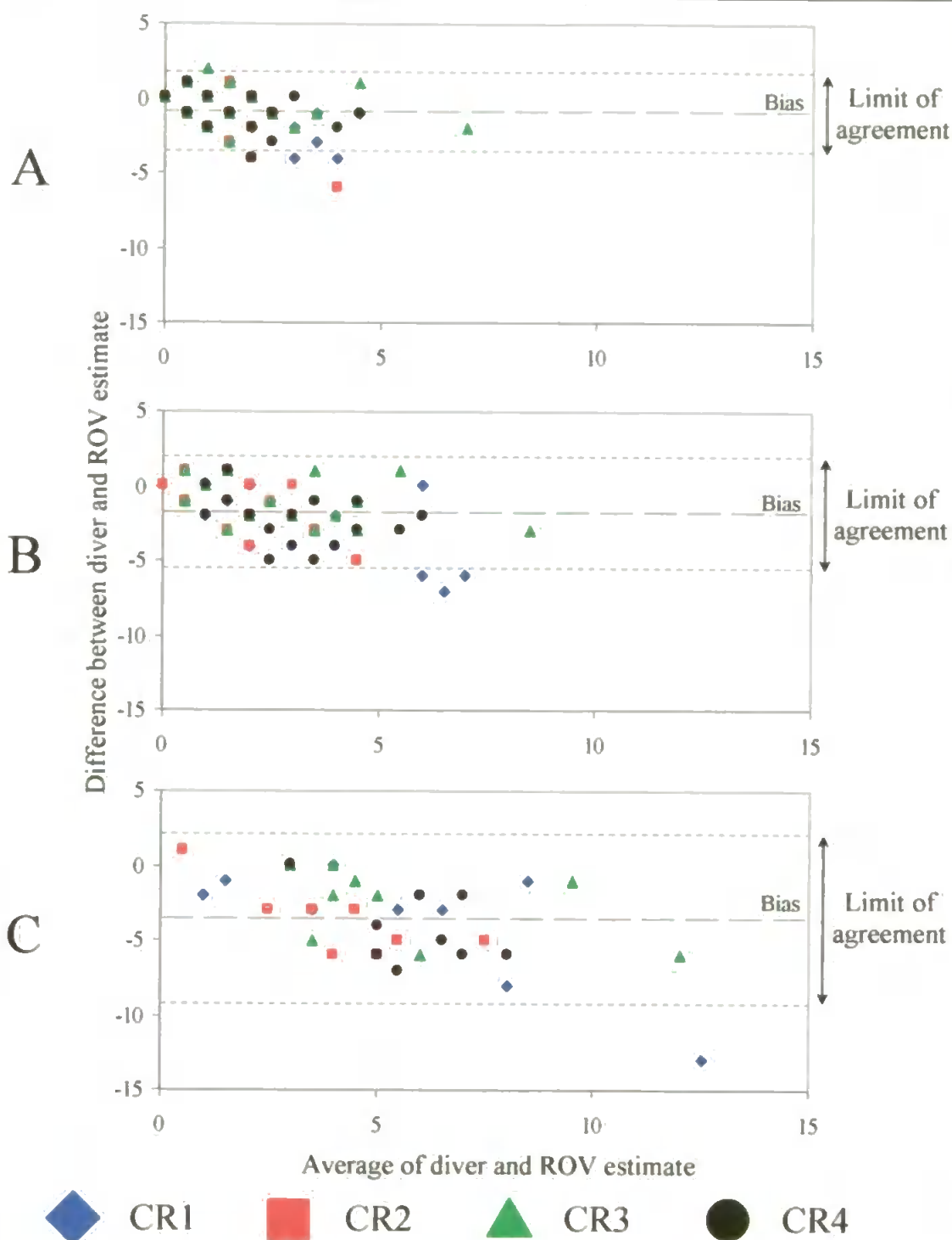


Figure 4.3: Bland and Altman plot of difference against mean for features greater than 15mm diameter in Loch Creran survey plots. Data are aggregated on grid size of A=0.25 m<sup>2</sup>; B=0.5 m<sup>2</sup>; C=1 m<sup>2</sup>. The bias, represented by the dashed line equals the mean difference between methods. The limits of agreement, represented by the dotted lines are equal to bias  $\pm$  2 standard deviations.

### 4.3.2 Jennycliff Bay

#### 4.3.2.1 Abundance estimates

In Jennycliff Bay, high feature density and restricted time for SCUBA diving limited observations by both diver and ROV to a single survey plot. The biotic features present in the Jennycliff Bay assemblage had similar dimensions, so different size fractions were not examined. Qualitative assessment of total biotic feature abundance data in Jennycliff Bay suggested that diver and ROV-derived estimates were similar (Table 4.3). Comparison of abundance estimates of specific feature types indicated that there were some differences between assignment of species identity to the biotic sediment features observed, and these were elucidated using the Bland and Altman plots of spatial coincidence at the scale of individual grid cells ( $0.25 \text{ m}^2$ ).

Table 4.3: Abundance estimates of biotic features counted during diver and ROV observations of the Jennycliff Bay survey plot. Area =  $9 \text{ m}^2$ .

Feature type	ROV-derived	Diver-derived
Total biotic features	621	635
Thalassinidean openings	180	94
Bivalve openings	425	507
Thalassinidean plus bivalve openings	605	601
Callianassa mounds	4	14

#### 4.3.2.2 Spatial coincidence

There was no significant bias between the estimates of total biotic feature abundance (Table 4.4 and Fig. 4.4). Data points that fell outside the limits of agreement at  $0.25 \text{ m}^2$  sample grain approached the methodological bias as samples were aggregated, which indicates that the effects of parallax on abundance estimates decreased as sample grain increased. Variation associated with the difference between abundance estimates (y-axis) at larger grain sizes indicated that some biotic features had not been detected by both

observation techniques, while variation between mean abundance estimates (x-axis) indicated variation of the spatial distribution of biotic features.

ROV-derived estimates of thalassinidean opening abundance were significantly greater than diver estimates, while ROV-derived estimates of bivalve abundance were significantly lower than diver estimates. However, there was no significant bias between diver and ROV estimates when these burrow types were aggregated (Table 4.3). *Callianassa subterranea* ejecta mounds were not detected in ROV images as effectively as by an experienced diver (Table 4.3).

Table 4.4: Mean bias ( $\pm 95\%$  CI) between diver and ROV estimates of features contained in Jennycliff Bay grid cells of  $0.25 \text{ m}^2$ . ns:  $p > 0.05$ ; \*  $p < 0.05$ ; \*\*  $p < 0.01$ . N=36

Feature type	Mean bias ( $\pm 95\%$ CI)
Total biotic features	$-0.4 \pm 1.3^{\text{ns}}$
Thalassinidean openings	$2.4 \pm 1.0^{**}$
Bivalve openings	$-2.3 \pm 1.2$
Thalassinidean plus bivalve openings	$0.1 \pm 1.3^{\text{ns}}$
Callianassa mounds	$-0.3 \pm 0.2^*$

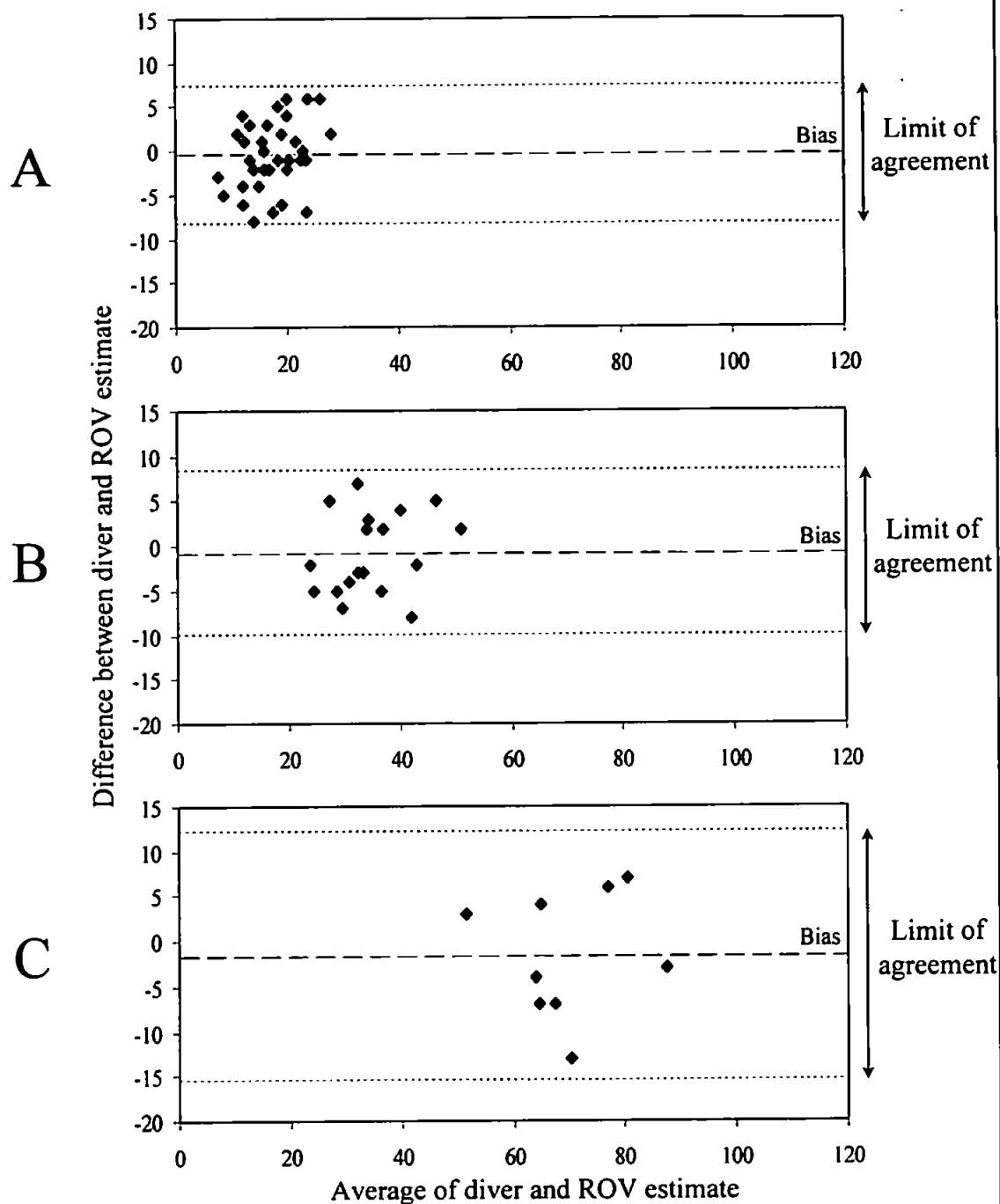


Figure 4.4: Bland and Altman plot of difference against mean for total biotic features in the Jennycliff Bay survey plot. Data are aggregated on grid size of A=0.25 m<sup>2</sup>; B=0.5 m<sup>2</sup>; C=1 m<sup>2</sup>. The bias, represented by the dashed line equals the mean difference between methods. The limits of agreement, represented by the dotted lines are equal to bias  $\pm$  2 standard deviations.

### 3.4 DISCUSSION

There was no significant difference between estimates of total biotic feature abundance between direct diver observation and remotely operated vehicle imaging in shallow unvegetated sedimentary environments. Although the benchmark for quantification of megafaunal biotic features has been direct observation by divers, the results presented here provide assurance that there was no systematic error associated with remote survey estimates of total biotic feature or conspicuous feature abundance. As a result, the confidence that may be applied to wider extent and deeper-water investigations of megafaunal diversity, bioturbational activity, standing stock, production or energy flux is increased (Chapters 5 and 6).

Much of the variability within the data presented can be accounted for by the different ways in which divers and camera systems observe the seabed. In the present study, survey frames were deployed close to (but not in contact with) the seabed to minimise sediment resuspension. The frame was a considerable aid when diver mapping; the divers could position themselves directly above the grid nodes to look vertically down. Conversely, the ROV camera was oriented obliquely to the sediment surface, causing small differences in abundance estimates due to parallax at the edges of the smallest grid cell size. The effect of parallax diminished as cell size increased because the ratio between sample area and sample perimeter decreased. The variation between abundance estimates that could not be explained by parallax was due to features that were not observed by one or other of the survey techniques.

Biotic features that were omitted by one or other of the survey techniques do not necessarily reflect lack of agreement between diver and ROV observations, as there was no consistent pattern to suggest bias between either technique. The ROV image data may be re-examined to identify which features were not recorded within the grids because diver

observations do not provide a permanent record of the seabed itself. Features recorded from ROV observations, but not recorded during diver observations, were measured from still images using *Benthic Imager*, and found to be approximately 2 cm diameter. Similarly, ROV images were re-examined to check for features that were recorded in diver maps only, yet no corresponding features were identified. However, the features recorded only in the diver maps were all small “unidentified holes” that were also approximately of 2 cm diameter. Since significant temporal variation in feature abundance may occur within 24 h in Loch Creran (Nickell [Dunstaffnage Marine Laboratory], pers. comm.), these small features may have been generated and/or eradicated during the inter-survey interval.

The significant differences detected between abundance estimates of different size fractions of the total biotic feature assemblage suggest that abundance estimates of the smaller features from remote observations were consistently lower than direct diver observations of the same area. However, feature dimensions from the diver and ROV observations were extracted in different ways; diver-derived measurements were calculated from the size of the object drawn *in situ*, while measurements of features in the ROV-generated maps were made from corresponding still images of the features themselves. Divers are known to overestimate significantly the size of objects (Ross, 1989), while the minimum size of feature that may be recorded in diver-generated maps depends on the size of the pencil tip, and will be reflected in feature dimensions extracted from *Scion Image* software. Conversely, the ABISS system is capable of measurements of features from images that are accurate to  $\pm 5\%$  (Pilgrim et al., 2000). Hence, greater confidence must be placed in the absolute dimensions of features derived from remote images, which may be used to define the minimum size of feature included in analyses.

The lack of bias between diver and ROV estimates at Jennycliff Bay suggests that remote observations may be cost effective where feature density is high, because the same area of

seabed may be surveyed in a fraction of the time required by diver observations. Subjective identification of burrows, rather than the ability to detect the openings, accounted for the differences between ROV and diver estimates of thalassinidean and bivalve openings, because there was no significant bias between abundance estimates when these groups were pooled. Thalassinidean shrimp and bivalve surface openings are generally distinctive. Thalassinidean shrimp burrows are connected to the surface by a number of vertical shafts, each of which form a funnel-shaped opening at the sediment surface (Atkinson and Nash, 1990); bivalve siphon tips are generally visible at the surface opening, which is flush with the sediment surface. However, bivalve openings may appear funnel-shaped if the siphons are retracted in response to predator activity, because the surface opening may slump when not supported by the siphons. Alternatively, competitive advantage may be derived from slumping of the opening, because funnel-shaped openings are associated with enhanced bioresuspension rates in comparison to a flat sediment surface; hence, the rate of pseudofaeces removal will be increased (Paterson and Black, 1999). In remote observations, the ability to discriminate between funnel-shaped bivalve openings and thalassinidean openings would be enhanced by increasing the image resolution, which may be achieved by reducing camera-object distance. Oblique camera and illumination angles would enhance further the detection of features characterised by subtle changes in bottom topography, such as the volcano-like mounds associated with *Callianassa subterranea* burrows (Atkinson and Nash, 1985), as shadows would be cast onto the seabed.

The ability to apply scale to the still ROV images using the laser array (described in Chapter 2) allowed feature measurement, which assisted with the identification of feature types (e.g. Marrs et al., 1996). The measurement of surface features may be used to infer size distributions of burrowing fauna and derive estimates of megafauna biomass, which will be presented in Chapter 5. In the present study, observations were made within metal



frames; however, the use of the ABISS permits abundance estimates to be expressed as absolute density estimates without the deployment of frames or other scaling aids. The laser array also provided a visual reference that assisted the pilot to maintain camera orientation, thus maintaining absolute resolution, to increase the amount of quantitative data that may be extracted from remote images.

Remote observations are less appropriate in topographically complex habitats, such as boulder fields and kelp forests, because the laser spot pattern becomes corrupted and cryptic organisms are more difficult to observe. Divers are more appropriate under such circumstances as they are able to manipulate the features to gain information on the fauna. However, the concordance between estimates derived from diver and ROV observations at both sites indicate that remote observations may be used to obtain accurate estimates of biotic feature abundance from unvegetated sediment environments on a wider extent, and from greater depths, than accessible to direct diver observation.

#### 4.5 CONCLUSIONS

There was strong agreement between abundance estimates of megafaunal features that were derived from direct diver and remote observation techniques. The results provide assurance that remote observation techniques may be deployed over wider spatial extent and to greater depths than divers may achieve without systematic errors in estimating megafaunal feature abundance. The spatial and temporal structure of a soft sediment megafaunal assemblage, based on quantitative images collected from an ROV, will be presented in the remaining chapters of this thesis.

## **CHAPTER 5**

### **Spatial and temporal pattern in community structure of a soft sediment megabenthic assemblage**

Sections of this chapter are contained in:

Parry, D.M, Kendall, M.A., Pilgrim, D.A., Jones, M.B. (in press)  
Identification of patch structure within marine benthic landscapes using a  
Remotely Operated Vehicle. *Journal of Experimental Marine Biology and  
Ecology*, 285–286.

## ABSTRACT

The spatial scale of megafaunal assemblage variation in apparently homogeneous subtidal sediment was investigated using quantitative observations from a remotely operated vehicle (ROV). Quantitative abundance estimates of surface-dwelling megafauna and biotic sediment features associated with burrowing megafauna were derived from video images using the Automated Benthic Image Scaling System (ABISS), a novel method of applying scale to images collected by ROVs. Spatially referenced images were collected to a maximum extent of 400 m within a broader area of apparently homogeneous sediment. Rank-correlograms were constructed to examine the extent and form of the megafaunal spatial structure. The megafaunal assemblage was neither uniformly distributed nor temporally stable. A nested hierarchy of spatial structure was detected within the megafaunal assemblage on a spatial extent up to 400 m. The approach described in this Chapter offers ways forward to address how variation of megafaunal spatial structure affects macrofaunal assemblage structure, and to elucidate fully the application of remote imaging to map and predict the conservation value of subtidal soft sediments.

## 5.1 INTRODUCTION

The fundamental role of ecology is to understand ecosystem dynamics and develop models that are sufficiently robust to make accurate predictions about changes in ecological systems (Peters, 1991). The biotic composition of ecosystems is shaped by biological and physical processes interacting within a complex hierarchy of spatial and temporal scales. Although there is no single correct scale at which to describe ecological patterns (Levin, 1992), generic methods for understanding and predicting relationships in ecosystems may be classified as either top-down or bottom-up. Top-down investigations suggest that only by observing patterns in assemblage structure may the distribution of individual species be understood. Conversely, the bottom-up approach requires an understanding of how each species in the assemblage is distributed and the way it interacts with all other species before community patterns may be understood. Understanding ecosystem dynamics is a multiphase process because patterns in assemblage structure are a function of top-down and bottom-up processes operating simultaneously. Large-scale patterns of species distribution within an assemblage (i.e. top-down investigation) result from relatively slow interactions between the environment and habitat, such as hydrodynamic regime and geological history, which might appear constant at smaller scales of observation. Conversely, small-scale distributional patterns are produced by interactions between individuals and species, such as competition and predation, which can operate at high rates and appear as noise in large-scale observations (O'Neill, 1989). No matter what the extent of investigation, processes operating at larger scales determine the conditions in which a distributional pattern occurs, while the processes responsible for the pattern itself operate at the next lowest level (O'Neill, 1989).

To understand ecosystem dynamics at any particular level of observation, the key components of an ecosystem must be identified. Once the key components have been determined, their spatial distribution may be quantified by mapping techniques.

Subsequently, hypotheses may be raised to examine the mechanism by which observed distributional patterns were created and maintained (i.e. top-down approach). Although small-scale manipulative experiments may be designed to test hypotheses that explain large-scale distribution patterns (i.e. bottom-up approach), they cannot be used in isolation to predict large-scale outcomes because many interactions contribute to variation in faunal abundance and distribution (Constable, 1999). In addition, different process rates do not necessarily scale up in the same way (Thrush et al., 1997b). Logically, therefore, experiments designed to elucidate the mechanisms that create and maintain a particular pattern require an ability to quantify the scale at which the features of interest are distributed.

Landscape ecology, a top-down approach to understanding ecosystem dynamics, considers all landscapes as a heterogeneous mosaic of landscape units, or habitat patches, which are repeated at intervals over space (Kent et al., 1997) and hypothesises that the spatial arrangement of ecosystems, habitats, or communities has ecological implications (Turner, 1990). In terrestrial landscape ecology, habitat patches are often defined on the basis of vegetation type and/or anthropogenic structures. Although a similar approach has been applied in the marine environment to investigate spatial distribution of seagrass habitats (Robbins and Bell, 1994), marine landscapes are defined usually using physical characteristics rather than biological structures (Zajac, 1999). Marine benthic habitats may be classified and mapped on a sub-regional scale using acoustic ground discriminating systems (AGDS) such as RoxAnn™ (Stenmar Micro Systems Ltd., Scotland) (e.g. Greenstreet et al., 1997) and QTC View™ (Quester Tangent Corporation, Canada) (e.g. Morrison et al., 2001), which group areas of seabed by their acoustic properties alone. Since the acoustic properties reflect sediment structure and water depth, the maps produced have little biological meaning when viewed in isolation. If the maps are to be used in ecological studies, it is necessary to link the acoustic properties of an area with the fauna

inhabiting it. Conservationists and environmental managers consider landscapes as a patchwork of 'biotopes', each representing the physical characteristics of a habitat and the specific species that are found commonly there. In the marine environment, direct observations, or grab sampling, may determine the biotope(s) associated with acoustically distinct patches of sediment. Since biotopes are differentiated by the specific species that live in a particular habitat, a number of similar biotopes are grouped functionally to define different 'life form' units (e.g. Entec, 1996), for which the acoustic signatures are determined. Consequently, maps of the acoustic characteristics of the seabed represent the predicted distribution of 'life form' units associated with apparently homogeneous areas of sediment (e.g. Greenstreet et al., 1997), yet little is known of the faunal variability within such patches.

Pearson and Rosenberg (1978) hypothesised that diverse benthic assemblages were established in previously azoic sediments through the process of succession. In the first stage of succession, opportunistic organisms (with rapid growth, small body size, short generation time, rapid reproduction and planktonic larvae) colonise the sediment surface and modify sediment characteristics through their feeding activity. The competitively dominant deeper-burrowing megafaunal organisms establish themselves gradually over time, turning the sediment into a complex three-dimensional fabric of burrows, tubes and feeding mounds, creating a variety of microhabitats for other species to colonise (Pearson and Rosenberg, 1978). However, the successional stage of a marine benthic assemblage may be impeded (or reset) by physical and biological disturbance events at spatial scales from individual ray feeding pits (Thrush et al., 1991) to large storm events (Posey et al., 1996) that occur at a range of temporal scales. Consequently, marine benthic assemblages may be considered as a mosaic of patches at different stages of recovery (i.e. succession) from disturbance events (Grassle and Morse-Porteous, 1987; Reise, 1991).

While the landscape of biogenic microhabitats produced by megafaunal individuals may be affected by the successional stage of the assemblage, the burrowing activity of megafaunal species (i.e. bioturbation) introduces a further source of disturbance that creates mosaic patterns in marine sediments (e.g. Thistle, 1981). Bioturbation by megafaunal species disturbs the geophysical and geochemical properties of sediments, particularly in areas of low abiotic disturbance (e.g. Hall, 1994), which influences the structure and composition of associated macrofaunal assemblages (e.g. Woodin, 1978; Brenchley, 1981; Posey, 1986). Changes in sediment granulometry (Aller and Dodge, 1974; Suchanek, 1983), sediment oxygenation (Forster and Graf, 1995; Astall et al., 1997), and nutrient fluxes (Hughes et al., 2000) associated with megafaunal bioturbation may affect assemblage structure through the direct or indirect effects on settlement and survival of macrofaunal larvae (Woodin, 1978). Therefore, the mechanisms of bioturbation, and the spatial and temporal distribution of the megafauna themselves, create and maintain environmental heterogeneity in an otherwise homogeneous environment (Levin and Paine, 1974).

Thrush et al. (2001) found that habitat structure was significantly correlated with macrofaunal species richness, evenness and Shannon-Weiner diversity, and hypothesised that observations of benthic habitat structure may be used as a surrogate for the rapid estimation of macrofaunal diversity at larger spatial scales. Remote observation of the seabed is used to validate biological classification of acoustic data, yet similar techniques could be used to quantify the spatial distribution of megafaunal population density; thus assessing habitat structure. Studies of the effects of bioturbation usually consider the size and frequency of disturbance (e.g. Petraitis, 1989). Experimental manipulations of bioturbating megafaunal species, however, showed that the response of the macrofaunal assemblage, particularly the rare species, was influenced by the identity of bioturbating species (Widdicombe and Austen, 1999). Consequently, quantification of megafaunal

assemblage distribution patterns may enhance techniques to rapidly map and predict macrofaunal assemblage structure by considering species identity with population density.

The abundance and identity of megafaunal organisms and the sediment structures that they construct may be extracted from ROV observations, and such data have been validated previously against those derived from direct diver observation (Chapter 3). Although diver/ROV validation was achieved over a limited spatial extent (9 m<sup>2</sup>), the Sonardyne International Ltd. underwater acoustic positioning system (Chapter 2) allows spatially-referenced ROV observations to be made on a larger survey extent. In this chapter, the results from ROV surveys designed to determine the composition and spatial structure of a megafaunal assemblage within an apparently homogeneous patch of sediment are described. The ROV surveys were designed specifically to test the null hypothesis that:

- a) The megafaunal assemblage within an extensive area of apparently homogeneous subtidal sediment was distributed homogeneously up to a maximum spatial extent of 400 m.

If the null hypothesis is falsified, the secondary hypotheses were:

- i) The size of megafaunal patches was consistent between years, and
- ii) the dimensions of megafaunal patches matched those of the macrofaunal patches.



## 5.2 MATERIALS AND METHODS

### 5.2.1 Survey location

Sampling of the spatial structure of the megafaunal assemblage of Jennycliff Bay, Plymouth Sound, took place on 30<sup>th</sup> and 31<sup>st</sup> May 2000, and 4<sup>th</sup> March 2001. The Jennycliff Bay sediment was described as a fairly extensive stretch of sandy mud by the Marine Biological Association (1957) and has been mapped using side-scan sonar as homogeneous sublittoral muddy sand (Moore et al., 1999). The site was also chosen specifically as a broad area of relatively homogeneous sediment in which macrofaunal heterogeneity had been quantified previously (Kendall and Widdicombe, 1999). A full description of the survey location is presented in Chapter 2. A long base line acoustic beacon array of approximately 200 × 300 m was deployed in Jennycliff Bay (Section 2.5.1). The positions of the seabed transponder beacons were determined using a differential global positioning system (DGPS) in combination with a vessel-mounted acoustic transponder, and converted to Universal Transverse Mercator (UTM) units in the Sonardyne *PharosLite* positioning software (Section 2.5).

### 5.2.2 Survey design

The survey was confined to an apparently homogeneous sublittoral muddy sand with bivalves habitat that was defined using side-scan sonar during a Joint Nature Conservation Committee project (Moore et al., 1999). To maximise the spatial coverage of the survey, yet remain within the same patch of sediment, four stations were established: Beacon, Central, Fylrix and Nearshore (Fig. 5.1). The research vessel was moored at each station during the ROV deployments. At each station, three parallel transects were defined, each of 100 m length and separated by 25 m, and the ROV was navigated as close to each transect line as hydrographic conditions permitted. All navigation data from *PharosLite* were recorded in a Microsoft Access database file, while real-time ROV position co-

ordinates and time were displayed on the video overlay. The video image and overlay information was recorded onto VHS videotape for later analysis.

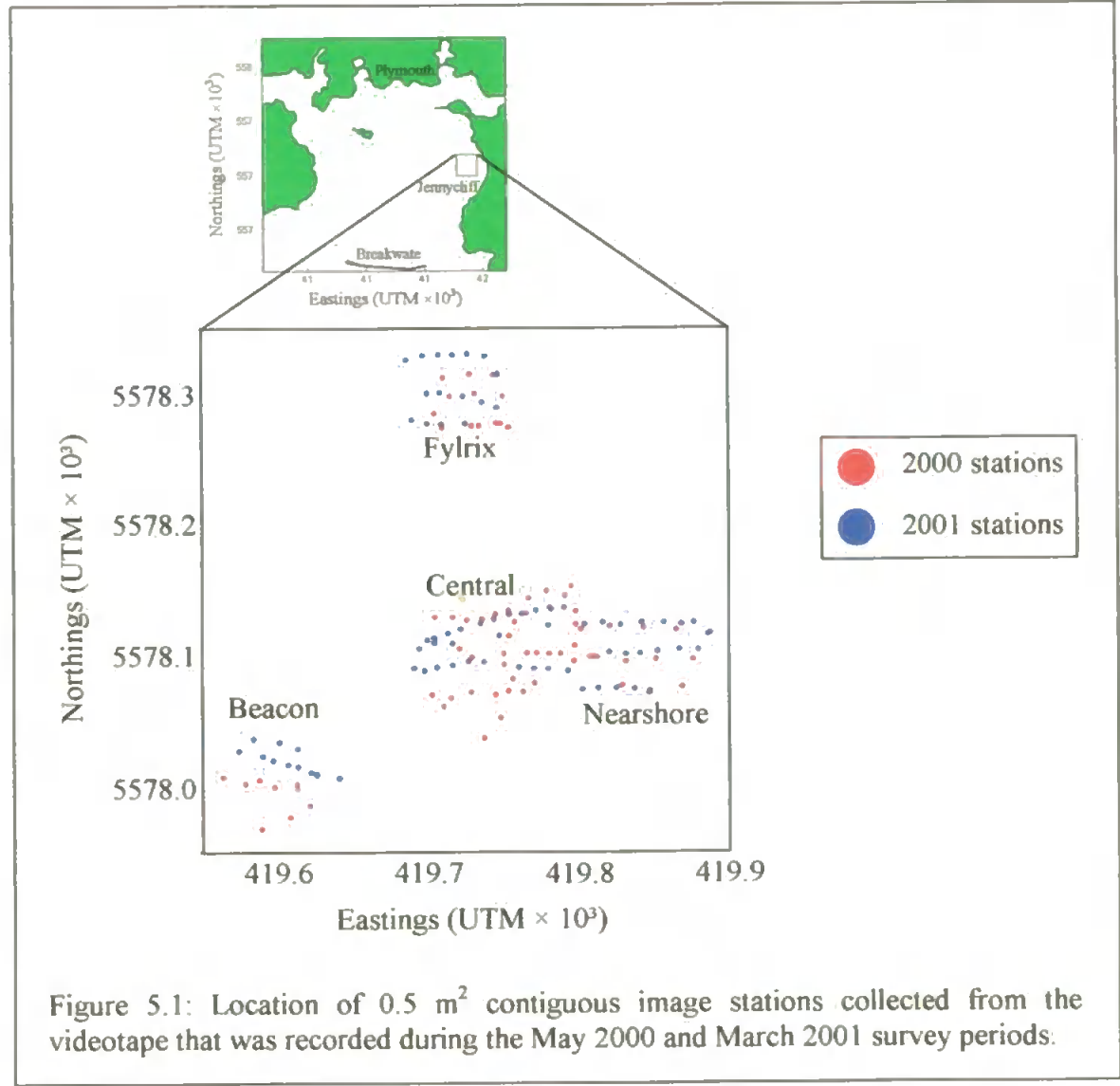
### 5.2.3 Data extraction

Still images were collected from the videotape using *MVPilot* frame grabbing software (MATRIX Vision GmbH, Oppenweiler, Germany). The area contained within each image was calculated using *Benthic Imager* and the UTM co-ordinates were recorded. To achieve a constant sample grain, a contiguous series of images was collected for each sample, onto which virtual quadrats totalling 0.5 m<sup>2</sup> were overlaid. The intended separation between samples (i.e. sample lag) was 10 m, but images were rejected if sediment resuspended by the wash from the ROV propellers obscured the seabed. Occasionally, position calculation by the *PharosLite* software was associated with large estimated position errors, which were recorded in the navigation database files (Section 2.5.3). Consequently, still images were rejected if the estimated position error exceeded 5 m, which is the same position accuracy achieved by differential GPS.

During May 2000, the videotape yielded seventy-three samples with a mean estimated position error of  $1.4 \pm 0.2$  m ( $\pm 95\%$  confidence interval). The March 2001 survey yielded seventy-two samples with a mean estimated position error of  $1.5 \pm 0.2$  m ( $\pm 95\%$  confidence interval). Although more samples could have been collected from the videotape in each survey year, the sample lag would have approached the spatial resolution of the acoustic positioning system.

All megafaunal sediment structures and surface-dwelling megafauna (henceforth, referred to as biotic features) within the virtual quadrat were identified using the still images and adjacent frames of the videotape. The still images were annotated accordingly and all biotic features were measured using *Benthic Imager* software (Chapter 6). The abundance

of biotic feature groups larger than 1 cm was recorded as these features could be identified consistently in the images. It was not possible to allocate all animals encountered to species, nor was it possible to identify the species responsible for all of the sediment structures observed. Wherever possible, surface-dwelling megafauna were identified to the lowest possible taxonomic level using the nomenclature of the Marine Species Directory (Howson and Picton, 1997). Megafaunal sediment structures, such as burrow openings and mounds, were identified to the best possible resolution using the morphological characteristics described by Marrs et al. (1996). Wherever possible, the identity of animals responsible for sediment structures not contained within Marrs et al. (1996) was investigated by a combination of SCUBA observation and the establishment of specimens recovered by anchor-dredging in laboratory aquaria.



The burrow openings of thalassinidean mud shrimp species (*Upogebia deltaura* and *Callinassa subterranea*) could not be distinguished. However, surface mounds were attributed to *C. subterranea*, as this species is a deposit feeder (Aller and Dodge, 1974; Rowden et al., 1998) while *U. deltaura* is a suspension feeder (Hill, 1981; Pinn et al., 1998) and would not produce such features. Three different bivalves with fused siphons were observed; one with dark viscera and two with light viscera. The latter were separated by the appearance of their siphon openings when the ROV passed overhead; 'species 1' resembled an hourglass while the inhalant and exhalant openings appeared separate in 'species 2'. The identity of these large bivalves was confirmed by collecting specimens with an anchor dredge. Individuals were returned to the laboratory, and allowed to rebury in sediment collected from Jennycliff Bay and maintained in tanks of circulating seawater (10–15°C) for 4 weeks. Images of the siphon openings at the sediment surface were collected, whereupon, the individuals were retrieved and identified to the species level. The bivalve species with dark viscera siphons was attributed to the common otter shell, *Lutraria lutraria*, while the light viscera siphons of species 2 were attributed to the cockle, *Acanthocardia* sp. Unsuccessful attempts were made to collect megafaunal specimens to identify those species responsible for making some of the unknown surface openings, such as the light viscera 'hourglass' bivalve siphons (bivalve species 1). Consequently, the morphology of these features, ranging in size from 0.5–2 cm diameter, was defined on size, shape and whether the opening was at the centre of a hollow or mound or flush with the sediment surface. These features were assigned a unique identification code that could be used to identify these features in subsequent images.

#### 5.2.4 Data analysis

Multivariate data analyses were carried out using the PRIMER (Plymouth Routines In Multivariate Ecological Research) software package, a suite of statistical routines developed at the Plymouth Marine Laboratory (Clarke and Warwick, 1994). A matrix of

between-sample similarity was constructed, using the Bray-Curtis similarity index, from biotic feature abundance data. The Bray-Curtis Similarity Index,  $S_{jk}$ , is given by:

$$S_{jk} = 100 \times \left( 1 - \frac{\sum_{i=1}^p |Y_{ij} - Y_{ik}|}{\sum_{i=1}^p (Y_{ij} + Y_{ik})} \right) \quad (\text{Bray and Curtis, 1957})$$

where  $Y_{ij}$  and  $Y_{ik}$  are the abundance of species  $i$  in samples  $j$  and  $k$  respectively ( $i = 1, 2, \dots, p$ ;  $j$  and  $k = 1, 2, \dots, n$ ). This index varies from 100% (total between-sample similarity) to 0% (total between-sample dissimilarity). Similarity matrices were constructed using untransformed biotic feature abundance data that emphasise the influence of common features and double root ( $\sqrt{\sqrt{\cdot}}$ ) transformed biotic feature abundance data, which represent a more balanced approach to analyses by increasing the influence of low abundance features on the whole assemblage.

Description of the spatial pattern at any particular scale within an assemblage can be addressed only after the null hypothesis that the assemblage is distributed homogeneously has been rejected. Examination of spatial structure within the megafaunal assemblage was approached in two different ways; by comparing variance within and between stations and by determining how assemblage similarity varied with distance. Differences between *a priori* groups of samples may be tested by analysis of variance (ANOVA) for single species or analysis of similarities (ANOSIM) for the distribution of an assemblage. However, investigation of spatial structure in the distribution of a species or assemblage implies that the abundance at one location is related to the abundance at another location; the spatial distribution is autocorrelated. Spatial autocorrelation between samples introduces difficulties with ANOVA tests because the samples are not statistically independent. ANOSIM tests are complicated further because values in each cell of a similarity matrix are not independent. While significance of difference in ANOSIM may still be assessed using a permutation procedure, the true number of degrees of freedom

used to assess significance in an ANOVA test are difficult to define because each new sample added to the analysis does not add a complete degree of freedom. While ANOVA and ANOSIM tests identify differences that may occur between groups of samples, the description of spatial pattern of a species or assemblage by these methods requires a complicated nested sampling design (e.g Underwood, 1997; Kendall and Widdicombe, 1999).

To date, most studies have examined spatial pattern within single species. They have been achieved by determining how spatial autocorrelation coefficients change with increasing sample lag, using Moran's  $I$  (Moran, 1950) and Geary's  $c$  (Geary, 1954), which are calculated by comparing the abundance between samples at different distances apart. By plotting the autocorrelation coefficient between samples against the distance separating them to produce a correlogram, the presence of patches can be detected and their size estimated (Angel and Angel, 1967; Jumars et al. 1977; Thrush et al., 1989). Multivariate techniques, such as the Mantel test statistic (Legendre and Fortin, 1989; Legendre, 1993), can be used to investigate spatial pattern in community data. The Mantel test statistic is based on parametric correlation between matrices of faunal similarity and distance (Legendre and Fortin, 1989) that may be over influenced by outlying values. In this thesis, a non-parametric rank-correlation technique has been used to examine the spatial structure of the benthic megafauna of Jennycliff Bay. This technique was chosen because the influence of large differences in values was diminished and the statistic was independent of scale (Somerfield and Gage, 2000).

#### *5.2.4.1 Megafaunal assemblage composition*

The significance of differences in megafaunal assemblage composition between years and stations was tested using a two-way crossed ANOSIM because the same transects were surveyed in both years. Although ANOSIM is equivalent to an ANOVA test for univariate

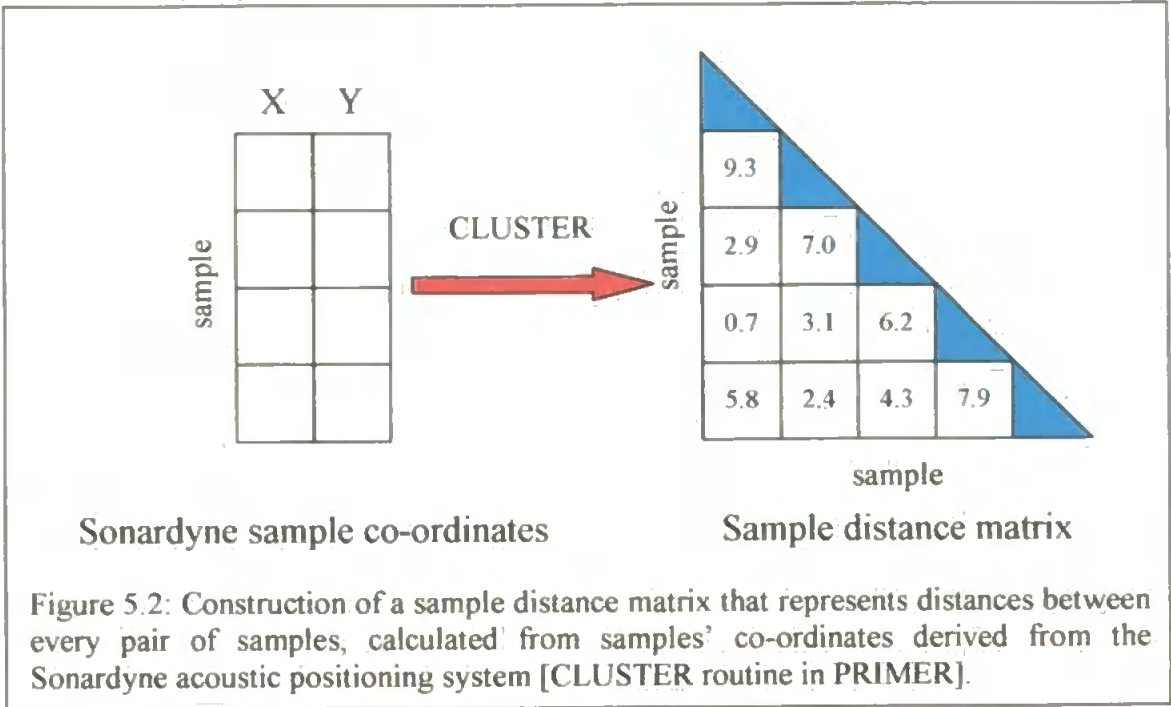
data, the former does not allow testing for interaction effects (Clarke, 1993). Where significant differences in assemblage structure were detected, the species/features responsible were identified using SIMPER (similarity of percentages) analysis. Non-parametric multidimensional scaling (MDS) was used to visualise the temporal stability of megafaunal assemblage structure between the two surveys. Two-way crossed ANOVA tests were performed to identify between-year and between-station differences in abundance of the discriminating features. Year and station were fixed factors in the analysis because station location was defined specifically to investigate assemblage variation in different parts of Jennycliff Bay. Pairwise tests using Tukey's HSD were used to identify which stations were significantly different from each other.

#### *5.2.4.2 Spatial structure of the megafaunal assemblage*

The spatial structure of the fauna, defined as a relationship between biotic similarity and sample lag, was explored by comparison of the biotic similarity matrix (Section 5.2.4) and a sample distance matrix. The latter was constructed from sample position data derived from the Sonardyne acoustic positioning system (Section 2.4.3) and expressed as the linear distance separating all pairs of samples (Fig. 5.2).

The spatial homogeneity of the megafaunal assemblage was tested by calculating Spearman's correlation coefficient,  $\rho$ , between corresponding elements of biotic similarity and sample distance matrices. The number of cells in each matrix, equivalent to the total number of possible pairs of samples, was 2628 and 2556 in May 2000 and March 2001, respectively. Spearman's rank correlation between matrices constructed from both untransformed and  $\sqrt{v}$ transformed faunal abundance data were performed using the RELATE routine in PRIMER (Clarke and Warwick, 1994). Since the lack of independence between elements of a similarity matrix invalidates the standard statistical

tables, the significance of correlations was determined using a Monte Carlo randomisation procedure with 5000 permutations (Somerfield and Gage, 2000).



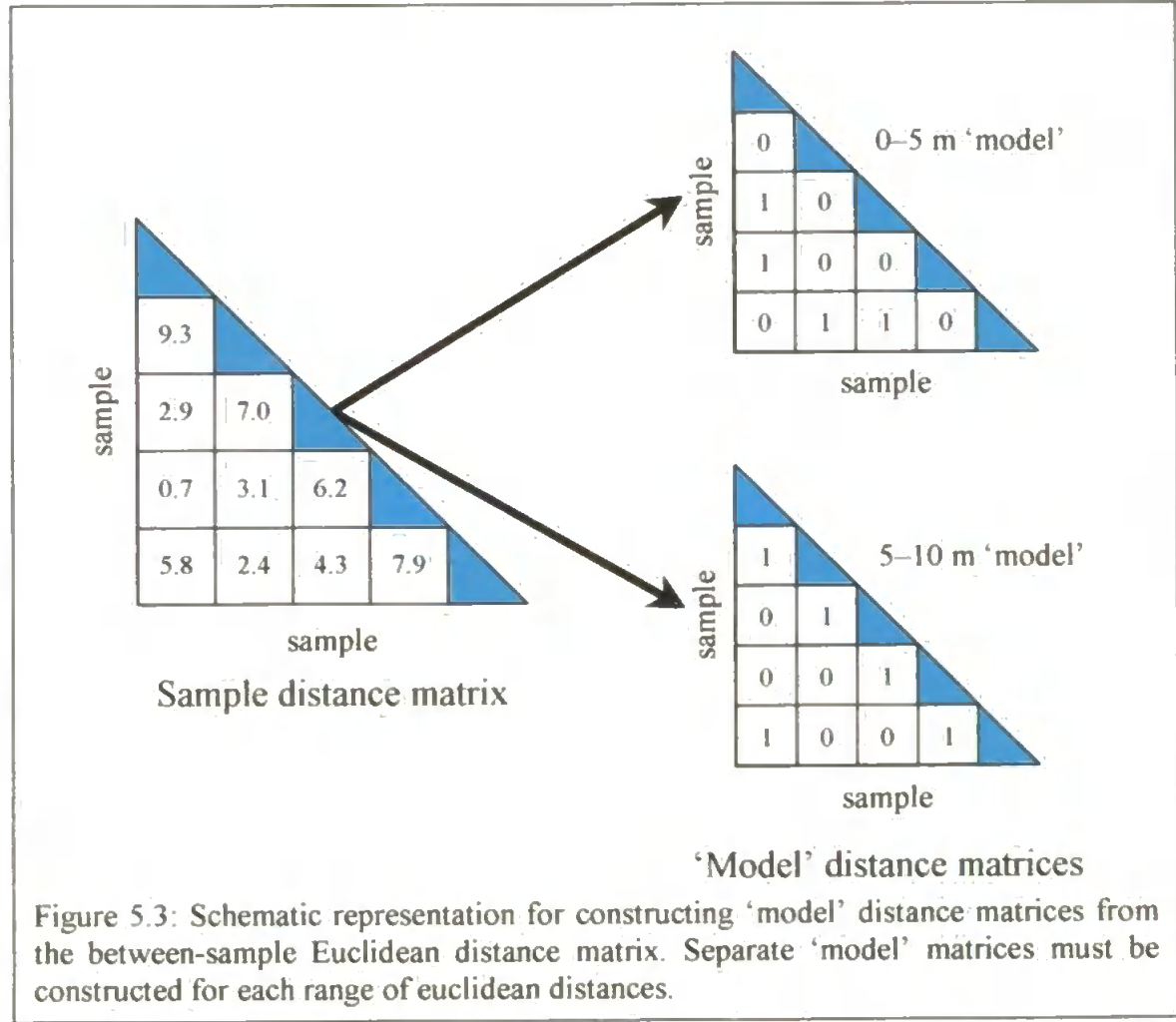
5.2.4.3 Spatial pattern of the megafaunal assemblage

The spatial pattern of the megafaunal assemblage was explored by constructing multivariate rank-correlograms (Somerfield and Gage, 2000), which allow the biotic similarity of samples within a pre-set distance class to be compared with the biotic similarity of all other samples. A separate 'model' distance matrix was constructed for each distance class by re-coding each cell of the sample distance matrix with '1' if the sample separation fell within the distance class and '0' for all other classes (Fig. 5.3).

The distance range chosen for each of the discrete 'model' distance matrices may be decided either by allocating an equal number of pairs of observations to each class or using fixed intervals to cover the maximum extent of the survey. Since the magnitude of Spearman's  $\rho$  depends on the number of observations in each test, the interpretation of spatial pattern from rank-correlograms constructed using equal numbers of observations per distance class is less susceptible to statistical artefacts (Somerfield [Plymouth Marine



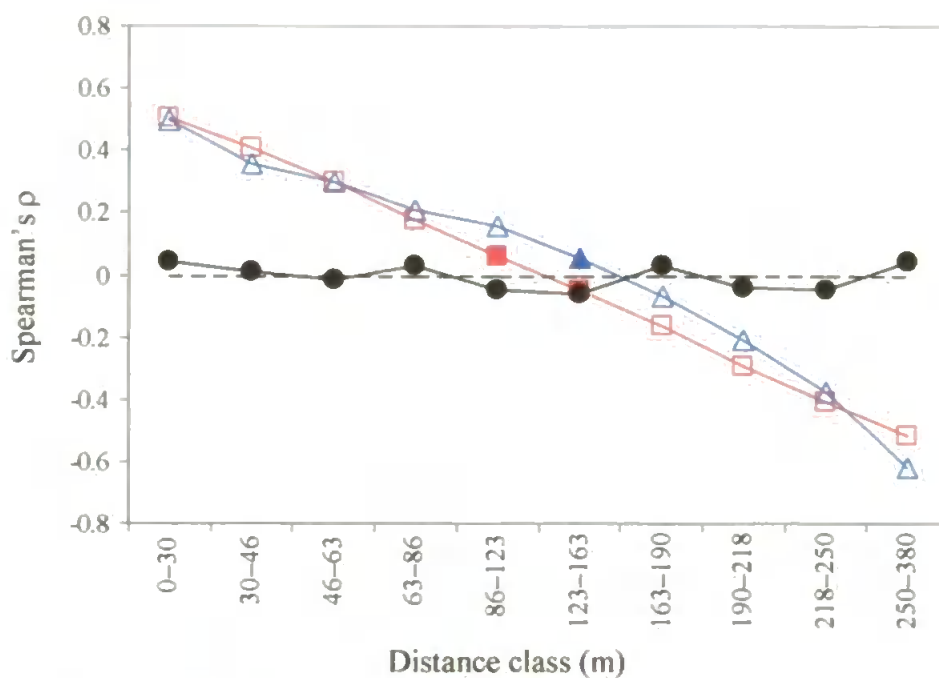
Laboratory], *pers.comm.*). Consequently, the May 2000 survey co-ordinates were used to define ten distance classes containing equal pairs of observations and a ‘model’ distance matrix was constructed for each class. The May 2000 distance class ranges were imposed on the March 2001 data, from which corresponding ‘model’ distance matrices were constructed from the March 2001 sample distance matrix. Since the distribution of pairs of observations allocated to each distance class in March 2001 was not significantly different to May 2000 (Kolmogorov-Smirnov test,  $p>0.05$ ,  $N=10$ ), the same distance class ranges were used to allow comparison of spatial pattern of the megafaunal assemblage between years. Consequently, each distance class contained approximately 260 observations in May 2000 and approximately 250 observations in March 2001.



In a similarity matrix, larger values indicate that samples are close together. In a distance matrix, however, larger values indicate that samples are further apart. Consequently, the

'model' distance matrices were treated as similarity rather than distance matrices so that positive Spearman's correlation coefficients corresponded to samples that were more alike than expected by chance, and *vice versa*. Spearman's correlation coefficient between the megafaunal similarity matrix and each 'model' distance matrix was calculated for both untransformed and  $\sqrt{\sqrt{}}$ transformed faunal abundance data using the RELATE routine in PRIMER (Clarke and Warwick, 1994). The significance of correlation within a particular distance-class was calculated using the Monte Carlo permutation technique (within RELATE). Correlation between megafaunal similarity and 'model' distance matrices represents a two-tailed test because samples within each distance class may be more or less similar than all other samples. Therefore, assuming significance of correlation at  $p=0.05$ , significant positive autocorrelation occurred when  $p<0.025$  and significant negative autocorrelation occurred when  $p>0.975$ .

A multivariate rank-correlogram (Somerfield and Gage, 2000) was constructed for both untransformed and  $\sqrt{\sqrt{}}$ transformed abundance data by plotting each correlation coefficient value against distance-class. In such diagrams, significant autocorrelation minima represent the distance between samples that are least similar biotically, and may be used to define the radius of a patch of similar fauna (Legendre and Fortin, 1989). Significant autocorrelation maxima in rank-correlograms that occur in distance classes greater than an autocorrelation minimum indicate the distance between successive patches of biotic similarity (Legendre and Fortin, 1989). Consequently, a spatially homogeneous megafaunal assemblage will be represented by a rank-correlogram in which no Spearman's  $\rho$  values are significantly different from zero (Fig. 5.4). Similarly, the multivariate rank-correlogram that would be obtained from a linear gradient may be constructed by calculating the correlation between the sample distance matrix rather than megafaunal similarity matrix and each 'model' distance matrix (Fig. 5.4).



**Significance value of Spearman's  $\rho$**

$0.025 < p < 0.975$ :



2000



2001



Homogeneous assemblage

$p < 0.025$  or  $p > 0.975$ :



2000



2001

Spearman's  $\rho = 0$



Figure 5.4: Rank-correlogram that would be obtained if biotic similarity and inter-sample distances were in a perfect series for each year and an example of a rank-correlogram for a homogeneous assemblage. Significance of Spearman's  $\rho$  value calculated by Monte Carlo permutation procedure [RELATE].

### 5.3 RESULTS

A total of thirty different megafaunal biotic feature types was identified from the images (Appendix I). Biogenic sediment features included thalassinidean mud shrimp burrow openings (*Upogebia deltaura* and *Callianassa subterranea*) and mounds (*Callianassa subterranea*), angular crab burrows (*Goneplax rhomboides*), and a variety of unknown surface openings and feeding pits. Megafaunal species included the infaunal bivalves *Lutraria lutraria*, *Acanthocardia* sp. and Unknown Bivalve 1, epibenthic decapods such as hermit crabs and decorator crabs (*Macropodia tenuirostris*), epibenthic gastropods (*Philine aperta*, *Hinia reticulata* and *Turitella* sp.) and ophiuroids.

Image resolution, measured by the pixel footprint (real size represented by a single pixel at the centre of the image), was  $1.3 \pm 0.3$  mm and  $1.1 \pm 0.1$  mm (mean  $\pm 95\%$  confidence) in May 2000 and March 2001 respectively. In May 2000, the camera range (distance between camera and the sediment at the centre of the image) and inclination angle (angle between sediment surface and the optical axis of the camera) were  $61 \pm 3$  cm and  $50 \pm 1^\circ$  (mean  $\pm 95\%$  confidence), respectively. In March 2001, the camera range and inclination angle were  $48 \pm 1$  cm and  $64 \pm 1^\circ$  (mean  $\pm 95\%$  confidence) respectively (Appendix II).

#### 5.3.1 Spatial structure of the megafaunal assemblage

The megafaunal assemblage was not distributed homogeneously within an extensive area of apparently homogeneous subtidal sediment in Jennycliff Bay. Significant positive Spearman's correlation (Table 5.1) indicated that simple distance-related spatial structure existed in both survey years, which implies that samples taken in close proximity to each other were more similar biotically than pairs of samples taken with greater separation (i.e. greater sample lag). Positive spatial autocorrelation of untransformed and  $\sqrt{\text{transformed}}$  abundance data (Table 5.1) indicated that the spatial structuring was reflected in both the abundance of dominant features and in the assemblage in general.

Table 5.1: Spearman's rank-correlation ( $\rho$ ) values between corresponding elements of biotic feature similarity and sample distance matrices to investigate spatial structure in the megafaunal assemblage of Jennycliff Bay. Bold values indicate significant correlation,  $p < 0.05$ , estimated by a Monte Carlo permutation procedure [RELATE routine in PRIMER] ( $p$ -values in parentheses).

	Survey Year	
Data transformation	2000	2001
Untransformed	<b>0.175 (0.002)</b>	<b>0.161 (0.012)</b>
$\sqrt{\sqrt{}}$ transformed	<b>0.173 (0.008)</b>	<b>0.187 (0.002)</b>

### 5.3.2 Spatial pattern of the megafaunal assemblage

The rank-correlograms show that the spatial pattern of the megafaunal assemblage in Jennycliff Bay was patchy in both years (Fig. 5.5). Each year, the rank-correlograms produced from untransformed and  $\sqrt{\sqrt{}}$ transformed data analyses were similar, indicating that the spatial pattern was reflected in the distribution of common features and in the assemblage as a whole. There were, however, between-year differences in the form of the rank-correlograms (Fig. 5.5), which indicated that the spatial pattern was not temporally stable.

#### 5.3.2.1 May 2000 survey

The spatial structure of the megafaunal assemblage during the May 2000 survey appears as a 'wide wave' (*sensu* Legendre and Fortin, 1989) across the extent of the survey. The significant positive correlation coefficient for samples separated by 0–30 m in both rank-correlograms (Fig. 5.5 2000A and 2000B) indicated that the minimum patch size was greater than 30 m. Biotic similarity of samples decreased as sample separation increased until a significant negative autocorrelation minimum occurred in the 123–163 m distance class (Fig. 5.5 2000A and B), which represented the distance between samples that were least similar biotically. The biotic similarity of samples separated by 163–250 m was significantly lower than the average assemblage, but greater than samples separated by

123–163 m, suggesting that a megafaunal patch with a minimum radius of 123–163 m (corresponding to the autocorrelation minimum) was present in the assemblage (Fig. 5.5 2000A and B).

Although Spearman's  $\rho$  for samples separated by 250–380 m was not significantly different from zero, the trend of increasing Spearman's  $\rho$  between 163 and 380 m suggested that the patch structure might be nested within yet larger patches beyond the spatial extent of the present survey.

The autocorrelation coefficients in the untransformed rank-correlogram (Fig. 5.5 2000A) were relatively constant between 0–86 m, which suggests that the dominant features were distributed homogeneously within the patch. The switch from significantly positive to significantly negative autocorrelation coefficient values occurred between 86–123 m, which suggests that the patch boundary was well defined. Conversely, the autocorrelation coefficients in the  $\sqrt{v}$ transformed rank-correlogram decreased gradually to the significant minimum value, which suggests a gradient of biotic similarity between samples where the location of the patch boundary was less distinct than for the dominant features.

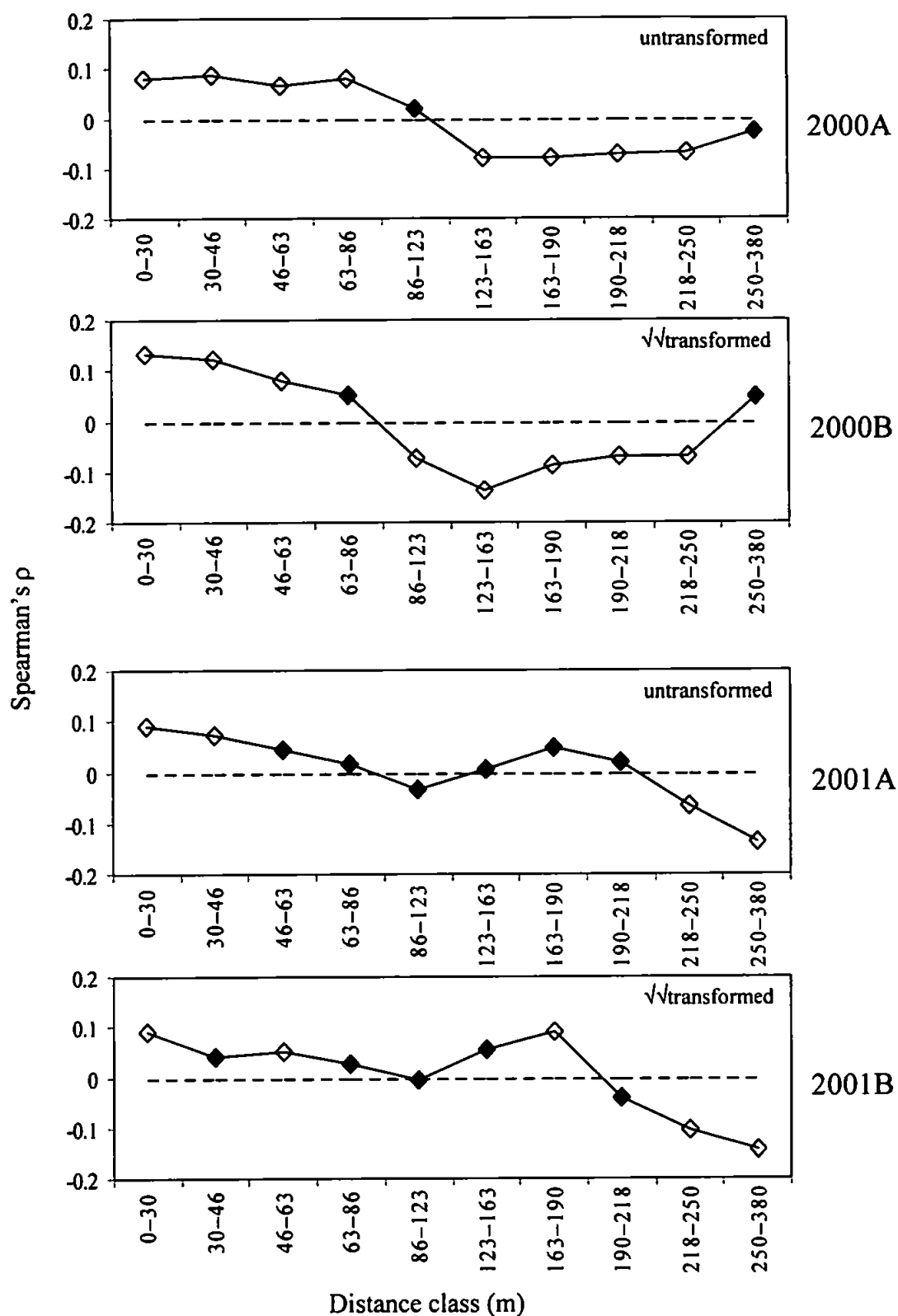


Figure 5.5: Rank-correlograms produced by correlation of Bray-Curtis similarities between samples separated by distance class in Jennycliff Bay, calculated using untransformed and  $\sqrt{\text{transformed}}$  abundance data for megafaunal biotic features. Open symbols  $p < 0.025$  or  $p > 0.975$ , closed symbols  $0.025 < p < 0.975$  estimated by Monte Carlo permutation [RELATE routine in PRIMER].

#### 5.3.2.2 March 2001 survey

The significant positive correlation coefficient for samples separated by 0–30 m in both rank-correlograms (Fig. 5.5 2001A and 2001B) indicated that the minimum patch size was greater than 30 metres. The biotic similarity of samples in the untransformed rank-correlogram decreased as sample separation increased (Fig. 5.5 2001A), suggesting that biotic feature distribution, biased towards the distribution of dominant features, represented a linear gradient across the survey extent. The minimum patch size detectable during March 2001 was between 250–380 m, inferred from the location of the autocorrelation minimum. Minimum patch size could be greater than 380 m if the value of the autocorrelation coefficient for samples greater than 380 m apart decreased further. Unfortunately, samples separated by more than 380 m were beyond the extent of the present survey, so minimum patch size could not be resolved. The transition between significant positive and significant negative autocorrelation coefficient values occurred over 46–218 m, in which Spearman's  $\rho$  was not significantly different from zero. This rank-correlogram pattern suggests that samples collected within the patch were not significantly different from the average biotic feature assemblage and the patch boundary was not clearly defined.

The general shape of the  $\sqrt{v}$  transformed rank-correlogram was similar to the untransformed rank-correlogram, indicating that the megafaunal assemblage was distributed in a patch with a radius of 250–380 m (Fig. 5.5 2001B). However, significant autocorrelation maxima in the 46–63 and 163–190 m distance classes suggested a nested pattern of megafaunal assemblage distribution within the 250–380 m radius patch. The radius of the nested patches could not be determined because the autocorrelation minima at the intermediate distance classes were not significantly different from zero.



#### 5.3.2.3 *Between-year differences in spatial pattern*

The spatial structure in the megafaunal assemblage in March 2001 was less clearly defined than in May 2000, because Spearman's  $\rho$  values in the rank-correlograms were lower in March 2001. The untransformed rank-correlograms (Fig. 5.5 2000A and 2001A) showed that dominant megafaunal features were distributed in a single patch in each year, although the March 2001 patch radius was larger than May 2000. Conversely, the  $\sqrt{d}$  transformed rank-correlograms indicated that the megafaunal assemblage in May 2000 was distributed in a single patch while there was a nested hierarchy of patches in the March 2001 megafaunal assemblage.

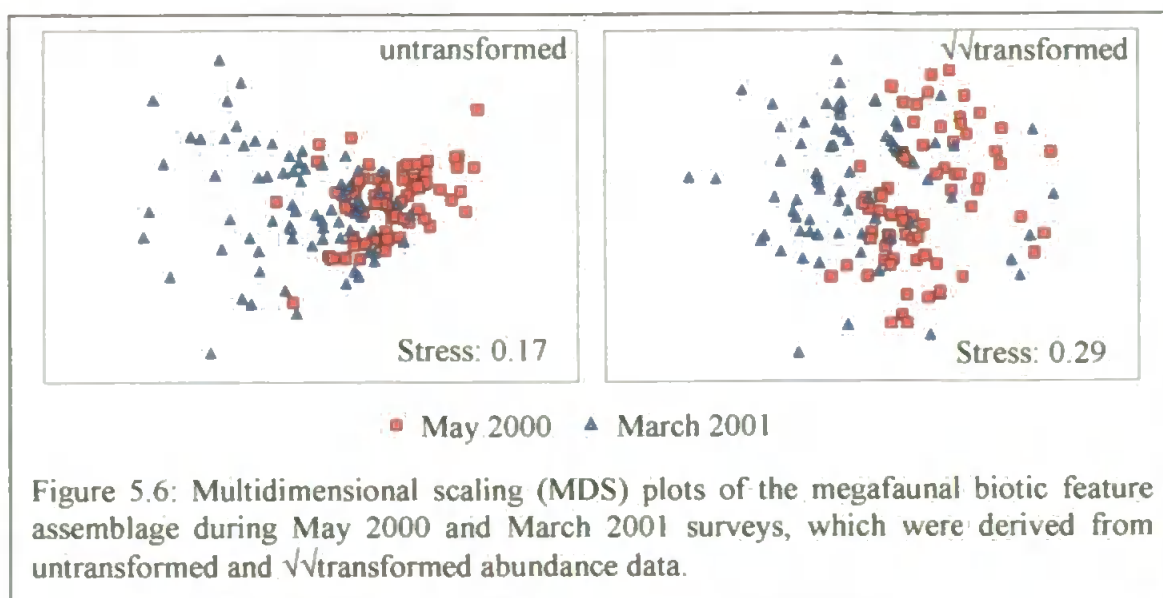
### 5.3.3 Megafaunal assemblage composition and spatial structure

Global tests using two-way crossed ANOSIM identified significant differences between years and stations (Table 5.2), indicating that the spatial structure of the megafaunal assemblage was not temporally stable. Significant between-year and between-station differences were observed in both untransformed and  $\sqrt{\sqrt{}}$ transformed abundance data, implying that the spatial structuring was reflected in the distribution of all the fauna.

Table 5.2: R-values from 2-way crossed ANOSIM test to test for significant differences in assemblage composition. Bold values indicate significant differences,  $p < 0.05$  ( $p$ -values in parentheses).

Factor	untransformed	$\sqrt{\sqrt{}}$ transformed
Year	<b>0.464 (0.001)</b>	<b>0.327 (0.001)</b>
Station	<b>0.276 (0.001)</b>	<b>0.301 (0.001)</b>

Non-parametric multidimensional scaling (MDS) plots of megafaunal biotic feature data provided a visualisation of between-year differences in megafaunal feature assemblage structure. The spread of points in the MDS plot for untransformed data showed that the variability in the distribution of common biotic features was greater in March 2001 than May 2000 (Fig. 5.6). However, the high stress values associated with the MDS plots, particularly using  $\sqrt{\sqrt{}}$ transformed data, suggested that an acceptable representation of the similarities in community structure had not been achieved. Consequently, interpretation of community structure within the megafaunal assemblage must be confined to the ANOSIM test statistic.



Pairwise tests, using one-way ANOSIM, were performed to identify which stations were significantly different from each other in each year (Table 5.3). Numerically dominant features (untransformed data) and the megafaunal assemblage ( $\sqrt{\sqrt{\phantom{x}}}$ transformed data) at the Central station were significantly different from all other stations during the May 2000 survey, indicating greater assemblage similarity at the centre of Jennycliff Bay compared to the edges of the patch (Fig. 5.1). Although the dominant features at the Fylrix and Nearshore stations were significantly different, the pattern was not reflected in the megafaunal assemblage as a whole. The distribution of common features, and the whole assemblage, in March 2001 was significantly different between all stations, except Central and Fylrix, which suggests complex spatial variation within the fauna. The lower R-values derived from the March 2001 survey indicated that between-station differences were not as well defined as in May 2000.

Table 5.3: R-values from pairwise comparisons of stations using 1-way ANOSIM. Bold values indicate significant differences,  $p < 0.05$  ( $p$ -values in parentheses).

Groups	Untransformed	$\sqrt{\sqrt{}}$ transformed
<i>May 2000</i>		
Beacon vs Central	<b>0.419 (0.001)</b>	<b>0.429 (0.000)</b>
Beacon vs Fylrix	0.090 (0.119)	0.012 (0.385)
Beacon vs Nearshore	0.141 (0.055)	0.081 (0.136)
Central vs Fylrix	<b>0.306 (0.001)</b>	<b>0.370 (0.000)</b>
Central vs Nearshore	<b>0.283 (0.001)</b>	<b>0.348 (0.000)</b>
Fylrix vs Nearshore	<b>0.185 (0.007)</b>	0.084 (0.058)
<i>March 2001</i>		
Beacon vs Central	<b>0.279 (0.003)</b>	<b>0.203 (0.015)</b>
Beacon vs Fylrix	<b>0.127 (0.042)</b>	<b>0.144 (0.025)</b>
Beacon vs Nearshore	<b>0.319 (0.000)</b>	<b>0.185 (0.018)</b>
Central vs Fylrix	0.073 (0.090)	0.059 (0.120)
Central vs Nearshore	<b>0.405 (0.000)</b>	<b>0.187 (0.000)</b>
Fylrix vs Nearshore	<b>0.323 (0.000)</b>	<b>0.334 (0.000)</b>

The biotic features that contributed most to the significant between-year differences in the megafaunal assemblage were identified using SIMPER analysis of untransformed abundance data. The common otter shell (*Lutraria lutraria*), thalassinidean burrow openings and rough/prickly cockles (cf. *Acanthocardia* sp.) were the best discriminating species, accounting for almost 70% of the dissimilarity between years (Table 5.4). Since the same discriminating species contributed to the majority of dissimilarity between stations in both survey years, the variation of abundance of these features was investigated further.

Table 5.4: Breakdown of the average dissimilarity of the biotic feature assemblage between years in Jennycliff Bay into contributions from each feature type [SIMPER routine in PRIMER]. Feature types are ordered in decreasing contribution; feature types in bold are discriminating species.

Biotic feature	Average dissimilarity	Average dissimilarity/ Standard deviation	Contribution (%)	Cumulative Contribution (%)
<b><i>Lutraria lutraria</i></b>	<b>25.70</b>	<b>1.59</b>	<b>50.4</b>	<b>50.4</b>
<b>Thalassinidean opening</b>	<b>5.54</b>	<b>1.17</b>	<b>10.9</b>	<b>61.3</b>
<b>cf <i>Acanthocardia</i></b>	<b>4.20</b>	<b>1.00</b>	<b>8.3</b>	<b>69.6</b>
<i>Turitella</i> sp.	3.02	0.70	5.9	75.5
<i>Callianassa</i> mound	1.98	0.94	3.9	79.4
Bivalve species 1	1.64	0.69	3.2	82.6
surface scrape	1.42	0.73	2.8	85.4
<i>Goneplax</i> burrow	0.86	0.42	1.7	87.1
Ophiuroid	0.84	0.48	1.7	88.8
<i>Hinia reticulata</i>	0.70	0.45	1.4	90.2

Two-way crossed ANOVA revealed significant between-year and between-station differences in *Lutraria lutraria* and in thalassinidean burrow opening abundance, while the abundance of cf. *Acanthocardia* sp. siphons was only significantly different between stations (Table 5.5). Significant interaction terms (i.e. Year×Station) indicate that the relative between-station differences were not consistent between years; thus the distribution of *Lutraria lutraria*, thalassinidean burrow openings and cf. *Acanthocardia* sp. was not consistent temporally.

Table 5.5: Results from 2-way crossed ANOVA analysis of abundance data (number of individuals per 0.5m<sup>2</sup> sample) for the biotic features discriminating between survey years (as identified by SIMPER routine). All factors were fixed. Bold values indicate significant differences,  $p < 0.05$ .

Source	df	SS	MS	F-ratio	<i>p</i> -value
<i>Lutraria sp</i>					
Year	1	<b>2673.21</b>	<b>2673.21</b>	<b>72.62</b>	<b>0.000</b>
Transect	3	<b>825.48</b>	<b>275.16</b>	<b>7.47</b>	<b>0.000</b>
Year × Station	3	<b>463.31</b>	<b>154.44</b>	<b>4.20</b>	<b>0.007</b>
<i>Thalassinidean openings</i>					
Year	1	<b>15.12</b>	<b>15.12</b>	<b>4.75</b>	<b>0.031</b>
Transect	3	<b>35.29</b>	<b>11.76</b>	<b>3.70</b>	<b>0.014</b>
Year × Station	3	<b>67.62</b>	<b>22.54</b>	<b>7.08</b>	<b>0.000</b>
<i>Callianassa mounds</i>					
Year	1	1.82	1.82	3.63	0.059
Transect	3	3.08	1.03	2.05	0.110
Year × Station	3	1.32	0.44	0.88	0.455
<i>cf Acanthocardia</i>					
Year	1	2.03	2.03	1.46	0.230
Transect	3	<b>53.29</b>	<b>17.76</b>	<b>12.76</b>	<b>0.000</b>
Year × Station	3	<b>111.04</b>	<b>37.01</b>	<b>26.59</b>	<b>0.000</b>

In May 2000, the mean abundance of *Lutraria lutraria* was significantly higher than in March 2001 (Table 5.6, Fig. 5.7); the mean abundance of this species at Central, Fylrix and Nearshore stations was significantly higher in May 2000 compared to March 2001. There was no significant between-year difference, however, in the mean abundance of *L. lutraria* at the Beacon station (Table 5.6 and Fig. 5.7). Significant between-station differences in *L. lutraria* abundance were detected only in May 2000, whereby, the mean abundance at the Fylrix station was significantly higher than at the Nearshore and Beacon stations (Table 5.6). At the Central station, the mean abundance of *L. lutraria* was less than at the Fylrix station, but greater than both Beacon and Nearshore stations (Fig. 5.7). The differences in *L. lutraria* abundance at the Beacon, Nearshore and Central stations were not statistically significant, however, which indicates that there was a spatial gradient in the abundance of *L. lutraria* within Jennycliff Bay during May 2000.

Table 5.6: Station differences in average abundance of dominant megafaunal features per 0.5m<sup>2</sup> sample in Jennycliff Bay. *P* values from Kruskal-Wallis tests; stations connected by lines are not significantly different ( $p < 0.05$ ) from each other (Tukey's HSD test). Stations are ordered, left-to right, from lowest to highest mean abundance, with minimum and maximum average abundance per 0.5m<sup>2</sup> sample presented for each feature. The integers 1 and 2 represent the May 2000 and March 2001 surveys, while B, C, F and N represent Beacon, Central, Fylrix and Nearshore stations, respectively.

	<i>p</i>	Station order	Min. – Max.
<i>Lutraria lutraria</i>	<0.000	N2 F2 C2 B2 N1 B1 C1 F1	5.3 – 24.4
Thalassinidean openings	<0.000	B2 N2 F2 C1 N1 B1 C2 F1	0.7 – 3.8
<i>Callianassa</i> mounds	<0.000	N1 N2 F1 B1 B2 C1 F2 C2	0.3 – 0.9
cf. <i>Acanthocardia</i> sp.	<0.000	B1 F2 N1 F1 B2 C2 C1 N2	0.0 – 2.8

In May 2000, the mean abundance of thalassinidean burrow openings was significantly higher than in March 2001, yet the mean abundance at each station was not significantly different between-years (Table 5.5, Fig. 5.7). Although there were no significant between-station differences in thalassinidean burrow opening abundance in May 2000, the highest mean abundance of thalassinidean burrow openings occurred at the Fylrix station. The highest mean abundance of *Lutraria lutraria* also occurred at the Fylrix station in May 2000, which suggests that the peak of megafaunal activity occurred at this station. Significant between-station differences detected in March 2001 showed that mean thalassinidean burrow opening abundance at the Central station was significantly higher than at all other stations (which did not differ significantly from each other) (Tables 5.5 and 5.6).

There were no significantly different between-year differences in the abundance of cf. *Acanthocardia* sp. siphons because the number of individuals in the samples was low in both years (Table 5.5, Fig. 5.7). cf. *Acanthocardia* sp. individuals were distributed in a patch that was located at the Central station in May 2000 and at the Nearshore station in

March 2001 (Fig. 5.7). Since the size distribution of *Acanthocardia* sp. siphons was not significantly different between years (mean diameter in May 2000 17.8 ±0.8 mm; March 2001 17.6 ±0.8 mm; Kolmogorov–Smirnov test,  $p=0.26$ ), the change in patch location may have been due to migration between survey years.

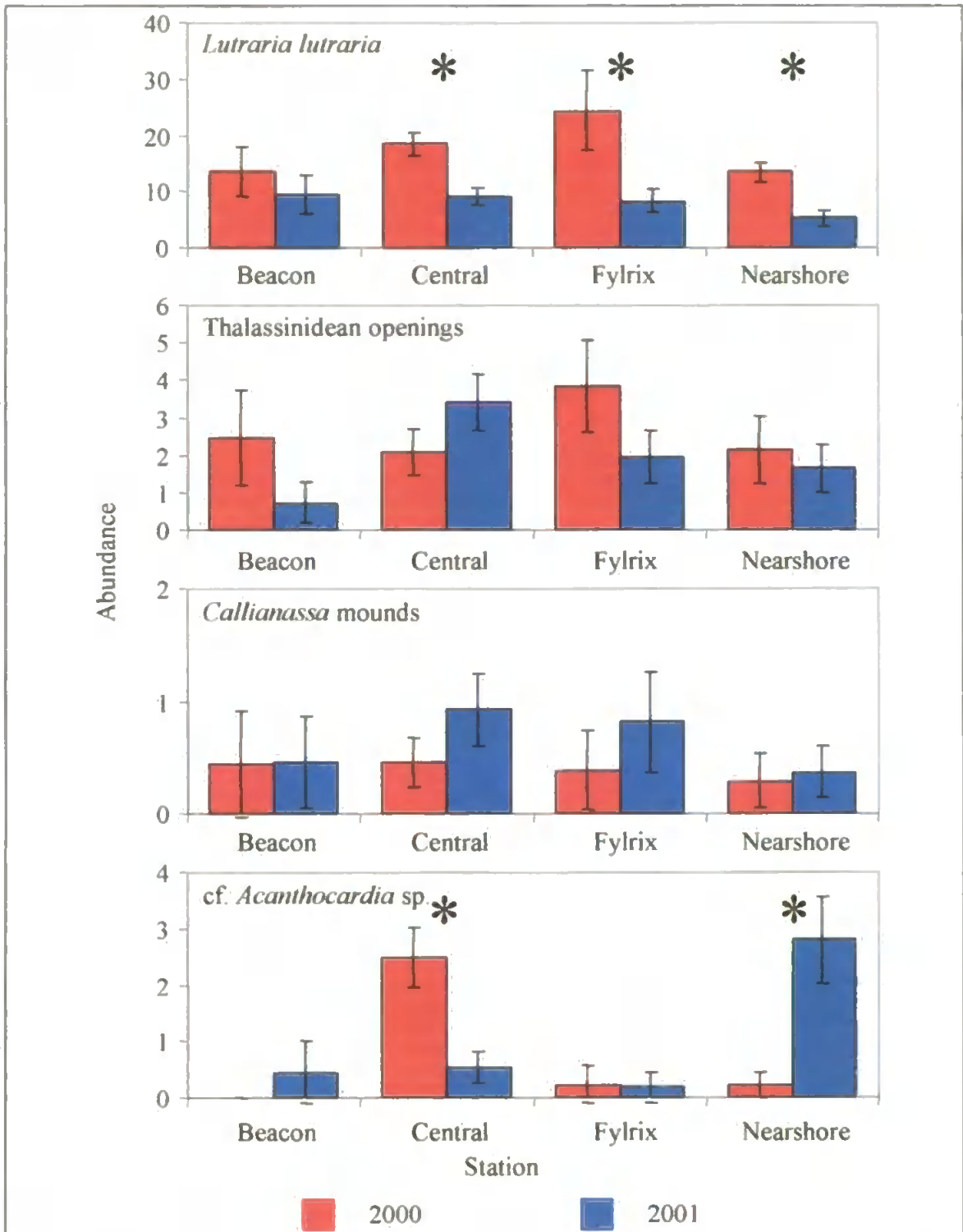


Figure 5.7: Mean abundance (number of individuals per 0.5m² video quadrat) in each station for four important megafaunal features, as identified by SIMPER analysis. Significant ( $p < 0.05$ ) between year differences within stations (Tukey's HSD) are marked with an asterisk.



### 5.3.4 Spatial pattern of *Lutraria lutraia* and thalassinidean openings

*Lutraria lutraria* and thalassinidean burrow openings were the discriminating features of the megafaunal assemblage both within and between surveys (Table 5.4). Since these features contributed most to between-station and between-year differences, their spatial pattern was investigated using rank-correlograms. In May 2000, the significant positive autocorrelation at the first distance class for *L. lutraria* indicated that minimum patch size exceeded 30 m (Fig. 5.8A), while the significant negative autocorrelation minima indicated patch radius was 218–250 m. Non-significant autocorrelation in the first distance class in March 2001 indicated that *L. lutraria* were arranged in patches less than 30 m radius, while these patches were separated by 30–46 m (significant autocorrelation maximum). The small patches of *L. lutraria* were nested within larger patches with radii of 250–380 m, indicated by a significant autocorrelation minimum.

The lack of significant autocorrelation at any distance class in the May 2000 rank-correlogram indicated that the thalassinidean burrow openings were spatially homogeneous during this month (Fig. 5.8B). In contrast, thalassinidean burrow openings were structured into patches with radius 123–163 m (significant autocorrelation minimum) separated by 250–380 m (significant autocorrelation maximum) during March 2001 (Fig. 5.8B). Figure 5.7 suggests that the patch structure of thalassinidean burrow openings was centred around the Central station.

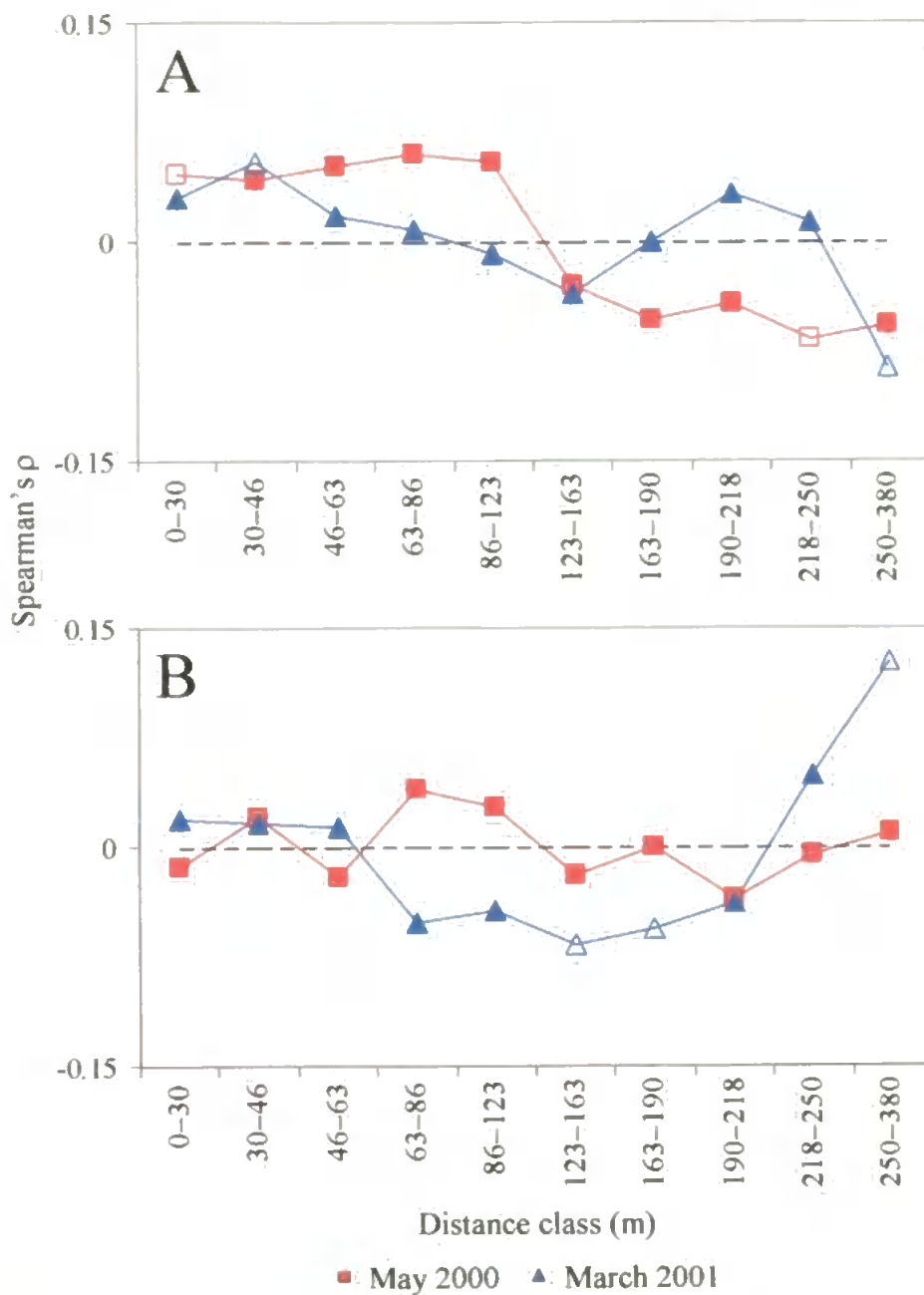


Figure 5.8: Rank-correlograms for (A) *Lutraria lutraria* and (B) thalassinidean burrow openings in Jennycliff Bay. Constructed from Spearman's  $\rho$  correlation between abundance and 'model' distance matrices using the RELATE routine.  $\square, \triangle$  symbols represent Spearman's  $\rho$  values where  $p < 0.025$  or  $p > 0.975$ ;  $\blacksquare, \blacktriangle$  symbols represent Spearman's  $\rho$  values where  $0.025 < p < 0.975$ .

## 5.4. DISCUSSION

The present study showed that the megafaunal assemblage, detected by quantitative spatially-referenced remote observations within a patch of homogeneous sediment, was neither uniformly distributed nor temporally stable. A nested hierarchy of spatial structure was detected within the megafaunal assemblage on a spatial extent up to 400 m. The significant between-year and between-station differences in megafaunal assemblage structure were best represented by abundance changes of thalassinidean burrow openings and *Lutraria lutraria* siphons.

### 5.4.1 Homogeneity of habitat and fauna

An apparently homogeneous habitat, such as Jennycliff Bay, should support a spatially homogeneous assemblage if a positive relationship between faunal diversity and habitat heterogeneity exists (e.g. Grassle and Maciolek, 1992; Cosson et al., 1997; Soltwedel and Vopel, 2001; Thrush et al., 2001). Homogeneous megafaunal distribution patterns may also result from intra- and inter-specific competition between the dominant animals within the assemblage, which, in the present study were thalassinidean shrimp (*Upogebia deltaura* and *Callianassa subterranea*) and the common otter shell (*Lutraria lutraria*). Thalassinideans construct complex burrows connected to the surface by a variable number of inhalant and exhalant openings and inhabited by a single individual. Although *C. subterranea* and *U. deltaura* are thought to deposit feed and suspension feed respectively (Aller and Dodge, 1974; Rowden et al., 1998), both species may change feeding modes to exploit the most advantageous food source (Nickell and Atkinson, 1995). Regular spacing of burrow openings may occur at the scale of individual burrows as a behavioural response to maximise the net benefit from the available food supply, which would result in homogeneous distribution of features. The minimum scale of thalassinidean homogeneity depends on the lateral extent of the burrow complex, which may reach 95 cm for callianassids (Suchanek et al., 1986), depending on the organic content of the sediment

(Berkenbusch and Rowden, 2000). The aggressive behaviour of thalassinideans (Ott et al., 1976) may cause individual burrow complexes to be separated, as burrow aggregation would increase the chance of meeting a conspecific individual. Consequently, a uniform distribution of individuals with a favourable habitat may be expected at the next largest scale.

Regular spacing of *Lutraria lutraria*, a suspension-feeding bivalve that lives permanently buried in a burrow approximately 30 cm below the sediment surface, may also occur in response to intra-specific competition for space and food. A weak foot limits the movement of *L. lutraria* within the burrow, so contact with the overlying water is maintained through partially retractable fused siphons (Holme, 1959). *L. lutraria* uses the sediment fabric for support rather than for a food supply, but surrounding sediment may become contaminated with pseudofaeces in hydrodynamically-quiescent habitats. Intra-specific competition for suspended particles, and the deleterious effects of pseudofaeces, combined with inter-specific competition for space in the sediment fabric may, therefore, result in a uniform distribution of dominant features within favourable habitats.

Despite an apparently homogeneous habitat and biological processes that may create homogeneous megafaunal distributions, a nested hierarchy of spatial structure was detected within the megafaunal assemblage on a spatial extent up to 400 m. Similarly, heterogeneous distributions of individual species (e.g. *Macomona liliana* and *Austrovenus stutchburyi* [Thrush et al., 1997a]) and assemblages (Zajac et al., 2000) within apparently homogeneous sediment habitats have been reported previously, so alternative hypotheses that may produce faunal heterogeneity must be considered. To identify the processes influencing the distribution of individuals and species within a habitat, the physical factors that operate at larger scales must be considered simultaneously with biological processes that operate on smaller spatial scales (Thrush et al., 1997a).

## 5.4.2 Alternative hypotheses for heterogeneous faunal distributions

The hydrodynamic regime and geological history set the boundary conditions within which a particular sediment habitat exists. Jennycliff Bay sediment was classified as homogeneous muddy sand using acoustic techniques that measure the reflectance of the seabed (Morrison et al., 2001). Acoustic reflectance of subtidal sediments, however, can be affected by water depth, geotechnical properties and pore water content as well as granulometry (Morrison et al., 2001). In addition, sediment granulometry covaries with other physical variables, such as organic content, microbial content and food supply, all of which may be affected hydrodynamically (Hall, 1994). Acoustic seabed classification techniques may, therefore, conceal subtle differences in the physical characteristics of sediment habitat. Consequently, faunal heterogeneity may occur in acoustically-homogeneous habitats in response to subtle variations in physical variables, which manifest themselves through biological structuring processes such as non-uniform settlement or non-uniform survival of the fauna.

### 5.4.2.1 Influence of physical processes on settlement of fauna

Many of the megafaunal features/species observed in the present study, including the numerically-dominant thalassinideans and *Lutraria lutraria*, have planktotrophic larvae (Dumbauld et al., 1996) that are transported passively in the water column. Consequently, the spatial distribution of larvae immediately preceding settlement may be affected by the hydrodynamic regime at the sediment–water interface, which is itself affected by the presence of burrow openings and mounds (Eckman, 1983). Although larval recruitment depends primarily on settlement to a suitable substratum (e.g. Feldman et al., 1997) the success of larval recruitment may be influenced further by spatial variation in sediment granulometry (or associated factor) within an area of suitable sediment. The hydrodynamic regime at the sediment–water interface may influence further the abundance and distribution of adults through dispersal of resuspended postlarvae (e.g. Ólafsson et al.,

1994; Hunt and Scheibling, 1997). Megafaunal bivalves may undergo postlarval dispersal in the water column either through passive erosion and transport with resuspended sediment (Emerson and Grant, 1991) or by active resuspension and byssal drifting (Armonies, 1992). The influence of postlarval transport may be greater for smaller bivalve individuals (e.g. less than 2 mm for *Mya arenaria* [Hunt and Mullineaux, 2002]) because resuspension is affected by particle size, but may also be significantly related to the ambient density of adults.

In the present study, the megafaunal features observed were greater than 1 cm diameter, which suggests that all bivalve siphons and burrow openings were associated with individuals that had survived larval settlement and reached adult size. Between-station differences in the abundance of *Lutraria lutraria* and thalassinidean burrow openings may, therefore, reflect spatial variation in the hydrodynamic regime at the sediment–water interface, which imposes spatial variation on megafaunal assemblage structure through direct and/or indirect effects on larval settlement post-settlement survival. Without prior knowledge of the scale of megafaunal variation, it was not possible to collect appropriate data to investigate further the relative importance of pre- and post-settlement processes at the sediment–water interface on the distribution and abundance of the megafaunal assemblage.

#### *5.4.2.2 Mechanisms by which resident fauna influence settlement and survival of fauna*

In addition to variation of the hydrodynamically induced habitat characteristics, megafaunal distribution patterns may be influenced further by the interaction of newly settled individuals with the resident fauna i.e. post-settlement processes. Bioturbation by megafaunal species disturbs the geophysical and geochemical properties of sediments, particularly in areas of low abiotic disturbance (e.g. Hall, 1994; Snelgrove and Butman, 1994), which influences the structure and composition of associated macrofaunal

assemblages (e.g. Woodin, 1978; Brenchley, 1981; Posey, 1986). Megafaunal bioturbation and suspension feeding may also influence the recruitment and survival of megafaunal individuals (Woodin, 1976), while fractions of the associated macrofaunal assemblage may prey upon megafaunal larvae. Consequently, spatial variation of the resident macro- and megafauna may further influence the spatial structure of megafaunal assemblages through bioturbation activity, which alters the available biotic/abiotic resources.

#### 5.4.2.2.1 Effects of megafaunal bioturbation on sediment reworking

The construction of burrows by thalassinidean shrimp in Jennycliff Bay affects sediment compaction and turbidity, while *Callianassa subterranea* can also expel significant volumes of sediment from the burrow (Rowden et al., 1998). Megafaunal burrowing activity may, therefore, create local patches of unstable sediment that smother animals with low mobility and inhibit larval settlement and/or recruitment (e.g. Posey et al., 1991). The burrow openings and mounds associated with thalassinidean and bivalve burrowing activity also increase the complexity of surface topography and may increase pore water content (Rhoads, 1974), all of which decreases bed shear stress, a measure of the erodability of the sediment surface. As a result, sediment resuspension from areas containing high densities of biogenic sediment structures will be greater than from a flat seabed under the same tidal currents (Widdows et al., 2000). While increased resuspension may benefit megafaunal individuals directly by increasing food availability and the rate pseudofaeces removal (Paterson and Black, 1999), the indirect effects on larval settlement and survival may impose further structure on mega- and macrofaunal assemblages.

#### 5.4.2.2.2 Effects of megafaunal bioturbation on sediment geochemistry

In addition to variation of the physical properties of the sediment, bioturbation may elicit non-uniform settlement and survival of megafauna by affecting the chemical characteristics of, and nutrient fluxes through, the sediment. Megafaunal burrow and tube

structures, and ventilation by the inhabitants, extends oxygenation to depths greater than ambient sediment conditions, which increases the habitat available to species that are sensitive to anoxic conditions (e.g. Forster and Graf, 1995; Astall et al., 1997). Sediment reworking may also incorporate organic material at the sediment–water interface into the sediment and expose buried material which, combined with increased oxygenation, increases the amount of food available to the associated fauna (Branch and Pringle, 1987).

The spatial variation of physical and chemical characteristics of the sediment habitat caused by bioturbating megafauna may affect the composition of the associated fauna in a predictable manner because animals with different life histories and functional roles display different responses to bioturbation. For example, the abundance of suspension feeding fauna may be reduced in areas of high bioturbation due to increased sediment reworking/resuspension, which may reduce the efficiency of food collection and block the filtering apparatus [cf. Trophic Group Amensalism hypothesis (Rhoads and Young, 1970)]. Similarly, mobile fauna may be able to withstand the effects of sediment reworking by the megafauna more efficiently than sessile fauna (Brenchley, 1981). Functional grouping may be extended and applied to megafaunal bioturbators as experimental evidence has shown that the mode, plus the intensity, of bioturbation by different megafaunal species can have a significant effect on the structure of macrofauna assemblages (Widdicombe and Austen, 1999). Various schemes for classifying bioturbation mode exist (e.g. Swift, 1993; Dauwe et al., 1998), which offer a way forward for investigating the influence of megafaunal distribution patterns on macrofaunal distribution patterns. However, further investigation to assess the robustness of functional group definitions and the potential for individual species to overlap different functional groups is required before megafaunal distribution patterns may be used as a surrogate to predict macrofaunal distribution patterns. The functional group approach to investigating megafaunal bioturbation and the



implications for the associated fauna remains an attractive technique, but is beyond the scope of this thesis.

#### 5.4.2.2.3 Effects of resident macrofauna on megafaunal distribution

The potential mechanisms by which megafaunal activity, specifically bioturbation, may create and maintain spatial heterogeneity in the mega- and macrofaunal assemblages have been discussed above. However, burrowing activity by macrofaunal-sized individuals may also contribute to sediment reworking and changes in sediment geochemistry. In addition, the spatial variation of macrofaunal assemblages may also feed back into megafaunal distribution patterns if newly settled megafaunal recruits represent a viable food supply for predatory macrofauna.

#### 5.4.2.2.4 Interaction between megafaunal and macrofaunal assemblage structure

Hypotheses may be raised to test whether megafaunal and macrofaunal assemblages influence each other, but assessing the relative importance of each contribution is difficult. Intensive grab sampling of Jennycliff Bay (July 1995) identified patches of macrofaunal animals at scales below 500 m and suggested that these patches were nested within larger areas that could be seen as homogeneous at larger spatial scales (Kendall and Widdicombe, 1999). Given that the extent of megafaunal and macrofaunal patches occurred at similar scale, the hypothesis that one influences the other cannot be rejected.

The lack of a single process that explains spatial pattern in benthic assemblages occurs because all species respond to the spatial and temporal variation in the environment at their own unique scale; the species ambit. Spatial heterogeneity of macrofaunal assemblages on the scale of hundreds of metres has been detected elsewhere (Thrush et al., 1989; Morrissey et al., 1992), which suggests that macrofaunal organisms have similar species ambits. It seems reasonable to assume that the small-bodied macrofauna respond to processes

associated with the larger-bodied megafauna because species ambit appears to be a function of body size and mobility (Hewitt et al., 1996).

Temporal variability of the megafaunal distribution patterns presented in this thesis suggest that macrofauna samples must be collected concurrently with megafaunal observations to assess directly the relationship between scales of megafaunal and macrofaunal distribution patterns. However, the similarity of scales of distribution encourages investigation of the potential use of megafaunal distribution patterns as a surrogate for mapping and predicting macrofaunal distribution.

As discussed earlier, megafaunal bioturbation affects physical and chemical processes that interact in a complex manner to modify the availability of resources to the associated fauna. Thalassinidean life span is 2–3 years (Witbaard and Duineveld, 1989), while a bivalve species similar to *Lutraria lutraria* (*Mya arenaria*) generally lives 10–12 years but may reach 28 years (Strasser, 1999). Therefore, established megafaunal individuals have the potential to affect the shorter-lived macrofaunal species in the surrounding sediment through direct and indirect effects of bioturbation. The critical role played by megafaunal species in creating and maintaining assemblage structure, particularly in areas of low abiotic disturbance, has been recognised by the term ‘ecosystem engineers’ (Lawton, 1994). An ecosystem engineer structures assemblages through disturbance rather than trophic processes [cf. Keystone species (Paine, 1966)]; autogenic engineers modify the environment via their own physical structures (e.g. coral reefs and trees) while allogenic engineers transform biotic/abiotic materials that are available to others (Lawton, 1994). Megafaunal species considered in the present study may, therefore, be considered as allogenic ecosystem engineers (Jones et al., 1994)

### **5.4.3 Legitimacy of homogeneous habitat**

The present study aimed to quantify the extent to which megafaunal assemblage heterogeneity could be detected in a homogeneous sediment. Although the survey location had been defined acoustically as a patch of apparently homogeneous sublittoral muddy sand (Moore et al., 1999), acoustic ground discrimination systems impose boundaries on the seabed to constrain areas that are acoustically different. However, classification of sediments represents artificial boundaries along a continuous gradient of grain size, which covaries with other habitat characteristics as described above. In the present study, the megafaunal assemblage/biotic feature landscape was defined based on statistical criteria. In practice, the seabed habitat is a mosaic of different sediment grades that support different assemblages and densities of fauna that respond to spatial and temporal variation in the environment at many overlapping scales. Consequently, the scales at which the key ecosystem processes operate must be identified so that techniques may be developed to map, monitor and, ultimately, predict the spatial arrangement of ecosystem functions.

### **5.4.4 Consideration of the sampling technique**

Megafaunal assemblage data extracted from remote observations of the seabed may be considered as a measure of the biologically-mediated landscape, rather than as an absolute estimate of megafaunal species abundance. The definition of megafaunal assemblage used in the present study encompassed surface dwelling megafauna and biogenic sediment features, such as burrow openings and mounds, because many soft-sediment megafaunal species bury deep in the sediment. Although surface features may be used to infer the identity of species responsible for constructing the features, it is not possible to use counts of features to make an absolute estimate of animal numbers because burrows have a variable number of openings. For example, a single thalassinidean burrow may have between 1–17 inhalant openings (Atkinson and Nash, 1985), which may vary between sexes and sediment type (Nickell and Atkinson, 1995; Rowden and Jones, 1995).

Nevertheless, within any single area the number of openings per burrow is reasonably consistent and at such a scale comparisons are possible.

In deep-sea observations, the presence of biogenic sediment features does not necessarily reflect concurrent megafaunal activity because low current conditions may allow traces to persist for long periods after formation (Wheatcroft et al., 1989). Biogenic sediment features are likely to have shorter persistence times in the shallow water of Jannycliff Bay because vacant burrow openings would fill rapidly in a heavily bioturbated sediment. Similarly, *Callianassa* sp. mounds can be dispersed easily by currents (Aller and Dodge, 1974), while detached *Laminaria* sp. fronds, dragged across the seabed in the current, flatten surface features (personal observation). The length of time that a vacated burrow persists may be influenced by a variety of local factors, such as local hydrography, bioturbation activity and sedimentation rate. Biogenic features, however, represent areas where the physical and chemical processes associated with bioturbation that may impose structure on macrofaunal assemblages, such as changes in sediment granulometry, chemistry and organic content, operate long after the bioturbating activity ceased. Quantification of epi-megafauna and biogenic sediment features is, therefore, a necessary requirement in the context of applying megafaunal assemblage structure as a surrogate for mapping and predicting macro-infaunal assemblages.

The minimum scale at which biotic feature variation can be investigated using remote observations is limited by the accuracy of the underwater positioning system (Chapter 2). The data presented in this thesis were extracted from images accurate to within 5 m of their true position, which is the same accuracy expected from differential GPS. While patchiness of the megafaunal assemblage at a sub-5 m scale is quite possible (Section 5.4.1), it could not be detected using the techniques employed in this thesis. The location of ROV stations used here was intended to maximise the spatial extent of the survey while

avoiding the edges of the patch. More images could have been collected within the extent of the survey. However, the number of pairs of observations that contribute to the Spearman's  $\rho$  correlation between matrices was very high. Consequently, many more samples would need to be collected to influence the value and significance of the correlation coefficient. Extra images could have been gathered outside the extent of the current survey, but these samples would have fallen outside the patch of apparently homogeneous sediment within Jennycliff Bay. Consequently, investigation of spatial pattern in the megafaunal assemblage at scales greater than 400 m may have been influenced by changes in the composition of the assemblage associated with a different sediment habitat rather than biotic interactions.

The design of any ecological study is affected by spatial scaling (Wiens, 1989), particularly when attempting to elucidate the relationship between a process and the faunal response. Spatial autocorrelation in an assemblage implies that samples taken close together will underestimate faunal variability, while the lack of independence between samples affects the number of degrees of freedom used to calculate statistical significance. To sample spatial variation within the megafaunal assemblage in the present study, sample lag should be 86–123 m because there was no significant spatial autocorrelation of these samples in either year. Similarly, it would be unwise to collect samples within 63 m of each other because positive spatial autocorrelation coefficients imply that the samples would be more alike than expected by chance. Increasing sample lag to between 218–250 m in the present study would encompass a greater proportion of faunal variability; thus the chances of incurring a Type I error are reduced (i.e. conclude a significant difference occurs when none exists). Investigation of megafaunal distribution patterns with limited resources should use replicate samples that are separated by at least 200 m to avoid confounding the survey objectives with spatial autocorrelation.

## 5.5 CONCLUSIONS

The detection of significant spatial heterogeneity in the megafaunal assemblage from an area classified (using acoustic techniques) as apparently homogeneous muddy sand suggested that quantitative remote observations allow collection of megafaunal assemblage data with greater spatial resolution than previously possible. The scale of spatial heterogeneity in the megafaunal assemblage was similar to that of the macrofaunal assemblage in the same site, which indicates that the application of megafaunal assemblage distribution patterns may elucidate the processes that impose structure on infaunal assemblages. Acoustic ground discrimination systems provide a low cost method for determining broad-scale sediment distribution patterns, from which crude estimates of the distribution of associated fauna may be inferred. Conversely, grab-sampling provides high resolution data on the structure of macrofaunal assemblages, but at relatively high costs. The approach described in this paper offers ways forward to address how variation of megafaunal assemblages at intermediate spatial scales might be related to, and interact with, the physical characteristics and macrofaunal assemblage structure of subtidal soft sediment habitats.

The significant between-year and between-station differences in megafaunal assemblage structure were best represented by changes in abundance of thalassinidean burrow openings and *Lutraria lutraria* siphons. The significant decrease in abundance of *L. lutraria* between May 2000 and March 2001 is of interest because these large bivalve species may represent a large proportion of the megafaunal biomass. Investigation of the population size structure of *L. lutraria* and estimates of their biomass will be presented in the following Chapter.

## **CHAPTER 6**

### **Population size structure and biomass of *Lutraria lutraria* in Jennycliff Bay**

## ABSTRACT

For marine benthic assemblages, assessment of biomass and oxygen consumption rarely includes the megafauna because the core samples that are collected and incubated to calculate sediment community oxygen consumption are not large enough to sample adequately the megafauna. Although megafauna contribute only a small proportion to total abundance, the contribution to total biomass, and hence respiration, may be much greater. This chapter investigates the population size structure of the megafaunal bivalve *Lutraria lutraria* by measuring the dimensions of the characteristic surface openings they produce. Biomass estimates were derived using size–weight relationships for a similar infaunal bivalve, *Mya arenaria*. The biomass estimates are associated with important caveats relating to the validity of applying size–weight relationships that were derived for a similar species and the extent to which the dimensions of surface openings relate to the width of the siphons. Hence, the contents of this chapter represent a proof of concept and the magnitude of the biomass estimates must be treated with caution.

Nevertheless, gross estimates of *Lutraria lutraria* biomass and respiration were estimated over two years. Results suggest that the population size structure of *L. lutraria* in Jennycliff Bay was stable between years, despite significant between-year differences in abundance. Gross estimates of *L. lutraria* biomass were  $96.5 \pm 9.1$  and  $48.6 \pm 7.1$  g AFDW per  $0.5 \text{ m}^2$  in May 2000 and March 2001 respectively, which represented approximately 90% of the endobenthic biomass. Results indicate that the assessment of benthic biomass and respiration by consideration of macrofaunal samples alone will underestimate severely the biomass and respiration of the entire endobenthic assemblage.



## 6.1 INTRODUCTION

To understand the functioning of ecosystems requires detailed knowledge of rates of various processes, particularly of energy flow (Thurston et al., 1994). Although direct measurement of energy flow rates in benthic habitats is difficult, measurement of biomass, and the partitioning between different fractions of the fauna, is a viable alternative (Platt, 1985; Piepenburg et al., 1995). The quality and quantity of organic matter that reaches the seabed from the water column governs ultimately the total organic content of marine sediments (Graf et al., 1982; Grebmeier and McRoy, 1989). In turn, the supply of organic matter depends on a variety of factors including primary production, particle sinking, zooplankton grazing and lateral advection. Organic matter that reaches the seabed is partitioned between the fully decayed fraction (refractory), the labile fraction (food) and the fraction contained within the fauna themselves (i.e. standing crop biomass) (Graf, 1992). To quantify the total organic content of sediments, and the pathways through which energy flows within and between the sediment and water column (i.e. benthic–pelagic coupling), the distribution and biomass of the key components of benthic and pelagic assemblages must be investigated.

Energy flow through benthic assemblages has been estimated through measurement of sediment community oxygen consumption (SCOC), which represents an integrated measurement of chemical and biological oxygen uptake (Pfannkuche, 1993; Drazen et al., 1998). SCOC is estimated from sediment cores that are incubated either *in situ* or under laboratory conditions. Normally, the sediment cores contain only the microbial, meio- and macrofaunal-sized fraction of the fauna because megafaunal-sized individuals are not sampled adequately by cores (Thurston et al., 1994). Indeed, any megafaunal and/or large macrofaunal individuals are usually removed from cores prior to incubation because their inclusion increases the magnitude of error terms around mean SCOC values. While SCOC estimates derived from short-lived macrofaunal-sized animals provide a measure of recent

carbon flux, the megafaunal-sized animals may represent a significant portion of the total biomass and, hence, community respiration (e.g. Schwinghamer, 1981). In addition, long-lived megafaunal individuals effectively average water column processes over seasonal and annual time scales, thus indicating longer-term trends in ecosystem processes (e.g. Graf et al., 1982). To improve benthic–pelagic coupling models, therefore, quantitative methods to estimate the spatial distribution and biomass of megafaunal individuals are required (Piepenburg and Schmid, 1996).

As megafaunal-sized individuals are not sampled adequately by traditional grab and core techniques (Thurston et al., 1994), remote imaging has been suggested as the most appropriate method of assessing the biomass of soft sediment megabenthic assemblages (Rice et al., 1982; Piepenburg et al., 1995). Remote camera systems have been used in this context as they may be deployed to collect epifaunal abundance data over a wide spatial extent where sample grain is larger than that of grabs and cores. To quantify energy flow, however, biomass must be estimated from individuals in images before carbon and oxygen uptake estimates may be derived. Remote imaging techniques have, thus far, been limited to estimating biomass of epifaunal species, such as ophiuroids, where biomass is extrapolated from the abundance and size distribution of individuals in images and size–weight relationships that are determined from sledge catches (Piepenburg and von Juterzenka, 1994; Piepenburg and Schmid, 1996).

The megafaunal assemblage in Jennycliff Bay was dominated by infaunal organisms, including the common otter shell (*Lutraria lutraria*) and thalassinidean mud shrimps (Chapter 4), so it was not possible to estimate the biomass of the dominant species through direct measurement of the individuals themselves. However, assuming that there is a relationship between the size of the burrowing individual and the size of the burrow they construct, the biomass of infaunal organisms may be extrapolated from measurements of

the surface openings. *L. lutraria* is a deep burrowing suspension-feeding bivalve that maintains contact with the water column through inhalant and exhalent siphons that are fused together along their length (Holme, 1959). Each individual is associated with a single surface opening in which the siphon tips were usually visible in video images (Appendix I), so the abundance of surface features is equal to the abundance of individuals. The diameter of the siphons, and the permanent burrow that they occupy, may be used to estimate indirectly the shell dimensions and, hence, body weight, so the population size structure of *L. lutraria* may be derived from abundance and size distribution of surface openings.

In the following sections of this chapter, the distribution of biomass within the *Lutraria lutraria* population will be investigated using the size distribution of surface openings. To assess partitioning of biomass between different fractions of the benthic assemblage, gross estimates of *L. lutraria* biomass will be derived as a measure of megafaunal biomass. Similarly, the rate of oxygen consumption by *L. lutraria* will be estimated as a function of biomass to assess respiration of the megafaunal assemblage.

## 6.2 MATERIALS AND METHODS

### 6.2.1 Survey location and design

The population size structure of the common otter shell, *Lutraria lutraria*, in Jennycliff Bay was investigated using individuals from sample images recorded to investigate the spatial and temporal structure of the megafaunal assemblage (Chapter 5). A full description of the survey design and method for extracting still image samples from the videotape is provided in Section 5.2. The diameter of individual surface openings was measured from annotated still images to the nearest millimetre using *Benthic Imager* software (Section 2.2.3). The width of the siphon that created each burrow was assumed to be equal to the diameter of the surface opening because the siphons appear to be in contact with the sediment along their length. A similar method of using the diameter of empty burrow shafts to measure indirectly the siphon width of *Mya arenaria* was proposed by Zwartz and Wanink (1989).

### 6.2.2 Data extraction

The relationship between siphon dimensions and shell length or body weight of *Lutraria lutraria* could not be quantified from the Jennycliff Bay population because insufficient numbers of individuals were recorded. There are also no data in the literature that relate the dimensions of siphons and shell size or body weight of other *L. lutraria* populations. Consequently, the weight of each *L. lutraria* individual was estimated by applying published conversion factors that relate siphon size and shell length and, subsequently, shell length and individual weight, which were derived for the sand gaper, *Mya arenaria*. Although *L. lutraria* and *M. arenaria* are members of different Orders (Veneroida and Myoida, respectively), the morphology of each species is very similar (the species may be distinguished by the hinge teeth pattern [Gibson et al., 2001]). Consequently, the body size–weight relationships for *M. arenaria* provided a reasonable approximation for estimating *L. lutraria* body size.

The relationship between siphon width and shell length in *Mya arenaria*, measured along the antero-posterior axis, may be expressed as:

$$\text{Siphon width} = 0.23 \times (\text{shell length})^{0.91} \quad \text{Equation 1}$$

(Zwarts and Wanink, 1989)

where siphon width and shell length were measured in millimetres;  $r^2=0.98$  and number of individuals was 166 (Zwarts and Wanink, 1989). Equation 1 may be arranged so that shell length is the subject of the equation as follows:

$$\text{Shell length} = \left( \frac{\text{siphon width}}{0.23} \right)^{\frac{1}{0.91}} \quad \text{Equation 2}$$

The relationship between shell length and ash-free dry weight (AFDW) of *Mya arenaria* may be expressed as:

$$\log_{10}[\text{AFDW}] = -2.3948 + (3.2478 \times \log_{10}[\text{shell length}]) \quad \text{Equation 3}$$

(Warwick and Price, 1975)

where AFDW and shell length were measured in grams and centimetres respectively;  $r^2=0.987$  and number of individuals was 20 (Warwick and Price, 1975). Equation 3 may be modified to calculate the AFDW of each individual as follows:

$$\text{AFDW} = 10^{(-2.3948 + [3.2478 \times \log_{10}(\text{shell length})])} \quad \text{Equation 4}$$

The relationship between siphon width and AFDW for *Mya arenaria* may be calculated by substituting Equation 2 into Equation 4 to produce the following:

$$\text{AFDW} = 10^{\left( -2.3948 + \left[ 3.2478 \times \log_{10} \left( \frac{(\text{siphon width}/0.23)^{1/0.91}}{10} \right) \right] \right)} \quad \text{Equation 5}$$

where ash-free dry weight (AFDW) was expressed in grams and siphon width was measured in millimetres.

To estimate the contribution of *Lutraria lutraria* to carbon flux models, the conversion factor of carbon biomass from AFDW was derived from published biomass size classes (Gerlach et al., 1985: Table 2, macrofauna):

$$\text{Carbon biomass} = \text{AFDW} \times 0.58 \quad \text{Equation 6}$$

To estimate the contribution of *Lutraria lutraria* to the benthic respiration, the AFDW of each individual was converted to oxygen consumption. As there are no published data on the relationship between individual weight and oxygen consumption for *Lutraria lutraria*, data relating individual weight and oxygen consumption in *Mya arenaria*, measured in the laboratory at 4.5 °C, were applied (Emerson et al., 1988):

$$\log_{10}[\text{Oxygen consumption}] = 0.461 + (0.558 \times \log_{10}[\text{dry weight}]) \quad \text{Equation 7}$$

(Emerson et al., 1988)

where oxygen consumption was expressed in  $\mu\text{l O}_2 \text{ h}^{-1}$  and dry weight was measured in milligrams;  $r^2=0.75$  (Emerson et al., 1988). In *Mya arenaria*, AFDW represents 15.6% of dry weight (Rumohr et al., 1987), so individual oxygen uptake may be derived from individual ash-free dry weight as follows:

$$\text{Oxygen uptake} = 10^{\left( \left( 0.558 \times \log_{10} \left[ \text{AFDW} \times \frac{100}{15.6} \right] \right) + 0.461 \right)} \quad \text{Equation 8}$$

where oxygen consumption (at 4.5°C) was expressed in  $\mu\text{l O}_2 \text{ h}^{-1}$  and ash-free dry weight (AFDW) was measured in milligrams.

The relationship between biomass and oxygen consumption was derived from data on *Mya arenaria* individuals at an ambient temperature of 4.5 °C, which is considerably lower than the 13–15 °C encountered by the megafaunal assemblage in Plymouth Sound in summer (Chapter 3). The effect of temperature on metabolic rate may be assessed by considering the  $Q_{10}$  value, which represents the factor by which metabolic rate increases when ambient temperature is raised by 10 °C. For *M. arenaria* in Chesapeake Bay, the  $Q_{10}$  value was

between 2–3 (Kennedy and Mihursky, 1972), which indicates that the metabolic rate will either double or treble in response to a 10 °C increase in ambient temperature. Therefore, the estimated respiration rate of *Lutraria lutraria* (Equation 8) was multiplied by 2.5 (median  $Q_{10}$  value) to account for the difference in temperature between Jennycliff Bay and laboratory conditions. While the temperature correction applied by  $Q_{10}$  values affects the magnitude of respiration rate estimates, the relative contribution of individuals to community respiration will be maintained (Schwinghamer et al., 1986).

### 6.2.3 Data analysis

To compare the population size structure of *Lutraria lutraria* in Jennycliff Bay between years, a size–frequency histogram was constructed. For both years, the siphon width measurements were used to allocate each individual to a siphon size class that ranged from 10–30 mm in intervals of 2 mm. The equivalent shell length and ash-free dry weight (AFDW) ranges associated with each siphon width class were calculated, and displayed as secondary and tertiary abscissae. Histograms were constructed using both the abundance and proportion of the population in each size class.

The relationships between siphon width, shell length and AFDW were generated from data on *Mya arenaria* populations in which the maximum shell length of individuals was 10 cm (Warwick and Price, 1975; Zwarts and Wanink, 1989), which corresponds to a siphon width equal to 15 mm. Size–weight relationships should not be applied to extrapolate estimates far beyond the size range from which the relationships were generated (Rumohr et al., 1987) because the range of data can affect significantly the linear regression used to derive the size–weight equation (Bland and Altman, 1986). The maximum siphon width of *Lutraria* measured in the present study was 28 mm, which extrapolates to an estimated shell length of approximately 20 cm (i.e. twice the size of individuals for which the size–weight relationships were generated). In the present study, extrapolation of shell length

(and subsequently AFDW) from siphon width was restricted to a maximum estimated shell length equal to 12 cm (corresponding to 18 mm siphon width), beyond which the error may be too large. Consequently, all individuals whose siphon width exceeded 18 mm were pooled into a single siphon width group in the size–frequency histogram.

To estimate the contribution of *Lutraria lutraria* to the total benthic biomass and infaunal assemblage respiration of Jennycliff Bay, the biomass and respiration rate of the *L. lutraria* population was calculated. Biomass was calculated by summing the weight of all individuals whose estimated shell length did not exceed 12 cm in each sample. Similarly, the respiration rate of the *L. lutraria* population was calculated by summing the corresponding individual oxygen consumption estimates (Equation 8). A conservative estimate of the weight and respiration rate of individuals whose estimated shell length exceeded 12 cm was achieved by using a standard individual with estimated shell length equal to 12 cm. Accordingly, the standard individual AFDW was equal to 13.0 g (Equation 4) and individual respiration rate was equal to  $4.0 \text{ mlO}_2\text{h}^{-1}$  (Equation 8). The contribution of individuals whose estimated shell length exceeded 12 cm was calculated by multiplying the abundance by the appropriate weight or respiration value, which was added to the relevant sample. Subsequently, mean biomass and respiration rate per  $0.5 \text{ m}^2$  sample was calculated.

Two-way crossed ANOVA tests were used to identify between-year and between-station differences in the mean *Lutraria lutraria* biomass and respiration, where year and station were fixed factors. Pairwise tests using Tukey's HSD were used to identify which stations were significantly different from each other.



## 6.3 RESULTS

### 6.3.1 Body size distribution of the *Lutraria lutraria* population

The size–frequency distribution of biomass in the *Lutraria lutraria* population was similar in both years despite large between-year differences in abundance (Fig. 6.1, Chapter 4). The *L. lutraria* population size–frequency histograms for May 2000 and March 2001 consisted of 1312 and 575 individuals, respectively, which were observed in seventy-three and seventy-two 0.5 m<sup>2</sup> grain samples, respectively. Of these, 142 individuals in May 2000 and 80 individuals in March 2001 had siphon width measurements greater than 18 mm (corresponding to an estimated shell length that exceeded 12 cm), and, therefore, AFDW was not extrapolated for these individuals (Section 6.2.3). Although individuals whose estimated shell length exceeded 12 cm represented less than 10% of the population in both years, the contribution of these individuals to total biomass estimates must be much greater.

In each year, the modal siphon width class was 10–12 mm (equivalent 1.6–3.1 g AFDW), which accounted for 43 and 33% of individuals in May 2000 and March 2001, respectively (Fig. 6.1). In May 2000, the median individual estimated AFDW was 4.1 g compared with 5.3 g in March 2001.

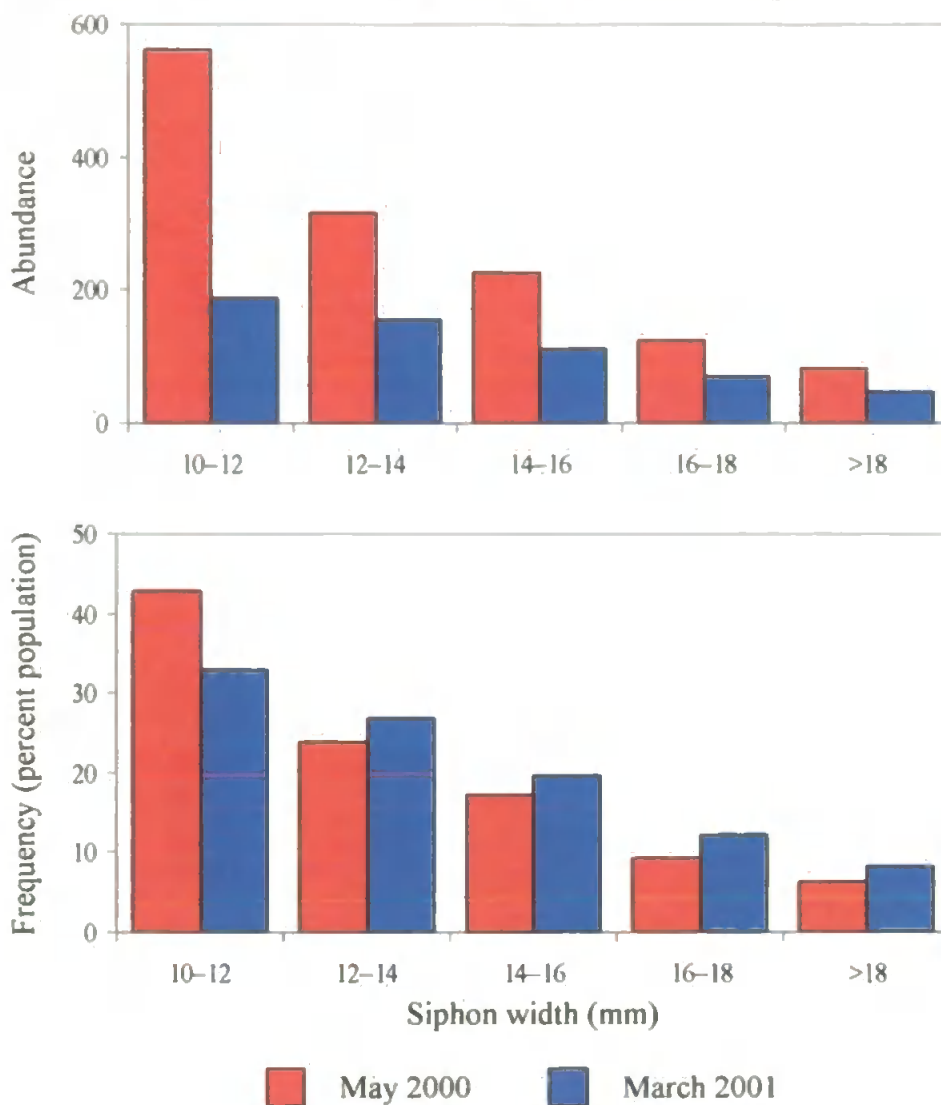


Figure 6.1: Size-frequency histogram of the *Lutraria lutraria* population in Jennycliff Bay based on siphon width measurements.

Table 6.1: Equivalent shell length and AFDW values corresponding to the siphon width groups, extracted from equations 2 and 5 respectively (Warwick and Price, 1975; Zwarts and Wanink, 1989).

Siphon width (mm)	10-12	12-14	14-16	16-18	>18
Shell length (cm)	6.3-7.7	7.7-9.1	9.1-10.6	10.6-12.0	>12.0
Ash-free dry weight (g)	1.6-3.1	3.1-5.3	5.3-8.6	8.6-13.0	>13.0

### 6.3.2 Estimates of *Lutraria lutraria* biomass and respiration

There were significant between-year and between-station differences in estimates of *Lutraria lutraria* biomass (Table 6.2). The significant interaction term (i.e. Year  $\times$  Station) indicated that between-station differences were not consistent between years and the distribution of biomass in the *L. lutraria* population between-stations was not consistent temporally.

Table 6.2: Results from 2-way crossed ANOVA of *Lutraria lutraria* biomass per 0.5 m<sup>2</sup> sample. All factors were fixed. Bold values indicate significant differences,  $p < 0.05$ .

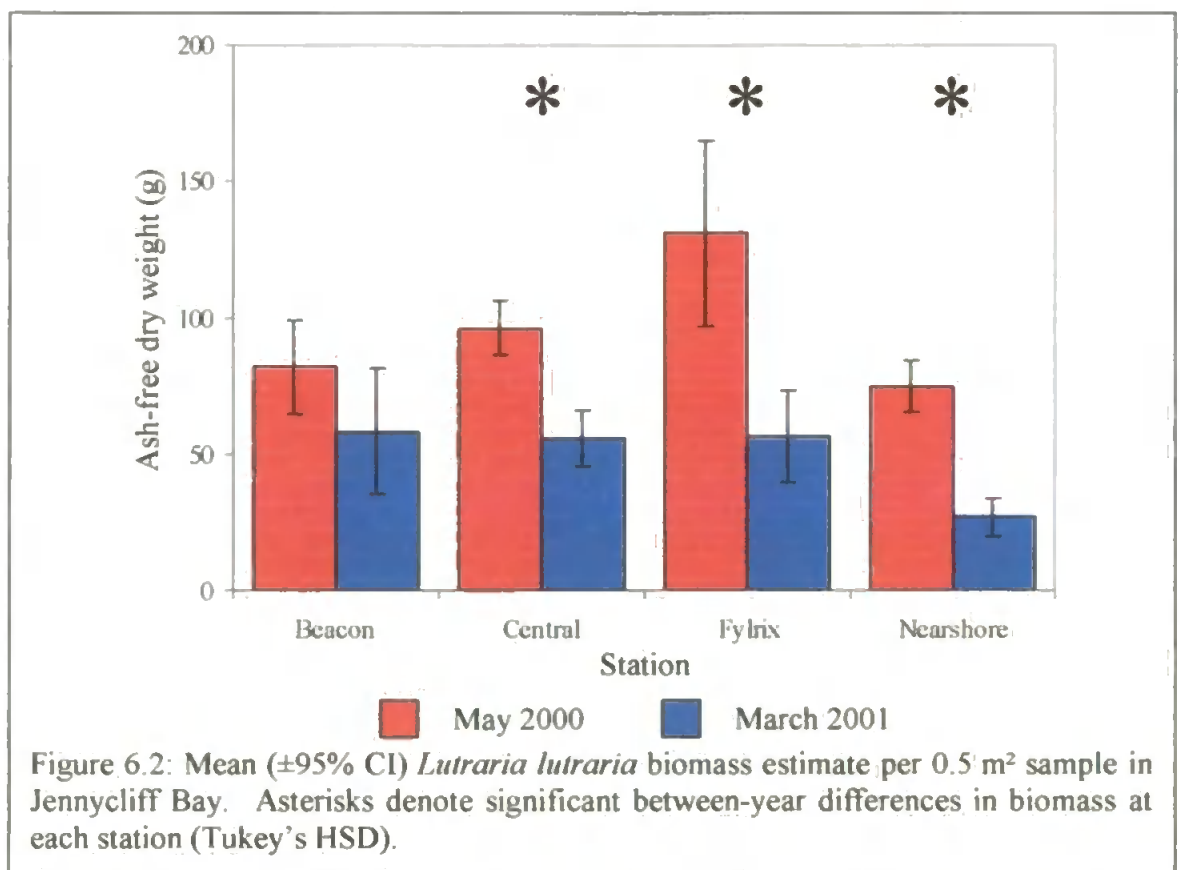
	df	MS	F-ratio	<i>p</i> -value
Year	<b>1</b>	<b>64331</b>	<b>60.70</b>	<b>&lt;0.000</b>
Station	<b>3</b>	<b>9171</b>	<b>8.65</b>	<b>&lt;0.000</b>
Year $\times$ Station	<b>3</b>	<b>2903</b>	<b>2.74</b>	<b>0.046</b>

The significant differences detected in gross estimates of *Lutraria lutraria* biomass were reflected in gross estimates of *L. lutraria* respiration, which was calculated as a function of individual body size (Equation 8).

Table 6.3: Mean ( $\pm 95\%$  CI) biomass and metabolism of *Lutraria lutraria* per 0.5 m<sup>2</sup> sample from Jennycliff Bay in each survey year. AFDW (ash-free dry weight) derived from equations based on surface opening measurements (Zwarts and Wanink, 1989 and Warwick and Davies, 1977). Individuals greater than 12 cm shell length were assigned standard AFDW equal to 13.0 g. AFDW estimates were used to derive estimates of individual dry weight and carbon biomass (Rumohr et al., 1987) and oxygen consumption at 14.5°C with Q<sub>10</sub> correction applied (Equation 8; Emerson et al., 1988).

	May 2000 n = 73	March 2001 n = 72
AFDW biomass (g)	96.5 $\pm$ 9.1	48.6 $\pm$ 7.1
Dry weight biomass (g)	618.7 $\pm$ 58.5	311.1 $\pm$ 45.4
Carbon biomass (g)	56.5 $\pm$ 5.3	28.4 $\pm$ 4.1
Oxygen consumption (ml O <sub>2</sub> h <sup>-1</sup> )	41.9 $\pm$ 3.9	23.5 $\pm$ 1.2

In May 2000, estimates of AFDW biomass per unit area and, hence, dry weight, carbon biomass and respiration rate were approximately double those in March 2001 (Table 6.3). In May 2000, the mean *Lutraria lutraria* biomass per sample was significantly higher at the Fylrix station than at all other stations, which were not significantly different from each other. In March 2001, however, the mean *L. lutraria* biomass per sample was significantly lower at the Nearshore station compared to all other stations, which were not significantly different from each other (Fig. 6.2). The spatial and temporal differences in gross biomass estimates reproduced the pattern of *L. lutraria* abundance (Fig. 6.7), suggesting that the larger biomass per unit area in May 2000 was due to greater abundance rather than the same number of larger individuals (Section 6.3.1 and Chapter 5).



## 6.4 DISCUSSION

### 6.4.1 Contribution of *Lutraria lutraria* to endobenthic biomass

In Jennycliff Bay, the population size structure of *Lutraria lutraria*, derived from measurements of characteristic surface openings, was stable between years despite significant between-year differences in population abundance. The biomass and, hence, respiration rate attributed to the *L. lutraria* population in each year differed significantly. The fact that the sample locations overlapped between years (Fig. 5.1) suggests that the between-year differences in population size structure and biomass estimates were real events rather than an artefact of the survey design. The siphon tips of *L. lutraria* were the most abundant megafaunal features detected in ROV images, representing 77.6 and 59.3% of epifauna and burrow openings in May 2000 and March 2001, respectively, so the biomass of *L. lutraria* may be a reasonable approximation of total megafaunal biomass in Jennycliff Bay. The abundance of other megafaunal features, such as thalassinidean burrow openings, was sufficiently large to indicate that the biomass of *L. lutraria* represents a conservative estimate of megafaunal biomass in Jennycliff Bay.

The magnitude of the *Lutraria lutraria* biomass estimates, presented in the current chapter, becomes more relevant when considering the contribution to the total endobenthic biomass of Jennycliff Bay. Although no macrofaunal samples were collected together with ROV deployments, boxcore samples collected during July 1995 to investigate small-scale patterns in assemblage structure provide a convenient approximation. The sample grain of the boxcore was 0.1 m<sup>2</sup>, which may be expected to sample adequately the small- and medium-bodied macrofauna while under-sampling megafaunal-sized individuals (Kendall, unpublished data). To allow direct comparison with *L. lutraria* biomass estimates, mean macrofaunal AFDW biomass was calculated by multiplying individual abundance by the appropriate biomass (Kendall, unpublished data) and conversion factor (Rumohr et al.,

1987); thus estimated macrofaunal biomass was  $6.3 \pm 2.3 \text{ g AFDW } 0.5 \text{ m}^{-2}$  (mean  $\pm 95\%$  confidence) (Table 6.4).

*Lutraria lutraria* individuals represented, on average, 94 and 89% of endobenthic biomass in May 2000 and March 2001, respectively, assuming that the macrofaunal AFDW in both years was equivalent to that estimated from boxcore samples (Table 6.4). The evidence presented in the current chapter, therefore, indicates that the megafaunal bivalve, *L. lutraria*, is a significant component of endobenthic biomass in Jennycliff Bay and that assessment of biomass using macrofaunal samples only under-estimates severely total endobenthic biomass, and hence respiration, in shallow subtidal soft sediment habitats.

Table 6.4: Contribution of *Lutraria lutraria* to total endobenthic AFDW biomass in Jennycliff Bay. Mean ( $\pm 95\%$  CI) *Lutraria* AFDW estimate from the present study and mean ( $\pm 95\%$  CI) macrofaunal AFDW estimate extrapolated from  $0.1 \text{ m}^2$  boxcore sampling in July 1995,  $n = 9$  (Kendall, unpublished data). Sample grain equals  $0.5 \text{ m}^2$ .

	May 2000	March 2001
Macrofaunal AFDW (g)	$6.3 \pm 2.3$	$6.3 \pm 2.3$
<i>Lutraria lutraria</i> AFDW (g)	$96.5 \pm 9.1$	$48.6 \pm 7.1$
Average Endobenthic AFDW (g)	102.8	54.9
Endobenthic AFDW range (g)	91.4–114.2	45.5–64.3
Average <i>Lutraria lutraria</i> proportion (%)	93.9	88.6
<i>Lutraria lutraria</i> proportion range (%)	91.0–96.4	82.8–93.3

Assessment of whether the pattern of endobenthic biomass partitioning, reported in the current chapter, is found at other locations is problematical because there are few studies where both the macro- and megafauna are sampled concurrently. Examples of locations where biomass partitioning between macro- and megafaunal components of marine benthic assemblages has been investigated are shown in Table 6.5. In Jennycliff Bay, the gross estimates of AFDW biomass and the megafaunal contribution to endobenthic biomass

(Table 6.4) were much greater than at any of the other locations in which biomass partitioning had been investigated (Table 6.5). Benthic–pelagic coupling, whereby, primary production, local hydrography, sedimentation and zooplankton grazing rates influence the quantity and quality of organic matter reaching the benthos (Grebmeier and McRoy, 1989) may explain the apparent differences in biomass estimates and partitioning patterns. In Jennycliff Bay, the organic content of the water column may be expected to be high because of the high organic content of the water in the Tamar and Plym rivers (0.3–3 mg C l<sup>-1</sup> [Morris et al., 1982]) both of which discharge into Plymouth Sound.

Table 6.5: Megafaunal contribution to endobenthic biomass (retained on 500µm mesh) at various locations. Water depth at each location is displayed in parentheses. Biomass was expressed as ash-free dry weight (AFDW); † indicates AFDW was derived from carbon mass, ‡ indicates AFDW was derived from wet weight. Mean (±95% confidence interval) values are marked with an asterisk.

Location	Endobenthic biomass (g/0.5 m <sup>2</sup> )	Megafaunal proportion (%)	Minimum megafaunal individual (mg)	Reference
Northumberland (80 m)	1.98	52.2	100	Buchanan and Warwick (1974)
Helgoland Bight (34 m)	17.8†	24.8	17.1†	Gerlach et al. (1985)
Kiel Bay (34 m)	52.0†	42.0	17.1†	Gerlach et al. (1985)
Barents Sea (246 ±108 m*)	8.70 ±5.7*	35.9 ±23.3*	55‡	Piepenburg et al. (1995)

*Lutraria lutraria* is a long-lived suspension-feeding bivalve that removes organic material from the water overlying the sediment–water interface, so the organic content of the water column may be particularly important in determining the *L. lutraria* population biomass. In Jennycliff Bay, the water depth was relatively shallow (10–15 m) compared to the other locations (Table 6.4), so benthic–pelagic coupling may be stronger at Jennycliff Bay

because of the shorter distance through which organic matter must pass before reaching the sediment–water interface. An additional factor that may explain the high megafaunal biomass at Jennycliff is the low rate of physical disturbance. Jennycliff Bay has a quiescent hydrodynamic regime and demersal trawling is prohibited, so the probability of disturbance to established *L. lutraria* individuals would be low. The long life expectancy of *L. lutraria* is well suited, therefore, to allow established individuals to flourish under the conditions of high organic content of the water column and low rates of physical disturbance.

#### **6.4.2 Sources of error in biomass estimation**

Benthic–pelagic coupling may be sufficient to support the high estimated *Lutraria lutraria* biomass in Jennycliff Bay, yet biomass estimates may contain artefacts resulting from the various assumptions made in the methodology of the current chapter. These assumptions may have significant effects on estimation of biomass and partitioning and will be addressed in the following paragraphs.

In the present chapter, individual *Lutraria lutraria* weight was calculated from measurement of siphon width, which was assumed to equal the diameter of the surface opening. However, the surface openings may slump to form a funnel-shaped opening rather than a vertical shaft (Chapter 4), so the surface opening diameter may be greater than the siphon width of the individual occupying the burrow. Consequently, measurement of surface openings affected by sediment slumping will produce the maximum estimate of individual weight, which will be carried through to gross estimates of biomass. To simulate the effect of sediment slumping on measurement of siphon width, estimates of biomass may be derived using siphon width measurements that are 75% of the value recorded by *Benthic Imager*. The resultant gross biomass estimates produced by coarse simulation of sediment slumping were  $38.4 \pm 4.0$  and  $19.0 \pm 3.0$  g AFDW  $0.5 \text{ m}^{-2}$  in May



2000 and March 2001, respectively, indicating that the *L. lutraria* biomass was greater than that of the megafaunal assemblage at any of the stations in Table 6.4.

The approximation of macrofaunal biomass was associated with caveats relating to scaling-up of biomass estimates from individual boxcore samples and assuming that macrofaunal biomass estimates were not affected by temporal variation between sampling dates. The macrofaunal biomass estimate was calculated from boxcore samples with sample grain equal to  $0.1 \text{ m}^2$ , and was multiplied by a factor of five to achieve the same sample grain as used for estimating *L. lutraria* biomass. Scaling-up of biomass estimates in this way assumes faunal homogeneity at sub-metre scales, which could not be investigated with the current data set. However, macrofaunal heterogeneity on sub-metre scales may not affect significantly mean biomass estimates; rather the variance might be expected to increase. The estimated macrofaunal component of endobenthic AFDW biomass used in the present study (6.3 g AFDW) was similar to the locations listed in Table 6.4 (0.95, 8.5, 17.52 and 5.58 g AFDW, respectively), which indicates that the macrofaunal biomass estimate was of a realistic magnitude. Macrofaunal assemblage structure, and hence biomass, within Jennycliff Bay has been stable temporally over the past 10 years (Kendall, unpublished data), which suggests that the macrofaunal biomass in May 2000 and March 2001 may be similar to that derived from boxcore sampling in July.

Errors associated with estimating biomass of either or both of the macrofauna and *Lutraria lutraria* will affect the magnitude of endobenthic biomass estimates, but the average contribution of *L. lutraria* to endobenthic biomass partitioning was greater than 60%, even under the most severe simulation conditions applied (Table 6.5). Consequently, the general conclusion of the present chapter remains: the megafaunal bivalve *L. lutraria* is the dominant component of endobenthic biomass in Jennycliff Bay and assessment of biomass

using macrofaunal samples alone under-estimates severely the total endobenthic biomass, and hence respiration, in shallow subtidal soft sediment habitats.

Table 6.6: Contribution of *Lutraria lutraria* to total endobenthic AFDW biomass in Jennycliff Bay. Mean ( $\pm 95\%$  CI) *Lutraria* AFDW estimate accounting for slumping of the sediment surface and mean ( $\pm 95\%$  CI) macrofaunal AFDW estimate extrapolated from 0.1 m<sup>2</sup> boxcore sampling in July 1995 (Kendall, unpublished data). Sample grain equals 0.5 m<sup>2</sup>.

	May 2000	March 2001
Macrofaunal AFDW (g)	6.3 $\pm$ 2.3	6.3 $\pm$ 2.3
<i>Lutraria lutraria</i> AFDW (g)	38.4 $\pm$ 4.0	19.0 $\pm$ 3.0
Average Endobenthic AFDW (g)	44.7	25.3
Endobenthic AFDW range (g)	38.4–51.0	20.0–30.6
Average <i>Lutraria lutraria</i> proportion (%)	86.0	75.1
<i>Lutraria lutraria</i> proportion range (%)	80.0–91.4	65.0–84.6

### 6.4.3 Validity of estimating biomass from size–weight relationships

#### 6.4.3.1 *Lutraria lutraria* biomass estimates

The *Lutraria lutraria* biomass data presented in the present chapter were calculated by applying size–weight relationships that were determined specifically for *Mya arenaria*. Although *L. lutraria* and *M. arenaria* are members of different bivalve orders (Veneroida and Myoida, respectively), the morphology of each species is very similar (the species may be distinguished by the hinge teeth pattern [Gibson et al., 2001]), so size–weight relationships for *M. arenaria* provide a reasonable approximation for estimating *L. lutraria* body size. The conversion factors from siphon width to shell length (Zwarts and Wanink, 1989), and from shell length to AFDW (Warwick and Price, 1975), were developed for individuals up to 90 and 100 mm shell length, respectively. The high  $r^2$  values associated with these relationships (Section 6.2.2) indicated that the majority of natural variation between individuals up to 100 mm shell length was accounted for. It was not possible to

clarify the robustness of size–weight relationships for individuals greater than 100 mm shell length, which were encountered in the present study, so a standard-sized individual was defined for all individuals for whom estimated shell length exceeded 120 mm. Ideally, size–weight relationships for *L. lutraria* across the entire shell size range would be determined, but insufficient individuals were collected for this to be achieved. Consequently, *L. lutraria* biomass estimates presented in the current chapter may be conservative, as the weight of individuals with shell length greater than 120 mm has been under-estimated.

#### 6.4.3.2 *Thalassinidean mud shrimp biomass estimates*

In both years, the siphon tips of *Lutraria lutraria* were the most abundant megafaunal features detected in ROV images. However, the abundance of thalassinidean mud shrimp burrows (Chapter 5) suggested that these crustaceans may make a further significant contribution to the total megafaunal biomass. Positive relationships between thalassinidean, particularly callianassid, burrow dimensions and burrow inhabitants have been described, where individual carapace length was related significantly to the diameter of tunnels and inhalant shafts (Rowden and Jones, 1995). However, estimates of thalassinidean biomass were not derived in the present chapter because only the surface openings can be measured from ROV images; tunnels are below the sediment surface, while inhalant shafts form funnel-shaped openings at the sediment surface (Atkinson and Nash, 1990). The funnel-shaped openings appear to form through sediment slumping at the surface rather than active construction by the burrow inhabitant (Rowden and Jones, 1995), so there is no general relationship between funnel diameter and inhalant shaft diameter. In addition, while surface features may be used to infer the identity of species, it is not possible to use counts of features to make an absolute estimate of abundance because burrows have a variable number of openings (Nickell and Atkinson, 1995). Nevertheless, thalassinidean population size structure may be compared at local scales because sediment

granulometry and hydrography affect the degree of sediment slumping and number of openings per burrow. However, the confidence that may be placed in estimates of thalassinidean biomass will be low. Consequently, biomass of *Lutraria lutraria*, which were derived from robust size–weight relationships, may be considered as a reasonable if somewhat conservative, estimate of megafaunal biomass in Jennycliff Bay.

#### **6.4.4 Interpretation of size–frequency histograms**

##### *6.4.4.1 Temporal stability of size–frequency histograms*

The size–frequency histograms presented in the current chapter showed that the distribution of biomass within the population was stable between years. To reduce the effects of natural variation on the structure of size–frequency histograms, a minimum of 500 individuals should be used to construct population size–frequency histograms (Grant et al., 1987). The number of *Lutraria lutraria* individuals included in the size–frequency histograms that are presented in this chapter was 1312 and 575 in May 2000 and March 2001, respectively, which provides assurance that the temporal stability of the population was not an artefact of the survey design as the same area was covered in both years.

To construct size–frequency histograms of the thalassinidean population, the maximum possible number of individuals would be obtained by assuming that each individual constructed one inhalant shaft with associated surface opening. Although the maximum possible number of individuals was 180, thalassinideans usually have 2–3 openings per burrow (Nickell and Atkinson, 1995; Hall-Spencer and Atkinson, 1999), which corresponds to 60–90 individuals. In Jennycliff Bay, therefore, there were insufficient numbers of burrows detected in ROV images from which to construct size–frequency histograms for the thalassinidean population. To recorded sufficient burrow openings to construct size–frequency histograms of the thalassinidean population, therefore, the area

surveyed must be increased either by increasing sample grain or collecting more samples i.e. decrease sample lag.

#### 6.4.4.2 *Detection of population recruitment*

To estimate population dynamics and production from size–frequency histograms, the number of age classes and the proportion of the population in each age class is required (Crisp, 1984; Grant et al., 1987). In the present study, the minimum size of surface opening (=siphon width) considered was 1 cm to ensure that small features were detected consistently in ROV images (Chapter 5). Size–frequency histograms produced from ROV observations cannot detect real recruitment of *Lutraria lutraria*, because the size of ‘O’ class individuals falls below the 1 cm siphon width threshold. However, apparent recruitment may be detected in size–frequency histograms because individuals that were below 1 cm siphon width in May 2000 may have grown sufficiently to be detected in March 2001.

#### 6.4.4.3 *Between-year difference in population abundance*

In March 2001, the number of *Lutraria lutraria* siphon tips detected was approximately half that detected in May 2000. The between-year difference in abundance may have resulted from low survival of the smallest individuals (siphon width 10–12 mm) or mortality within all size classes in the population. Survival of the smallest individuals did not cause the between-year differences in abundance because the population size structure was similar between years; hence, the population may have declined in response to a mortality event that acted on individuals of all sizes. Although the agent responsible for a mortality event is unknown, high numbers of dead and moribund *L. lutraria* were collected in benthic trawls after a large phytoplankton bloom (*Phaeocystis* sp.) occurred between the years surveyed (author’s personal observation). The sediment surface may become anoxic as phytoplankton blooms decay, while *Phaeocystis* sp. also releases toxins into the water

column (Aanensen et al., 1998), both of which may influence the survival of infaunal organisms. *Lutraria lutraria* may be particularly susceptible to the *Phaeocystis* sp. bloom because their low mobility within the burrow (Holme, 1959) restricts their ability to avoid unfavourable conditions.

#### 6.4.5 Modelling energy flux through ecosystems

In the present chapter, the estimated biomass of *Lutraria lutraria* represented a significant proportion of the endobenthic biomass in Jennycliff Bay. The repercussions of excluding megafaunal biomass from estimates of endobenthic biomass are particularly relevant when constructing models of energy flux through ecosystems. The European Regional Seas Ecosystem Model II (ERSEM II) aims to describe the benthic and pelagic ecosystems and the coupling between them, modelling the North Sea with a spatial resolution of 1° latitude × 1° longitude (Baretta et al., 1995). Macrofaunal biomass estimates are the main output of the benthic biological submodel, where the benthic habitat consists of three layers (oxygenated, oxidised and reduced) through which organic detritus is distributed. Although ERSEM II produces qualitatively correct results at a broad scale, the model under-predicts consistently macrofaunal biomass in areas where measured biomass exceeds approximately 13 g C m<sup>-2</sup> (Blackford, 1997). In Jennycliff Bay, the estimated carbon biomass of *L. lutraria* was between 4–9 times greater than the threshold below which the model provided an adequate representation of field data, which suggests that the megafaunal role in benthic ecosystems and models should be investigated further. A sampling programme that integrated megafaunal-sized organisms with the macro- and microfauna may contribute to the “synthesis of process measurements, fitting and educated guesswork” (Blackford, 1997) on which modelling of energy flow through ecosystems is currently based.

In recent years, the biological processes operating within ecosystems, particularly pelagic ecosystems, have been modelled using body size distributions as an indicator of process rate (Moloney and Field, 1991; Gin et al., 1998). Benthic biomass distributions have been investigated for meio- and macrofauna-sized animals, in which a characteristic bimodal pattern separates meio- and macrofauna (Schwinghamer, 1981; Warwick, 1984). In the present study, the median-sized *Lutraria lutraria* individual would fall within geometric ( $\times 2$ ) body size class 32, which is beyond the normal range of macrofaunal-sized species (Kendall et al., 1997). The addition of other megafaunal-sized species present in the Jennycliff Bay assemblage, such as thalassinideans and *Acanthocardia* sp., may result in a second biomass minimum between macro- and megafauna, which provides further evidence that the megafauna may form another functional component distinct from the macro- and meiofauna (Lampitt et al., 1986; Parry et al., 1999).

#### **6.4.6 Suggestions for sampling endobenthic biomass and respiration**

In the present study, estimates of *Lutraria lutraria* biomass, and the partitioning of biomass within the endobenthic fauna, were obtained for Jennycliff Bay, a shallow muddy sand substratum. While biomass is influenced primarily by food supply from the pelagic zone (Grebmeier and McRoy, 1989), the pattern of biomass partitioning may be related to sediment granulometry (Piepenburg et al., 1995). To investigate the role of megafaunal individuals in energy flux through marine ecosystems, therefore, further investigations are required to assess megafaunal biomass in a variety of sediment habitats. However, an inter-disciplinary sampling strategy that accounts adequately for all size fractions of the fauna would be required to elucidate fully the patterns of biomass partitioning in a variety of soft sediment assemblages.

## 6.5 CONCLUSION

In Jennycliff Bay, the population size–frequency structure of *Lutraria lutraria*, derived from measurements of surface openings, was stable between May 2000 and March 2001 despite significant between-year differences in population abundance. The estimated biomass of *L. lutraria* represented at least 90% of the endobenthic biomass, which suggests that assessment of community oxygen uptake based on SCOC measurement alone underestimates severely the total benthic community oxygen consumption. To quantify the flux of energy through marine benthic ecosystems, an inter-disciplinary sampling strategy that accounts for all size fractions of the benthic assemblage is recommended. Observation of epifauna and sediment structures associated with burrowing megafauna by ROV offers a way forward to estimate megafaunal biomass, and hence oxygen consumption, which may improve models of energy flux through marine ecosystems.



# **CHAPTER 7**

## **General discussion and conclusions**

## 7.1 INTRODUCTION

This thesis has demonstrated that the abundance, spatial distribution and biomass of epibenthic and conspicuous infaunal megafauna may be assessed using quantitative underwater observations from a remotely operated vehicle. This chapter provides an overview of the way in which the work described in earlier chapters has advanced quantitative underwater observation techniques and presents an assessment of the ways in which observations have advanced understanding of the distribution and functioning of soft sediment assemblages.

## 7.2 ADVANCES IN REMOTE IMAGING TECHNIQUES

The Automated Benthic Image Scaling System (ABISS) (Chapter 2) has advanced remote underwater imaging techniques by allowing rapid calculation of image scale that can be applied across the whole image, accounting for variations due to perspective. Rapid calculation of image scale is vital for underwater observations because, to investigate faunal assemblages quantitatively, the sample grain (i.e. area of seabed in the image) must be determined and maintained throughout a particular study. Traditionally, image scale is calculated using camera-object distance and inclination angle that are maintained by contact with the seabed, which is impossible with freely-moving cameras mounted on ROVs and manned submersibles. The ABISS now provides flexibility of camera movement (for use in topographically complex areas) with the ability to scale images. Underwater cameras equipped with the ABISS may, therefore, be deployed on Remotely Operated Vehicles (and manned submersibles) without making contact with the seabed, allowing quantitative non-destructive observations that minimise sediment resuspension and the ability to observe features from a variety of angles to assist with identification. By calculating image scale for each image independently, the ABISS allows sample grain to be defined within individual images, or to be controlled *a posteriori* by analysing

contiguous images; hence quantitative data may be extracted from underwater images to investigate megafaunal abundance and distribution patterns.

Megafauna have been defined as those organisms large enough to be observed by a camera (Grassle et al., 1975), while meio- and macrofauna are defined using the size of sieve mesh. In reality, the megafaunal definition cannot be supported because the absolute dimensions of an organism on an image depend upon image resolution, which, in turn, is a function of camera-object distance, acceptance angle and camera inclination angle (Chapter 2). The ABISS calculates pixel footprint, a measure of image resolution (Section 2.3.3.2), from which the minimum size of organism detected consistently in images may be estimated. Hence, the megafaunal definition is refined and strengthened because the absolute size of individual/feature considered may be imposed, allowing images without the appropriate resolution to be rejected. In this thesis, epibenthic megafaunal individuals and biotic sediment structures associated with burrowing megafauna were considered only if the diameter exceeded 10 mm. A consistent definition of megafaunal size provides rigor to spatial and temporal comparisons of megafaunal assemblages that was unobtainable previously. Hence, between-year differences in megafaunal abundance and spatial pattern reported in this thesis were real events rather than variation in the ability to detect features.

The ABISS afforded additional benefits to underwater observations because the ability to measure surface features assisted with their identification. The majority of biotic features encountered could be attributed to different burrowing species using published descriptions of shape and size (Atkinson and Nash, 1985; Nickell and Atkinson, 1995; Marrs *et al.*, 1996), but there were a number of features whose identity could not be determined with confidence. Hence, unidentified surface features were given a consistent temporary name (e.g Unknown bivalve 1) and described by their shape and size as measured from *Benthic Imager* software (Section 5.2.3). As quantitative underwater observations are extended to

different benthic habitats, there will be more megafaunal surface features for which species identity cannot be resolved, so it will be important to develop the image library begun during research for this thesis (Appendix I).

Although the ABISS was developed primarily to provide scale in images, the operational capabilities of the ROV were enhanced because the pattern of laser spots provided a real-time visual reference that assisted the pilot in maintaining camera orientation during ROV deployment. In so doing, the ABISS maximised the proportion of videotape in which images were acceptable for analysis shortening analysis time in the laboratory. The ABISS was developed specifically for deployment on an ROV-mounted underwater camera, but the principles of image scale calculation apply to all methods of camera deployment. Hence, quantitative megafaunal observations may be made using any underwater camera that is deployed in conjunction with the ABISS.

## **7.3 MEGAFUNAL ASSEMBLAGE STRUCTURE AND FUNCTION**

### **7.3.1 Spatial pattern of the megafaunal assemblage**

The spatial pattern of the Jennycliff Bay megafaunal assemblage was neither uniform nor stable temporally within an area of homogeneous muddy sand; a hierarchy of spatial structure was detected, in which patches with a minimum radius between 123–163 m were nested within patches of up to 400 m radius. The image scaling and position-fixing techniques developed in this thesis have great potential for deployment in future studies of the scale of megafaunal variation within soft sediment habitats.

The spatial scale of variation within the megafaunal assemblage, investigated in this thesis, was similar to that of the macrofaunal assemblage of the same area of Jennycliff Bay that was sampled using a complex array of diver collected cores in July 1995 (Kendall and Widdicombe, 1999). The similar scales of variation between the macro- and megafaunal

components suggests that: 1) the megafaunal assemblage influences the structure and composition of macrofaunal assemblage; or 2) the macrofaunal assemblage influences the structure and composition of megafaunal assemblage; or 3) both macro- and megafaunal assemblages respond to physical structuring processes in a similar manner, or 4) that a combination of interactions influence the structure of the total benthic assemblage. To elucidate the processes structuring benthic assemblages, the physical and biological characteristics of habitats should be investigated concurrently using spatially referenced samples within a wide survey extent. Deployment of the ABISS with underwater cameras mounted on grabs and/or corers would allow the structure and composition of macrofaunal assemblages to be placed in context with the structure and composition of the associated megafaunal assemblage.

### 7.3.2 The role of megafauna in ecosystem function

The full importance of the megafauna in the functioning of benthic assemblages is not appreciated at present. It is evident from Chapter 6 that megafaunal species make a significant contribution to endobenthic biomass and respiration. Such data are required for an appreciation of energy and nutrient flux at the sediment–water interface. Chapter 6 showed that it is relatively straightforward to use ABISS to estimate and map benthic biomass of some megafaunal species. This approach is novel. In Chapter 6, the biomass of the infaunal bivalve *Lutraria lutraria* was estimated from measurements of its characteristic siphon opening and size–weight relationships for a similar species, *Mya arenaria*. The size and shape of *L. lutraria* is broadly similar to that of *M. arenaria* and so estimates of biomass and respiration are considered broadly appropriate but there would be greater confidence if species specific data had been available. Similarly, size–weight relationships for other common megafaunal organisms should be developed beyond existing data for ophiuroids (Piepenburg et al., 1997), infaunal bivalves (*M. arenaria* [Warwick and Price, 1975; Emerson et al., 1988; Zwarts and Wanink, 1989], *Scrobicularia*

*plana* and *Macoma balthica* [Zwarts et al., 1994]) and thalassinidean shrimps (Witbaard and Duineveld, 1989; Richardson et al., 2000). Furthermore, it would be necessary to investigate the way in which local factors relating to the physical properties of sediment might modify any broad relationship between the size of surface openings and individual weight.

In addition to contributing a significant proportion of endobenthic biomass, some megafaunal species also have a strong influence on ecosystem structure and function. For example, suspension feeding bivalves and some infaunal shrimps (e.g. *Upogebia deltarua*) extract food particles and planktonic larvae from the water column, which enhances the flux of energy across the sediment–water interface and influences the composition of the local assemblage (Woodin, 1976). Additionally, bioirrigation of burrows (Graf, 1992) may increase the depth that oxygen penetrates into the sediment fabric thereby increasing the depth (i.e. volume) to which bacteria, meiofauna and macrofauna may respire aerobically. In contrast, sediment reworking by thalassinideans during burrow construction and maintenance (Rowden et al., 1998) may influence sediment permeability and oxygenation (Meadows and Tait, 1989; Meadows and Meadows, 1991), settlement and survival of post-larvae (Posey et al., 1991) and interfere with nearby suspension feeders (Rhoads and Young, 1970). The direct and indirect mechanisms by which megafaunal species influence ecosystem processes have been demonstrated for a variety of species, yet the rate at which megafaunal species affect ecosystem processes may be related to the size distribution (Rowden et al., 1998), as well as the abundance, of individuals. The ABISS enhances underwater observations because the size–frequency distribution of individuals or biotic features may be determined in addition to their abundance. Hence, spatial variation in the composition and size–frequency distribution of the megafaunal assemblage may be used as a surrogate to predict the spatial variation of certain ecosystem process rates.

## 7.4 IMPLICATIONS FOR QUANTIFYING SPATIAL STRUCTURE IN BENTHIC ASSEMBLAGES

In this thesis, the scales of spatial variation were quantified formally (Chapter 5) because each sample was referenced spatially using an underwater acoustic positioning system (Chapter 2). Spatial heterogeneity has been regarded generally as a hindrance in ecology due to the increased variance imposed on sampling, while spatial autocorrelation between samples may confound statistical analyses as samples are not truly independent (Legendre, 1993). Traditionally, survey strategies have been devised to minimise variance between samples either by increasing the number of samples collected (i.e. increase replication) or by increasing the sample grain, which may be achieved either by pooling samples collected separately or by using large sample units such as trawls. However, high sample replication increases the time and cost of data extraction, while important information on spatial variation is lost when sample grain is increased because abundance is integrated over large areas. Although a successful sampling strategy may control between-sample variation, the confounding effects of spatial autocorrelation between samples on statistical analyses remain.

An alternative approach to survey design suggests that between-sample variance is important information that should be retained to allow a formal description of the natural heterogeneity in the system under study (Legendre, 1993). Technological developments, such as differential global positioning systems (dGPS) and the underwater acoustic positioning system described in this thesis (Chapter 2), have enhanced the ability to collect samples that are referenced spatially with high accuracy. In combination with statistical techniques that consider the degree of spatial autocorrelation (Angel and Angel, 1967; Jumars et al. 1977; Thrush et al., 1989), spatially referenced samples allow the scales of spatial pattern to be quantified, which is a first step in the interpretation of any ecological data. It seems sensible, therefore, to reference all samples spatially to quantify the scales

of spatial pattern in the continued attempts to infer the processes that create and maintain the patterns observed.

The image scaling and positioning techniques that have been developed during this thesis have allowed quantitative assessment of patterns of spatial distribution for epibenthic megafauna, and those burrowing megafauna that produce characteristic surface openings. However, as yet no remote imaging techniques can detect burrowing megafaunal species such as echinoids that do not produce characteristic surface openings. To quantify burrowing megafauna that do not produce conspicuous surfaces, large numbers of spatially referenced box-cores remain the most appropriate technique. To enhance understanding of the structure and function of benthic assemblages, an integrated stratified sampling design using spatially referenced direct and indirect sampling methods is recommended. The underwater imaging techniques developed in this thesis offer a way forward to quantify the distribution of megafaunal assemblages and assess the role of certain megafaunal species in the structure and function of soft sediment habitats.

## 7.5 CONCLUSIONS

- The Automated Benthic Image Scaling System (ABISS) allows quantitative megafaunal abundance data to be extracted rapidly from images, accounting for perspective, collected from cameras mounted on a remotely operated vehicle, and may be deployed similarly with any underwater camera. Additionally, the ABISS offers the potential for benthic survey in waters deeper than accessible to divers.
- The spatial pattern of assemblages may be determined formally using statistical techniques such as correlograms that require quantitative samples that are referenced spatially. The ability to locate marine benthic samples accurately has improved with the development of global positioning systems and underwater acoustic positioning



systems. To infer process from pattern, therefore, any future investigations should determine sample lag and survey extent by collecting spatially referenced samples.

- Estimates of biomass, respiration and energy flux may be derived from measurements of epibenthic megafauna, and the surface openings of burrowing megafauna, to assess the megafaunal contribution to a variety of ecosystem processes. Current models of energy flux through the benthos do not consider the contribution of megafauna, so further investigation of megafaunal assemblages would appear to be long overdue.
- To describe and monitor benthic assemblages, an integrated stratified sampling design to include megafaunal species with the traditional macro- and meiofaunal samples is required. Quantitative underwater observations offer a way forward to sample adequately the abundance and biomass of the megafaunal fraction of benthic assemblages and assess the use of megafaunal distribution patterns as surrogates for estimating spatial variation in macrofaunal diversity and ecosystem function.

## REFERENCES

- Aanesen, R.T., Eilertsen, H.C., Stabell, O.B. (1998) Light-induced toxic properties of the marine alga *Phaeocystis pouchetii* towards cod larvae. *Aquatic Toxicology* 40, 109–121.
- Addicot, J.F., Aho, J.M., Antolin, M.F., Padilla, D.K., Richardson, J.S., Soluk, D.A. (1987). Ecological neighborhoods: scaling environmental patterns. *Oikos* 49, 340–346.
- Aller, R.C., Dodge, R.E. (1974). Animal-sediment relations in a tropical lagoon, Discovery Bay, Jamaica. *Journal of Marine Research* 32, 209–232.
- Andrew, N.L., Mapstone, B.D. (1987). Sampling and the description of spatial pattern in marine ecology. *Oceanography and Marine Biology: an Annual Review* 25, 39–90.
- Angel, H.H., Angel, M.V. (1967). Distribution pattern analysis in a marine benthic community. *Helgolander Meeresuntersuchungen* 15, 445–454.
- Armonies, W. (1992). Migratory rhythms of drifting juvenile molluscs in tidal waters of the Wadden Sea. *Marine Ecology Progress Series* 83, 197–206.
- Armstrong, J.D., Bagley, P.M., Priede, I.G. (1992). Photographic and acoustic tracking observations of the behaviour of the grenadier *Coryphaenoides (Nematonurus) armatus*, the eel *Synphobranchus bathybius*, and other abyssal demersal fish in the North Atlantic Ocean. *Marine Biology* 112, 535–544.
- Astall, C.M., Taylor, A.C., Atkinson, R.J.A. (1997). Behavioural and physiological implications of a burrow-dwelling lifestyle for two species of upogebiid mud-shrimp (Crustacea: Thalassinidea). *Estuarine Coastal Shelf Science* 44, 155–168.
- Atkinson, R.J.A., Nash, R.D.M. (1985). Burrows and their inhabitants. *Progress in Underwater Science* 10, 109–115.
- Atkinson, R.J.A., Nash, R.D.M. (1990). Some preliminary observations on the burrows of *Callianassa subterranea* from the West Coast of Scotland. *Journal of Natural History* 24, 403–413.
- Atkinson, R.J.A., Frogli, C., Arneri, E., Antolini, B. (1998). Observations on the burrows and burrowing behaviour of *Brachynotus gemmellari* and on the burrows of several other species occurring on *Squilla* grounds off Ancona, central Adriatic. *Scientia Marina* 62, 91–100.
- Baretta, J.W., Ebenhö, W., Ruurdij, P. (1995). The European Regional Seas Ecosystem Model, a complex marine ecosystem model. *Netherlands Journal of Sea Research* 33, 233–246.
- Barker, B.A., Helmond, I., Bax, N., Williams, A., Davenport, S., Wadley, V.A. (1999). Vessel-towed camera platform for sea-floor surveys of the continental shelf. *Continental Shelf Research* 19, 1161–1170.
- Barthel, D., Gutt, J., Tendal, O.S. (1991). New information on the biology of Antarctic deep-water sponges derived from underwater photography. *Marine Ecology Progress Series* 69, 303–307.

- Bax, N., Kloser, R., Williams, A., Gowlett-Holmes, K., Ryan, T. (1999). Seafloor habitat definition for spatial management in fisheries: a case study on the continental shelf of southeast Australia. *Oceanologica Acta* **22**, 705–719.
- Bengtsson, J., Jones, H., Setälä, H. (1997). The value of biodiversity. *Trends in Ecology and Evolution* **12**, 334–336.
- Bergstedt, R.A., Anderson, D. R. (1990). Evaluation of line transect sampling based on remotely sensed data from underwater video. *Transactions of the American Fisheries Society* **119**, 86–91.
- Berkenbusch, K., Rowden, A.A. (2000). Intraspecific burrow plasticity of an intertidal population of *Callinassa filholi* (Crustacea: Decapoda: Thalassinidea) in relation to environmental conditions. *New Zealand Journal of Marine and Freshwater Research* **34**, 397–408.
- Bett, B.J., Rice, A.L., Thurston, M.H. (1995). A quantitative photographic survey of spoke-burrow type lebensspuren on the Cape Verde abyssal plain. *Internationale Revue Der Gesamten Hydrobiologie* **80**, 153–170.
- Blackburn, T.M., Harvey, P.H., Pagel, M.D. (1990). Species number, population density and body size relationships in natural communities. *Journal of Animal Ecology* **59**, 335–345.
- Blackford, J.C. (1997). An analysis of benthic biological dynamics in a North Sea ecosystem model. *Journal of Sea Research* **38**, 213–230.
- Bland, J.M., Altman, D.G. (1986). Statistical methods for assessing agreement between two methods of clinical measurement. *Lancet* **1**, 307–310.
- Blundon, J.A., Kennedy, V.S. (1982). Refuges for infaunal bivalves from the blue crab, *Callinectes sapidus* (Rathbun), predation in Chesapeake Bay. *Journal of Experimental Marine Biology and Ecology* **65**, 67–81.
- Bowen, A.D., Walden, B.B. (1992). Manned versus unmanned systems: a complementary approach. *Marine Technology Society Journal* **26**, 79–80.
- Branch, G.M., Pringle, A. (1987). The impact of the prawn *Callinassa kraussi* Stebbing on sediment turnover and on bacteria, meiofauna, and benthic microflora. *Journal of Experimental Marine Biology and Ecology* **107**, 217–235.
- Bray, J.R., Curtis, J.T. (1957). An ordination of the upland forest communities of Southern Wisconsin. *Ecological Monographs* **27**, 325–349.
- Brenchley, G.A. (1981). Disturbance and community structure: an experimental study of bioturbation in marine soft-bottom environments. *Journal of Marine Research* **39**, 767–790.
- Briggs, K.B., Richardson, M.D. (1997). Small-scale fluctuations in acoustic and physical properties in surficial carbonate sediments and their relationship to bioturbation. *Geo-Marine Letters* **17**, 306–315.
- Brodeur, R.D. (1998). In situ observations of the association between juvenile fishes and scyphomedusae in the Bering Sea. *Marine Ecology Progress Series* **163**, 11–20.

- Buchanan, J.B. (1984). Sediment analysis. In: *Methods for study of the marine benthos*. (Eds. Holme, N.A., McIntyre, A.D.). Blackwell Scientific Publications, London, pp. 41–65.
- Buchanan, J.B., Warwick, R.M. (1974). An estimate of benthic macrofaunal production in the offshore mud of the Northumberland coast. *Journal of the Marine Biological Association* **54**, 197–222.
- Buller, A.T., McManus, J. (1979). Sediment sampling and analysis. In: *Estuarine hydrography and sedimentation*. (Ed. Dyer, K.R.). Cambridge University Press, Cambridge, pp. 87–130.
- Caddy, J.F. (1973). Underwater observation on tracks of dredges and trawls and some effects of dredging on a scallop ground. *Journal of the Fisheries Research Board of Canada* **30**, 173–180.
- Chapman, C.J. (1979). Some observations on populations of Norway lobster, *Nephrops norvegicus* (L), using diving, television and photography. *Rapports et Proces-Verbaux de Reunions, Conseil Internationale pour l'Exploration de la mer* **175**, 127–133.
- Chivers, R.C., Emerson, N., Burns, D. (1990). New acoustic processing for underway surveying. *The Hydrographic Journal* **56**, 9–17.
- Clarke, A., Lidgard, S. (2000). Spatial patterns of diversity in the sea: bryozoan species richness in the North Atlantic. *Journal of Animal Ecology* **69**, 799–814.
- Clarke, K.R. (1993). Non-parametric multivariate analysis of changes in community structure. *Australian Journal of Ecology* **18**, 117–143.
- Clarke, K.R., Warwick, R.M. (1994). Changes in marine communities: an approach to statistical analysis and interpretation. Plymouth: Natural Environment Research Council, Plymouth Marine Laboratory.
- Coelho, V.R., Cooper, R.A., De Almeida Rodrigues, S. (2000). Burrow morphology and behavior of the mud shrimp *Upogebia omissa* (Decapoda: Thalassinidea: Upogebiidae). *Marine Ecology Progress Series* **200**, 229–240.
- Coffen-Smout, S.S., Rees, E.I.S. (1999). Burrowing behaviour and dispersion of cockles *Cerastoderma edule* L. following simulated fishing disturbance. *Fisheries Research* **40**, 65–72.
- Collie, J.S., Escanero, G.A., Valentine, P.C. (2000). Photographic evaluation of the impacts of bottom fishing on benthic epifauna. *ICES Journal of Marine Science* **57**, 987–1001.
- Collins, W., Gregory, R., Anderson, J. (1996). A digital approach to seabed classification. Habitat assessment for juvenile cod is just one application of this acoustic method. *Sea Technology* **37**, 83–87.
- Connell, J.H. (1978). Diversity in tropical rain forests and coral reefs. *Science* **199**, 1302–1309.
- Constable, A.J. (1999). Ecology of benthic macro-invertebrates in soft-sediment environments: A review of progress towards quantitative models and predictions. *Australian Journal of Ecology* **24**, 452–476.

- Cosson, N., Sibuet, M., Galeron, J. (1997). Community structure and spatial heterogeneity of the deep-sea macrofauna at three contrasting stations in the tropical northeast Atlantic. *Deep Sea Research Part I-Oceanographic Research Papers* **44**, 247–269.
- Costanza, R., d'Arge, R., de Groot, R., Farber, S., Grasso, M., Hannon, B., Limburg, K., Naeem, S., O'Neill, R.V., Paruelo, J., Raskin, R.G., Sutton, P., van der Belt, M. (1997). The value of the world's ecosystem services and natural capital. *Nature* **387**, 253–260.
- Council of the European Communities (1992). Council Directive 92/43/EEC: on the conservation of natural habitats and of wild flora and fauna. *Official Journal of the European Communities* L206/7. Communities, C.o.t.E., 1992. Council Directive 92/43/EEC: on the conservation of natural habitats and of wild flora and fauna. *Official Journal of the European Communities* L206/7.
- Crame, J.A. (2000). Evolution of taxonomic diversity gradients in the marine realm: evidence from the composition of recent bivalve faunas. *Paleobiology* **26**, 188–214.
- Crisp, D.J. (1984). Energy flow measurements. In *Methods for the study of marine benthos* (ed. N. A. Holme, McIntyre, A.D.), pp. 284–372. London: Blackwell Scientific Publications.
- Crone, D. R. (1963). Elementary photogrammetry, pp. 197. New York: Frederick Ungar.
- Cummings, V.J., Thrush, S.F., Hewitt, J.E., Turner, S.J. (1998). The influence of the pinnid bivalve *Atrina zelandica* (Gray) on benthic macroinvertebrate communities in soft-sediment habitats. *Journal of Experimental Marine Biology and Ecology* **228**, 227–240.
- Dauwe, B., Herman, P.M., Heip, C.H.R. (1998). Community structure and bioturbation potential of macrofauna at four North Sea stations with contrasting food supply. *Marine Ecology Progress Series* **173**, 67–83.
- Davis, D.L., Pilskalns, C.H. (1992). Measurements with underwater video: camera field width calibration and structured lighting. *Marine Technology Society Journal* **26**, 13–19.
- Dawber, M., Powell, R.D. (1995). Observations made by remotely operated vehicle of epifauna near the Mackay Glacier tongue. *Antarctic Journal of the United States* **30**, 152–153.
- Dawber, M., Powell, R.D. (1997). Epifaunal distributions at marine-ending glaciers: influences of ice dynamics and sedimentation. *The Antarctic Region: Geological Evolution and Processes* 875–884.
- Dayton, P.K. (1992). Community landscape: scale and stability in hard bottom marine communities. In: *Aquatic Ecology: scale, pattern and process*. (Eds. Giller, P.S., Hildrew, A.G., Raffaelli, D.G.). Blackwell Science Ltd., London, pp. 289–332.
- DeRidder, C., Lawrence, J.M. (1982). Food and feeding mechanisms: Echinoidea. In: *Echinoderm Nutrition* (Eds. Jangoux, M., Lawrence, J.M.). A.A. Balkema, Rotterdam, pp. 57–115.
- de Vaugelas, J., Buscail, R. (1990). Organic matter distribution in burrows of the thalassinid crustacean *Callichurus laureae*, Gulf of Aqaba (Red Sea). *Hydrobiologia* **207**, 269–277.

- Dowdeswell, J.A., Powell, R.D. (1996). Submersible remotely operated vehicles (ROVs) for investigations of the glacier-ocean-sediment interface. *Journal of Glaciology* **42**, 176–183.
- Drazen, J.C., Baldwin, R.J., Smith Jr., K.L. (1998). Sediment community response to a temporally varying food supply at an abyssal station in the NE Pacific. *Deep Sea Research Part II- Topical Studies in Oceanography* **45**, 893–913.
- Duarte, C.M. (2000). Marine biodiversity and ecosystem services: an elusive link. *Journal of Experimental Marine Biology and Ecology* **250**, 117–131.
- Dumbauld, B.R., Armstrong, D.A., Feldman, K.L. (1996). Life-history characteristics of two sympatric thalassinidean shrimps, *Neotrypaea californiensis* and *Upogebia pugettensis*, with implications for oyster culture. *Journal of Crustacean Biology* **16**, 689–708.
- Dyer, K.R. (1986). Coastal and estuarine sediment dynamics. Wiley, Chichester, 342 pp.
- Eckman, J.E. (1983). Hydrodynamic processes affecting benthic recruitment. *Limnology and Oceanography* **28**, 241–257.
- Eckman, J.E., Nowell, A.R.M., Jumars, P.A. (1981). Sediment destabilisation by animal tubes. *Journal of Marine Research* **39**, 361–374.
- Ellis, D.V., Heim, C. (1985). Submersible surveys of benthos near a turbidity cloud. *Marine Pollution Bulletin* **16**, 197–203.
- Emerson, C.W., Minchinton, T.E., Grant, J. (1988). Population structure, biomass, and respiration of *Mya arenaria* L. on temperate sandflat. *Journal of Experimental Marine Biology and Ecology* **115**, 99–111.
- Emerson, C.W., Grant, J. (1991). The control of soft-shell clam (*Mya arenaria*) recruitment on intertidal sandflats by bedload sediment transport. *Limnology and Oceanography* **36**, 1288–1300.
- Entec. (1996). Broad scale habitat mapping of intertidal and subtidal coastal areas: Loch Maddy, North Uist: Scottish Natural Heritage Research, Survey and Monitoring Report No. 76.
- Etchemendy, S., Davis, D. (1991). Designing an ROV for oceanographic research. *Sea Technology* **February**, 21–24.
- Feldman, K.L., Armstrong, D.A., Eggleston, D.B., Dumbauld, B.R. (1997). Effects of substrate selection and post-settlement survival on recruitment success of the thalassinidean shrimp *Neotrypaea californiensis* to intertidal shell and mud habitats. *Marine Ecology Progress Series* **150**, 121–136.
- Feral, J.-P. (1999). Indicators of marine and coastal biodiversity of the Mediterranean Sea. United Nations Environment Program, Tunis, Tunisia.
- Forman, R.T.T. (1995). Land mosaics: the ecology of landscapes and regions. Cambridge University Press, Cambridge, 632 pp.
- Forster, S., Graf, G. (1995). Impact of irrigation on oxygen flux into the sediment - intermittent pumping by *Callinassa subterranea* and piston-pumping by *Lanice conchilega*. *Marine Biology* **123**, 335–346.

- Franklin, A., Pickett, G.D., Holme, N.A., Barrett, G.D. (1980). Surveying stocks of Scallops (*Pecten maximus*) and Queens (*Chlamys opercularis*) with underwater television. *Journal of the Marine Biological Association of the United Kingdom* **60**, 181–191.
- Gage, J. (1972). A preliminary survey of the benthic macrofauna and sediments in Lochs Etive and Creran, sea-lochs along the west coast of Scotland. *Journal of the Marine Biological Association of the United Kingdom* **52**, 237–276.
- Gage, J. (1974). Shallow-water zonation of sea-loch benthos and its relation to hydrographic and other physical features. *Journal of the Marine Biological Association of the United Kingdom* **54**, 223–249.
- Gardner, W.D., Sullivan, L.G., Thorndike, E.M. (1984). Long-term photographic, current, and nephelometer observations of manganese nodule environments in the Pacific. *Earth and Planetary Science Letters* **70**, 95–109.
- Gaston, K.J., Blackburn, T.M. (1995). Mapping biodiversity using surrogates for species richness: Macro-scales and New World birds. *Proceedings of the Royal Society of London Series B-Biological Sciences* **262**, 335–341.
- Geary, R.C. (1954). The continuity ratio and statistical mapping. *Incorporated Statistician* **5**, 115–145.
- Gerlach, S.A., Hahn, A.E., Schrage, M. (1985). Size spectra of benthic biomass and metabolism. *Marine Ecology Progress Series* **26**, 161–173.
- Gibbs, P.E. (1969). A quantitative study of the polychaete fauna of certain fine deposits in Plymouth Sound. *Journal of the Marine Biological Association of the United Kingdom* **49**, 311–326.
- Gibson, R., Hextall, B., Rogers, A. (2001). Photographic guide to the sea and shore life of Britain and North-west Europe, pp. 436. Oxford: Oxford University Press.
- Gilbert, F., Stora, G., Bonin, P. (1998). Influence of bioturbation on denitrification activity in Mediterranean coastal sediments: an *in situ* experimental approach. *Marine Ecology Progress Series* **163**, 99–107.
- Gin, K.Y.H., Guo, J.H., Cheong, H.F. (1998). A size-based ecosystem model for pelagic waters. *Ecological Modelling* **112**, 53–72.
- Graf, G., Bengtsson, W., Diesner, U., Schultz, R., Theede, H. (1982). Benthic responses to sedimentation of a spring phytoplankton bloom: process and budget. *Marine Biology* **67**, 201–208.
- Graf, G. (1992). Benthic-Pelagic Coupling: a Benthic View. *Oceanography and Marine Biology: An Annual Review* **30**, 149–190.
- Graf, G., Rosenberg, R. (1997). Bioresuspension and biodeposition: A review. *Journal of Marine Systems* **11**, 269–278.
- Grant, A., Morgan, P.J., Olive, P.J.W. (1987). Use made in marine ecology of methods for estimating demographic parameters from size/frequency data. *Marine Biology* **95**, 201–208.



- Grassle, J.F., Sanders, H.L., Hessler, R.R., Rowe, G.T., McLellan, T. (1975). Pattern and zonation: a study of the bathyal megafauna using the research submersible *Alvin*. *Deep Sea Research* **22**, 457–481.
- Grassle, J.F., Morse-Porteous, L.S. (1987). Macrofaunal colonisation of disturbed deep-sea environments and the structure of deep-sea benthic communities. *Deep Sea Research Part I-Oceanographic Research Papers* **34**, 1911–1950.
- Grassle, J.F., Maciolek, N.J. (1992). Deep-sea species richness - regional and local diversity estimates from quantitative bottom samples. *American Naturalist* **139**, 313–341.
- Gray, J.S. (1974). Animal sediment relationships. *Oceanography and Marine Biology: an Annual Review* **12**, 223–261.
- Gray, J.S. (1997). Marine biodiversity: patterns, threats and conservation needs. *Biodiversity and Conservation* **6**, 153–175.
- Gray, J.S. (2000). The measurement of marine species diversity, with an application to the benthic fauna of the Norwegian continental shelf. *Journal of Experimental Marine Biology and Ecology* **250**, 23–494.
- Grebmeier, J.M., McRoy, C.P. (1989). Pelagic-benthic coupling on the shelf of the northern Bering and Chukchi Seas. III. Benthic food-supply and carbon cycling. *Marine Ecology Progress Series* **53**, 46–79.
- Grebmeier, J.M., Harrison, N.M. (1992). Seabird activity on benthic amphipods facilitated by gray whale activity in the northern Bering Sea. *Marine Ecology Progress Series* **80**, 125–133.
- Greene, C.H., Wiebe, P.H., Miyamoto, R.T., Burczynski, J. (1991). Probing the fine structure of the ocean sound-scattering layers with ROVERSE technology. *Limnology and Oceanography* **36**, 193–204.
- Greenstreet, S.P.R., Tuck, I.D., Grewar, G.N., Armstrong, E., Reid, D.G., Wright, P.J. (1997). An assessment of the acoustic survey technique, RoxAnn, as a means of mapping seabed habitat. *ICES Journal of Marine Science* **54**, 939–959.
- Griffis, R.B., Suchanek, T.K. (1991). A model of burrow architecture and trophic modes in thalassinidean shrimps (Decapoda: Thalassinidea). *Marine Ecology Progress Series* **79**, 171–183.
- Gutt, J., Ekau, W. (1996). Habitat partitioning of dominant high Antarctic demersal fish in the Weddell Sea and Lazarev Sea. *Journal of Experimental Marine Biology and Ecology* **206**, 25–37.
- Gutt, J., Starmans, A., Dieckmann, G. (1996). Impact of iceberg scouring on polar benthic habitats. *Marine Ecology Progress Series* **137**, 311–316.
- Hall, S.J., Raffaelli, D., Thrush, S.F. (1992). Patchiness and disturbance in shallow water benthic assemblages. In: *Aquatic Ecology: scale, pattern and process*. (Eds. Giller, P.S., Hildrew, A.G., Raffaelli, D.G.). Blackwell Science Ltd., London, pp. 333–376.

- Hall, S.J. (1994). Physical disturbance and marine benthic communities: life in unconsolidated sediments. *Oceanography and Marine Biology: an Annual Review* 32, 179–239.
- Hall-Spencer, J.M., Atkinson, R.J.A. (1999). *Upogebia deltaura* (Crustacea: Thalassinidea) in Clyde Sea maerl beds, Scotland. *Journal of the Marine Biological Association of the United Kingdom* 79, 871–880.
- Hamada, E., Numanami, H., Naito, Y., Taniguchi, A. (1986). Observation of the marine benthic organisms at Syowa Station in Antarctica using a remotely operated vehicle. *Memoirs of the National Institute for Polar Research* 40, 289–298.
- Hamilton, L.J., Mulhearn, P.J., Poeckert, R. (1999). Comparison of RoxAnn and QTC-View acoustic bottom classification system performance for the Cairns area, Great Barrier Reef, Australia. *Continental Shelf Research* 19, 1577–1597.
- Hardin, D.D., Graves, D., Imamura, E. (1992). Investigating seafloor disturbances with a small ROV. *Marine Technology Society Journal* 26, 40–45.
- Harrold, C., Light, K., Lisin, S. (1998). Organic enrichment of submarine-canyon and continental-shelf benthic communities by macroalgal drift imported from nearshore kelp forests. *Limnology and Oceanography* 43, 669–678.
- Hensley, R.T. (1996). Preliminary survey of benthos from the *Nephrops norvegicus* mud grounds in the North-western Irish Sea. *Estuarine, Coastal and Shelf Science* 42, 457–465.
- Hewitt, J.E., Thrush, S.F., Cummings, V.J., Pridmore, R.D. (1996). Matching patterns with processes: Predicting the effect of size and mobility on the spatial distributions of the bivalves *Macomona liliana* and *Austrovenus stutchburyi*. *Marine Ecology Progress Series* 135, 57–67.
- Hill, B. (1981). Respiratory adaptations of three species of *Upogebia* (Thalassinidea, Crustacea) with special reference to low tide periods. *Biological Bulletin (Woods Hole, Mass.)* 160, 272–279.
- Hiscock, K. (1987). Subtidal rock and shallow sediments using diving. In: *Biological surveys of estuaries and coasts* (Eds. Baker, J.M., Wolff, W.J.). Cambridge University Press, Cambridge, UK, pp. 198–237.
- Holme, N.A. (1959). The British species of *Lutraria* (Lamellibranchia), with a description of *L. angustior* Philippi. *Journal of the Marine Biological Association of the United Kingdom* 38, 557–568.
- Holme, N.A., Barrett, R.L. (1977). A sledge with television and photographic cameras for quantitative investigation of the epifauna on the continental shelf. *Journal of the Marine Biological Association of the United Kingdom* 57, 391–403.
- Holme, N.A., McIntyre, A.D. (1984). Methods for the study of marine benthos. Blackwell Scientific Publications, London, 387 pp.
- Hovland, M., Mortensen, P.B., Brattegard, T., Strass, P., Rokoengen, K. (1998). Ahermatypic coral banks off Mid-Norway: Evidence for a link with seepage of light hydrocarbons. *Palaios* 13, 189–200.

- Howson, C.M., Picton, B.E. (1997). The species directory of the marine fauna and flora of the British Isles and surrounding seas. Ulster Museum.
- Hughes, D.J., Atkinson, R.J.A. (1997). A towed video survey of megafaunal bioturbation in the north-eastern Irish Sea. *Journal of the Marine Biological Association of the United Kingdom* 77, 635–653.
- Hughes, D.J., Ansell, A.D., Atkinson, R.J.A., Nickell, L.A. (1993). Underwater television observations of surface-activity of the echiuran worm *Maxmuelleria lankesteri* (Echiura, Bonelliidae). *Journal of Natural History* 27, 219–248.
- Hughes, D.J., Ansell, A.D., Atkinson, R.J.A. (1996). Distribution, ecology and life-cycle of *Maxmuelleria lankesteri* (Echiura: Bonelliidae): a review with notes on field identification. *Journal of the Marine Biological Association of the United Kingdom* 76, 897–908.
- Hughes, D.J., Atkinson, R.J.A., Ansell, A.D. (2000). A field test of the effects of megafaunal burrows on benthic chamber measurements of sediment-water solute fluxes. *Marine Ecology Progress Series* 195, 189–199.
- Hunt, H.L., Scheibling, R.E. (1997). Role of early post-settlement mortality in recruitment of benthic marine invertebrates. *Marine Ecology Progress Series* 155, 269–301.
- Hunt, H.L., Mullineaux, L.S. (2002). The roles of predation and postlarval transport in recruitment of the soft shell clam (*Mya arenaria*). *Limnology and Oceanography* 47, 151–164.
- Huston, M.A. (1979). A general hypothesis of species diversity. *American Naturalist* 113, 81–101.
- Irlandi, E.A. (1994). Large-scale and small-scale effects of habitat structure on rates of predation - how percent coverage of seagrass affects rates of predation and siphon nipping on an infaunal bivalve. *Oecologia* 98, 176–183.
- Jones, C.G., Lawton, J.H., Shachak, M. (1994). Organisms as ecosystem engineers. *Oikos* 69, 373–386.
- Jones, C.G., Lawton, J.H., Shachak, M. (1997). Positive and negative effects of organisms as physical ecosystem engineers. *Ecology* 78, 1946–1957.
- Jones, D.T., Eggleton, P. (2000). Sampling termite assemblages in tropical forests: testing a rapid biodiversity assessment protocol. *Journal of Applied Ecology* 37, 191–203.
- Jones, N.S. (1950). Marine bottom communities. *Biological Review* 25, 283–313.
- Jumars, P.A., Thistle, D., Jones, M.L. (1977). Detecting two-dimensional spatial structure in biological data. *Oecologia* 28, 109–123.
- Kaiser, M.J., Edwards, D.B., Armstrong, P.J., Radford, K., Lough, N.E.L., Flatt, R.P., Jones, H.D. (1998). Changes in megafaunal benthic communities in different habitats after trawling disturbance. *ICES Journal of Marine Science* 55, 353–361.
- Kanazawa, K. (1995). How spatangoids produce their traces - relationship between burrowing mechanism and trace structure. *Lethaia* 28, 211–219.
- Kendall, M.A., Warwick, R.M., Somerfield, P.J. (1997). Species size distributions in Arctic benthic communities. *Polar Biology* 17, 389–392.

- Kendall, M.A., Widdicombe, S. (1999). Small scale patterns in the structure of macrofaunal assemblages of shallow soft sediments. *Journal of Experimental Marine Biology and Ecology* **237**, 127–140.
- Kennedy, V.S., Mihursky, J.A. (1972). Effects of temperature on the respiratory metabolism of three Chesapeake Bay bivalves. *Chesapeake Science* **13**, 1–22.
- Kent, M., Gill, W.J., Weaver, R.E., Armitage, R.P. (1997). Landscape and plant community boundaries in biogeography. *Progress in Physical Geography* **21**, 315–353.
- Kidwell, S.M. (2001). Ecological fidelity of molluscan death assemblages. In: *Organism–sediment interactions* (Eds. Aller, J.Y., Woodin, S.A., Aller, R.C.). University of South Carolina Press, Columbia, South Carolina, pp. 199–221.
- Kotliar, N., Weins, J. (1990). Multiple scales of patchiness and spatial structure: a hierarchical framework for the study of heterogeneity. *Oikos* **59**, 253–260.
- Krebs, C.J. (1972). *Ecology*. Harper and Row, New York.
- Lamont, P.A., Gage, J.D. (1998). Dense brittle star population on the Scottish continental slope. In: *Proceedings of the Ninth International Echinoderm Conference* (Eds. Mooi, R., Telford, M.). A.A. Balkema, San Francisco, California, USA, pp. 377–382.
- Lampitt, R.S., Burnham, M.P. (1983). A free-fall time-lapse camera and current-meter system BATHYSNAP with notes on the foraging behavior of a bathyal decapod shrimp. *Deep Sea Research Part I-Oceanographic Research Papers* **30**, 1009–1017.
- Lampitt, R.S., Billet, D.S.M., Rice, A.L. (1986). Biomass of the invertebrate megabenthos from 500 to 4100 m in the northeast Atlantic. *Marine Biology* **93**, 69–81.
- Lampitt, R.S., Raine, R.C.T., Billett, D.S.M., Rice, A.L. (1995). Material supply to the European continental slope: A budget based on benthic oxygen demand and organic supply. *Deep Sea Research I-Oceanographic Research Papers* **42**, 1865–1880.
- Lauerman, L.M.L., Kaufmann, R.S. Smith Jr., K.L. (1996). Distribution and abundance of epibenthic megafauna at a long time-series station in the northeast Pacific. *Deep Sea Research I-Oceanographic Research Papers* **43**, 1075–1103.
- Lawton, J.H. (1989). What is the relationship between population density and body size in animals? *Oikos* **5**, 429–433.
- Lawton, J.H. (1994). What do species do in ecosystems? *Oikos* **71**, 367–374.
- Legendre, P., Fortin, M.-J. (1989). Spatial pattern and ecological analysis. *Vegetatio* **80**, 107–138.
- Legendre, P. (1993). Spatial autocorrelation: trouble or new paradigm? *Ecology* **74**, 1659–1673.
- Lettau, H. (1969). Note on aerodynamic roughness parameter estimation on the basis of roughness-element description. *Journal of Applied Meteorology* **8**, 828–832.
- Levin, S.A., Paine, R.T. (1974). Disturbance, patch formation and community structure. *Proceedings of the National Academy of Sciences of the United States of America* **71**, 2744–2747.

- Levin, S.A. (1992). The problem of pattern and scale in ecology. *Ecology* **73**, 1943–1967.
- Levin, S.A. (2000). Multiple scales and the maintenance of biodiversity. *Ecosystems* **3**, 498–506.
- Loreau, M., Naeem, S., Inchausti, P., Bengtsson, J., Grime, J.P., Hector, A., Hooper, D.U., Huston, M.A., Raffaelli, D., Schmid, B., Tilman, D., Wardle, D.A. (2001). Ecology - Biodiversity and ecosystem functioning: Current knowledge and future challenges. *Science* **294**, 804–808.
- Lundälv, T.L. (1971). Quantitative studies on rocky bottom biocenoses by underwater photogrammetry. A methodological study. *Thalassia Jugoslavica* **7**, 201–208.
- Lundälv, T.L. (1976). A stereophotographic method for quantitative studies on rocky-bottom biocenoses. In: *Underwater Research* (Eds. Drew, E.A., Nythgoe, J.N., Woods, J.D.). Academic Press, London, pp. 299–302.
- Lutz, R.A., Desbruyères, D., Shank, T.M., Vrijenhoek, R.C. (1998). A deep-sea hydrothermal vent community dominated by Stauromedusae. *Deep Sea Research II-Topical Studies in Oceanography* **45**, 329–334.
- MacDonald, I.R., Boland, G.S., Baker, J.S., Brooks, J.M., Kennicutt, M.C., Bidigare, R.R. (1989). Gulf of Mexico hydrocarbon seep communities II. Spatial distribution of seep organisms and hydrocarbons at Bush Hill. *Marine Biology* **101**, 235–247.
- Machan, R., Fedra, K. (1975). A new towed underwater camera system for wide-range benthic surveys. *Marine Biology* **33**, 75–84.
- Magorrian, B.H., Service, M. (1998). Analysis of underwater visual data to identify the impact of physical disturbance on Horse Mussel (*Modiolus modiolus*) beds. *Marine Pollution Bulletin* **36**, 354–359.
- Magorrian, B.H., Service, M., Clarke, W. (1995). An acoustic bottom classification survey of Strangford Lough, Northern Ireland. *Journal of the Marine Biological Association of the United Kingdom* **75**, 987–992.
- Marine Biological Association, (1957). Plymouth Marine Fauna, pp. 457. Plymouth: Latimer, Trend & Co. Ltd.
- Marrs, S.J., Atkinson, R.J.A., Smith, C.J., Hills, J.M. (1996). Calibration of the towed underwater TV technique for use in stock assessment of *Nephrops norvegicus*, pp. 155: Final Report to the European Commission 94/069.
- Maybeck, P.S. (1979). Stochastic models, estimation, and control, vol. 1. London: Academic Press.
- Meadows, P., Tait, J. (1989). Modification of sediment permeability and shear strength by two burrowing invertebrates. *Marine Biology* **101**, 75–82.
- Meadows, P.S., Meadows, A. (1991). The environmental impact of burrowing animals and animal burrows. *Symposia of the Zoological Society of London* **63**, 157–181.
- Michalopoulos, C., Auster, P.J., Malatesta, R.J. (1992). A comparison of transect and species-time counts for assessing faunal abundance from video surveys. *Marine Technology Society Journal* **26**, 27–31.

- Milne, B.T. (1992). Spatial aggregation and neutral models in fractal landscapes. *American Naturalist* **139**, 32–54.
- Moloney, C.L., Field, J.G. (1991). The size-based dynamics of plankton food webs. I. a simulation model of carbon and nitrogen flows. *Journal of Plankton Research* **13**, 1003–1038.
- Moore, J.J., Smith, J., Northern, K.O. (1999). Marine Nature Conservation Review Sector 8. Inlets in the western English Channel: area summaries. Peterborough: Joint Nature Conservation Committee.
- Moran, P.A.P. (1950). Notes on continuous stochastic phenomena. *Biometrika* **37**, 17–23.
- Morris, A.W., Loring, D.H., Bale, A.J., Howland, R.J.M., Mantoura, R.F.C., Woodward, E.M.S. (1982). Particle dynamics, particulate carbon and the oxygen minimum in an estuary. *Oceanologica Acta* **5**, 349–353.
- Morrisey, D.J., Howitt, L., Underwood, A.J., Stark, J.S. (1992). Spatial variation in soft-sediment benthos. *Marine Ecology Progress Series* **81**, 197–204.
- Morrison, M.A., Thrush, S.F., Budd, R. (2001). Detection of acoustic class boundaries in soft sediment systems using the seafloor acoustic discrimination system QTC VIEW. *Journal of Sea Research* **46**, 233–243.
- Mortensen, P.B., Roberts, J.M., Sundt, R.C. (2000). Video-assisted grabbing: a minimally destructive method of sampling azooxanthellate coral banks. *Journal of the Marine Biological Association of the United Kingdom* **80**, 365–366.
- Nash, R.D.M., Chapman, C.J., Atkinson, R.J.A., Morgan, P.J. (1984). Observations on the burrows and burrowing behaviour of *Calocaris macandreae* (Crustacea: Decapoda: Thalassinidea). *Journal of the Zoological Society of London* **202**, 425–439.
- Nickell, L.A., Atkinson, R.J.A. (1995). Functional morphology and trophic modes of three thalassinidean shrimp species, and a new approach to the classification of thalassinidean burrow morphology. *Marine Ecology Progress Series* **128**, 181–197.
- Nickell, L.A., Hughes, D.A., Atkinson, R.J.A. (1995). Megafaunal bioturbation in organically enriched Scottish sea lochs. In: *Biology and Ecology of Shallow Coastal Waters. Proceedings of the 28th European Marine Biology Symposium* (Eds. Eleftheriou, A., Ansell, A.D., Smith, C.J.). Olsen and Olsen, Fredensborg, Iraklio, Crete, pp. 315–322.
- Norkko, A., Cummings, V.J., Thrush, S.F., Hewitt, J.E., Hume, T. (2001). Local dispersal of juvenile bivalves: implications for sandflat ecology. *Marine Ecology Progress Series* **212**, 131–144.
- Ólafsson, E.B., Peterson, C.H., Ambrose Jr, W.G. (1994). Does recruitment limitation structure populations and communities of macro-invertebrates in marine soft sediments: the relative significance of pre- and post-settlement processes. *Oceanography and Marine Biology: and Annual Review* **32**, 65–110.
- Oliver, I., Beattie, A.J. (1993). A possible method for the rapid assessment of biodiversity. *Conservation Biology* **7**, 562–568.

- Oliver, J.S., Slattery, P.N. (1985). Destruction and opportunity on the seafloor: effects of gray whale feeding. *Ecology* **66**, 1965–1975.
- Olsgard, F., Somerfield, P.J., Carr, M.R. (1998). Relationships between taxonomic resolution, macrobenthic community patterns and disturbance. *Marine Ecology Progress Series* **172**, 25–36.
- O'Neill, R.V. (1989). Perspectives in hierarchy and scale. In: *Perspectives in Ecological Theory* (Eds. Roughgarden, J., May, R.M., Levin, S.A.). Princeton University Press, Princeton, New Jersey, pp. 140–156.
- O'Neill, R.V., Gardner, R.H., Milne, B.T., Turner, M.G., Jackson, B. (1991). Heterogeneity and spatial hierarchies. In: *Ecological heterogeneity* (Eds. Kolasa, J., Pickett, S.T.A.). Springer-Verlag, New York, pp. 85–96.
- Ott, J.A., Fuchs, B., Fuchs, R., Malasek, A. (1976). Observations on the biology of *Callinassa stebbingi* Borradaile and *Upogebia littoralis* Risso and their effect upon the sediment. *Senckenbergiana Maritima* **6**, 61–79.
- Paine, R.T. (1966). Food web complexity and species diversity. *American Naturalist* **100**, 65–75.
- Parry, D.M., Kendall, M.A., Rowden, A.A., Widdicombe, S. (1999) Species body size distribution patterns of marine benthic macrofauna assemblages from contrasting sediment types. *Journal of the Marine Biological Association of the United Kingdom* **79**, 793–801
- Paterson, D.M., Black, K.S. (1999). Water flow, sediment dynamics and benthic biology. *Advances in Ecological Research* **29**, 155–193.
- Patterson, K.R. (1984). Distribution patterns of some epifauna in the Irish Sea and their ecological interactions. *Marine Biology* **83**, 103–108.
- Pearson, T.H., Rosenberg, R. (1978). Macrobenthic succession in relation to organic enrichment and pollution in the marine environment. *Oceanography and Marine Biology: an Annual Review* **16**, 229–311.
- Pemberton, G.S., Risk, M.J., Buckley, D.E. (1976). Supershrimp: deep bioturbation in the Strait of Canso, Nova Scotia. *Science* **192**, 790–791.
- Peters, R.H. (1991). A critique for ecology. Cambridge: Cambridge University Press.
- Peters, R.H., Wassenberg, K. (1983). The effect of body size on animal abundance. *Oecologia* **60**, 89–96.
- Petersen, C.G.J. (1913). Valuation of the sea II. The animal communities of the sea bottom and their importance for marine zoogeography. *Report from the Danish Biological Station* **21**, 1–44.
- Petratis, P.S., Latham, R.E., Niesenbaum, R.E. (1989). The maintenance of species diversity by disturbance. *Quarterly Review of Biology* **64**, 393–418.
- Pfannkuche, O. (1993). Benthic response to the sedimentation of particulate organic-matter at the BIOTRANS Station, 47°N, 20°W. *Deep Sea Research Part II-Topical Studies in Oceanography* **40**, 135–149.

- Phillips, J.D., Driscoll, A.H., Peal, K.R., Marquet, W.M., Owen, D.M. (1979). A new undersea geological survey tool: ANGUS. *Deep Sea Research I-Oceanographic Research Papers* **26**, 211–225.
- Pickett, S.T.A., Thompson, J.N. (1978). Patch dynamics and the design of nature reserves. *Biological Conservation* **13**, 27–37.
- Piepenburg, D., von Juterzenka, K. (1994). Abundance, biomass and spatial distribution patterns of brittle stars (Echinodermata: Ophiuroidea) on the Kolbeinsey Ridge north of Iceland. *Polar Biology* **14**, 185–194.
- Piepenburg, D., Blackburn, T.H., von Dorrien, C.F., Gutt, J., Hall, P.O.J., Hulth, S., Kendall, M.A., Opalinski, K.W., Rachor, E., Schmid, M.K. (1995). Partitioning of benthic community respiration in the Arctic (northwestern Barents Sea). *Marine Ecology Progress Series* **118**, 199–213.
- Piepenburg, D., Schmid, M.K. (1996). Distribution, abundance, biomass, and mineralisation potential of the epibenthic megafauna of the Northeast Greenland shelf. *Marine Biology* **125**, 321–332.
- Piepenburg, D., Schmid, M.K. (1997). A photographic survey of the epibenthic megafauna of the Arctic Laptev Sea shelf: distribution, abundance, and estimates of biomass and organic carbon demand. *Marine Ecology Progress Series* **147**, 63–75.
- Piepenburg, D., Voss, J., Gutt, J. (1997). Assemblages of sea stars (Echinodermata: Asteroidea) and brittle stars (Echinodermata: Ophiuroidea) in the Weddell Sea (Antarctica) and off Northeast Greenland (Arctic): A comparison of diversity and abundance. *Polar Biology* **17**, 305–322.
- Pilgrim, D.A. (1998). The observation of underwater light – Part 1. *The Hydrographic Journal* **90**, 23–27.
- Pilgrim, D.A., Parry, D.M., Jones, M.B., Kendall, M.A. (2000). ROV image scaling with laser spot patterns. *Underwater Technology* **24**, 93–103.
- Pinn, E.H., Robertson, M.R. (1998). The effect of bioturbation on Roxann® a remote acoustic seabed discrimination system. *Journal of the Marine Biological Association of the United Kingdom* **78**, 707–715.
- Pinn, E.H., Robertson, M.R. (2001). Further analysis of the effect of bioturbation by *Nephrops norvegicus* (L.) on the acoustic return of the RoxAnn™ seabed discrimination system. *ICES Journal of Marine Sciences* **58**, 216–219.
- Pinn, E.H., Atkinson, R.J.A., Rogerson, A. (1998). The diet of two mud-shrimps, *Calocaris macandreae* and *Upogebia stellata* (Crustacea: Decapoda: Thalassinidea). *Ophelia* **48**, 211–223.
- Platt, T. (1985). Structure of the marine ecosystem: its allometric basis. *Canadian Bulletin on Fisheries and Aquatic Sciences* **213**, 55–64.
- Posey, M.H. (1986). Changes in a benthic community associated with dense beds of a burrowing deposit feeder, *Callinassa californiensis*. *Marine Ecology Progress Series* **31**, 15–22.



- Posey, M.H., Dumbauld, B.R., Armstrong, D.A. (1991). Effects of a burrowing mud shrimp, *Upogebia pugettensis* (Dana), on abundances of macro-infauna. *Journal of Experimental Marine Biology and Ecology* **148**, 283–294.
- Posey, M.H., Lindberg, W., Alphin, T., Vose, F. (1996). Influence of a storm disturbance on an offshore benthic community. *Bulletin of Marine Science* **59**, 523–529.
- Preston, J.M., Collins, W.T. (1999). Bottom classification in very shallow water by high-speed data acquisition. Quester Tangent Corporation.
- Priede, I.G., Bagley, P.M., Smith, A., Creasey, S., Merrett, N.R. (1994). Scavenging deep demersal fishes of the Porcupine Seabight, North-East Atlantic: observations by baited camera, trap and trawl. *Journal of the Marine Biological Association of the United Kingdom* **74**, 481–498.
- Rees, E.I.S., Nicholaidou, A., Laskaridou, P. (1977). The effects of storms on the dynamics of shallow water associations. In: *Biology of Benthic Organisms*. (Eds. Keegan, B.F., Ceidigh, P.O., Boaden, P.J.S.). Pergamon Press, New York, pp. 465–474.
- Reise, K. (1991). Mosaic cycles in the marine benthos. In *The mosaic-cycle concept of ecosystems* (ed. H. Remmert), pp. 61–82.
- Rhoads, D.C. (1974). Organism-sediment relations on the muddy seafloor. *Oceanography and Marine Biology: An Annual Review* **12**, 263–300.
- Rhoads, D.C., Young, D.K. (1970). The influences of deposit-feeding organisms on sediment stability and community trophic structure. *Journal of Marine Research* **28**, 150–178.
- Rice, A.L., Aldred, R.G., Billett, D.S.M., Thurston, M.H. (1979). The combined use of an epibenthic sledge and a deep-sea camera to give quantitative relevance to macro-benthos samples. *Ambio Special Report*, 59–72.
- Rice, A.L., Aldred, R.G., Darlington, E., Wild, R.A. (1982). The quantitative estimation of the deep-sea megabenthos; a new approach to an old problem. *Oceanologica Acta* **5**, 63–72.
- Richardson, A.J., Lamberts, C., Isaacs, G., Moloney, C.L., Gibbons, M.J. (2000). Length–weight relationships of some important forage crustaceans from South Africa. *Naga Report, The ICLARM Quarterly* **23**, 29–33.
- Robbins, B., Bell, S. (1994). Seagrass landscapes: A terrestrial approach to the marine subtidal environment. *Trends in Ecology and Evolution* **9**, 301–304.
- Robison, B.H. (1992). Midwater research methods with MBARI's ROV. *Marine Technology Society Journal* **26**, 32–39.
- Ross, H.E. (1989). Orientation, movement and motor skills in divers. *Progress in Underwater Science* **13**, 147–167.
- Rowden, A.A., Jones, M.B. (1993). Critical evaluation of sediment turnover rates for Callianassidae (Decapoda: Thalassinidea). *Journal of Experimental Marine Biology and Ecology* **173**, 265–272.

- Rowden, A.A., Jones, M.B. (1995). The burrow structure of the mud shrimp *Callinassa subterranea* (Decapoda: Thalassinidea) from the North Sea. *Journal of Natural History* **29**, 1155–1165.
- Rowden, A.A., Jones, M.B., Morris, A.W. (1998). The role of *Callinassa subterranea* (Montagu) (THALASSINIDEA) in sediment resuspension in the North Sea. *Continental Shelf Research* **18**, 1365–1380.
- Rumohr, H., Brey T., Ankar, S. (1987). A compilation of biometric conversion factors for benthic invertebrates of the Baltic Sea. In *Baltic Marine Biologists Publication*, vol. 9, pp. 56.
- Sanders, H.L. (1968). Marine benthic diversity: a comparative study. *American Naturalist* **102**, 243–282.
- Schneider, D.C. (1994). *Quantitative Ecology: Spatial and Temporal Scaling*. Academic Press, San Diego, 396 pp.
- Schwinghamer, P. (1981). Characteristic size distributions of integral benthic communities. *Canadian Journal of Fisheries and Aquatic Science* **38**, 1255–1263.
- Schwinghamer, P., Hargrave, B., Peer, D., Hawkins, C.W. (1986). Partitioning of production and respiration among size groups of organisms in an intertidal benthic community. *Marine Ecology Progress Series* **31**, 131–142.
- Schwinghamer, P., Guigné, J.Y., Siu, W.C. (1996). Quantifying the impact of trawling on benthic habitat structure using high resolution acoustics and chaos theory. *Canadian Journal of Fisheries and Aquatic Science* **53**, 288–296.
- Shepherd, K., Juniper, S.K. (1997). ROPOS: creating a scientific tool from an industrial ROV. *Marine Technology Society Journal* **31**, 48–54.
- Siddorn, J.R., Allen, J.I., Uncles, R.J. (submitted). Heat, salt and tracer transport in the Plymouth Sound coastal region: A 3D modelling study. *Journal of the Marine Biological Association of the United Kingdom*.
- Smith, C.R., Hamilton, S.C. (1983). Epibenthic megafauna of a bathyal basin off southern California: patterns of abundance, biomass, and dispersion. *Deep Sea Research I-Oceanographic Research Papers* **30**, 907–928.
- Smith, C.R., Maybaum, H.L., Baco, A.R., Pope, R.H., Carpenter, S.D., Yager, P.L., Macko, S.A., Deming, J.W. (1998). Sediment community structure around a whale skeleton in the deep Northeast Pacific: Macrofaunal, microbial and bioturbation effects. *Deep Sea Research II-Topical Studies in Oceanography* **45**, 335–364.
- Smith, J.R. (1997). Introduction to geodesy: the history and concepts of modern geodesy. In *Wiley series in surveying and boundary control* (ed. R. Minnink), pp. 224. New York: John Wiley and Sons, Inc.

- Smith, K.L., Kaufmann, R.S., Wakefield, W.W. (1993). Mobile megafaunal activity monitored with a time-lapse camera in the abyssal North Pacific. *Deep Sea Research I-Oceanographic Research Papers* **40**, 2307–2324.
- Snelgrove, P.V.R., Butman, C.A. (1994). Animal-sediment relationships revisited: cause versus effect. *Oceanography and Marine Biology: an Annual Review* **32**, 11–117.
- Snelgrove, P.V.R., Austen, M.C., Boucher, G., Heip, C., Hutchings, P., King, G., Koike, I., Lambshead, P.J., Smith, C. (2000). Sediments-up and water column-down: linking biodiversity above and below the sediment–water interface. *Bioscience* **50**, 1108–1120.
- Soltwedel, T., Vopel, K. (2001). Bacterial abundance and biomass in response to organism-generated habitat heterogeneity in deep-sea sediments. *Marine Ecology Progress Series* **219**, 291–298.
- Somerfield, P.J., Gage, J.D. (2000). Community structure of the benthos in Scottish Sea-lochs. IV. Multivariate spatial pattern. *Marine Biology* **136**, 1133–1145.
- Soulsby, R.L. (1997). Dynamics of marine sands: a manual for practical applications. HR Wallingford, Wallingford, pp. 141.
- Sprunk, H.J., Auster, P.J., Stewart, L.L., Lovalvo, D.A., Good, D.H. (1992). Modifications to low-cost remotely operated vehicles for scientific sampling. *Marine Technology Society Journal* **26**, 54–58.
- Stamhuis, E.J., Schreurs, C.E., Videler, J.J. (1987). Burrow architecture and turbatory activity of the Thalassinid shrimp *Callianassa subterranea* from the central North Sea. *Marine Ecology Progress Series* **151**, 155–163.
- Steele, J.H. (1985). Spatial patterns in planktonic communities. Plenum Press, New York.
- Strasser, M. (1999). *Mya arenaria* - an ancient invader of the North Sea coast. *Helgoländer Meeresuntersuchungen* **52**, 309–324.
- Suchanek, T.H. (1983). Control of seagrass communities and sediment distribution by *Callianassa* (Crustacea, Thalassinidea) bioturbation. *Journal of Marine Research* **41**, 281–298.
- Suchanek, T.H., Colin, P.L. (1986). Rates and effects of bioturbation by invertebrates and fishes at Enewetak and Bikini Atolls. *Bulletin of Marine Science* **38**, 25–34.
- Summers, R.W. (1980). The diet and feeding behaviour of the flounder *Platichthys flesus* (L.) in the Ythan Estuary, Aberdeenshire, Scotland. *Estuarine, Coastal and Marine Science* **11**, 217–232.
- Swift, D.J. (1993). The macrobenthic infauna off Sellafield (north-eastern Irish Sea) with special reference to bioturbation. *Journal of the Marine Biological Association of the United Kingdom* **73**, 143–162.
- Takagawa, T. (1995). Advanced technology used in Shinkai 6500 and full ocean depth ROV Kaiko. *Marine Technology Society Journal* **29**, 15–25.

- Thayer, C.W. (1983). Sediment-mediated biological disturbance and the evolution of marine benthos. In: *Biotic interactions in recent and fossil benthic communities* L. (Eds. Tevesz, M.J.S., McCall, P.). Plenum Press, New York, pp. 479–625.
- The Hydrographic Office (1991). Tidal Stream Atlas: Plymouth Harbour and Approaches. Edition 2. The United Kingdom Hydrographic Office, Taunton, pp. 41.
- The Hydrographic Office (2001). Admiralty Tide Tables. Volume 1. United Kingdom and Ireland (including European Channel Ports). The United Kingdom Hydrographic Office.
- Thorndike, E.M. (1959). Deep-sea cameras of the Lamont Observatory. *Deep Sea Research* **5**, 234–237.
- Thistle, D. (1981). Natural physical disturbances and communities in marine soft bottoms. *Marine Ecology Progress Series* **6**, 223–228.
- Thrush, S.F. (1986). Spatial heterogeneity in subtidal gravel generated by the pit-digging activities of *Cancer pagurus*. *Marine Ecology Progress Series* **30**, 221–227.
- Thrush, S.F., Townsend, C.R. (1986). The sublittoral macrobenthic community composition of Lough Hyne, Ireland. *Estuarine Coastal and Shelf Science* **23**, 551–573.
- Thrush, S.F., Hewitt, J.E., Pridmore, R.D. (1989). Patterns in the spatial arrangements of polychaetes and bivalves in intertidal sandflats. *Marine Biology* **102**, 529–534.
- Thrush, S.F., Pridmore, R.D., Hewitt, J.E., Cummings, V.J. (1991). Impact of ray feeding disturbances on sandflat macrobenthos - do communities dominated by polychaetes or shellfish respond differently. *Marine Ecology Progress Series* **69**, 245–252.
- Thrush S.F., Cummings, V.J., Dayton, P.K., Ford, R., Grant, J., Hewitt, J.E., Hines, A.H., Lawrie, S.M., Pridmore, R.D., Legendre, P., McArdle, B.H., Schneider, D.C., Turner, S.J., Whitlatch, R.B., Wilkinson, M.R. (1997a) Matching the outcome of small-scale density manipulation experiments with larger scale patterns: an example of bivalve adult/juvenile interactions. *Journal of Experimental Marine Biology and Ecology* **216**, 153–169.
- Thrush, S.F., Schneider, D.C., Legendre, P., Whitlatch, R.D., Dayton, P.K., Hewitt, J.E., Hines, A.H., Cummings, V.J., Lawrie, S.M., Grant, J., Pridmore, R.D., Turner, S.J., McArdle, B.H. (1997b). Scaling-up from experiments to complex ecological systems: Where to next? *Journal of Experimental Marine Biology and Ecology* **216**, 243–254.
- Thrush, S.F., Hewitt, J.E., Cummings, V.J., Dayton, P.K., Cryer, M., Turner, S.J., Funnell, G., Budd, R., Milburn, C., Wilkinson, M.R. (1998). Disturbance of the marine benthic habitat by commercial fishing: impacts at the scale of the fishery. *Ecological Applications* **8**, 866–879.
- Thrush, S.F., Hewitt, J.E., Funnell, G.A., Cummings, V.J., Ellis, J., Schultz, D., Talley, D., Norkko, A. (2001). Fishing disturbance and marine biodiversity: the role of habitat structure in simple soft-sediment systems. *Marine Ecology Progress Series* **221**, 255–264.
- Thurston, M.H., Bett, B.J., Rice, A.L., Jackson, P.A.B. (1994). Variations in the invertebrate abyssal megafauna in the North Atlantic Ocean. *Deep Sea Research I-Oceanographic Research Papers* **41**, 1321–1348.

- Tilman, D. (1997). Biodiversity and ecosystem functioning. In: *Nature's Services. Societal dependence on natural ecosystems* (Ed. Daily, G.C.). Island Press, Washington DC, pp. 93–112.
- Tuck, I.D., Chapman, C.J., Atkinson, R.J.A., Bailey, N., Smith, R.S.M. (1997). A comparison of methods for stock assessment of the Norway lobster, *Nephrops norvegicus*, in the Firth of Clyde. *Fisheries Research* **32**, 89–100.
- Turner, M.G. (1990). Spatial and temporal analysis of landscape patterns. *Landscape Ecology* **4**, 21–30.
- Turner, M.G., O'Neill, R.V., Gardner, R.H., Milne, B.T. (1989). Effects of changing spatial scale on the analysis of landscape pattern. *Landscape Ecology* **3**, 153–162.
- Tusting, R.F., Caimi, F.M., Taylor, L.D. (1989). Special purpose illumination systems for remotely operated vehicles. In *ROV 89 Conference*, pp. 170–175: Washington, D.C., Marine Technology Society.
- Underwood, A.J. (1986). What is a community? In: *Patterns and processes in the history of life* (Eds. Raup, D.M., Jablonski, D.). Dahlem Konferenzen. Springer-Verlag, Berlin, pp. 351–367.
- Underwood, A.J., Chapman, M.G., Connell, S.D. (2000). Observations in ecology: you can't make progress on processes without understanding the patterns. *Journal of Experimental Marine Biology and Ecology* **250**, 97–115.
- Uzmann, J.R., Cooper, R.A., Theroux, R.B., Wigley, R.L. (1977). Synoptic comparison of three sampling techniques for estimating abundance and distribution of selected megafauna: submersible vs camera sled vs otter trawl. *Marine Fisheries Review* **39**, 11–19.
- Valentine, J.F., Heck, K.L., Harper, P., Beck, M. (1994). Effects of bioturbation in controlling turtlegrass (*Thalassia testudinum* Banks ex König) abundance - evidence from field enclosures and observations in the northern Gulf-of-Mexico. *Journal of Experimental Marine Biology and Ecology* **178**, 181–192.
- Veisze, P., Karpov, K. (2002). Geopositioning a Remotely Operated Vehicle for marine species and habitat analysis. In: *Undersea with GIS*. (Ed. Wright, D.J.). ESRI Press, Redlands, CA, USA, pp. 105–116.
- Vevers, H.G. (1951). Photography of the sea floor. *Journal of the Marine Biological Association of the United Kingdom* **30**, 101–111.
- Vézina, A.F. (1988). Sampling variance and the design of quantitative surveys of the marine benthos. *Marine Biology* **97**, 151–155.
- Wakefield, W.W., Genin, A. (1987). The use of a Canadian (perspective) grid in deep-sea photography. *Deep Sea Research I-Oceanographic Research Papers* **34**, 469–478.

- Warwick, R.M. (1984). Species size distributions in marine benthic communities. *Oecologia* **61**, 32–41.
- Warwick, R.M., Price, R. (1975). Macrofauna production in an estuarine mud-flat. *Journal of the Marine Biological Association of the United Kingdom* **55**, 1–18.
- Warwick, R.M., Davies, J.R. (1977). The distribution of sublittoral macrofauna communities in the Bristol Channel in relation to the substrate. *Estuarine and Coastal Marine Science* **5**, 267–288.
- Warwick, R.M., Uncles, R.J. (1980). Distribution of macrofauna associations in the Bristol Channel in relation to tidal stress. *Marine Ecology Progress Series* **3**, 97–103.
- Warwick, R.M., Light, J. (2002). Death assemblages of molluscs on St Martin's Flats, Isles of Scilly: a surrogate for regional biodiversity? *Biodiversity and Conservation* **11**, 99–112.
- Watters, G., Bergström, B., Gutt, J., Pettersson, J.-A. (1995). AMLR program: Preliminary report of AMLR 1995 Leg III, epibenthic surveys of bays, anchorages, and fjords around South Georgia. *Antarctic Journal of the United States* **30**, 237–240.
- Wheatcroft, R.A., Smith, C.R., Jumars, P.A. (1989). Dynamics of surficial trace assemblages in the deep sea. *Deep Sea Research I-Oceanographic Research Papers* **36**, 71–91.
- White, P.S., Pickett, S.T.A. (1985). Natural disturbance and patch dynamics: an introduction. In: *The ecology of natural disturbances and patch dynamics* (Eds. Pickett, S.T.A., White, P.S.). Academic Press, London, pp. 3–13.
- Whittaker, R.H. (1960). Vegetation of the Siskiyou Mountains, Oregon and California. *Ecological Monographs* **30**, 279–338.
- Whittaker, R.H. (1975). Communities and ecosystems. Macmillan, New York, 385 pp.
- Widdicombe, S. (2001). Disturbance and diversity in marine benthic communities. PhD thesis. *Department of Biological Sciences*. Plymouth: University of Plymouth.
- Widdicombe, S., Austen, M.C. (1998). Experimental evidence for the role of *Brissopsis lyrifera* (Forbes, 1841) as a critical species in the maintenance of benthic diversity and the modification of sediment chemistry. *Journal of Experimental Marine Biology and Ecology* **228**, 241–255.
- Widdicombe, S., Austen, M.C. (1999). Mesocosm investigation into the effects of bioturbation on the diversity and structure of a subtidal macrobenthic community. *Marine Ecology Progress Series* **189**, 181–193.
- Widdicombe, S., Austen, M.C., Kendall, M.A., Warwick, R.M., Jones, M.B. (2000). Bioturbation as a mechanism for setting and maintaining levels of diversity in subtidal macrobenthic communities. *Hydrobiologia* **440**, 369–377.
- Widdows, J., Brinsley, M.D., Salkeld, P.N., Lucas, C.H. (2000). Influence of biota on spatial and temporal variation in sediment erodability and material flux on a tidal flat (Westerschelde, The Netherlands). *Marine Ecology Progress Series* **194**, 23–37.
- Wiens, J.A. (1989). Spatial scaling in ecology. *Functional Ecology* **3**, 385–397.

- Winer, B.J., Brown, D.R., Michels, K.M. (1991). Statistical principles in experimental design. New York: McGraw-Hill, Inc.
- Witbaard, R., Duineveld, G.C.A. (1989). Some aspects of the biology and ecology of the burrowing shrimp *Callianassa subterranea* (Montagu) (Thalassinidae) from the southern North Sea. *Sarsia* 74, 209–219.
- Woodin, S.A. (1976). Adult–larval interactions in dense faunal assemblages: patterns of abundance. *Journal of Marine Research* 34, 25–41.
- Woodin, S.A. (1978). Refuges, disturbance, and community structure: a marine soft-bottom example. *Ecology* 59, 274–284.
- Zajac, R.N. (1999). Understanding the sea floor landscape in relation to impact assessment and environmental management in coastal marine sediments. In *Biogeochemical Cycling and Sediment Ecology*, vol. 59 (ed. J. S. Gray), pp. 211–227: Kluwer Academic Publishers.
- Zajac, R.N., Lewis, R.S., Poppe, L.J., Twichell, D.C., Vozarik, J., DiGiacomo-Cohen, M.L. (2000) Relationships among sea-floor structure and benthic communities in Long Island Sound at regional and benthoscape scales. *Journal of Coastal Research* 16, 627–640.
- Zwarts, L., Wanink, J. (1989). Siphon size and burying depth in deposit- and suspension-feeding bivalves. *Marine Biology* 100, 227–240.
- Zwarts, L., Blomert, A-M., Spaak, P., de Vries, B. (1994). Feeding radius, burying depth and siphon size of *Macoma balthica* and *Scrobicularia plana*. *Journal of Experimental Marine Biology and Ecology* 183, 193–212.

# **APPENDIX I**

## **Description of megafaunal features**



Table A1.1: Megafaunal species and biogenic sediment structures associated with burrowing megafauna identified from ROV images in Jannycliff Bay.

Megafaunal species or biogenic sediment feature	Description
Thalassinidean opening	Circular funnel-shaped opening leading to vertical shaft. Opening approximately 2–4 cm diameter. <i>Melinna palmata</i> tubes often visible within the opening.
Extinct thalassinidean opening	As above, but shaft appears to be in-filled
<i>Callianassa subterranea</i> pelletised mound	Sediment mound that is darker than sediment surface. Diameter of mound at base approximately 8 cm. Crater-like depression at the summit of mound gives the appearance of a volcano.
cf <i>Callianassa subterranea</i> pelletised mound (flattened)	Patch of dark (anoxic) sediment "smeared" across sediment surface. Approximately 8 cm wide.
<i>Callianassa subterranea</i> open mound	Sediment mound that is darker than sediment surface (anoxic). Mound diameter at base approximately 8 cm. Circular opening approximately 2 cm diameter at the summit of mound.
<i>Goneplax rhomboides</i> burrow	Oblique burrow opening approximately 4 cm wide. Ejected sediment often visible as scree from burrow entrance.
Unknown oblique opening	Oblique burrow opening approximately 2 cm wide with no ejected sediment
Hermit crab	Gastropod shell (usually <i>Turitella</i> or <i>Hinia</i> ) from which legs are visible.
<i>Macropodia</i> sp.	Triangular carapace with elongated rostrum. Long and slender pereopods.
<i>Cancer pagurus</i>	Oval carapace, large robust chelae.
Pair of 1 cm diameter holes surrounded by ejected sediment	Pair of circular holes, each approximately 1 cm diameter, surrounded by ejected sediment.
Circular 1 cm flush opening	Circular hole approximately 1 cm diameter, flush with sediment surface
Circular 1 cm in a depression	Circular hole approximately 1 cm diameter, sloping hole entrance.
"3-siphoned opening"	Single surface opening approximately 2 cm diameter containing three circular holes, each approximately 5 mm diameter.
Two openings in a common depression	Single surface opening approximately 2 cm diameter containing three circular holes, each approximately 5 mm diameter.
<i>Philine aperta</i>	Rounded diamond-shaped translucent grey-white epifaunal mollusc. Approximately 3 cm length.
<i>Pecten maximus</i>	Epifaunal bivalve with flat ears either side of umbones. Sometimes partially buried below sediment surface.
<i>Acanthocardia</i> sp.	Single surface opening with fused bivalve siphon tips visible at surface. Pale viscera siphon tips that appear as two spots when contracted in response to ROV passing overhead.
<i>Lutraria lutraria</i>	Single surface opening with fused bivalve siphon tips visible at the surface. Dark viscera siphon tips.
Unknown bivalve siphon 1	Single surface opening with fused bivalve siphon tips visible at surface. Pale viscera siphon tips that appear hourglass-shaped when contracted in response to ROV passing overhead.
Bivalve shell on surface	Bivalve shell protruding from sediment surface. No viscera visible.
<i>Hinia reticulata</i>	Epifaunal gastropod with reticulated shell. Tracks often visible.
<i>Turitella communis</i>	Epifaunal gastropod with sharply pointed shell approximately 6 cm tall. Whorls separated by distinct suture line. Reddish brown colour.
Burrowing anemone	Anemone tentacles protruding from sediment surface.
<i>Myxicola infundibulum</i>	Funnel-shaped tentacular crown with dark distal edge.
Ejected sediment patch	Patch of dark (anoxic) sediment originating from point. Approximately 3 cm wide.
Surface scrape/feeding pit	Large depression in the sediment surface with distinct edges but not leading to a burrow opening
Detritus obscured feature	Biogenic sediment structure partially obscured by <i>Laminaria</i> sp. or other detritus
Ophiuroid	Large brittlestar with disc diameter approximately 35 mm. Arm length approximately 4 times disc diameter. Probably <i>Ophiura ophiura</i>
White detritus patch	White patch on sediment surface. Probably <i>Beggiatoa</i> sp.

Table A1.2: Megafaunal species and biogenic sediment structures associated with burrowing megafauna identified from ROV images in Loch Creran.

Megafaunal species or biogenic sediment feature	Description
<i>Nephrops norvegicus</i> burrow	Oblique opening greater than 4 cm wide. Ejected sediment often visible in scree pattern. Chela(e) may protrude from opening
<i>Nephrops norvegicus</i> vertical opening	Circular opening leading to a vertical shaft that appears to penetrate to <i>N. norvegicus</i> tunnel. Opening approximately 2–4 cm diameter
<i>Maxmuelleria lankesteri</i> mound	Large mound of pale sediment approximately 50 cm diameter. Sediment fine and not covered in diatom bloom.
Thalassinidean opening	Circular funnel-shaped opening leading to vertical shaft. Opening approximately 2–4 cm diameter. <i>Melinna palmata</i> tubes often visible within the opening.
<i>Goneplax rhomboides</i> burrow	Oblique burrow opening approximately 4 cm wide. Ejected sediment often visible as scree from burrow entrance.
<i>Virgularia mirabilis</i>	slender cream–yellow sea pen with polyps on both sides of a slender column. Approximately 20 cm in height, but may reach 50 cm.
Large circular hole	Large circular hole approximately 6 cm diameter, no funnel, vertical shaft.
Circular 1 cm flush opening	Circular hole approximately 1 cm diameter, flush with sediment surface.
Circular 1 cm in a depression	Circular hole approximately 1 cm diameter, sloping entrance to hole.
Circular 1 cm on a mound	Circular hole approximately 1 cm diameter at the top of a small mound, base of diameter approximately 3 cm.
“3-siphoned opening”	Single surface opening, approximately 2 cm diameter containing three circular holes, each approximately 5 mm diameter.
“Kidney” opening	Kidney-shaped opening, 2 cm diameter.
<i>Myxicola infundibulum</i>	Funnel-shaped tentacular crown with dark distal edge.
Bivalve siphon	Single surface opening with fused bivalve siphon tips visible at the sediment surface.
Bivalve shell on surface	Bivalve shell protruding from sediment surface. No viscera visible.
Burrowing anemone	Anemone tentacles protruding from the sediment surface.
Surface scrape/feeding pit	Large depression in the sediment surface with distinct edges but not leading to a burrow opening.
cf egg case	Gelatinous epifaunal structure approximately 2 cm long, disturbed by propeller wash.
White detritus patch	White patch on sediment surface. Probably <i>Beggiatoa</i> sp.

## **APPENDIX II**

### **Raw abundance data**

Table A2.1: Abundance of megafaunal features observed by direct diver and ROV observations in Loch Creran grid CR1.

Grid Location	Direct diver observations			ROV observations		
	Total Features	Conspicuous features	Features greater than 15 mm diameter	Total Features	Conspicuous features	Features greater than 15 mm diameter
CR1_A1	1	0	1	1	0	0
CR1_A2	1	1	1	1	1	1
CR1_A3	0	0	0	0	0	0
CR1_A4	1	0	1	2	0	2
CR1_A5	6	1	5	2	2	2
CR1_A6	5	1	5	1	1	1
CR1_B1	3	1	2	1	0	1
CR1_B2	3	2	3	3	2	2
CR1_B3	1	0	1	0	0	0
CR1_B4	3	0	3	1	0	0
CR1_B5	6	3	6	4	2	2
CR1_B6	3	2	3	1	1	1
CR1_C1	0	0	0	1	1	1
CR1_C2	3	1	3	2	0	1
CR1_C3	1	0	1	0	0	0
CR1_C4	0	0	0	0	0	0
CR1_C5	4	4	4	4	3	3
CR1_C6	1	1	1	3	1	1
CR1_D1	5	4	5	6	4	4
CR1_D2	1	1	1	2	2	2
CR1_D3	1	0	1	2	0	0
CR1_D4	0	0	0	3	0	0
CR1_D5	1	0	1	3	1	1
CR1_D6	2	0	2	1	1	0
CR1_E1	7	4	6	5	1	2
CR1_E2	4	2	4	5	2	2
CR1_E3	0	0	0	1	0	1
CR1_E4	2	2	2	1	1	1
CR1_E5	0	0	0	0	0	0
CR1_E6	1	1	1	1	0	0
CR1_F1	3	2	2	4	0	0
CR1_F2	0	0	0	3	0	0
CR1_F3	2	1	2	5	1	1
CR1_F4	0	0	0	3	0	1
CR1_F5	1	1	1	1	0	0
CR1_F6	0	0	0	1	0	1
Total	72	35	68	74	27	34

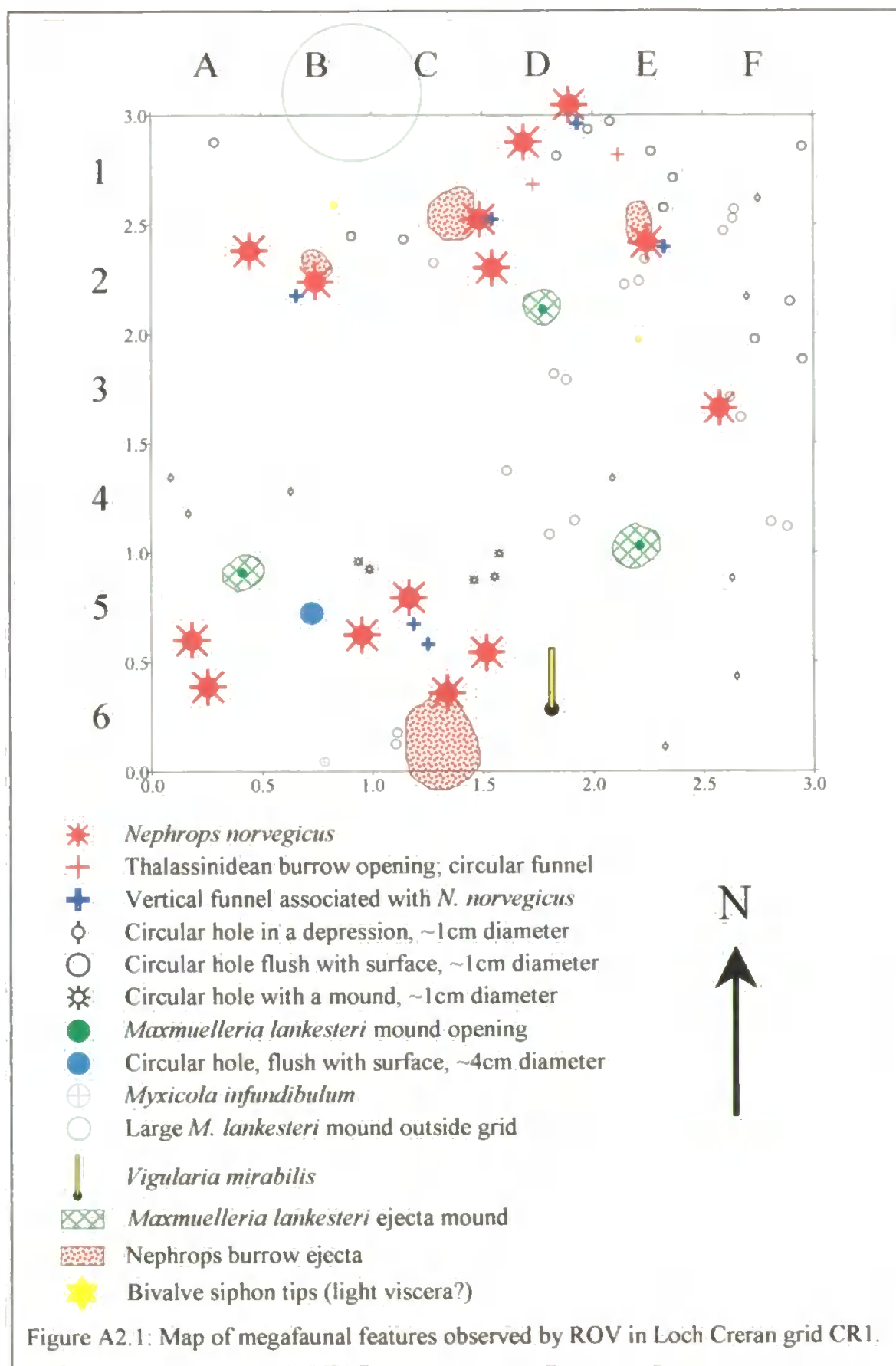


Table A2.2: Abundance of megafaunal features observed by direct diver and ROV observations in Loch Creran grid CR2.

Grid Location	Direct diver observations			ROV observations		
	Total Features	Conspicuous Features	Features greater than 15 mm diameter	Total Features	Conspicuous Features	Features greater than 15 mm diameter
CR2_A1	2	2	2	2	1	0
CR2_A2	2	0	1	6	1	1
CR2_A3	1	1	1	2	1	1
CR2_A4	2	2	2	2	2	2
CR2_A5	0	0	0	0	0	0
CR2_A6	4	1	4	2	0	0
CR2_B1	1	0	1	3	0	1
CR2_B2	3	1	2	1	1	1
CR2_B3	8	1	7	6	1	1
CR2_B4	0	0	0	1	0	1
CR2_B5	8	0	3	5	0	1
CR2_B6	1	0	1	2	0	1
CR2_C1	0	0	0	0	0	0
CR2_C2	3	1	3	1	1	1
CR2_C3	1	1	1	1	1	1
CR2_C4	2	1	2	1	0	0
CR2_C5	2	0	2	2	0	1
CR2_C6	1	0	1	0	0	0
CR2_D1	0	0	0	0	0	0
CR2_D2	2	0	1	4	0	0
CR2_D3	3	3	3	2	2	2
CR2_D4	2	1	2	1	0	0
CR2_D5	0	0	0	0	0	0
CR2_D6	4	0	4	2	0	0
CR2_E1	0	0	0	2	0	0
CR2_E2	1	1	1	5	1	2
CR2_E3	3	1	3	1	0	0
CR2_E4	0	0	0	0	0	0
CR2_E5	0	0	0	0	0	0
CR2_E6	0	0	0	1	1	1
CR2_F1	1	0	1	0	0	0
CR2_F2	3	0	3	1	0	0
CR2_F3	1	1	1	0	0	0
CR2_F4	1	1	1	2	1	2
CR2_F5	0	0	0	0	0	0
CR2_F6	0	0	0	0	0	0
Total	62	19	53	58	14	20

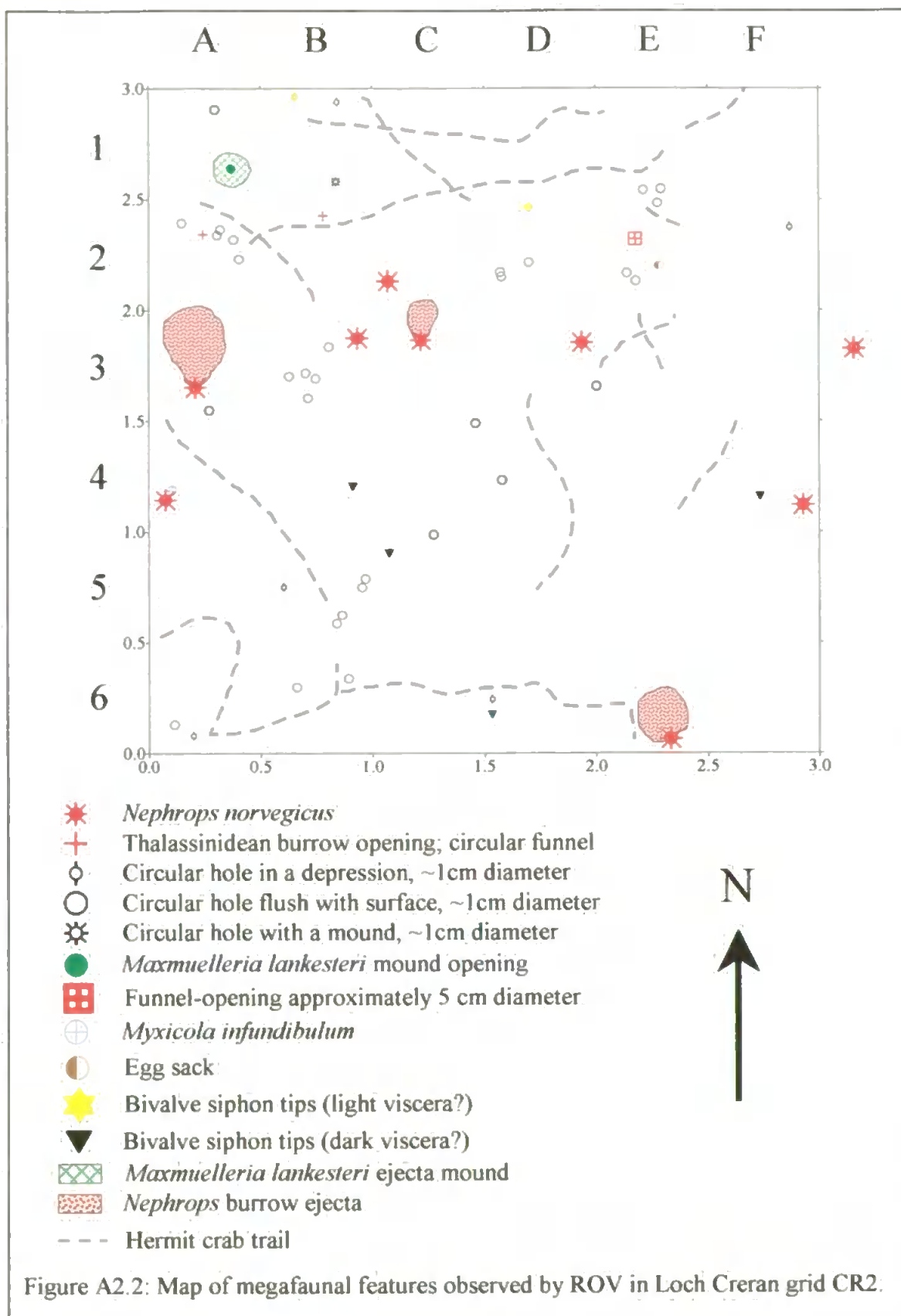


Table A2.3: Abundance of megafaunal features observed by direct diver and ROV observations in Loch Creran grid CR3.

Grid Location	Direct diver observations			ROV observations		
	Total Features	Conspicuous Features	Features greater than 15 mm diameter	Total Features	Conspicuous Features	Features greater than 15 mm diameter
CR3_A1	2	2	2	2	2	2
CR3_A2	1	0	1	1	0	0
CR3_A3	3	1	2	2	1	0
CR3_A4	2	0	1	2	0	0
CR3_A5	1	0	1	2	0	0
CR3_A6	0	0	0	2	0	2
CR3_B1	0	0	0	1	0	1
CR3_B2	0	0	0	0	0	0
CR3_B3	2	2	2	3	1	1
CR3_B4	4	2	4	3	2	2
CR3_B5	2	2	2	5	2	2
CR3_B6	2	0	2	1	0	0
CR3_C1	2	0	1	0	0	0
CR3_C2	0	0	0	1	0	1
CR3_C3	4	3	4	2	2	2
CR3_C4	1	1	1	1	1	1
CR3_C5	1	1	1	1	1	1
CR3_C6	5	1	4	5	1	3
CR3_D1	3	2	3	2	1	2
CR3_D2	1	1	1	0	0	0
CR3_D3	1	1	1	2	1	1
CR3_D4	4	3	4	8	5	5
CR3_D5	0	0	0	0	0	0
CR3_D6	1	0	1	2	0	0
CR3_E1	2	2	2	2	2	2
CR3_E2	1	1	1	2	2	2
CR3_E3	9	4	8	6	5	6
CR3_E4	2	1	2	1	1	1
CR3_E5	1	0	1	0	0	0
CR3_E6	2	1	2	4	0	1
CR3_F1	1	0	1	1	0	0
CR3_F2	0	0	0	0	0	0
CR3_F3	2	2	2	2	2	2
CR3_F4	3	0	3	1	0	0
CR3_F5	0	0	0	0	0	0
CR3_F6	3	1	3	1	0	0
Total	68	34	63	68	32	40



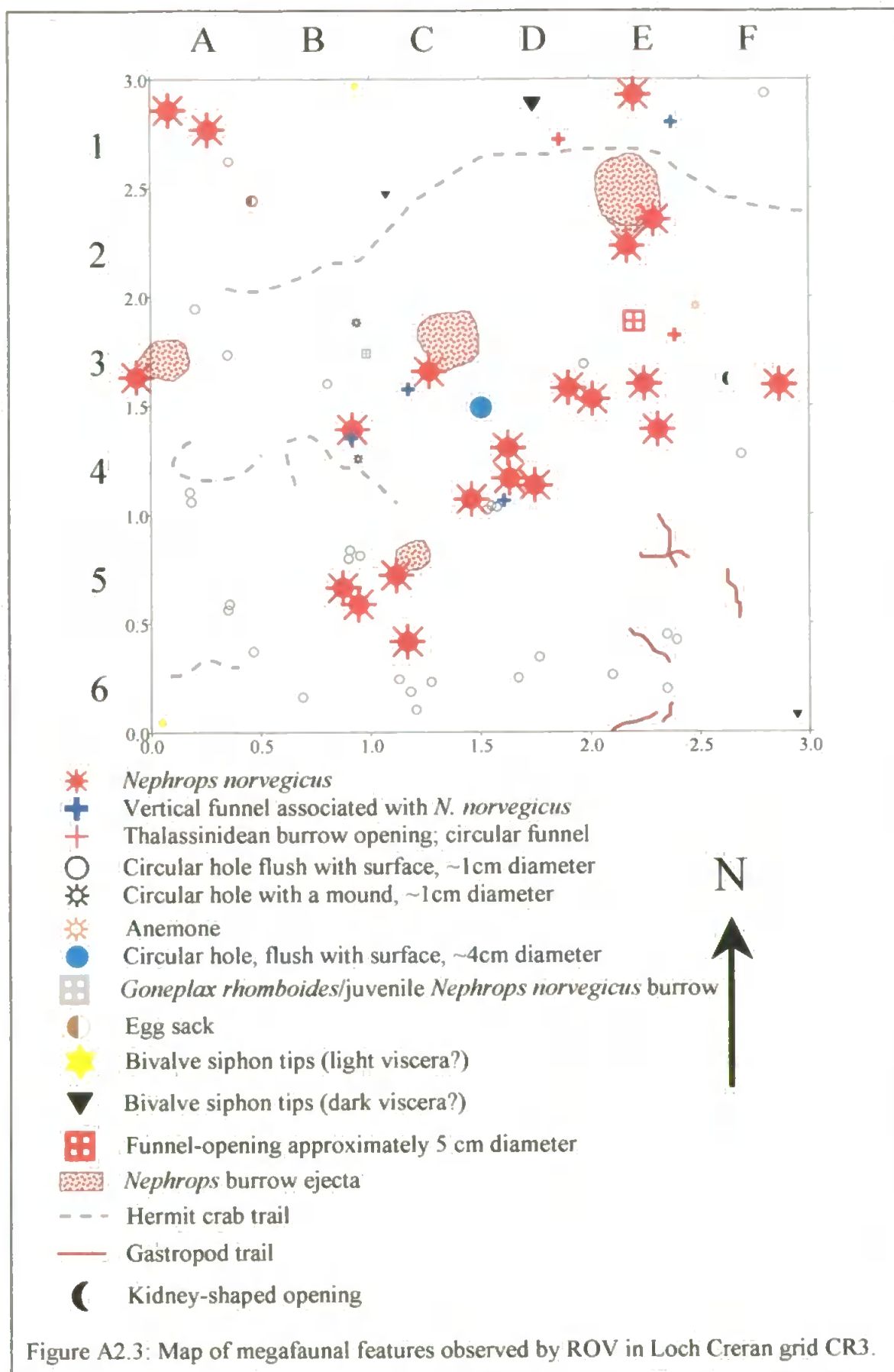


Table A2.4: Abundance of megafaunal features observed by direct diver and ROV observations in Loch Creran grid CR4.

Grid Location	Direct diver observations			ROV observations		
	Total Features	Conspicuous Features	Features greater than 15 mm diameter	Total Features	Conspicuous Features	Features greater than 15 mm diameter
CR4_A1	4	1	4	3	1	1
CR4_A2	3	0	2	2	0	0
CR4_A3	1	1	1	3	1	1
CR4_A4	0	0	0	1	0	1
CR4_A5	1	0	1	0	0	0
CR4_A6	1	0	1	1	0	0
CR4_B1	1	0	0	0	0	0
CR4_B2	5	0	3	2	0	1
CR4_B3	1	1	1	0	0	0
CR4_B4	1	1	1	5	3	1
CR4_B5	2	1	2	3	1	1
CR4_B6	4	0	4	4	0	1
CR4_C1	1	1	1	1	1	1
CR4_C2	0	0	0	1	0	1
CR4_C3	3	3	3	1	1	1
CR4_C4	2	0	2	0	0	0
CR4_C5	3	1	3	2	1	2
CR4_C6	1	0	1	1	0	0
CR4_D1	3	1	3	1	1	1
CR4_D2	3	2	3	2	2	2
CR4_D3	2	1	2	1	1	1
CR4_D4	3	0	2	4	2	2
CR4_D5	3	2	2	1	0	0
CR4_D6	1	0	1	1	1	1
CR4_E1	5	2	4	2	1	1
CR4_E2	3	3	3	4	3	3
CR4_E3	6	3	5	4	3	3
CR4_E4	2	2	2	2	2	2
CR4_E5	1	1	1	1	0	0
CR4_E6	5	0	4	0	0	0
CR4_F1	4	1	4	1	1	1
CR4_F2	0	0	0	1	0	0
CR4_F3	1	0	1	4	1	1
CR4_F4	0	0	0	0	0	0
CR4_F5	0	0	0	0	0	0
CR4_F6	5	2	5	4	3	4
Total	81	30	72	63	30	34

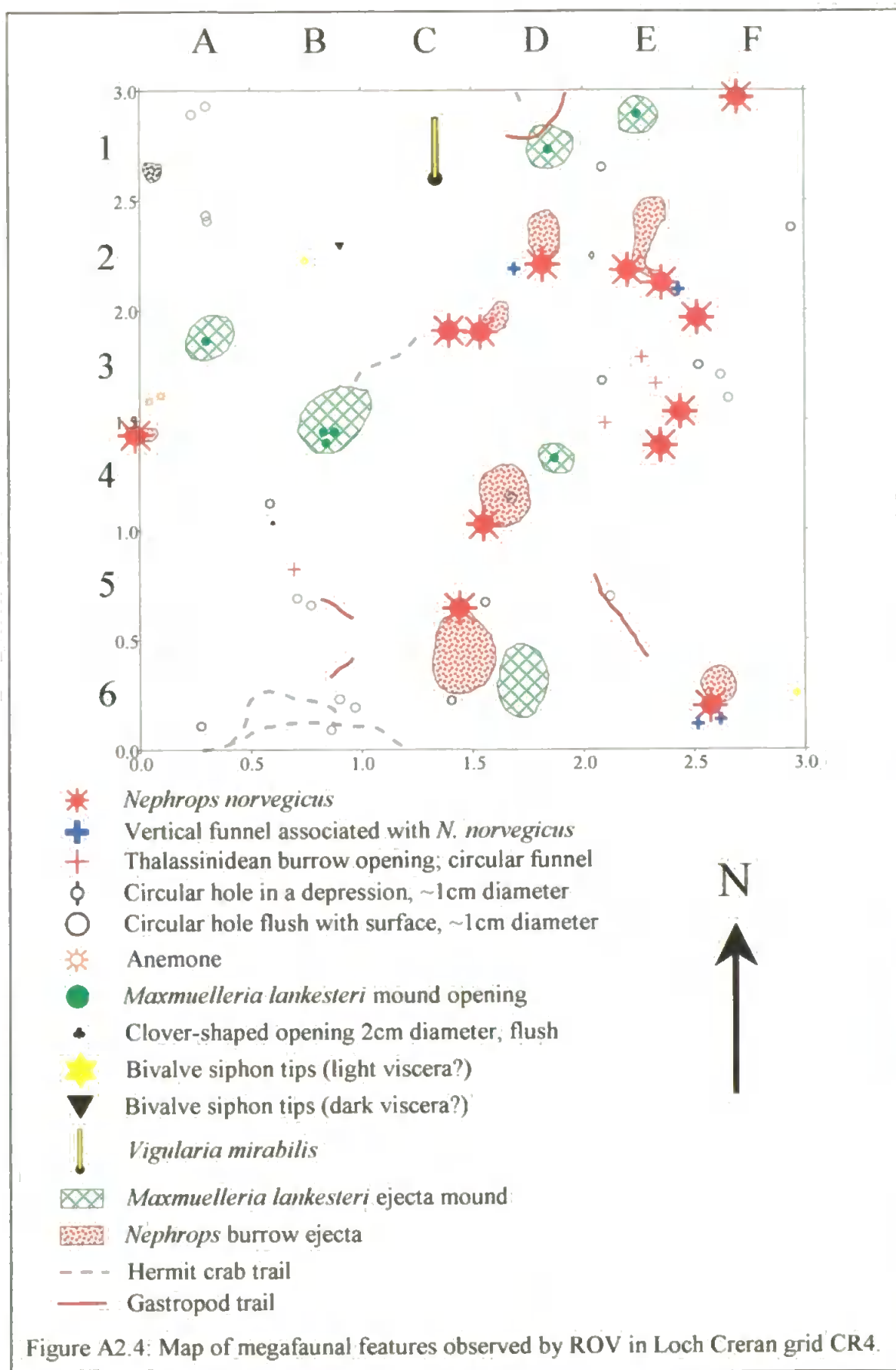


Table A2.5: Abundance of megafaunal features observed by direct diver and ROV observations in Jennycliff Bay grid.

Grid Location	Direct diver observations					ROV observations				
	Total Features	Thalassinidean Opening	Callianassa Mound	Bivalve	Thalassinidean opening plus bivalve	Total Features	Thalassinidean Opening	Callianassa Mound	Bivalve	Thalassinidean opening plus bivalve
JCI_A1	16	1	1	14	15	21	12	1	8	20
JCI_A2	17	3	1	13	16	15	2	0	13	15
JCI_A3	15	1	1	13	14	9	1	0	8	9
JCI_A4	10	1	0	8	9	14	1	0	13	14
JCI_A5	9	0	0	6	6	6	1	0	2	3
JCI_A6	24	3	1	20	23	23	3	0	20	23
JCI_B1	15	0	0	12	12	16	6	0	9	15
JCI_B2	18	0	0	18	18	10	0	0	10	10
JCI_B3	10	2	0	8	10	12	2	1	9	11
JCI_B4	15	2	1	12	14	18	4	0	14	18
JCI_B5	14	2	0	12	14	10	1	0	9	10
JCI_B6	21	5	0	14	19	22	4	0	16	20
JCI_C1	17	0	1	16	16	23	5	0	18	23
JCI_C2	12	4	0	7	11	13	7	0	6	13
JCI_C3	23	2	0	21	23	29	5	0	24	29
JCI_C4	15	0	0	15	15	13	0	0	13	13
JCI_C5	12	5	0	7	12	15	8	0	7	15
JCI_C6	21	1	0	19	20	20	4	0	15	19
JCI_D1	22	6	0	16	22	16	7	0	9	16
JCI_D2	12	3	1	8	11	15	4	0	11	15
JCI_D3	18	4	2	12	16	16	5	0	11	16
JCI_D4	18	3	0	15	18	22	9	1	12	21
JCI_D5	21	3	0	18	21	27	7	0	20	27
JCI_D6	23	11	0	12	23	22	13	0	9	22
JCI_E1	21	6	0	15	21	14	6	0	8	14
JCI_E2	18	2	0	15	17	20	7	0	11	18
JCI_E3	27	6	1	20	26	20	9	0	11	20
JCI_E4	19	4	1	14	18	18	7	0	11	18
JCI_E5	23	3	1	19	22	23	8	0	15	23
JCI_E6	21	1	2	16	17	19	2	0	17	19
JCI_F1	23	3	0	20	23	23	14	0	9	23
JCI_F2	27	2	0	23	25	29	8	1	19	27
JCI_F3	17	0	0	17	17	13	2	0	11	13
JCI_F4	14	3	0	9	12	13	3	0	9	12
JCI_F5	16	1	0	13	14	16	1	0	14	15
JCI_F6	11	1	0	10	11	6	2	0	4	6
Total	635	94	14	507	601	621	180	4	425	605

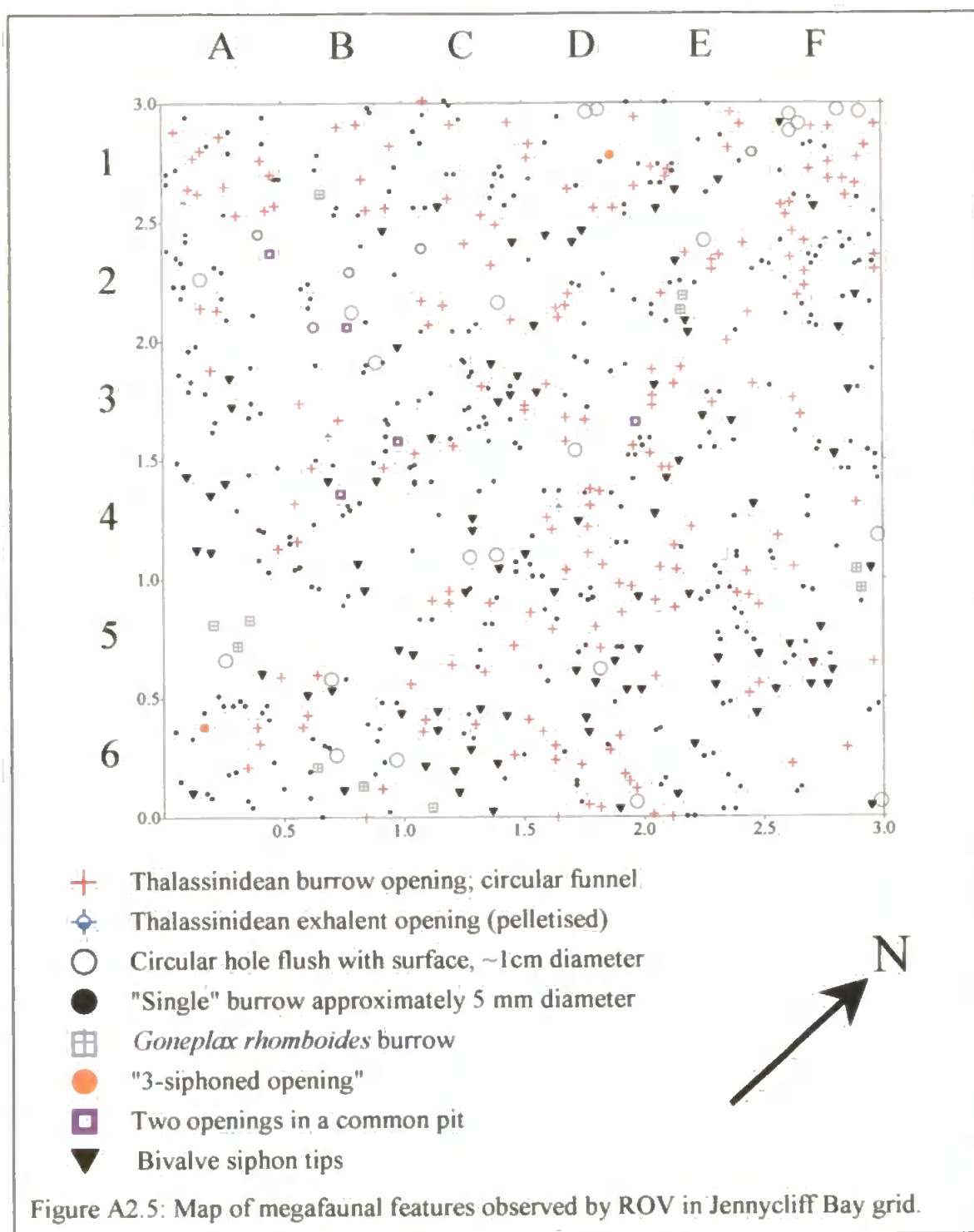


Table A2.6: Abundance of each megafaunal species and biogenic sediment feature associated with burrowing megafauna in 0.5 m<sup>2</sup> sample images at the Beacon station in May 2000.

Megafaunal species or biogenic sediment feature	2000_B01	2000_B02	2000_B03	2000_B04	2000_B05	2000_B06	2000_B07	2000_B08	2000_B09
Thalassinidean Opening	5	1	2	5	1	2	0	4	3
cf extinct thalassinidean opening	0	0	0	0	0	0	0	0	0
<i>Callianassa subterranea</i> pelletised mound	0	0	0	0	2	1	1	0	0
<i>C. subterranea</i> pelletised mound (flattened)	0	0	0	0	0	0	0	0	0
<i>C. subterranea</i> open mound	0	0	0	0	0	0	0	0	0
<i>Goneplax rhomboides</i> burrow	1	0	0	0	0	0	0	1	0
Unknown oblique opening	0	0	0	0	0	0	0	0	0
Hermit crab	0	0	0	0	0	0	0	0	0
<i>Macropodia</i> sp.	0	0	0	0	0	0	0	0	0
<i>Cancer pagurus</i>	0	0	0	0	0	0	0	0	0
pair of 1 cm diameter holes surrounded by ejected sediment	0	0	0	0	0	0	0	0	0
circular 1 cm flush opening	1	0	0	0	0	0	0	0	0
circular 1 cm in a depression	0	0	0	0	0	0	0	0	0
"3-siphoned opening"	0	0	1	0	0	0	0	0	0
two openings in a common depression	0	0	0	0	0	0	0	0	0
<i>Philine aperta</i>	0	0	0	0	0	0	0	0	0
<i>Acanthocardia</i> sp.	0	0	0	0	0	0	0	0	0
Unknown bivalve siphon 1	0	1	1	2	1	2	0	2	2
<i>Pecten maximus</i>	0	0	1	0	0	0	0	0	0
<i>Lutraria lutraria</i>	13	11	16	8	11	6	9	25	24
bivalve shell on surface	0	0	0	0	0	0	0	0	0
<i>Hinia reticulata</i>	2	0	0	0	0	0	0	0	0
<i>Turitella communis</i>	0	0	0	0	0	0	0	0	0
Burrowing Anemone	0	0	0	1	0	0	0	0	0
<i>Myxicola infundibulum</i>	0	0	0	0	0	0	0	0	0
ejected sediment patch	0	0	0	0	0	0	0	0	0
surface scrape/feeding pit	1	0	0	0	0	0	0	0	1
detritus obscured feature	1	0	0	0	0	0	0	0	0
Ophiuroid	0	1	0	0	0	0	0	0	0
white detritus patch	0	0	0	0	0	0	0	0	0
Number of species/features	7	4	5	4	4	4	2	4	4
Number of individuals	24	14	21	16	15	11	10	32	30

Table A2.7: Abundance of each megafaunal species and biogenic sediment feature associated with burrowing megafauna in 0.5 m<sup>2</sup> sample images at the Central station in May 2000.

Megafaunal species or biogenic sediment feature	2000_C 01	2000_C 02	2000_C 03	2000_C 04	2000_C 05	2000_C 06	2000_C 07	2000_C 08	2000_C 09	2000_C 10	2000_C 11	2000_C 12	2000_C 13	2000_C 14	2000_C 15	2000_C 16	2000_C 17	2000_C 18	2000_C 19	2000_C 20
Thalassinidean Opening	2	0	1	2	5	0	2	0	5	3	3	1	2	1	0	4	5	9	2	2
cf extinct thalassinidean opening	0	0	0	0	0	0	0	0	0	0	0	0	0	0	0	0	0	0	0	0
<i>Callianassa subterranea</i> pelletised mound	1	0	0	0	1	0	1	0	0	1	0	0	0	0	0	0	0	1	0	1
<i>C. subterranea</i> pelletised mound (flattened)	0	0	0	0	0	0	0	0	0	0	0	0	0	0	0	0	1	0	1	0
<i>C. subterranea</i> open mound	0	0	0	0	0	0	0	0	0	1	0	0	0	0	0	0	1	0	1	0
<i>Goneplax rhomboides</i> burrow	0	0	0	0	0	0	0	1	0	0	0	0	0	0	0	0	0	0	1	0
Unknown oblique opening	0	0	0	0	0	0	0	0	0	0	0	0	0	0	0	0	0	0	0	0
Hermit crab	0	1	0	1	0	0	0	0	0	0	0	0	0	0	0	0	0	0	0	0
<i>Macropodia</i> sp.	0	0	0	0	0	0	0	0	0	0	0	0	0	0	0	0	0	0	0	0
<i>Cancer pagurus</i>	0	0	0	0	0	0	0	0	0	0	0	0	0	0	0	0	1	0	0	0
pair of 1 cm diameter holes surrounded by ejected sediment	0	0	0	0	0	0	0	0	1	0	0	0	0	0	0	0	0	0	0	0
circular 1 cm flush opening	0	0	0	0	0	0	0	0	0	0	0	0	0	0	0	0	1	0	0	0
circular 1 cm in a depression	0	0	0	0	0	0	0	0	0	0	0	0	0	0	0	0	0	0	0	0
"3-siphoned opening"	1	0	0	0	0	0	0	0	0	0	0	0	0	0	0	0	0	0	0	0
two openings in a common depression	0	0	0	0	0	0	0	0	0	0	0	0	0	0	0	0	0	0	0	0
<i>Philine aperta</i>	0	0	0	0	0	0	0	0	0	0	0	0	0	0	0	0	0	0	0	0
<i>Acanthocardia</i> sp.	1	0	2	2	4	3	1	5	5	2	4	4	3	3	0	0	1	2	4	6
Unknown bivalve siphon 1	0	0	1	1	0	1	0	0	0	1	0	0	0	0	0	0	0	0	0	0
<i>Pecten maximus</i>	0	0	0	0	0	0	1	0	0	0	0	0	0	0	0	0	0	0	0	0
<i>Lutraria lutraria</i>	24	20	29	13	23	9	16	13	23	17	22	17	17	33	29	15	16	8	18	23
bivalve shell on surface	0	1	0	0	0	0	0	0	0	0	0	0	0	0	2	0	0	1	0	0
<i>Hinia reticulata</i>	0	0	0	0	0	0	0	0	0	0	0	0	0	0	0	0	0	0	0	0
<i>Turritella communis</i>	0	0	0	0	0	0	0	0	0	0	0	0	0	0	0	0	0	0	0	0
Burrowing Anemone	0	0	0	0	0	0	0	0	0	0	0	0	0	0	0	0	0	0	0	0
<i>Myxicola infundibulum</i>	0	0	0	0	0	0	0	0	0	0	0	0	0	0	0	0	0	0	0	2
ejected sediment patch	0	0	0	0	1	0	0	0	0	0	0	0	0	0	0	0	0	0	0	0
surface scrape/feeding pit	0	0	2	0	1	0	0	0	2	1	1	0	1	3	0	0	0	1	0	0
detritus obscured feature	0	0	0	0	0	0	0	0	0	0	0	0	0	1	0	0	0	0	0	0
Ophiuroid	0	0	2	0	0	0	0	0	0	0	1	0	0	0	1	0	0	0	0	0
white detritus patch	0	0	0	0	0	0	0	0	0	0	0	0	1	0	0	0	0	0	0	0
Number of species/features	5	3	6	5	6	3	5	3	5	7	5	3	5	5	3	2	7	6	6	5
Number of individuals	29	22	37	19	35	13	21	19	36	26	31	22	24	41	32	19	26	22	27	34

Table A2.7 continued..

Megafaunal species or biogenic sediment feature	2000_C21	2000_C22	2000_C23	2000_C24	2000_C25	2000_C26	2000_C27	2000_C28	2000_C29	2000_C30	2000_C31	2000_C32	2000_C33	2000_C34	2000_C35	2000_C36	2000_C37
Thalassinidean Opening	1	0	4	0	3	2	0	2	4	1	1	0	2	4	1	0	2
cf extinct thalassinidean opening	0	0	1	0	0	0	0	0	1	0	0	0	0	0	0	0	0
<i>Callianassa subterranea</i> pelletised mound	1	0	1	0	3	2	0	1	1	0	0	0	1	0	0	0	1
<i>C. subterranea</i> pelletised mound (flattened)	0	0	1	0	0	0	0	1	0	0	1	0	0	0	1	0	0
<i>C. subterranea</i> open mound	0	0	0	0	0	0	0	0	1	0	0	0	0	1	0	1	1
<i>Goneplax rhomboides</i> burrow	0	0	0	0	0	0	0	0	0	0	2	0	0	0	0	0	0
Unknown oblique opening	0	0	0	0	0	0	0	0	0	0	0	0	0	0	0	0	0
Hermit crab	0	0	0	0	0	0	0	0	0	0	0	0	0	0	0	0	1
<i>Macropodia</i> sp.	0	0	0	0	0	0	0	0	0	0	0	0	0	0	0	0	0
<i>Cancer pagurus</i> pair of 1 cm diameter holes surrounded by ejected sediment	0	0	0	0	0	0	0	0	0	0	0	0	0	0	0	0	0
circular 1 cm flush opening	0	0	0	0	0	0	0	0	0	0	0	0	0	0	0	0	0
circular 1 cm in a depression	0	0	0	0	0	0	0	0	0	0	0	0	0	0	0	0	0
"3-siphoned opening"	0	0	0	0	0	0	0	0	0	0	0	0	0	0	0	0	0
two openings in a common depression	0	0	0	0	0	0	0	0	0	0	0	0	0	0	0	0	0
<i>Philine aperta</i>	0	0	0	0	0	0	0	0	0	0	0	0	0	0	0	0	0
<i>Acanthocardia</i> sp.	5	3	3	1	3	0	2	1	1	4	2	1	2	1	4	2	6
Unknown bivalve siphon 1	1	2	1	0	0	1	0	0	0	0	0	1	0	0	1	0	0
<i>Pecten maximus</i>	0	0	0	0	0	0	0	0	0	0	0	0	0	0	0	0	0
<i>Lutraria lutraria</i>	27	10	16	21	11	23	11	17	29	21	18	9	16	17	17	14	18
bivalve shell on surface	1	0	1	0	0	0	0	0	0	0	0	0	0	0	0	1	1
<i>Hinia reticulata</i>	0	0	0	0	0	0	0	0	0	1	0	0	0	0	0	0	0
<i>Turritella communis</i>	0	0	0	0	0	0	0	0	0	0	0	0	0	0	0	0	0
Burrowing Anemone	0	0	0	0	0	0	0	0	0	0	0	0	0	0	0	0	0
<i>Myxicola infundibulum</i>	0	0	0	0	0	0	1	0	0	0	0	0	0	0	0	0	0
ejected sediment patch	0	0	0	0	0	0	0	0	0	0	0	0	0	0	0	0	0
surface scrape/feeding pit	0	1	0	0	0	1	2	0	1	0	2	0	0	1	2	0	1
detritus obscured feature	0	0	0	0	0	0	0	0	0	0	0	0	0	0	0	0	0
Ophiuroid	0	0	0	0	1	0	0	0	0	0	0	0	0	0	0	0	1
white detritus patch	0	0	0	0	0	0	0	0	0	0	0	0	0	0	0	0	0
Number of species/features	6	4	8	2	5	5	4	5	7	4	6	3	4	5	6	4	9
Number of individuals	36	16	28	22	21	29	16	22	38	27	26	11	21	24	26	18	32



Table A2.8: Abundance of each megafaunal species and biogenic sediment feature associated with burrowing megafauna in 0.5 m<sup>2</sup> sample images at the Fylrix station in May 2000.

Mega faunal species or biogenic sediment feature	2000_F01	2000_F02	2000_F03	2000_F04	2000_F05	2000_F06	2000_F07	2000_F08	2000_F09	2000_F10	2000_F11	2000_F12	2000_F13
Thalassinidean Opening	9	5	3	2	4	4	3	4	3	1	4	3	2
cf extinct thalassinidean opening	0	0	0	0	0	0	0	0	0	0	1	0	0
<i>Callinassa subterranea</i> pelletised mound	1	2	0	0	0	0	0	1	0	0	0	0	1
<i>C. subterranea</i> pelletised mound (flattened)	0	0	0	0	0	0	0	0	0	0	0	0	0
<i>C. subterranea</i> open mound	0	0	0	0	0	0	0	0	0	0	0	0	0
<i>Goneplax rhomboides</i> burrow	0	1	0	0	0	0	0	0	0	2	0	0	1
Unknown oblique opening	0	0	0	0	0	0	0	0	0	0	0	0	0
Hermit crab	0	1	0	0	0	0	0	0	0	0	1	0	0
<i>Macropodia</i> sp.	0	0	0	0	0	0	0	0	0	0	0	0	0
<i>Cancer pagurus</i>	0	0	0	0	0	0	0	0	0	0	0	0	0
pair of 1 cm diameter holes surrounded by ejected sediment	0	0	0	0	0	0	0	0	0	0	0	0	0
circular 1 cm flush opening	0	1	1	0	1	0	0	1	0	0	0	0	0
circular 1 cm in a depression	1	0	0	0	0	0	0	0	0	0	0	0	0
"3-siphoned opening"	0	0	0	0	1	1	1	1	0	0	0	0	0
two openings in a common depression	0	0	0	0	0	0	0	0	0	0	0	0	0
<i>Philine aperta</i>	0	0	0	0	0	0	0	1	0	0	0	0	0
<i>Acanthocardia</i> sp.	0	0	2	0	0	0	0	0	1	0	0	0	0
Unknown bivalve siphon 1	4	2	1	3	2	0	1	1	0	1	1	0	0
<i>Pecten maximus</i>	0	0	0	0	0	0	0	0	0	0	0	0	0
<i>Lutraria lutraria</i>	49	14	37	15	12	22	35	19	17	14	35	11	40
bivalve shell on surface	0	0	0	1	0	0	0	0	0	0	0	0	1
<i>Hinia reticulata</i>	0	1	0	0	0	0	0	0	1	0	0	0	0
<i>Turritella communis</i>	0	0	0	0	0	0	0	0	0	0	0	0	0
Burrowing Anemone	0	0	0	0	0	0	0	0	0	0	0	0	0
<i>Myxicola infundibulum</i>	0	0	0	0	0	0	0	0	0	0	0	0	0
ejected sediment patch	0	0	0	1	0	0	0	2	0	0	0	0	1
surface scrape/feeding pit	0	0	1	0	0	0	0	1	0	1	0	0	1
detritus obscured feature	1	0	2	0	0	1	0	0	0	0	0	0	0
Ophiuroid	0	0	1	0	0	0	0	0	0	0	0	0	0
white detritus patch	0	0	0	0	0	0	0	0	0	0	0	0	0
Number of species/features	6	8	8	5	5	4	4	9	4	5	5	2	7
Number of individuals	65	27	48	22	20	28	40	31	22	19	42	14	47

Table A2.9: Abundance of each megafaunal species and biogenic sediment feature associated with burrowing megafauna in 0.5 m<sup>2</sup> sample images at the Nearshore station in May 2000.

Megafaunal species or biogenic sediment feature	2000_N01	2000_N02	2000_N03	2000_N04	2000_N05	2000_N06	2000_N07	2000_N08	2000_N09	2000_N10	2000_N11	2000_N12	2000_N13	2000_N14
Thalassinidean Opening	4	1	0	4	4	4	0	0	0	2	4	2	3	2
cf extinct thalassinidean opening	0	0	0	0	0	0	0	0	0	0	0	0	0	0
<i>Callianassa subterranea</i> pelletised mound	0	0	1	0	0	0	1	0	0	0	0	1	0	1
<i>C. subterranea</i> pelletised mound (flattened)	0	0	0	0	0	0	0	0	0	0	0	0	0	0
<i>C. subterranea</i> open mound	0	0	0	1	0	1	0	0	1	0	0	0	0	0
<i>Goneplax rhomboides</i> burrow	0	1	0	0	0	0	0	0	0	0	0	0	0	0
Unknown oblique opening	0	0	0	0	0	0	0	0	0	0	0	0	0	0
Hermit crab	0	0	0	0	0	0	0	0	0	0	0	0	1	0
<i>Macropodia</i> sp.	0	0	0	0	0	0	0	0	0	0	0	0	0	0
<i>Cancer pagurus</i>	0	0	0	0	0	0	0	0	0	0	0	0	0	0
pair of 1 cm diameter holes surrounded by ejected sediment	0	0	0	0	0	0	0	0	0	0	0	0	0	0
circular 1 cm flush opening	0	0	1	0	0	0	0	0	0	0	0	0	0	0
circular 1 cm in a depression	0	0	0	0	0	0	0	0	0	0	0	0	0	0
"3-siphoned opening"	2	1	0	0	0	0	0	1	0	0	0	0	0	0
two openings in a common depression	0	1	0	0	0	0	0	0	0	0	0	0	0	0
<i>Philine aperta</i>	0	0	0	0	0	0	0	0	0	0	0	0	0	0
<i>Acanthocardia</i> sp.	0	0	1	0	0	1	0	0	0	0	0	0	0	1
Unknown bivalve siphon 1	0	0	0	0	0	4	0	0	1	0	0	0	0	0
<i>Pecten maximus</i>	0	0	0	0	0	0	0	0	0	0	0	0	0	0
<i>Lutraria lutraria</i>	12	13	13	12	11	13	12	6	15	17	16	21	15	12
bivalve shell on surface	0	0	0	2	0	0	0	0	0	0	0	0	0	0
<i>Hinia reticulata</i>	0	1	1	0	0	0	1	0	0	0	1	0	0	1
<i>Turritella communis</i>	0	0	0	0	0	0	0	0	0	0	0	0	0	0
Burrowing Anemone	0	0	0	0	0	0	0	0	0	0	0	0	0	0
<i>Myxicola infundibulum</i>	0	0	0	0	0	0	0	0	0	0	0	0	0	1
ejected sediment patch	0	0	0	0	0	0	0	0	0	0	0	0	0	1
surface scrape/feeding pit	0	0	0	0	0	0	0	0	0	0	2	0	2	0
detritus obscured feature	0	0	0	1	0	0	0	0	0	0	0	0	1	1
Ophiuroid	0	0	0	0	0	0	0	0	0	0	0	0	0	0
white detritus patch	0	0	0	0	0	0	0	0	0	0	0	0	0	0
Number of species/features	3	6	5	5	2	5	3	2	3	2	4	3	5	7
Number of individuals	18	18	17	20	15	23	14	7	17	19	23	24	22	19

Table A2.10: Abundance of each megafaunal species and biogenic sediment feature associated with burrowing megafauna in 0.5 m<sup>2</sup> sample images at the Beacon station in March 2001.

Megafaunal species or biogenic sediment feature	2001_B_01	2001_B_02	2001_B_03	2001_B_04	2001_B_05	2001_B_06	2001_B_07	2001_B_08	2001_B_09	2001_B_10	2001_B_11
Thalassinidean Opening	0	1	0	1	1	0	3	1	0	0	1
cf extinct thalassinidean opening	0	0	0	0	0	0	0	0	0	0	0
<i>Callianassa subterranea</i> pelletised mound	0	0	1	1	2	0	0	0	0	0	1
<i>C. subterranea</i> pelletised mound (flattened)	0	0	0	0	0	1	0	1	1	1	0
<i>C. subterranea</i> open mound	0	0	0	0	0	0	1	0	0	0	0
<i>Goneplax rhomboides</i> burrow	1	0	0	0	0	0	0	0	0	0	0
Unknown oblique opening	0	0	0	0	0	0	0	0	0	0	0
Hermit crab	0	0	0	0	0	0	0	0	0	0	0
<i>Macropodia</i> sp.	0	0	0	0	0	0	0	0	0	0	0
<i>Cancer pagurus</i>	0	0	0	0	0	0	0	0	0	0	0
pair of 1cm diameter holes surrounded by ejected sediment	0	0	0	0	0	0	0	0	0	0	0
circular 1cm flush opening	0	0	0	0	0	0	0	0	0	0	0
circular 1cm in a depression	0	0	0	0	0	0	0	0	0	0	0
"3-siphoned opening"	0	0	0	0	0	0	0	0	0	0	0
two openings in a common depression	0	0	0	0	0	0	0	0	0	0	0
<i>Philine aperta</i>	0	0	0	0	0	0	0	0	0	0	0
<i>Acanthocardia</i> sp.	0	0	0	0	3	0	1	0	0	1	0
Unknown bivalve siphon 1	0	0	0	0	0	0	0	0	0	0	1
<i>Pecten maximus</i>	0	0	0	0	0	0	0	0	0	1	0
<i>Lutraria lutraria</i>	9	12	16	10	19	4	2	13	5	12	2
bivalve shell on surface	0	0	0	0	0	0	0	0	0	0	0
<i>Hinia reticulata</i>	0	0	1	0	0	0	0	0	0	0	1
<i>Turritella communis</i>	0	2	1	2	2	9	2	5	1	0	0
Burrowing Anemone	0	0	0	0	0	2	0	0	0	0	0
<i>Myxicola infundibulum</i>	0	0	0	0	0	0	0	0	0	0	0
ejected sediment patch	0	0	0	0	0	1	0	0	0	0	0
surface scrape/feeding pit	2	0	0	0	0	0	0	0	0	0	0
detritus obscured feature	1	0	0	0	0	0	0	0	0	0	0
Ophiuroid	0	0	3	0	0	0	2	2	2	0	0
white detritus patch	0	0	0	0	0	0	0	0	0	0	0
Number of species/features	4	3	5	4	5	5	6	5	4	4	5
Number of individuals	13	15	22	14	27	17	11	22	9	15	6

Table A2.11: Abundance of each megafaunal species and biogenic sediment feature associated with burrowing megafauna in 0.5 m<sup>2</sup> sample images at the Central station in March 2001.

Mega faunal species or biogenic sediment feature	2001_ C 01	2001_ C 02	2001_ C 03	2001_ C 04	2001_ C 05	2001_ C 06	2001_ C 07	2001_ C 08	2001_ C 09	2001_ C 10	2001_ C 11	2001_ C 12	2001_ C 13	2001_ C 14	2001_ C 15	2001_ C 16	2001_ C 17	2001_ C 18	2001_ C 19	2001_ C 20	2001_ C 21	2001_ C 22	2001_ C 23	2001_ C 24	2001_ C 25	2001_ C 26
Thalassinidean Opening	5	5	2	5	3	3	2	6	8	4	5	0	6	6	2	2	2	1	1	2	1	4	2	4	3	4
cf extinct thalassinidean opening	0	0	0	0	0	0	0	0	0	0	0	0	0	0	0	0	0	0	0	0	0	0	0	0	0	0
<i>Callinassa subterranea</i> pelletised mound	1	2	1	1	0	1	1	2	2	1	0	0	0	2	0	0	2	0	1	0	0	0	2	1	2	2
<i>C. subterranea</i> pelletised mound (flattened)	0	0	0	0	0	0	0	0	0	0	1	0	1	0	0	1	1	1	1	0	0	0	0	0	0	0
<i>C. subterranea</i> open mound	0	0	0	1	0	0	0	0	0	0	0	0	0	1	0	0	0	0	0	0	0	1	0	1	0	0
<i>Goneplax rhomboides</i> burrow	0	0	0	0	0	0	4	1	0	0	0	2	0	0	0	0	0	1	0	0	0	0	0	0	0	0
Unknown oblique opening	0	0	0	0	0	0	0	0	0	0	0	0	0	0	0	0	0	0	0	0	0	0	0	0	0	0
Hermit crab	0	0	0	0	0	0	0	0	0	0	0	0	0	0	1	0	0	0	0	0	0	0	0	0	0	0
<i>Macropodia</i> sp.	0	0	0	0	0	0	0	0	0	0	0	0	0	0	0	0	0	0	0	0	0	0	0	0	0	0
<i>Cancer pagurus</i>	0	0	0	0	0	0	0	0	0	0	0	0	0	0	0	0	0	0	0	0	0	0	0	1	0	0
pair of 1cm diameter holes surrounded by ejected sediment	0	0	0	0	0	0	0	0	0	0	0	0	0	0	0	0	0	0	0	0	0	0	0	0	0	0
circular 1cm flush opening	0	0	0	0	0	0	0	0	0	0	0	0	0	0	0	0	0	0	0	0	0	0	0	0	0	0
circular 1cm in a depression	0	0	0	0	0	0	0	0	0	0	0	0	0	0	0	0	0	0	0	0	0	0	0	0	0	0
"3-siphoned opening"	0	0	0	0	0	0	0	0	0	0	1	0	0	0	0	0	0	0	0	0	0	0	0	0	0	1
two openings in a common depression	0	0	0	1	0	0	0	0	0	0	0	0	0	0	0	0	0	0	0	0	0	0	0	0	0	0
<i>Philine aperta</i>	0	0	0	0	0	0	0	0	0	0	0	0	0	0	0	0	0	0	0	0	0	0	0	0	0	0
<i>Acanthocardia</i> sp.	0	0	1	1	1	0	0	0	0	0	0	0	1	0	1	1	0	2	0	1	3	1	0	1	0	0
Unknown bivalve siphon 1	0	0	0	0	0	0	0	0	1	0	0	0	0	0	1	0	0	0	1	0	0	0	0	0	0	0
<i>Pecten maximus</i>	0	0	0	0	0	0	0	0	0	0	0	0	0	0	0	0	0	0	0	0	0	0	0	0	0	0
<i>Lutraria lutraria</i>	3	7	9	7	13	13	3	7	11	11	17	10	6	10	9	7	17	14	9	13	7	7	10	11	3	4
bivalve shell on surface	0	0	2	0	0	0	0	0	1	0	0	0	0	0	0	0	0	0	0	0	0	0	0	0	0	0
<i>Hinia reticulata</i>	0	0	0	0	0	0	0	0	0	0	0	0	1	0	0	0	0	0	0	0	0	0	0	0	1	0
<i>Turitella communis</i>	2	3	0	1	0	0	0	0	0	0	2	0	0	3	0	3	2	1	0	1	0	0	0	0	1	2
Burrowing Anemone	0	0	0	0	0	0	0	0	0	0	0	0	0	0	1	0	0	1	0	0	0	0	0	0	0	0
<i>Myxicola infundibulum</i>	0	0	0	0	0	0	0	0	0	0	0	0	0	0	0	0	0	0	0	0	0	0	0	0	0	0
ejected sediment patch	0	0	0	0	0	0	0	0	0	0	0	0	0	0	0	0	0	0	0	0	0	0	0	0	0	0
surface scrape/feeding pit	1	0	0	0	1	0	1	0	0	0	0	0	0	0	0	0	0	1	1	0	0	1	0	0	0	0
detritus obscured feature	0	0	0	0	0	0	0	0	0	0	1	0	0	0	0	0	0	0	0	0	0	1	0	1	0	0
Ophiuroid	0	0	2	0	1	0	0	0	0	0	0	0	0	0	0	2	0	0	1	0	0	0	0	0	0	0
white detritus patch	0	0	0	0	0	0	0	0	0	0	0	0	0	0	0	0	0	0	0	0	0	0	0	0	0	0
Number of species/features	5	4	6	7	5	3	5	4	5	3	6	2	4	6	6	6	5	8	7	4	3	6	3	7	5	5
Number of individuals	12	17	17	17	19	17	11	16	23	16	27	12	14	23	15	16	24	22	15	17	11	15	14	20	10	13

Table A2.12: Abundance of each megafaunal species and biogenic sediment feature associated with burrowing megafauna in 0.5 m<sup>2</sup> sample images at the Fylrix station in March 2001.

Mega faunal species or biogenic sediment feature	2001_ F 01	2001_ F 02	2001_ F 03	2001_ F 04	2001_ F 05	2001_ F 06	2001_ F 07	2001_ F 08	2001_ F 09	2001_ F 10	2001_ F 11	2001_ F 12	2001_ F 13	2001_ F 14	2001_ F 15	2001_ F 16
Thalassinidean Opening	1	2	0	2	0	0	2	2	5	2	2	4	3	1	4	1
cf extinct thalassinidean opening	0	0	0	0	0	0	0	0	0	0	0	0	0	0	0	0
<i>Callianassa subterranea</i> pelletised mound	0	1	0	0	0	1	2	0	2	2	0	2	1	0	2	0
<i>C. subterranea</i> pelletised mound (flattened)	0	0	0	0	0	0	0	0	0	0	0	0	0	0	0	0
<i>C. subterranea</i> open mound	0	0	0	1	0	0	0	0	1	0	1	1	0	0	0	0
<i>Goneplax rhomboides</i> burrow	0	0	1	0	0	0	0	0	0	0	0	0	0	0	0	0
Unknown oblique opening	0	0	0	0	0	0	0	0	0	0	0	0	0	0	0	0
Hermit crab	0	0	0	0	0	0	0	0	0	0	0	0	0	0	0	1
<i>Macropodia</i> sp.	0	0	0	1	0	0	0	0	0	0	0	0	0	0	0	0
<i>Cancer pagurus</i>	0	0	0	0	0	0	0	0	0	0	0	0	0	0	0	0
pair of 1cm diameter holes surrounded by ejected sediment	0	0	0	0	0	0	0	0	0	0	0	0	0	0	0	0
circular 1cm flush opening	0	0	0	0	0	0	0	0	0	0	0	0	0	0	0	0
circular 1cm in a depression	0	0	0	0	0	0	0	0	0	0	0	0	0	0	0	0
"3-siphoned opening"	0	0	0	0	0	0	0	0	0	0	0	0	0	0	0	0
two openings in a common depression	0	0	0	0	0	0	0	0	0	0	0	0	0	0	0	0
<i>Philine aperta</i>	0	0	0	0	0	0	0	0	0	0	0	0	0	0	0	0
<i>Acanthocardia</i> sp.	0	0	0	0	0	0	0	0	0	1	0	0	0	2	0	0
Unknown bivalve siphon 1	0	0	0	0	0	0	0	0	0	0	0	0	0	0	0	0
<i>Pecten maximus</i>	0	0	0	0	0	0	0	0	0	0	0	0	0	0	0	0
<i>Lutraria lutraria</i>	19	7	12	10	10	6	7	10	8	2	13	12	5	5	5	2
bivalve shell on surface	0	0	0	0	2	0	0	0	0	0	0	0	0	0	0	1
<i>Hinia reticulata</i>	0	0	0	0	1	1	0	0	0	0	1	0	0	0	0	0
<i>Turritella communis</i>	0	0	0	0	0	0	0	0	1	1	1	0	0	1	0	3
Burrowing Anemone	0	0	0	1	0	0	0	0	0	0	0	0	0	0	0	0
<i>Myxicola infundibulum</i>	0	0	0	0	0	0	0	0	0	0	0	0	0	0	0	0
ejected sediment patch	0	0	0	0	0	1	0	0	0	0	0	0	0	0	0	0
surface scrape/feeding pit	0	1	1	2	0	3	0	1	0	0	0	0	0	1	0	0
detritus obscured feature	1	0	0	0	0	0	0	0	1	0	1	0	1	0	1	0
Ophiuroid	0	0	0	0	0	0	0	0	0	0	0	0	1	1	1	0
white detritus patch	0	0	0	0	0	0	0	0	0	0	0	0	0	0	0	0
Number of species/features	3	4	3	6	3	5	3	3	6	5	6	4	5	6	5	5
Number of individuals	21	11	14	17	13	12	11	13	18	8	19	19	11	11	13	8

Table A2.13: Abundance of each megafaunal species and biogenic sediment feature associated with burrowing megafauna in 0.5 m<sup>2</sup> sample images at the Nearshore station in March 2001.

Mega faunal species or biogenic sediment feature	2001_ N 01	2001_ N 02	2001_ N 03	2001_ N 04	2001_ N 05	2001_ N 06	2001_ N 07	2001_ N 08	2001_ N 09	2001_ N 10	2001_ N 11	2001_ N 12	2001_ N 13	2001_ N 14	2001_ N 15	2001_ N 16	2001_ N 17	2001_ N 18	2001_ N 19
Thalassinidean Opening	1	4	1	1	1	5	1	0	0	1	1	2	0	4	2	3	2	2	0
cf extinct thalassinidean opening	0	1	0	0	0	0	0	0	0	0	0	0	0	0	0	0	1	0	0
<i>Callinassa subterranea</i> pelletised mound	0	0	0	0	1	0	0	0	0	1	0	1	1	0	0	1	1	1	0
<i>C. subterranea</i> pelletised mound (flattened)	0	1	0	0	0	1	0	1	0	1	0	0	0	0	1	0	1	0	0
<i>C. subterranea</i> open mound	0	0	0	0	0	0	0	0	0	0	0	0	0	0	0	0	0	0	0
<i>Goneplax rhomboides</i> burrow	1	0	0	2	0	0	0	0	0	0	0	0	0	0	0	0	0	0	1
Unknown oblique opening	0	0	0	0	0	1	3	1	0	0	1	0	0	0	0	0	0	0	0
Hermit crab	0	0	0	0	0	0	0	0	0	0	0	0	0	0	0	0	0	0	0
<i>Macropodia</i> sp.	0	0	1	0	0	0	0	0	0	0	0	0	0	0	0	0	0	0	0
<i>Cancer pagurus</i>	0	0	0	0	0	0	0	0	0	0	0	0	0	0	0	0	0	0	0
pair of 1cm diameter holes surrounded by ejected sediment	0	0	0	0	0	0	0	0	0	0	0	0	0	0	0	0	0	0	0
circular 1cm flush opening	0	0	0	0	0	0	0	0	0	0	0	0	0	0	0	0	0	0	0
circular 1cm in a depression	0	0	0	0	0	0	0	0	0	0	0	0	0	0	0	0	0	0	0
"3-siphoned opening"	0	0	0	0	0	0	0	0	0	0	0	0	0	0	0	0	0	0	0
two openings in a common depression	0	0	0	0	0	0	0	0	0	0	0	0	0	0	0	0	0	0	0
<i>Philine aperta</i>	0	0	0	0	0	0	0	0	0	0	0	0	0	0	0	0	0	0	0
<i>Acanthocardia</i> sp.	0	3	5	4	2	4	0	3	0	1	6	3	3	2	2	5	3	4	3
Unknown bivalve siphon 1	0	1	0	0	1	1	0	0	0	0	0	0	0	1	0	0	0	2	0
<i>Pecten maximus</i>	0	0	0	0	0	0	0	0	0	0	0	0	0	0	0	0	0	0	0
<i>Lutraria lutraria</i>	6	14	9	1	7	8	6	5	3	7	5	3	2	4	5	7	1	2	6
bivalve shell on surface	0	0	0	0	0	0	1	0	0	0	0	0	0	0	0	0	0	0	1
<i>Hinia reticulata</i>	0	0	0	0	0	0	0	0	0	0	0	0	0	0	0	4	0	0	0
<i>Turritella communis</i>	3	4	1	1	0	3	1	0	2	0	2	2	3	1	6	3	0	0	0
Burrowing Anemone	0	0	0	0	0	0	0	1	0	0	0	0	0	0	0	0	0	0	0
<i>Myxicola infundibulum</i>	0	0	0	0	1	0	0	1	0	0	1	0	0	0	0	0	0	0	0
ejected sediment patch	0	0	0	0	0	0	0	0	0	0	1	0	0	1	0	0	0	0	0
surface scrape/feeding pit	1	0	0	0	0	0	0	0	0	0	0	0	0	0	0	0	0	0	1
detritus obscured feature	0	0	0	0	0	0	0	0	1	0	0	0	0	1	0	0	0	0	1
Ophiuroid	0	0	0	0	0	0	0	0	0	0	0	0	0	0	0	0	0	0	0
white detritus patch	0	0	0	0	0	0	0	0	0	0	0	0	0	0	0	0	0	0	0
Number of species/features	5	7	5	5	6	7	5	6	3	5	7	5	4	7	5	6	6	5	6
Number of individuals	12	28	17	9	13	23	12	12	6	11	17	11	9	14	16	23	9	11	13

## **APPENDIX III**

### **Image scale information**

Table A3.1: Location of sample images in Jenncyliff Bay, May 2000, and camera orientation information derived from *PharosLite* (Sonardyne International Ltd.) and *Benthic Imager*.

Station	Average Easting (UTM)	Average Northing (UTM)	Average Inclination Angle (°)	Average Camera Height (cm)	Average Camera Distance (cm)	Average Range (cm)	Average Pixel Footprint (mm)
2000_B01	419565.4	5578007.7	59	35	22	42	0.7
2000_B02	419580.0	5578003.2	54	44	32	54	1.0
2000_B03	419589.2	5578005.6	57	40	26	48	0.9
2000_B04	419599.2	5578000.4	55	30	21	37	0.7
2000_B05	419614.2	5578002.2	52	41	32	52	1.0
2000_B06	419614.4	5577998.4	54	44	31	54	1.0
2000_B07	419622.5	5577986.2	50	33	35	55	1.1
2000_B08	419609.7	5577977.3	55	40	28	49	0.9
2000_B09	419590.5	5577968.8	50	33	29	44	0.9
2000_C01	419711.5	5578061.6	50	54	45	71	1.4
2000_C02	419738.2	5578037.2	48	62	56	84	1.6
2000_C03	419749.6	5578052.6	53	48	37	61	1.2
2000_C04	419754.7	5578072.8	50	45	38	59	1.2
2000_C05	419757.6	5578082.1	46	45	44	64	1.3
2000_C06	419751.8	5578092.9	46	57	56	80	1.6
2000_C07	419751.4	5578101.1	54	57	41	70	1.3
2000_C08	419755.1	5578114.9	48	63	56	85	1.6
2000_C09	419758.5	5578125.3	52	52	41	67	1.3
2000_C10	419766.1	5578132.2	58	54	33	64	1.2
2000_C11	419782.1	5578136.6	55	50	34	61	1.1
2000_C12	419792.1	5578145.4	53	57	43	72	1.3
2000_C13	419799.1	5578133.7	61	46	25	53	1.0
2000_C14	419799.1	5578124.0	53	45	34	56	1.0
2000_C15	419798.2	5578107.6	46	52	50	72	1.4
2000_C16	419788.9	5578101.4	62	58	31	66	1.2
2000_C17	419781.5	5578101.2	58	44	28	53	1.0
2000_C18	419773.5	5578102.0	69	51	20	55	1.0
2000_C19	419766.5	5578101.8	61	60	33	69	1.2
2000_C20	419730.4	5578098.5	58	59	37	70	1.2
2000_C21	419722.0	5578105.3	56	55	37	67	1.2
2000_C22	419704.1	5578070.0	48	68	62	92	1.7
2000_C23	419716.6	5578067.5	55	59	41	72	1.3
2000_C24	419730.0	5578072.5	58	61	37	71	1.3
2000_C25	419746.0	5578070.0	54	52	38	65	1.2
2000_C26	419764.4	5578072.6	52	50	40	65	1.2
2000_C27	419771.7	5578079.0	55	56	40	69	1.3
2000_C28	419797.6	5578095.7	57	62	40	74	1.3
2000_C29	419796.4	5578152.7	63	53	27	60	1.1
2000_C30	419780.0	5578149.1	52	58	44	73	1.3
2000_C31	419768.1	5578143.6	56	51	35	62	1.2
2000_C32	419754.7	5578134.3	55	63	44	77	1.4
2000_C33	419746.1	5578131.5	62	58	30	66	1.2
2000_C34	419736.9	5578127.4	59	52	31	61	1.1
2000_C35	419726.7	5578127.0	53	45	35	57	1.1
2000_C36	419717.8	5578129.1	58	60	37	71	1.3
2000_C37	419705.8	5578129.1	58	46	29	54	1.0
2000_F01	419755.2	5578274.0	58	36	23	45	0.8
2000_F02	419749.7	5578277.0	58	35	21	41	0.8
2000_F03	419746.8	5578277.5	56	39	27	47	0.9
2000_F04	419735.6	5578275.0	56	64	43	77	1.4
2000_F05	419730.9	5578275.1	50	65	54	85	1.6
2000_F06	419711.2	5578273.6	55	54	38	66	1.2
2000_F07	419706.0	5578284.6	66	57	25	63	1.1
2000_F08	419716.5	5578297.5	59	49	28	56	1.0
2000_F09	419732.8	5578299.5	59	66	40	77	1.4
2000_F10	419751.2	5578297.7	70	66	23	72	1.2
2000_F11	419745.0	5578313.9	59	55	32	64	1.1
2000_F12	419729.1	5578314.5	56	43	31	54	1.0
2000_F13	419711.6	5578311.7	53	45	33	56	1.1
2000_N01	419813.0	5578098.9	49	43	37	57	1.1
2000_N02	419808.0	5578099.1	57	31	22	39	0.8
2000_N03	419876.5	5578097.1	50	45	39	60	1.2
2000_N04	419852.2	5578097.1	58	44	27	52	0.9
2000_N05	419832.0	5578095.5	45	39	39	56	1.2
2000_N06	419811.1	5578099.2	59	34	20	40	0.8
2000_N07	419888.1	5578117.2	60	47	28	55	1.0
2000_N08	419865.6	5578119.2	58	50	29	58	1.1
2000_N09	419844.2	5578121.2	58	33	20	39	0.8
2000_N10	419821.6	5578122.0	51	34	28	44	0.9
2000_N11	419802.3	5578119.9	51	36	30	48	0.9
2000_N12	419869.5	5578076.4	63	63	33	72	1.2
2000_N13	419847.2	5578071.2	60	32	20	39	0.7
2000_N14	419829.5	5578077.4	61	34	21	41	0.8
Average			56	49	34	61	1.1
Standard Deviation			5	10	9	13	0.2
95% confidence			1	2	2	3	0.1



Table A3.2: Location of sample images in Jenncyliff Bay, March 2001, and camera orientation information derived from *PharosLite* (Sonardyne International Ltd.) and *Benthic Imager*.

Station	Average Easting (UTM)	Average Northing (UTM)	Average Inclination Angle (°)	Average Camera Height (cm)	Average Camera Distance (cm)	Average Range (cm)	Average Pixel Footprint (mm)
2001_B_01	419642.2	5578006.7	66	42	18	46	1.2
2001_B_02	419627.4	5578009.7	65	42	20	47	1.2
2001_B_03	419623.8	5578011.2	67	39	17	42	1.1
2001_B_04	419615.1	5578015.3	67	40	17	43	1.1
2001_B_05	419608.2	5578017.0	62	40	22	46	1.2
2001_B_06	419598.5	5578020.5	66	41	18	45	1.1
2001_B_07	419591.4	5578023.6	67	42	18	47	1.2
2001_B_08	419575.7	5578027.7	63	40	20	45	1.2
2001_B_09	419585.5	5578036.9	61	42	24	48	1.3
2001_B_10	419602.6	5578034.3	65	46	22	51	1.4
2001_B_11	419614.4	5578029.3	66	41	19	45	1.1
2001_C_01	419700.5	5578111.6	72	39	13	42	1.0
2001_C_02	419705.3	5578113.3	59	45	23	50	1.4
2001_C_03	419714.6	5578116.6	65	47	19	51	1.4
2001_C_04	419722.9	5578119.8	67	41	18	45	1.1
2001_C_05	419735.9	5578124.1	72	46	15	48	1.3
2001_C_06	419745.2	5578127.5	61	43	24	49	1.3
2001_C_07	419755.2	5578130.8	63	42	22	47	1.3
2001_C_08	419763.1	5578131.7	66	42	18	46	1.2
2001_C_09	419772.7	5578134.2	64	41	20	46	1.2
2001_C_10	419782.6	5578135.5	63	38	20	43	1.1
2001_C_11	419791.2	5578136.3	62	43	23	49	1.3
2001_C_12	419780.9	5578122.8	60	45	26	52	1.4
2001_C_13	419748.6	5578115.2	66	43	19	47	1.2
2001_C_14	419717.9	5578109.1	69	42	16	45	1.2
2001_C_15	419705.4	5578109.8	69	42	16	45	1.1
2001_C_16	419695.6	5578104.9	71	45	16	48	1.3
2001_C_17	419698.9	5578088.1	70	46	17	50	1.3
2001_C_18	419707.3	5578090.9	67	45	19	49	1.3
2001_C_19	419718.1	5578092.6	66	42	19	46	1.2
2001_C_20	419727.7	5578095.6	66	43	20	47	1.3
2001_C_21	419738.3	5578095.0	59	46	28	55	1.6
2001_C_22	419691.9	5578090.4	67	41	17	45	1.2
2001_C_23	419761.2	5578090.7	71	49	17	52	1.5
2001_C_24	419771.2	5578089.7	66	43	19	47	1.2
2001_C_25	419780.9	5578089.9	64	42	21	47	1.3
2001_C_26	419793.7	5578088.4	63	42	21	48	1.3
2001_F_01	419687.2	5578325.7	58	38	24	45	1.2
2001_F_02	419698.3	5578328.5	56	39	26	46	1.3
2001_F_03	419708.9	5578329.3	59	40	24	47	1.2
2001_F_04	419718.3	5578329.2	61	40	22	46	1.2
2001_F_05	419727.8	5578329.7	61	43	24	50	1.4
2001_F_06	419739.4	5578328.4	64	42	20	47	1.2
2001_F_07	419748.0	5578314.5	60	43	25	50	1.4
2001_F_08	419737.4	5578293.3	61	41	23	47	1.2
2001_F_09	419725.1	5578297.8	59	39	24	46	1.3
2001_F_10	419709.6	5578300.2	60	41	24	47	1.3
2001_F_11	419701.3	5578299.9	61	42	23	47	1.3
2001_F_12	419691.1	5578279.7	56	42	28	51	1.4
2001_F_13	419700.9	5578276.6	61	41	22	47	1.2
2001_F_14	419710.7	5578276.4	60	40	23	46	1.2
2001_F_15	419726.7	5578276.6	58	39	86	46	1.2
2001_F_16	419747.3	5578289.0	57	39	25	47	1.3
2001_N_01	419848.1	5578073.2	62	45	24	51	1.4
2001_N_02	419837.7	5578074.4	68	44	18	47	1.2
2001_N_03	419825.9	5578074.9	64	42	21	47	1.3
2001_N_04	419814.0	5578074.9	65	43	20	48	1.3
2001_N_05	419803.3	5578074.0	60	45	26	52	1.5
2001_N_06	419821.1	5578102.3	69	43	16	46	1.2
2001_N_07	419832.3	5578100.6	71	39	14	41	1.0
2001_N_08	419841.8	5578101.5	72	43	14	46	1.2
2001_N_09	419853.1	5578102.8	73	43	14	46	1.2
2001_N_10	419867.7	5578104.7	67	44	19	48	1.3
2001_N_11	419879.8	5578104.0	65	42	20	47	1.2
2001_N_12	419886.7	5578116.0	66	48	22	52	1.5
2001_N_13	419877.2	5578124.9	63	45	22	50	1.4
2001_N_14	419868.8	5578123.8	61	42	24	48	1.3
2001_N_15	419857.7	5578125.0	62	45	23	50	1.4
2001_N_16	419842.7	5578124.6	60	45	26	52	1.4
2001_N_17	419828.6	5578123.0	68	46	19	50	1.3
2001_N_18	419817.0	5578125.0	63	45	23	51	1.4
2001_N_19	419804.9	5578123.7	60	44	25	51	1.4
Average			64	42	22	48	1.3
Standard Deviation			4	2	8	3	0.1
95% confidence			1	1	2	1	0.0

## APPENDIX IV

### **Sample images**



Figure A4.1: Benthic Imager screenshot showing the 5-spot laser pattern around a burrow of the angular crab, *Goneplax rhomboides*. The image has been overlaid with a 20 × 20 cm square quadrat that has been corrected to account for perspective. Reproduced from Figure 2.7.



Figure A4.2: Typical image of the seabed at Jennycliff Bay with the laser spot pattern. Megafaunal features include thalassinidean burrow openings, and the openings of the infaunal bivalves *Lutraria lutraria* and cf. *Acanthocardia* sp.. The video overlay displays ROV orientation with a date-time and depth stamp.



Figure A4.3: Typical image of the seabed at Jennycliff Bay with the laser spot pattern. Megafaunal features include a *Callianassa* mound and the surface openings produced by the infaunal bivalves *Lutraria lutraria* and cf. *Acanthocardia* sp.. The video overlay displays ROV orientation with a date-time and depth stamp.

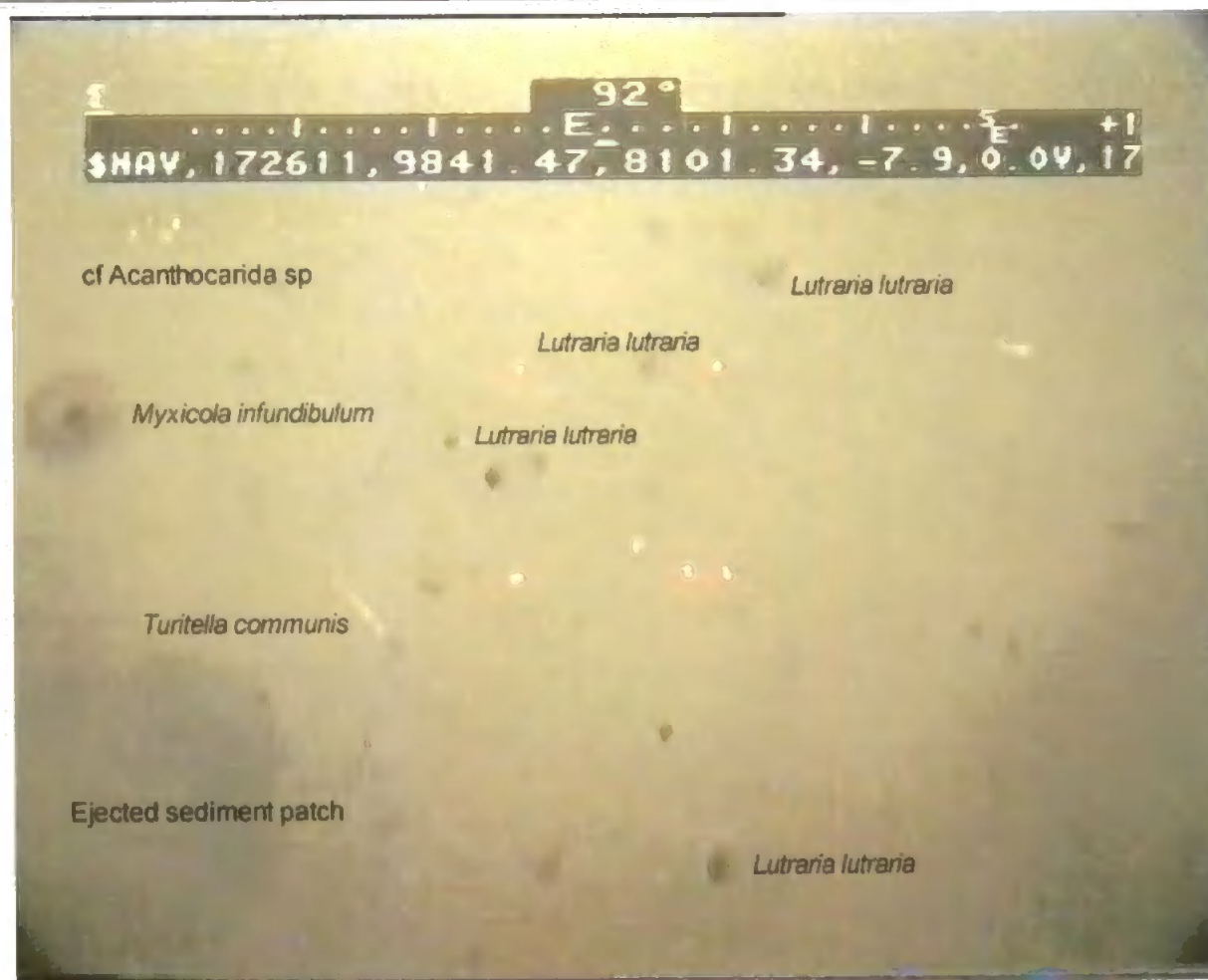


Figure A4.4: Typical image of the seabed at Jennycliff Bay with the laser spot pattern. Megafaunal features include the openings of the infaunal bivalves *Lutraria lutraria* and cf. *Acanthocardia* sp. with the polychaete *Myxicola infundibulum*, the epifaunal gastropod, *Turitella communis*, and an ejected sediment patch. The video overlay displays ROV orientation, time stamp and UTM co-ordinates derived from the Sonardyne underwater acoustic positioning system.





Figure A4.5: Typical image of the seabed at the Upper Basin of Loch Creran showing the laser spot pattern. The dominant megafaunal burrow (right of image) is constructed by the Norway lobster, *Nephrops norvegicus*, one individual being visible in a burrow entrance. Two colonies of the seapen, *Virgularia mirabilis*, are also present.

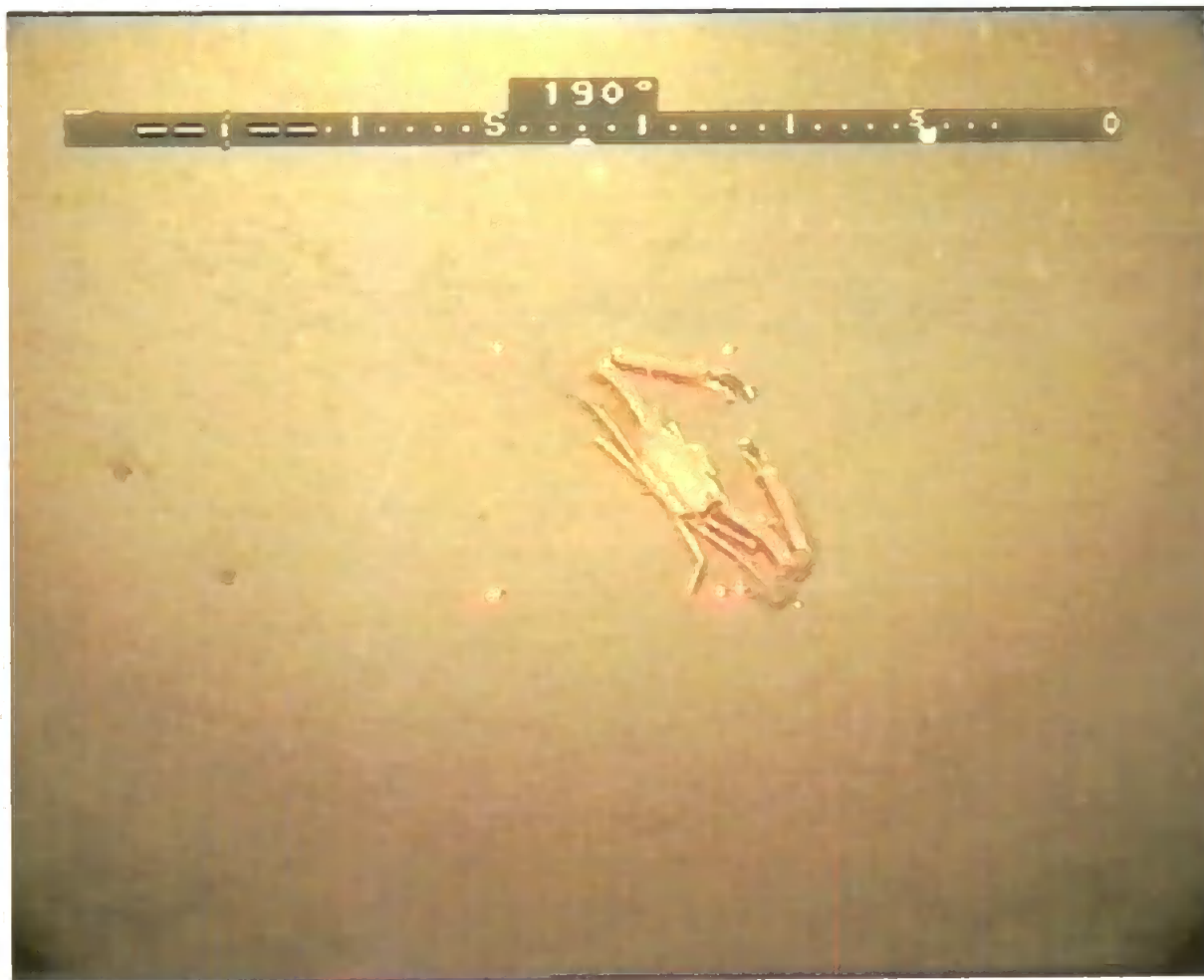


Figure A4.6: A rare foray of the angular crab, *Goneplax rhomboides*, from its burrow at the Upper Basin of Loch Creran. A typical burrow opening may be seen in Figure A4.1. The video overlay displays ROV orientation only as current speeds were negligible.